Shape optimization by the level-set method

Frédéric de Gournay

THÈSE
présentée devant
l'ECOLE POLYTECHNIQUE
pour l'obtention du
DIPLÔME DE DOCTORAT

présentée et soutenue publiquement le 07 Juillet 2005 par

Frédéric de GOURNAY

SPÉCIALITÉ : MATHÉMATIQUES APPLIQUEES

Optimisation de formes par la méthode des lignes de niveaux

Au vu des rapports de :

M. Mohamed MASMOUDI
M. Michel PIERRE.

Devant la commission d'examen formée de :

M. Grégoire ALLAIRE (Directeur de thèse)
M. Eric BONNETIER
M. Fançois JOUVE
M. Mohamed MASMOUDI
M. Michel PIERRE.

Remerciements

tout seigneur tout honneur, c'est donc Grégoire que je remercierai en premier pour m'avoir tant appris pendant ces trois années et avoir fait preuve d'une si grande patience pendant nos discussions. Merci aussi pour tes connaissances encyclopédiques et tes conseils avisés. Je veux remercier aussi François qui forme la deuxième voix de ce duo complémentaire et qui a su m'initier aux arcanes mystérieuse de Fortran 77. Merci aussi François de savoir me changer les idées aussi vite que tu sais changer de sujet quand le mot 'bug' apparaît dans la conversation.

Merci aussi aux menbres du jury, Eric, Mohammed et Michel pour leurs commentaires et leurs propositions d'améliorations toujours pertinentes. Merci surtout d'avoir eu le courage de lire cette thèse jusqu'au bout.

Merci aussi aux différents menbres du labo et surtout à Vincent, notre estimé chef, à Robert pour sa passion du karaté (quoique un peu trop communicative), à Jeanne pour sa gentillesse et à Sylvain qui a supporté sans -trop- broncher les exactions que j'ai commis envers son réseau. On m'a dit que le CMAP était un des labos de mathématiques les plus agréables à vivre, je n'en doute pas.

Je pense aussi à ceux qui en dehors du labo m'ont aidé à supporter les différentes épreuves que doit surmonter un jeune apprenti :

Merci à Jean-Baptiste d'avoir vécu avec moi ces différentes années de thésard et d'avoir cru bon essayer de me démontrer que les soucis du thésard sont solvables (solubles) dans l'Armagnac.

Merci à ma mère d'avoir toujours su mettre entre nous pendant ces dernières années une distance d'au moins huit cent kilomètres.

Merci à mon père d'avoir pris pendant cinq minutes un air concentré en lisant mes premiers efforts tout en se demandant quel vin il allait bien pouvoir servir à table.

Merci finalement à Jean-Yves de m'avoir rappelé avec sa diplomatie habituelle et par des discrets quoiques très éloquents soupirs que les mathématiques n'intéressent que très peu les gens normaux.

Introduction

'optimisation des structures élastiques est un problème d'une importance telle qu'il a monopolisé nombre d'attentions dans les dernières années. Les méthodes numériques utilisées pour résoudre ce problème peuvent se diviser en deux classes : Les méthodes topologiques et les méthodes géométriques.

Les méthodes topologiques représentent les formes par leur densité sur un maillage fixe et optimisent la forme maille par maille tandis que les méthodes géométriques bougent la frontière du domaine. Chaque méthode présente ses inconvénients, ce qui a motivé un couplage de deux de ces méthodes dans le **chapitre 2**.

Parmi les méthodes topologiques, la plus utilisée est la méthode SIMP (cf [Ben95]) qui optimise la densité de la forme (comprise entre 0 et 1) avec un facteur de pénalisation pour éviter les densités intermédiaires et obtenir une forme "classique" (ie, la densité vaut partout 0 ou 1). Une des plus élégantes est la méthode d'homogénéisation (cf [All01]) qui relaxe le problème dans la fermeture des formes admissibles pour le critère considéré. Malheureusement, la méthode d'homogénéisation n'est disponible que pour des cas simples : la compliance ou les valeurs propres. De plus la forme optimale est généralement une forme composite et une méthode de pénalisation est nécessaire pour obtenir une forme usuelle. De plus, ces deux méthodes présentent le même défaut : Comme la séparation entre le vide et la forme n'est pas claire, il y a apparition de modes "fictifs". Un mode fictif est un mode qui est localisé dans le vide. Comme nous travaillerons beaucoup avec des valeurs propres, ces deux méthodes ont été éliminées d'office.

Deux autres méthodes topologiques existent : le gradient topologique (cf [SZ99],[GGM01]) qui place de manière optimale des trous dans la forme mais qui ne peut pas augmenter le volume de la forme et la méthode des ligaments de Sokolowski [NS04] qui relie deux parties de la forme par un fin ligament. Cette dernière méthode n'a jamais été implémentée et semble d'ailleurs difficile à traiter numériquement.

Les méthodes géométriques quant à elles bougent la forme du domaine. Ce sont des méthodes de gradient où on utilise le formalisme de la dérivation par rapport au domaine (voir [MS76] et **chapitre 1**). Elles présentaient comme principal défaut la nécessité de remailler le domaine quant deux parties de la frontière coalescaient. Ce problème fut résolu par la méthode "level-set" (voir

[OS88]) qui permet de considérer une frontière comme la courbe de niveau 0 d'une fonction. La forme est définie comme l'ensemble des points ou la fonction est négative. Ceci permet de traiter les formes sur des maillages fixes et permet de changer efficacement la topologie de la forme. Advecter la frontière de la forme revient à appliquer une simple équation de type Hamilton-Jacobi à la fonction level-set. Cependant cette approche conserve certains de ses autres défauts initiaux comme la faculté de rester très facilement coincé dans des minima locaux. La théorie mathématique de l'optimisation géométrique s'applique cependant à bien plus de cas que celle de l'homogénéisation.

Plan de la thèse

Le **chapitre 1** est un rappel des différentes notions pré-requises pour comprendre les méthodes géométriques. Sans prétention d'exhaustivité, ce chapitre présente aussi quelques résultats intéressants sur l'existence et la régularité des formes optimales. On y définit la topologie avec laquelle la dérivation par rapport au domaine est effectuée, il s'agit de celle de l'espace tangent aux difféomorphismes $W^{1,\infty}(\mathbb{R}^d;\mathbb{R}^d)$, inversibles et pris au point identité. Cette topologie s'identifie naturellement avec celle des champs de vecteurs $W^{1,\infty}(\mathbb{R}^d;\mathbb{R}^d)$. On y rappelle le fameux *théorème de structure d'Hadamard* qui consiste à dire que la valeur de la différentielle ne dépend que de la valeur de la normale du champs de vecteur sur la frontière de la forme à l'itération k. Ainsi il existe sur cette forme une "pression" définie sur sa frontière qui indique si on doit en ce point augmenter ou diminuer le volume de la forme pour l'améliorer. Nous définissons ensuite la méthode des courbes de niveaux qui est essentiellement un artefact numérique pour transformer le domaine.

Nous démontrons aussi quelques propriétés simples des formes optimales du problème de la compliance. En regardant l'équation d'Euler-Lagrange des formes optimales, nous arrivons à démontrer que celles-ci doivent présenter des points de rebroussements dans le cas du Laplacien. Pour l'élasticité, sous des conditions de symétrie, elles doivent présenter des coins. Nous arrivons à calculer pour l'élasticité l'angle entre la forme et l'endroit où elle est accrochée (la condition de Dirichlet), si on suppose la solution régulière. Cet angle ne dépend que de la valeur du coefficient de Poisson de la forme.

Mon travail de thèse a d'abord porté sur l'implémentation numérique du couplage entre la méthode level-set et le gradient topologique. Nous avons développé un algorithme efficace qui permet d'advecter la frontière d'une forme et de créer des trous à l'intérieur. Ce travail permet d'essayer d'affranchir la méthode level-set de ses principaux défauts : les minima locaux et la dépendance par rapport à l'initialisation. Ce travail est résumé au **chapitre 2**. La méthode topologique qui consiste à calculer la dérivé de la fonction objectif quand un trou est percé dans la forme est couplée avec la méthode de variation de frontière. La méthode de couplage est des plus simple, elle consiste à effectuer une itération de gradient topologique toutes les n itérations d'avancement de la frontière.

Nous nous sommes ensuite intéressés à l'extension de la vitesse de la méthode level-set. En effet, la pression qui essaye d'advecter la frontière du domaine n'est définie *que* sur cette frontière (doit-on ou non en ce point augmenter ou diminuer le volume ?). Dans le formalisme de la méthode level-set, on transporte la fonction qui définit le domaine par une équation d'Hamilton-Jacobi définie sur tout le maillage. D'où la nécessité de trouver une vitesse définie de manière cohérente partout. La méthode d'extension que nous proposons consiste simplement à multiplier la vitesse par le Laplacien inverse. Nous en avons profité dans la foulée pour démontrer que cette extension pouvait aussi s'interpréter comme une régularisation, ce qui améliore l'algorithme.

En comprenant l'extension de la vitesse comme une méthode de recherche de la plus grande pente, nous avons aussi pu établir un formalisme satisfaisant permettant de résoudre des problèmes jusqu'ici non traités comme l'optimisation de la première valeur propre d'une structure quand elle est double ou l'optimisation robuste (voir plus loin). Le **chapitre 3** est le résumé de cet axe de recherche.

Nous nous sommes aussi intéressés à différentes notions de stabilité des structures. Il ne suffit pas qu'une structure soit optimale pour un certain jeu de forces, il faut aussi qu'elle résiste bien aux perturbations et qu'elle reste assez longtemps en régime linéaire. Nous avons donc développé la théorie de la compliance robuste qui permet de trouver la pire des perturbations et d'optimiser par rapport à cette dernière et nous avons traité le problème du flambage.

Le problème de la compliance robuste est le problème de trouver la perturbation d'une force qui maximise l'énergie interne (ou compliance) d'une structure élastique. L'ensemble des perturbations autorisées est défini comme une boule dans un certain espace de Hilbert. Le problème est du type : trouver le couple (u, s) optimal tel que :

$$\max_{\|s\| \leq m} \max_{u} -(\mathbf{A}u, u) + 2(\mathbf{f}, u) + 2(B^* s, u) \tag{1}$$

Où $\mathbf{A}$ est un opérateur linéaire coercif et représente l'opérateur de l'élasticité. $\mathbf{f}$ est le terme source, s est la perturbation, m est la taille des perturbations, u est le déplacement et B est *l'opérateur de localisation des perturbations.*

Ce problème est le problème classique de la compliance si $m = 0$ et est un problème de valeur propre si $f = 0$. Il peut donc être considéré comme une extension des deux problèmes. Nous prouvons au **chapitre 4** l'existence d'une perturbation la pire et nous caractérisons l'ensemble des pires perturbations. Nous montrons qu'il s'agit d'une sphère de dimension finie inscrite dans l'ensemble des perturbations admissibles. Essentiellement le résultat final dit que si on introduit un multiplicateur de Lagrange z pour la contrainte $\|s\| \leq m$, alors les min et les max peuvent s'échanger. L'algorithme produit pour trouver les couples (u, s) optimaux sera essentiellement une méthode de Newton sur $\min g(z)$ où $g(z)$ est la fonction convexe (là ou le minimum sera cherché) :

$$g(z) = \max_{s} \max_{u} -(\mathbf{A}u, u) + 2(\mathbf{f}, u) + 2(B^* s, u) + z(m - (s, s))$$

Des bornes efficaces pour la méthode de Newton seront données.

Ensuite, dans le **chapitre 5** nous calculons la dérivée directionelle de la compliance robuste par rapport au domaine. Le problème pouvant être interprété comme un mélange du problème de la compliance et d'un problème aux valeurs propres, nous montrerons que c'est un problème auto-adjoint. Les perturbations qui maximisent l'équation (1) peuvent être multiples, c'est pourquoi nous utilisons la méthode de régularisation introduite au **chapitre 3** et son utilisation aux problèmes des valeurs propres multiples pour produire un algorithme d'optimisation par la méthode level-set.

Le problème du flambage est traité dans le **chapitre 6**. Il s'agit d'un critère permettant de caractériser la limite du régime linéaire d'une forme soumise à un jeu de forces. La modélisation simplifiée du flambage que nous étudierons ici, le "flambage linéaire" est un problème aux valeurs propres généralisé dont l'opérateur du second membre dépend de la solution du système de l'élasticité linéaire. Ce problème aux valeur propres ne présente pas de compacité, nous ne savons toujours pas si la plus petite valeur propre est atteinte. En postulant cette atteignabilité, nous pouvons démontrer la dérivabilité de la plus petite valeur propre par rapport au domaine quand celle-ci est simple. Nous pouvons calculer la collection des dérivées directionnelles quand la plus petite valeur propre est multiple. En utilisant le formalisme développé au **chapitre 3**, nous pouvons donner un algorithme d'optimisation du flambement. Nous utilisons cet algorithme sur des mécanismes pour essayer de s'affranchir du problème des "hinges" (charnières, articulations).

Le **chapitre 7** est un pot-pourri de résultats numériques supplémentaires.

Le **chapitre 8** est un exposé des principales difficultés rencontrées lors de l'implémentation numérique du problème d'optimisation de forme par la méthode level-set. Les solutions adoptées y sont développées et argumentées. Ces deux chapitres sont destinés à apporter des éléments de réponse et de comparaison à tous ceux qui se lancent dans l'implémentation de cette méthode.

Nouvelles approches de la thèse

$\diamond$ Parmi les nouvelles approches abordée dans cette thèse, nous retiendrons en premier lieu une nouvelle manière de calculer la dérivée par rapport au domaine de certaines fonction coût. En effet, certaines fonctions coût s'expriment comme un maximum (compliance, valeurs propres, compliance robuste,..) sur un espace qui varie avec le domaine :

$$\mathcal{J}(\Omega) = \max_{u \in H(\Omega)} F(u, \Omega)$$

Par exemple pour la fonction coût "énergie de Dirichlet", l'analogue de la compliance, on a :

$$\mathcal{J}(\Omega) = \max_{u \in H_0^1(\Omega)} -\int_\Omega \nabla u \cdot \nabla u + 2\int_\Omega fu \tag{2}$$

L'approche classique consistait à dériver $u(\Omega)$ (le maximiseur) par rapport au domaine pour obtenir la dérivée de $\mathcal{J}$. Ici, nous ne montrerons plus l'existence de la dérivée de u mais bien celle de $\mathcal{J}$ en utilisant le résultat suivant :
Définissons

$$\mathcal{J}(\theta) = \max_{u \in H} F(u, \theta)$$

Si l'ensemble sur lequel est maximisé F (ie H) ne dépend pas de θ, alors, sous des conditions très peu restrictives, $\mathcal{J}$ est directionnellement différentiable par rapport à θ et la dérivée directionelle au point θ_0 est donnée par :

$$\frac{\partial \mathcal{J}}{\partial \theta}(\theta_0).\theta = \max_{u \in \mathcal{M}} \frac{\partial F}{\partial \theta}(u, \theta_0).\theta$$

Où $\mathcal{M}$ représente l'ensemble des u maximiseurs de $F(u, \theta_0)$.
Ici $\theta \in W^{1,\infty}(\mathbb{R}^d; \mathbb{R}^d)$ est un vecteur tangent à la topologie de dérivation par rapport au domaine (voir **chapitre 1** pour une présentation de cette topologie) et θ_0 vaut toujours 0.

Cette manière de dériver (voir [SJP92] et aussi [AB03] pour un résultat analogue), exprimée à la section 3.5 pour les valeurs propres multiples et à la section 5.2 pour la compliance robuste permet de calculer la dérivée par rapport au domaine de nouvelles fonction coût, qui ne sont plus globalement dérivables, seulement directionellement.

Un dernier problème est à résoudre, comment faire pour que l'ensemble sur lequel on maximise l'équation (2) (ie $H_0^1(\Omega)$) ne dépende pas de Ω ? La réponse est assez simple et nécessite la connaissance de la topologie de dérivation par rapport au domaine (**chapitre 1**). L'ensemble des domaines atteignables est défini comme l'ensemble des $\Omega_\theta = T(\Omega)$ où $T = \mathrm{Id} + \theta$ et θ décrit $W^{1,\infty}(\mathbb{R}^d; \mathbb{R}^d)$. Il suffit de remarquer ensuite que, avec $v = u \circ T^{-1}$:

$$\begin{aligned} & \max_{u \in H_0^1(\Omega_\theta)} -\int_{\Omega_\theta} \nabla u \cdot \nabla u + 2\int_{\Omega_\theta} fu \\ = & \max_{v \in H_0^1(\Omega)} -\int_{\Omega_\theta} \nabla(v \circ T^{-1}) \cdot \nabla(v \circ T^{-1}) + 2\int_{\Omega_\theta} f(v \circ T^{-1}) \end{aligned}$$

Par un changement de variable on se ramène à une intégrale sur Ω et on peut donc dériver l'intégrande par rapport à θ. Le max lui-même ne dépend plus de θ. On peut remarquer tout de suite que la plus grosse contrainte de régularité sur Ω que l'on demande est que Ω supporte bien les changements de variable (Ω Lipschitz). Dans le formalisme de la dérivation par rapport au domaine, cette approche n'utilise que la notion de *dérivée Lagrangienne* sans utiliser celle de la *dérivée Eulerienne*.

$\diamond$ La méthode level-set étant une méthode de gradient, nous retiendrons aussi l'interprétation de la régularisation de la vitesse comme une méthode de plus grande descente. Trouver la direction de descente s'exprimera par :

$$\min_{\|V\|_K=1} (\frac{\partial \mathcal{J}}{\partial \theta}(\theta_0), V)$$

Où K est un espace de Hilbert (typiquement $H^1(D)$) et V représente la direction de descente (voir le **chapitre 3** pour une discussion sur la faisabilité d'une telle approche). Nous montrerons que le problème :

$$\min_{\|V\|_K=1} \max_{u\in\mathcal{M}} (\frac{\partial F}{\partial \theta}(u, \theta_0), V) \tag{3}$$

est un problème très facile à résoudre pour les fonctions coût considérées. Il s'agit d'un problème de type SDP en dimension petite (voir le **chapitre 1**). La technique de transformation de l'équation (3) en un problème SDP est basée sur les deux propriétés suivantes :
-La fonctionnelle $(u, V) \mapsto (\frac{\partial F}{\partial \theta}(u, \theta_0), V)$ est quadratique en u et linéaire en V.
-L'ensemble des maximiseurs $\mathcal{M}$ est une sphère dans un certain espace de Hilbert.

$\diamond$ Le problème de compliance robuste (voir équation 1) qui est formalisé au **chapitre 4** est un problème du genre "trust-region" en dimension infinie. En dimension finie, ce problème est bien connu et les solutions clairement identifiées. Les méthodes de preuve d'existence et d'unicité apportées sont, tout du moins à notre connaissance, des techniques purement de dimension finies. Nous avons donc du établir des techniques valables en dimension infinie pour ce problème. Ces dernières donnent les mêmes résultats que les techniques finies. L'étendue des connaissances en problèmes de type "trust-region" et le fait qu'il ait surtout été étudié sous son angle "dimension finie" rend probable l'existence d'une démonstration qui nous soit inconnue en dimension infinie.

Notations

Elasticité

u	:	Déplacement ; champs de vecteur
$\mathbf{f_1}$	:	Terme source de volume ; champs de vecteur
$\mathbf{f_2}$	:	Terme source de bord (Neumann) ; champs de vecteur
$\mathbf{f} = (\mathbf{f_1}, \mathbf{f_2})$	:	Notation générique de l'ensemble des termes sources
$e(\cdot)$	:	Déformations ; champs de matrice
$\varepsilon(\cdot)$	:	Partie linéaire des déformations
σ	:	Contraintes ; champs de matrice
A	:	Loi de Hooke ; tenseur sur les matrice
$\mathbf{A}$	:	Opérateur d'élasticité
$\mathbf{B}$	:	Opérateur de localisation des perturbations (compliance robuste)

Géométrie

D	:	Domaine de travail
$\Omega \subset D$	:	Forme à optimiser
$\partial\Omega$	:	Frontière de Ω
Γ	:	Sous-ensemble de $\partial\Omega$
n	:	Normale extérieure de Ω
H	:	Courbure moyenne de Ω
θ	:	Champs de vecteur d'advection de Ω
ϕ	:	Level-set définissant Ω ; fonction sur D

Optimisation

$\mathcal{U}_{ad}$	:	Domaines admissibles
$\mathcal{J}(\Omega)$	:	Fonction objectif
η	:	Multiplicateur de Lagrange pour le volume
$\mathcal{L}(\Omega)$	:	Lagrangien pour la contrainte de volume
$\mathcal{J}'(\theta)$	:	Différentielle par rapport au domaine de $\mathcal{J}$
$\mathcal{L}^c$	:	Lagrangien de Céa

Indices

$_{vp}$	:	Première valeur propre
$_{cp}$	:	Compliance
$_{bu}$	:	Flambement
$_{lse}$	:	Erreur au déplacement cible
$_{rob}$	:	Compliance robuste

Table des matières

1 Quelques rappels et propriétés **1**
1.1 Position des problèmes 1
1.2 Dérivation par rapport au domaine 4
1.3 Définition et résultats 4
1.3.1 La méthode du Lagrangien de Céa 7
1.3.2 Démontrer la différentiabilité de la solution 9
1.4 La méthode des courbes de niveaux 11
1.4.1 Calcul numérique de l'EDP 13
1.4.2 Vitesse d'advection 13
1.4.3 Schéma numérique de l'équation d'Hamilton-Jacobi 14
1.5 Existence de formes optimales 14
1.5.1 Les théorèmes d'existence pour la convergence de Hausdorff complémentaire 14
1.5.2 Présence de cusps pour le Laplacien 16
1.5.3 Propriétés des formes optimales en élasticité 17
1.6 Les problèmes SDP 20

2 Structural optimization using topological and shape sensitivity via a level set method **23**
2.1 Introduction 24
2.2 Setting of the problem 25
2.3 Shape derivative 26
2.4 Topological derivative 27
2.5 Level set method for shape optimization 30
2.6 Optimization algorithm 31
2.7 Numerical examples in 2-d 33
2.8 Numerical examples in 3-d 38
2.9 Conclusion 41

3 Velocity extension for the Level-set method **43**
3.1 Introduction 44
3.2 Presentation of the problem 45
3.3 The weak material approximation and the natural extension method 46

3.4 Velocity regularization by the Hilbertian method 47
3.4.1 Definition of the Hilbertian method 47
3.4.2 Advantages of the method 47
3.4.3 Numerical example : Eigenvalues of a cantilever 49
3.4.4 Numerical example : The compliance of the cantilever . . 51
3.4.5 Numerical example : A 2-d gripping-mechanism 52
3.4.6 Numerical example : More 2-d mechanism 54
3.4.7 Numerical example : A 3-d gripping mechanism 57
3.5 Optimizing multiple eigenvalues 58
3.5.1 A general theorem about eigenvalue differentiation 59
3.5.2 Calculus of the directional derivative of $\mathcal{L}_{vp}$ 60
3.5.3 Calculating V^* 64
3.6 Numerical results 66
3.6.1 The 3-d eigenvalue of a beam 66
3.6.2 The short cantilever 69

4 The direct problem of the robust compliance 71
4.1 Motivation 72
4.2 The problem 73
4.2.1 Setting 73
4.2.2 Equivalent formulation 74
4.2.3 An overview of chapter 4 75
4.3 The maximum is a critical value 76
4.3.1 The maximum is attained 77
4.3.2 The maximum is a critical value 77
4.4 The critical point problem 78
4.4.1 The Fredholm alternative 78
4.4.2 The set of critical points 80
4.5 Finding ρ^* 81
4.5.1 Restriction on the maximizers 81
4.5.2 The function g 82
4.6 An algorithm 85
4.6.1 A stable algorithm 85
4.6.2 Bounds on s 86
4.7 Numerical results 88
4.7.1 Monotonic properties 88
4.7.2 Non-dependency of the bounds with respect to the mesh . 90

5 Shape optimization of the robust compliance 93
5.1 Shape optimization setting 94
5.2 Shape differentiability 94
5.2.1 Introduction : Lagrange derivation 95
5.2.2 A general theorem about robust derivation 96
5.2.3 Application of theorem 5.2.1 to shape optimization 98
5.3 An algorithm of shape optimization 100
5.3.1 The SDP problem 101

5.3.2 The choice of descent direction . . . 102
5.4 Numerical results . . . 104
5.4.1 From the beam to a cantilever . . . 104
5.4.2 The Wheel-bridge . . . 105
5.4.3 The 2-d mast . . . 106
5.4.4 The 3-d beam . . . 109
5.4.5 The 3-d bridge . . . 110
5.4.6 The 3-d chair . . . 111
5.5 Conclusion . . . 111

6 Shape optimization of the buckling load 113
6.1 The direct problem . . . 113
6.1.1 Definition of the linearized buckling load . . . 113
6.2 Shape sensitivity of the buckling load . . . 116
6.2.1 Multiplicity equal to one . . . 116
6.2.2 Multiplicity greater than one . . . 119
6.2.3 The algorithm . . . 120
6.3 Numerical example . . . 121
6.3.1 The loaded beam . . . 121
6.3.2 The two beams reinforcement . . . 123
6.3.3 The compliant bridge . . . 125
6.3.4 The buckling of a grip . . . 126
6.4 Conclusion . . . 129

7 D'autres résultats numériques 131
7.1 Compliance robuste de la console courte . . . 131
7.2 Valeur propre de la console courte . . . 133
7.3 La pince du CEA . . . 135
7.4 Une autre pince . . . 138
7.5 Le mécanisme à coefficient de Poisson négatif . . . 139

8 Numerical results : beyond the mirror 143
8.1 2-d issues for the compliance and the robust compliance . . . 144
8.1.1 The thin bar problem . . . 144
8.1.2 The tolerance parameter solution is not available for the robust compliance . . . 145
8.1.3 Topological gradient as a solution to the thin bar problem 146
8.1.4 The reload method as the chosen solution for the robust compliance . . . 147
8.2 The fiber problem in 3-d compliance . . . 147
8.3 Modes in disconnected parts of the shape . . . 148
8.4 Mechanism design . . . 151
8.4.1 The Hinges and Horn's problem . . . 151
8.4.2 Disconnection of the mechanism . . . 153
8.4.3 The Natural extension method and the Lagrange multiplier 154
8.5 Conclusion . . . 156

A Existence of a local maximum for the direct problem of the robust compliance **157**

B Proof of Theorem 5.2.1 **161**
B.1 The subgradient of $\mathcal{J}_{rob}$ 161
B.2 The directional derivative 163

Index **165**

Table des Figures **165**

Bibliographie **169**

Chapitre 1

Quelques rappels et propriétés

Résumé

Ce chapitre est destiné à rappeler le contexte de l'optimisation de formes par la méthode level-set et à poser les problématiques actuelles soulevées par ce problème. Nous en profiterons aussi pour définir certaines des notations utilisés lors de la suite de cette thèse. Sont aussi présentées quelques propriétés simples des formes optimales pour le problème de la compliance.

1.1 Position des problèmes 1
1.2 Dérivation par rapport au domaine 4
1.3 Définition et résultats 4
1.3.1 La méthode du Lagrangien de Céa 7
1.3.2 Démontrer la différentiabilité de la solution 9
1.4 La méthode des courbes de niveaux 11
1.4.1 Calcul numérique de l'EDP 13
1.4.2 Vitesse d'advection 13
1.4.3 Schéma numérique de l'équation d'Hamilton-Jacobi . 14
1.5 Existence de formes optimales 14
1.5.1 Les théorèmes d'existence pour la convergence de Hausdorff complémentaire 14
1.5.2 Présence de cusps pour le Laplacien 16
1.5.3 Propriétés des formes optimales en élasticité 17
1.6 Les problèmes SDP 20

1.1 Position des problèmes

Un problème d'optimisation de forme consiste en : une équation aux dérivées partielles, une fonction objectif dépendant de la solution de l'EDP et un en-

semble de formes admissibles. L'EDP modèle que nous utilisons est celle de l'élasticité linéaire. Soit $\Omega \subset \mathbb{R}^d$ ($d = 2$ ou 3) un ouvert borné contenant un matériau isotrope linéaire de Loi de Hooke A. Où le tenseur A est défini par :

Définition 1.1.1 *Pour toute matrice symétrique ξ, $A\xi$ est la matrice définie par*

$$A\xi = 2\mu\xi + \lambda\big(\mathrm{Tr}\xi\big)Id, \tag{1.1}$$

Où μ et λ sont les coefficients de Lamé du matériau qui vérifient :

$$\mu > 0 \quad et \quad 2\mu + d\lambda > 0 \tag{1.2}$$

Pour un champs vectoriel u, on définit le champs de déformations linéaires et les contraintes par :

Définition 1.1.2 *Pour tout champs vectoriel u, les déformations linéaires et les contraintes sont deux champs de matrice symétriques définis respectivement par*

$$e(u) = \frac{1}{2}(\nabla u + \nabla u^*) \quad et \quad \sigma = Ae(u) \tag{1.3}$$

La frontière de la forme de travail Ω est décomposée en deux sous-ensembles complémentaires :

$$\partial\Omega = \Gamma_N \cup \Gamma_D, \tag{1.4}$$

Où des conditions de Dirichlet seront imposées sur Γ_D et des conditions de type Neumann sur Γ_N.

L'ensemble des formes admissibles est l'ensemble des Ω inclus dans une grande boîte D et de volume fixé V.

$$\mathcal{U}_{ad} = \Big\{\Omega \subset D \text{ tel que } |\Omega| = V\Big\}. \tag{1.5}$$

Optimisation de la première valeur propre

Le problème spectral est : Trouver une valeur propre γ et un vecteur propre $u \neq 0$ tels que :

$$\left\{\begin{array}{rcll} -div\,(A\,e(u)) & = & \gamma\rho u & \text{dans } D \\ u & = & 0 & \text{sur } \Gamma_D \\ \big(A\,e(u)\big)n & = & 0 & \text{sur } \Gamma_N. \end{array}\right. \tag{1.6}$$

Le champs scalaire ρ défini sur D représente la densité du matériau, le cas usuel étant $\rho = 1$ dans Ω et $\rho = 0$ ailleurs. Le spectre de l'élasticité $Sp(\Omega)$ est défini comme l'ensemble des valeurs propres qui est ici un ensemble dénombrable de réels tendant vers l'infini et qui atteint sa plus petite valeur propre $\gamma_1(\Omega) > 0$ (si Γ_D interdit les déplacements rigides, ce qui sera toujours supposé).

Le problème d'optimisation de la première valeur propre est donné par :

$$\min_{\Omega\in\mathcal{U}_{ad}} \mathcal{J}_{vp}(\Omega) \quad \text{où} \quad \mathcal{J}_{vp}(\Omega) = -\gamma_1(\Omega) \tag{1.7}$$

Optimisation de la compliance

Pour un jeu de forces $\mathbf{f} = (\mathbf{f_1}, \mathbf{f_2})$ avec $\mathbf{f_1} \in L^2(\Omega)^d$ et $\mathbf{f_2} \in H^1(\Omega)^d$ où $\mathbf{f_1}$ est le champs vectoriel des forces volumiques et $\mathbf{f_2}$ celui des forces surfaciques, le déplacement $u \in H^1(\Omega)^d$ est la solution du système de l'élasticité linéaire :

$$\left\{ \begin{array}{rcll} -div\,(A\,e(u)) & = & \mathbf{f_1} & \text{in } \Omega \\ u & = & 0 & \text{on } \Gamma_D \\ (A\,e(u))n & = & \mathbf{f_2} & \text{on } \Gamma_N. \end{array} \right. \tag{1.8}$$

Il faut de plus assurer que Γ_D interdit les déplacements rigides au sens où il n'existe pas de rotation-translation non nulles qui s'annulent sur Γ_D. Si ce n'est pas le cas, il faut imposer des conditions d'équilibre sur $\mathbf{f} = (\mathbf{f_1}, \mathbf{f_2})$ et travailler dans l'espace des champs de vecteurs quotienté par les déplacements rigides.

Il existe une unique solution au problème (1.8) dans $H^1_D(\Omega)^d$, où l'indice D signifie que les fonctions sont nulles sur Γ_D. De plus u est le maximiseur de la fonctionnelle énergie sur l'espace $H^1_D(\Omega)^d$:

$$E_\Omega(v, \mathbf{f}) = -\int_\Omega A\,e(v) : e(v)\,dx + 2\int_\Omega \mathbf{f_1} \cdot v\,dx + 2\int_{\Gamma_N} \mathbf{f_2} \cdot v\,ds$$

La valeur du-dit maximum, $C_\Omega(\mathbf{f})$, est appelée la compliance. C'est un bon indice de la rigidité de la structure soumise au jeu de forces $\mathbf{f}$. Le problème d'optimisation de forme de la compliance est donné par

$$\min_{\mathcal{U}_{ad}} \mathcal{J}_{cp}(\Omega) \quad \text{où} \quad \mathcal{J}_{cp}(\Omega) = C_\Omega(\mathbf{f}). \tag{1.9}$$

Optimisation du déplacement cible

Un autre choix de fonctions objectives très utile pour l'optimisation de mécanisme compliants est la minimisation de l'erreur entre le déplacement u (défini comme dans l'équation 1.8) et un déplacement cible u_0.

$$\min_{\mathcal{U}_{ad}} \mathcal{J}_{lse}(\Omega) \quad \text{où} \quad \mathcal{J}_{lse}(\Omega) = \left(\int_\Omega k(x)|u - u_0|^\alpha dx \right)^{1/\alpha}, \tag{1.10}$$

Où $\alpha \geq 2$,$u_0 \in L^\infty(D)$ et $k \in L^\infty(D)$ est un facteur de poids qui permet de pondérer la zone d'intérêt.

Contrainte de volume

Au lieu d'imposer aux ouverts admissibles d'être de volume V (cf (1.5)) nous utiliserons un multiplicateur de Lagrange η pour vérifier cette contrainte de volume sur les ouverts admissibles. Le problème que nous aurons à traiter sera donc :

$$\min_{\Omega \subset D} \mathcal{L}(\Omega) \quad \text{où} \quad \mathcal{L}(\Omega) = \mathcal{J}(\Omega) + \eta|\Omega| \tag{1.11}$$

Le multiplicateur de Lagrange η doit être adapté pour satisfaire la contrainte de volume. Cependant nous travaillerons rarement avec des multiplicateurs de Lagrange évoluant. La raison principale est que si η est fixé, alors on essaie de minimiser $\mathcal{L}(\Omega)$, l'historique de son évolution a un sens bien défini et on peut plus facilement analyser le comportement de l'algorithme.

1.2 Dérivation par rapport au domaine

1.3 Définition et résultats

La notion de dérivabilité par rapport au domaine est comprise au sens suivant, qui remonte à Hadamard (voir [MS76], [Pir84], [Sim80], [SJP92]).

Définition 1.3.1 *Soit Ω supposé régulier le domaine actuel de travail. Pour tout champs de vecteur $\theta \in W^{1,\infty}(D;D)$, soit*

$$\Omega_\theta = (Id + \theta) \circ \Omega = \{x + \theta(x) \text{ tel que } x \in \Omega\} \tag{1.12}$$

Pour toute fonctionnelle $\mathcal{J}(\Omega)$, la dérivabilité par rapport au domaine est la dérivabilité par rapport à l'espace $W^{1,\infty}(D;D)$ de la fonctionnelle $\theta \mapsto \mathcal{J}(\Omega_\theta)$ prise au point $\theta = 0$.

La différentielle de cette application appliquée à la direction θ sera notée $\mathcal{J}'(\theta)$.

On peut remarquer que la classe des domaines atteints à partir d'un domaine Ω appartient toujours à la classe d'homotopie du domaine de départ Ω. En 2-d, cela signifie que le nombre de composantes connexes du complémentaire est toujours le même. La méthode de variation de frontière n'est, en ce sens, pas capable de supporter les changements de topologies.

Un résultat classique est que la dérivée par rapport au domaine ne dépend que de la valeur de $\theta \cdot n$ sur la frontière de Ω. La raison en est que $\Omega_{t\theta}$ lui même ne dépend au premier ordre en t que de la valeur de $\theta \cdot n$ sur $\partial\Omega$.

Théorème 1.3.1 (de structure d'Hadamard) *Soit Ω un ouvert régulier et $\mathcal{J}(\Omega)$ une fonctionnelle Fréchet différentiable en Ω. Pour tout champs θ_1 et θ_2 tels que $\theta_1 - \theta_2$ est $C^1(\mathbb{R}^d;\mathbb{R}^d)$ et tels que $\theta_1 \cdot n = \theta_2 \cdot n$ sur $\partial\Omega$ alors :*

$$\mathcal{J}'(\theta_1) = \mathcal{J}'(\theta_2)$$

On peut donner deux exemples simples de dérivation par rapport au domaine de fonctionnelles qui sont la clef d'un calcul de type "dérivation avec un Lagrangien" ou "dérivation de Céa" (voir la section 6.2.1 et [Céa86]).

Lemme 1.3.1 *Soit $\phi_1 \in W^{1,1}(\mathbb{R}^d)$ et $\phi_2 \in W^{2,1}(\mathbb{R}^d)$ et soit les deux fonctionnelles suivantes :*

$$\mathcal{J}_1(\Omega) = \int_\Omega \phi_1 \quad et \quad \mathcal{J}_2(\Omega) = \int_{\partial\Omega} \phi_2$$

Alors $\mathcal{J}_1$ et $\mathcal{J}_2$ sont Fréchet-différentiables par rapport au domaine et

$$\mathcal{J}_1'(\theta) = \int_\Omega div(\theta\phi_1) \quad et \quad \mathcal{J}_2'(\theta) = \int_{\partial\Omega} \phi_2(div(\theta) - \partial_n(\theta\cdot n)) + \nabla\phi_2\theta \quad (1.13)$$

Quand Ω est assez régulier, une intégration par partie donne :

$$\mathcal{J}_1'(\theta) = \int_{\partial\Omega} (\theta\cdot n)\phi_1 \quad et \quad \mathcal{J}_2'(\theta) = \int_{\partial\Omega} (\theta\cdot n)(H\phi_2 + \frac{\partial\phi_2}{\partial n}) \quad (1.14)$$

Où n est la normale extérieure à Ω et $H = div(n)$ est la courbure moyenne de $\partial\Omega$.

Preuve La démonstration de l'équation (1.13) est juste un développement au premier ordre en θ des formules de changement de variable suivants, obtenus en notant $T = \mathrm{Id} + \theta$:

$$\mathcal{J}_1(\Omega_\theta) = \int_{\Omega_\theta} \phi_1 = \int_\Omega |det\nabla T|(\phi_1 \circ T)$$

$$\mathcal{J}_2(\Omega_\theta) = \int_{\partial\Omega_\theta} \phi_2 = \int_{\partial\Omega} |det\nabla T||\nabla T^{-*} n|_{\mathbf{R}^n}(\phi_2 \circ T)$$

Pour l'équation (1.14), l'intégration par partie pour $\mathcal{J}_1$ est évidente, celle de $\mathcal{J}_2$ nécessite une extension locale de la normale (nécessaire pour définir $\partial_n(\theta\cdot n)$ de toute façon). En décomposant $\theta = (\theta\cdot n)n + \theta_\tau$ selon la composant normale de θ et sa composante tangentielle, il vient :

$$\begin{aligned} div(\theta) &= \partial_n(\theta\cdot n) + (\theta\cdot n)div(n) + div(\theta_\tau) \\ \nabla\phi_2.\theta &= (\partial_n\phi_2)(\theta\cdot n) + \nabla\phi_2.\theta_\tau \end{aligned}$$

De telle sorte que

$$\mathcal{J}_2'(\theta) = \int_{\partial\Omega} (\theta\cdot n)(H\phi_2 + \frac{\partial\phi_2}{\partial n}) + \int_{\partial\Omega} (div(\theta_\tau)\phi_2 + \nabla\phi_2\theta_\tau)$$

Une intégration par partie permet d'obtenir le résultat. □

Corollaire 1.3.2 *Si $\mathcal{J}_2(\Omega)$ est défini par $\mathcal{J}_2(\Omega) = \int_\Gamma \phi_2$ avec Γ un sous-ensemble régulier de $\partial\Omega$ alors :*

$$\mathcal{J}_2'(\theta) = \int_\Gamma (\theta\cdot n)(H\phi_2 + \frac{\partial\phi_2}{\partial n}) + \int_{\partial\Gamma} (\theta\cdot n_\Gamma)(\phi_2)$$

Où ∂_Γ est la frontière de Γ par rapport à $\partial\Omega$ et n_Γ est le champs de vecteur tangent à $\partial\Omega$ qui représente la normale de Γ quand Γ est comprise comme une sous-variété de $\partial\Omega$.

Preuve Le développement est le même que pour la preuve de (1.14), il suffit d'utiliser l'intégration par partie suivante :

$$\int_\Gamma (div(\theta_\tau)\phi_2 + \nabla\phi_2\theta_\tau) = \int_\Gamma div(\phi_2\theta_\tau) = \int_{\partial\Gamma} (\theta \cdot n_\Gamma)(\phi_2)$$

□

Nous donnons maintenant sans démonstration les formules des différentielles par rapport au domaine des fonctions coût de la compliance $\mathcal{J}_{cp}$, de la première valeur propre $\mathcal{J}_{vp}$ et de l'erreur au déplacement $\mathcal{J}_{lse}$ qui sont valables pour des termes sources réguliers et un déplacement u régulier, par exemple $\mathbf{f_1} \in H^1(\Omega)^d$, $\mathbf{f_2} \in H^2(\Omega)^d$, $u \in H^2(\Omega)^d$.

Proposition 1.3.3 (Dérivation de la compliance)
Soit Ω un domaine régulier et le déplacement u défini par (1.8)*. Soit la fonction coût $\mathcal{J}_{cp}$ définie par* (1.9)*. Si $\mathbf{f_1} \in H^1(\Omega)^d$, $\mathbf{f_2} \in H^2(\Omega)^d$ et $u \in H^2(\Omega)^d$ alors $\mathcal{J}_{cp}$ est dérivable par rapport au domaine et*

$$\begin{aligned} \mathcal{J}'_{cp}(\theta) &= \int_{\Gamma_N} (\theta\cdot n)\left(-Ae(u)\colon e(u) + 2[\mathbf{f_1}\cdot u + \frac{\partial \mathbf{f_2}\cdot u}{\partial n} + H\mathbf{f_2}\cdot u]\right) \\ &+ \int_{\Gamma_D} (\theta\cdot n) Ae(u)\colon e(u) \end{aligned} \tag{1.15}$$

Proposition 1.3.4 (Dérivation de la première valeur propre)
Soit Ω un domaine régulier et la première valeur propre γ_1 associée au premier vecteur propre u définis par (1.6)*. Soit la fonction coût $\mathcal{J}_{vp}$ définie par* (1.7)*. Si $u \in H^2(\Omega)^d$ et si la dimension du premier espace propre est* 1 *alors $\mathcal{J}_{vp}$ est dérivable par rapport au domaine et*

$$\begin{aligned} \mathcal{J}'_{vp}(\theta) &= \int_{\Gamma_N} (\theta\cdot n)\left(Ae(u)\colon e(u) - \gamma_1 \rho u\cdot u\right) \\ &- \int_{\Gamma_D} (\theta\cdot n) Ae(u)\colon e(u) \end{aligned} \tag{1.16}$$

Où u est normalisé par $\int_\Omega \rho u \cdot u = 1$

Proposition 1.3.5 (Dérivation de l'erreur à un déplacement cible)
Soit Ω un domaine régulier et le déplacement u défini par (1.8)*. Soit la fonction coût $\mathcal{J}_{lse}$ définie par* (1.10)*. Si $\mathbf{f_1} \in H^1(\Omega)^d$, $\mathbf{f_2} \in H^2(\Omega)^d$ et $u \in H^2(\Omega)^d$ alors $\mathcal{J}_{lse}$ est dérivable par rapport au domaine et*

$$\begin{aligned} \mathcal{J}'_{lse}(\theta) &= \int_{\Gamma_N} (\theta\cdot n)\left(\frac{C_0}{\alpha} k|u-u_0|^\alpha - 2Ae(p)\colon e(u) + 2\mathbf{f_1}\cdot p + 2\frac{\partial(\mathbf{f_2}\cdot p)}{\partial n} + 2H\mathbf{f_2}\cdot p\right) \\ &+ \int_{\Gamma_D} (\theta\cdot n)\left(\frac{C_0}{\alpha} k|u-u_0|^\alpha + 2Ae(u)\colon e(p)\right) \end{aligned}$$

Où p est l'état adjoint, supposé régulier, i.e. $p \in H^2(\Omega)^d$, défini comme

$$\left\{ \begin{array}{rcll} -div\,(A\,e(p)) & = & C_0 k(x)|u-u_0|^{\alpha-2}(u-u_0) & in\ \Omega \\ p & = & 0 & on\ \Gamma_D \\ \big(Ae(p)\big)n & = & 0 & on\ \Gamma_N, \end{array} \right. \tag{1.17}$$

et C_0 est la constante donnée par :

$$C_0 = \frac{1}{2}\left(\int_\Omega k(x)|u(x)-u_0(x)|^\alpha dx\right)^{1/\alpha-1}. \tag{1.18}$$

Remarque 1.3.1 *Dans tous les cas étudiés, la dérivée par rapport au domaine s'exprime par :*

$$\mathcal{J}'(\theta) = \int_{\partial\Omega} (\theta \cdot n) v$$

ce qui est en accord avec le théorème de structure d'Hadamard (Théorème 1.3.1). La vitesse v dépend implicitement de Ω, de la solution de l'EDP et éventuellement de l'état adjoint si celui-ci est nécessaire. Cette vitesse v a le sens physique d'une pression définie sur la frontière de Ω qui, en tout point de la frontière indique si on doit augmenter le volume ($v > 0$) ou le diminuer ($v < 0$) pour diminuer la valeur de $\mathcal{J}$.

1.3.1 La méthode du Lagrangien de Céa

La façon la plus simple de calculer la dérivation par rapport au domaine, n'est malheureusement que formelle. Elle fut introduite dans [Céa86] pour le Laplacien et s'étend facilement à tout type d'EDP et de fonction objectif.

Soit u le déplacement associé à un jeu de forces $\mathbf{f} = (\mathbf{f_1}, \mathbf{f_2})$. Supposons que la fonction objectif soit de la forme :

$$\mathcal{J}(\Omega) = \int_\Omega j(x, u(x))\, dx$$

Soit le Lagrangien $\mathcal{L}^c(\Omega, v, q, v_D, q_D)$ défini pour $(v, q, v_D, q_D) \in [H^1(\mathbb{R}^d; \mathbb{R}^d)]^4$.

$$\begin{aligned} \mathcal{L}^c(\Omega, v, q, v_D, q_D) &= \int_\Omega j(x, v(x))\, dx - 2\int_\Omega Ae(v) : e(q) \\ + \quad 2\int_\Omega \mathbf{f_1}\cdot q + 2\int_{\Gamma_N} \mathbf{f_2}\cdot q &+ 2\int_{\Gamma_D} (v\cdot v_D + q\cdot q_D) \end{aligned} \tag{1.19}$$

Où v_D et q_D sont des multiplicateurs de Lagrange pour les conditions de Dirichlet. Le problème adressé est :

$$\min_{v,q_D}\max_{q,v_D} \mathcal{L}^c(\Omega, v, q, v_D, q_D)$$

L'équation des points critiques de $\mathcal{L}^c$ donne les équations de (u, p, u_D, p_D) le point-selle. Les dérivées partielles de $\mathcal{L}^c$ par rapport à v_D et q_D donnent respectivement $u = 0$ et $p = 0$ sur Γ_D. La dérivée partielle de $\mathcal{L}^c$ par rapport à q

donne l'équation du déplacement u qui est défini comme dans l'équation (1.8) ainsi que l'équation $p_D = Ae(u) \cdot n$. La dérivée partielle de $\mathcal{L}^c$ par rapport à v donne l'équation de p :

$$\left\{ \begin{array}{rcll} -div\,(A\,e(p)) & = & \frac{1}{2} j_1' & \text{dans } D \\ p & = & 0 & \text{sur } \Gamma_D \\ \big(A\,e(p)\big)n & = & \frac{1}{2} j_2' & \text{sur } \Gamma_N. \end{array} \right. \tag{1.20}$$

Où (j_1', j_2') est la différentielle de j par rapport à v, prise au point u et vue comme une distribution, ie :

$$\int_\Omega j_1' \cdot X + \int_{\partial\Omega} j_2' \cdot X = \int_\Omega D_v j(x, u(x)).X \quad \text{pour tout } X \in H^1(\mathbb{R}^d; \mathbb{R}^d)$$

Quand $D_v j(x, u(x)).X$ représente la différentielle de j par rapport à v, prise au point u et appliquée au vecteur tangent X. Dans le cas de la compliance, qui est une fonction objectif auto-adjointe, l'équation (1.20) donne $p = u$. En effet dans le cas :

$$\begin{array}{rl} & j(x, v(x)) = Ae(v) \colon e(v) \\ \Longrightarrow & \displaystyle\int_\Omega D_v j(x, u(x)).X = 2 \int_\Omega Ae(u) \colon e(X) \\ \Longrightarrow & \displaystyle\int_\Omega D_v j(x, u(x)).X = 2 \int_\Omega -div(Ae(u)) \cdot X + 2 \int_{\partial\Omega} Ae(u)n \cdot X \\ \Longrightarrow & j_1' = -2div(Ae(u)) \text{ et } j_2' = 2Ae(u)n \end{array}$$

Pour finir, L'équation de u_D est donnée par la dérivée de $\mathcal{L}^c$ par rapport à v et vaut $u_D = -\frac{1}{2} j_2' + Ae(p) \cdot n$

En remarquant que $\mathcal{J} = \mathcal{L}^c((\Omega, v, q, v_D, q_D)$, les dérivées des deux fonctionnelles par rapport au domaine coïncident. :

$$\mathcal{J}'(\theta) = \mathcal{L}^{c\prime}(\Omega, u, p, u_D, p_D)(\theta)$$

Car le Lagrangien $\mathcal{L}^c$ est défini pour $(v, q, v_D, q_D) \in [H^1(\mathbb{R}^d; \mathbb{R}^d)]^4$ qui sont des espaces **indépendant** de Ω. La dérivée du Lagrangien par rapport au paramètre Ω est donc égale à la dérivée partielle du-dit Lagrangien par rapport à Ω prise au point-selle. Ce qui nous donne, en utilisant les équations (1.14) :

$$\begin{array}{rcl} \mathcal{J}'(\theta) & = & \displaystyle\int_{\partial\Omega} (\theta \cdot n) \left[j - 2Ae(u) \colon e(p) + 2\mathbf{f_1} \cdot p + 2H\mathbf{f_2} \cdot p + 2\frac{\partial \mathbf{f_2} \cdot p}{\partial n} \right] \\ & + & \displaystyle 2\int_{\Gamma_D} (\theta \cdot n) \left[\frac{\partial u}{\partial n} [-\frac{1}{2} j_2' + Ae(p) \cdot n] + \frac{\partial p}{\partial n} Ae(u) \cdot n \right] \end{array}$$

Où on a utilisé $u = 0 = p$ sur Γ_D pour simplifier les termes dans l'intégrande de Γ_D. Ces termes peuvent être encore simplifiés si on remarque que comme Γ_D est une courbe de niveau de u et de p alors

$$\frac{\partial p}{\partial n} Ae(u) \cdot n = Ae(u) \colon e(p) = \frac{\partial u}{\partial n} Ae(p) \cdot n$$

Sous forme plus synthétique, $\mathcal{J}'$ est donné par :

$$\begin{aligned}\mathcal{J}'(\theta) &= \int_{\Gamma_N} (\theta \cdot n)\left[j - 2Ae(u)\colon e(p) + 2\mathbf{f_1}\cdot p + 2H\mathbf{f_2}\cdot p + 2\frac{\partial \mathbf{f_2}\cdot p}{\partial n}\right] \\ &+ \int_{\Gamma_D} (\theta \cdot n)\left[j + 2Ae(u)\colon e(p) - \frac{\partial u}{\partial n} j_2'\right] \end{aligned} \tag{1.21}$$

On retrouve l'équation de la dérivée de la compliance en remplaçant :

$$j = Ae(u)\colon e(u) \quad \text{et} \quad p = u \quad \text{et} \quad j_2' = 2Ae(u)\cdot n$$

On retrouve l'équation de la dérivée de l'erreur au déplacement cible en posant :

$$j = k|u-u_0|^\alpha \quad \text{et} \quad j_1' = \alpha k|u-u_0|^{\alpha-2}(u-u_0) \quad \text{et} \quad j_2' = 0$$

1.3.2 Démontrer la différentiabilité de la solution

La dérivation avec un Lagrangien de Céa est formelle au sens où il faut montrer que le déplacement u est dérivable par rapport au domaine pour pouvoir assurer que la différentielle de $\mathcal{J}$ existe bien. D'où la nécessité d'une autre technique pour pouvoir assurer que u est différentiable par rapport au domaine. Nous ne montrerons cette technique que dans un cas simplifié où la fonction objectif est :

$$\mathcal{J}(\Omega) = \int_\Omega |u(\Omega) - u_0|^2$$

Où u est un champs scalaire solution de l'équation de Laplace avec conditions limites homogènes de Dirichlet :

$$\left\{\begin{array}{rcll} -\Delta u(\Omega) &=& f & \text{dans } \Omega \\ u(\Omega) &=& 0 & \text{sur } \partial\Omega \end{array}\right. \tag{1.22}$$

On rappelle que si $\Omega_\theta = \Omega \circ T$ avec $T = Id + \theta$, on essaye de dériver l'application $\theta \mapsto J(\Omega_\theta)$.

Il existe deux dérivées de u, la dérivée Lagrangienne Y et la dérivée Eulerienne U. La dérivée Y s'exprime comme la dérivée de l'application :

$$W^{1,\infty} \mapsto H_0^1(\Omega_0) \quad : \quad \theta \mapsto \bar{u} = u(\Omega_\theta)\circ(Id+\theta)$$

La dérivée Eulerienne U n'a qu'un sens "point par point" , elle est définie en chaque point x comme la dérivée de l'application :

$$W^{1,\infty} \mapsto \mathbb{R} \quad : \quad \theta \mapsto u(\Omega_\theta)(x)$$

Il existe une relation entre ces deux dérivées donnée par

$$U(\theta) = Y(\theta) - \nabla u(\Omega).\theta \tag{1.23}$$

La dérivée Y a bien un sens évident, cependant la définition de U fait qu'elle n'a pas forcément de sens. Pour donner un sens à U nous définirons U comme solution de l'équation (1.23). nous remarquons tout de suite que la dérivée Eulerienne U n'appartient plus forcément à l'espace H^1.

Proposition 1.3.6 *Si $u(\Omega)$ est définie par (1.22), alors la dérivée Lagrangienne existe et est donnée par :*

$$\left\{ \begin{array}{rcll} -\Delta Y(\theta) & = & -\Delta(\nabla u(\Omega).\theta) & dans\ \Omega \\ Y(\theta) & = & 0 & sur\ \partial\Omega \end{array} \right. \tag{1.24}$$

Dans ce cas, la dérivée Eulerienne vaut :

$$\left\{ \begin{array}{rcll} -\Delta U(\theta) & = & 0 & dans\ \Omega \\ U(\theta) & = & -(\theta \cdot n)\frac{\partial u(\Omega)}{\partial n} & sur\ \partial\Omega \end{array} \right. \tag{1.25}$$

Démonstration
$\diamond$ Effectuons un changement de variable dans la formulation variationnelle de l'équation (1.22), pour que les intégrales soient posées sur le domaine Ω. Nous obtenons, avec $T = Id + \theta$:

$$\int_\Omega |det(\nabla T)| \left[\nabla\left(\bar{u}(\Omega_\theta)\right)\nabla T^{-1}\right] \cdot \left[\nabla(\phi \circ T)\nabla T^{-1}\right] = \int_\Omega |det(\nabla T)|(f \circ T) \cdot (\phi \circ T)$$

Où ϕ dénote une fonction test arbitraire et $\bar{u} = u \circ T$
$\diamond$ Utilisons le fait que $\psi = \phi \circ T$ est une fonction test admissible, puis nous dérivons par rapport à θ pour obtenir, après un peu d'algèbre :

$$\int_\Omega \nabla Y \cdot \nabla\psi + \int_\Omega \left(div\theta \mathrm{Id} - \nabla\theta - \nabla\theta^*\right)\nabla u(\Omega) \cdot \nabla\psi = \int_\Omega div(f\theta) \cdot \psi \tag{1.26}$$

$\diamond$ Quand ϕ décrit $H_0^1(\Omega_\theta)$, alors $\psi = \phi \circ T$ décrit $H_0^1(\Omega)$, l'équation (1.26) est donc la formulation variationelle de l'expression suivante de la dérivée $Y \in H_0^1(\Omega)$:

$$\left\{ \begin{array}{rcll} -\Delta Y(\theta) & = & div\left[\left(div\theta \mathrm{Id} - \nabla\theta - \nabla\theta^*\right)\nabla u(\Omega)\right] + div(f\theta) & \text{dans } \Omega \\ Y(\theta) & = & 0 & \text{sur } \partial\Omega \end{array} \right. \tag{1.27}$$

$\diamond$ Puis passer de l'équation (1.27) à l'équation (1.24) se fait en remarquant que $-\Delta u = f$ et que :

$$\Delta(\nabla v.\theta) = div\left((\Delta v)\theta - (div\theta)\nabla v + \left(\nabla\theta + \nabla\theta^*\right)\nabla v\right)$$

Pour toute distribution v. $\square$

Théorème 1.3.7 *Soit Ω un ouvert borné régulier. L'application*

$$\mathcal{J}(\Omega) = \int_\Omega |u(\Omega) - u_0|^2$$

est différentiable

$$\mathcal{J}'(\theta) = \int_{\partial\Omega} |u(\Omega) - u_0|^2 + 2\frac{\partial p}{\partial n}\frac{\partial u(\Omega)}{\partial n} \tag{1.28}$$

Où $p \in H_0^1(\Omega)$ est l'état adjoint défini par :

$$\left\{ \begin{array}{rcll} -\Delta p & = & u(\Omega) - u_0 & dans\ \Omega \\ p & = & 0 & sur\ \partial\Omega \end{array} \right. \tag{1.29}$$

Démonstration
$\diamond$ On effectue un changement de variable sur $\mathcal{J}$ pour ramener la fonction objectif à une intégrale sur Ω et on dérive par rapport à θ, ce qui donne :

$$\begin{aligned}\mathcal{J}(\Omega_\theta) &= \int_\Omega |det\nabla T||\bar{u}(\Omega_\theta) - u_0 \circ T|^2 \\ \mathcal{J}'(\theta) &= \int_\Omega div(\theta)|u(\Omega) - u_0|^2 - 2(Y(\theta) - \nabla u_0.\theta)(u(\Omega) - u_0)\end{aligned}$$

$\diamond$ On utilise successivement la définition de l'état adjoint (1.29) puis la formulation variationelle de $Y(\theta)$ (1.24) pour faire disparaître le terme en $Y(\theta)$ dans $\mathcal{J}'(\theta)$

$$\int_\Omega (u(\Omega) - u_0)Y(\theta) = \int_\Omega \nabla[Y(\theta)]\nabla p = \int_\Omega -[\Delta(\nabla u(\Omega).\theta)]p \tag{1.30}$$

On fait deux intégrations par partie successives sur $\nabla u.\theta$ et en utilisant la définition de l'adjoint (1.29), on obtient :

$$\begin{aligned}\int_\Omega (u(\Omega) - u_0)Y(\theta) &= \int_\Omega -[\Delta(\nabla u(\Omega).\theta)]p = \int_\Omega \nabla(\nabla u(\Omega).\theta) \cdot \nabla p \\ &= \int_\Omega -(\nabla u(\Omega).\theta) \cdot \Delta p + \int_{\partial\Omega} \frac{\partial p}{\partial n} \nabla u(\Omega).\theta \\ \int_\Omega (u(\Omega) - u_0)Y(\theta) &= \int_\Omega \nabla u(\Omega).\theta(u(\Omega) - u_0) + \int_{\partial\Omega} \frac{\partial p}{\partial n} \nabla u(\Omega).\theta \quad (1.31)\end{aligned}$$

$\diamond$ On en déduit de l'équation (1.31) l'équation suivante pour $\mathcal{J}'$:

$$\mathcal{J}'(\theta) = \int_\Omega div(\theta)|u(\Omega) - u_0|^2 + 2(\nabla u(\Omega).\theta - \nabla u_0.\theta)(u(\Omega) - u_0) + \int_{\partial\Omega} 2\frac{\partial p}{\partial n} \nabla u(\Omega).\theta$$

Il suffit ensuite de remarquer que :

$$div(\theta)|u(\Omega) - u_0|^2 + 2(\nabla u(\Omega).\theta - \nabla u_0.\theta)(u(\Omega) - u_0) = div(\theta|u(\Omega) - u_0|^2)$$

et de faire une intégration par partie sur θ et d'utiliser $\nabla u(\Omega).\theta = \frac{\partial u(\Omega)}{\partial n}(\theta \cdot n)$ sur le bord de Ω pour conclure à l'équation (1.28). $\square$

L'équation (1.28) correspond à l'équation (1.21) du calcul de la dérivée par rapport au domaine avec la méthode du Lagrangien de Céa quand on remarque que $\Gamma_N = \emptyset$ et si on identifie $Ae(u)\colon e(p)$ avec $\nabla u \cdot \nabla p = \frac{\partial u}{\partial n}\frac{\partial p}{\partial n}$ sur Γ_D.

1.4 La méthode des courbes de niveaux

Une fois que le calcul de la dérivée par rapport à la forme Ω_k a été établi, il ne reste plus qu'à avancer le domaine Ω_k en $\Omega_{k+1} = (\mathbb{I}d + t\theta_k)\Omega_k$. Nous supposerons ici que la dérivée par rapport au domaine Ω_k est de la forme (voir la remarque (1.3.1)) :

$$\mathcal{J}'(\theta) = \int_{\partial\Omega_k} (\theta \cdot n)v_k$$

La méthode de gradient la plus simple consiste à choisir θ_k tel que $\theta_k \cdot n = -v_k$. Les premiers algorithmes d'optimisation géométriques avançaient les domaine en $\Omega_{k+1} = (\mathrm{Id} + t(-v_k n)) \circ \Omega_k$ en bougeant les coordonnées des noeuds qui définissent la frontière de Ω_k et, si nécessaire, remaillaient le domaine quand les frontières coalescaient ou quand le maillage devenait localement trop grossier ou trop mal conditionné. Ces étapes coûtaient très cher et pouvaient rendre instable l'algorithme de gradient.

La méthode level-set a donc été développée et a été appliquée avec succès dans les travaux de [OS01], [SW00] ou [AJT02]. L'idée est de travailler sur des maillages fixes et de représenter le domaine Ω_k par le biais de fonctions ϕ_k définies sur D de la manière suivante :

$$x \in \Omega_k \Longleftrightarrow \phi_k(x) < 0 \tag{1.32}$$

Une fois ce formalisme posé, transformer Ω_k en Ω_{k+1} est une opération des plus simples, due au lemme suivant :

Lemme 1.4.1 *Soit une forme $\Omega(t)$ dépendant du temps dont la frontière évolue à la vitesse normale $V(x,t)$. Si $\phi(0)$ est une fonction level-set pour $\Omega(0)$ (au sens de l'équation (1.32)). Alors $\phi(t)$ définie par l'équation d'Hamilton-Jacobi suivante :*

$$\frac{\partial \phi}{\partial t} = V|\nabla \phi| \tag{1.33}$$

est une fonction level-set pour $\Omega(t)$.

Démonstration L'équation définissant la frontière de Ω est :

$$\phi(x(t), t) = 0$$

En dérivant cette équation par rapport au temps, on obtient :

$$\frac{\partial \phi}{\partial t} + \nabla \phi . x'(t) = 0$$

Comme la frontière avance à la vitesse normale $V(x,t)$, alors $x'(t) = V(x,t)n$. Il suffit pour conclure de se souvenir que comme la frontière est une courbe de niveau de ϕ, alors $n = \frac{\nabla \phi}{|\nabla \phi|}$. Ce qui donne l'équation recherchée (1.33). □

Un autre avantage de la représentation par la méthode level-set est que la normale est étendue presque partout par $n = \frac{\nabla \phi}{|\nabla \phi|}$. La courbure $H = div(n)$ a aussi un sens presque partout.

En se souvenant de l'équation (1.33), nous utiliserons l'équation d'Hamilton-Jacobi suivante pour définir ϕ_{k+1} en fonction de ϕ_k et implicitement transformer Ω_k en Ω_{k+1}.

$$\begin{aligned} \phi(0) &= \phi_k \\ \frac{\partial \phi}{\partial t} + V^* |\nabla \phi| &= 0 \\ \phi_{k+1} &= \phi(T) \end{aligned} \tag{1.34}$$

Où $T > 0$ est le pas de la méthode de gradient et V^* est la direction de descente qui est choisit en accord avec le calcul de la différentielle de $\mathcal{J}$ (voir la section 1.4.2).

1.4.1 Calcul numérique de l'EDP

Nous voyons d'abord comment calculer numériquement le déplacement u solution du système de l'élasticité. Nous utiliserons un maillage de D quadrangulaire et des éléments finis $Q1$. La fonction level-set définit sur tout D une densité de la forme θ. Cette densité est constante par morceaux, définie sur les cellules. Nous utiliserons deux matériaux, l'un de loi de Hooke A là où $\theta = 1$ et l'autre de loi εA pour $\theta = 0$. Une interpolation est utilisée pour les valeurs intermédiaires de θ.

Quand ε tend vers 0, cette approximation consiste donc, physiquement, à mettre un "matériau mou" dans le vide. Il est montré dans [SHSP89] que, au premier ordre en ε, on calcule bien la solution de l'élasticité avec condition de Neumann homogènes sur les frontières entre le plein et le vide. Pour les problèmes aux valeurs propres, il suffit de mettre la matrice de second membre (matrice de masse) nulle dans le vide pour calculer le premier vecteur propre avec une précision de l'ordre de ε. On évite ainsi les problèmes liés à l'apparition des "modes fictifs", c-a-d, les modes localisés dans le vide.

1.4.2 Vitesse d'advection

Le choix le plus simple pour V^*, la vitesse de l'équation d'Hamilton-Jacobi (1.34), est d'étendre v qui détermine la différentielle de $\mathcal{J}$ (cf remarque 1.3.1) à tout le domaine. Par exemple, pour la minimisation de la compliance $\mathcal{L}_{cp}(\Omega) = \mathcal{J}_{cp}(\Omega) + \eta|\Omega|$. Supposons que la partie de Dirichlet ne bouge pas et que là où les forces sont appliquées, la forme ne soit pas optimisable. Dans ce cas, la dérivée par rapport au domaine de $\mathcal{L}_{cp}$ est donnée de manière univoque par :

$$\mathcal{L}'_{cp}(\theta) = \int_{\partial\Omega} (\theta \cdot n) v$$

avec $v = -Ae(u) : e(u) + \eta$ (voir équation (1.15)) ce qui a un sens dans tout D. La vitesse V^* utilisée dans l'équation d'Hamilton-Jacobi sera donnée par $V^* = Ae(u) : e(u) - \eta$.

Nous remarquons que quand la dérivée de forme implique la normale ou la courbure H, celles-ci ont bien un sens sur tout D comme étant égales à :

$$n = \frac{\nabla\phi}{|\nabla\phi|} \quad \text{et} \quad H = div(n)$$

Nous discuterons plus en détail dans le chapitre 3 la pertinence de cette extension.

1.4.3 Schéma numérique de l'équation d'Hamilton-Jacobi

Le schéma numérique utilisé pour résoudre l'équation d'Hamilton-Jacobi :

$$\frac{\partial \phi}{\partial t} + V^* |\nabla \phi| = 0 \quad \text{dans } D$$

est un schéma de différence finie, explicite, upwind d'ordre 1. Il s'exprime sur une grille quadrangulaire comme :

$$\frac{\phi_{i,j}^{n+1} - \phi_{i,j}^n}{\Delta t} + V_{i,j}^n g^{sign}(D_x^+ \phi_{i,j}^n, D_x^- \phi_{i,j}^n, D_y^+ \phi_{i,j}^n, D_y^- \phi_{i,j}^n) = 0$$

Où $sign = +$ ou $-$ est le signe de $V_{i,j}^n$ avec

$$D_x^+ \phi_{i,j}^n = \frac{\phi_{i+1,j}^n - \phi_{i,j}^n}{\Delta x} \quad D_x^- \phi_{i,j}^n = \frac{\phi_{i,j}^n - \phi_{i-1,j}^n}{\Delta x}$$
$$D_y^+ \phi_{i,j}^n = \frac{\phi_{i,j+1}^n - \phi_{i,j}^n}{\Delta y} \quad D_y^- \phi_{i,j}^n = \frac{\phi_{i,j}^n - \phi_{i,j-1}^n}{\Delta y}$$

Où Δx et Δy représentent usuellement la taille des mailles quadrangulaires et où $\phi_{i,j}^n$ représente la valeur de ϕ^n sur le $(i,j)^{eme}$ noeud de la grille. La fonction g est définie par :

$$g^+(d_x^+, d_x^-, d_y^+, d_y^-) = \sqrt{\min(d_x^+, 0)^2 + \max(d_x^-, 0)^2 + \min(d_y^+, 0)^2 + \max(d_y^-, 0)^2}$$

$$g^-(d_x^+, d_x^-, d_y^+, d_y^-) = \sqrt{\max(d_x^+, 0)^2 + \min(d_x^-, 0)^2 + \max(d_y^+, 0)^2 + \min(d_y^-, 0)^2}$$

Ce schéma introduit dans [Set99], [OS01] nécessite une condition CFL ce qui limite le pas de temps Δt. Comme une itération de ce schéma est bien plus économique au sens du temps CPU qu'un calcul de l'élasticité, plusieurs itérations successives de ce schéma seront effectuées par calcul de l'élasticité. Le nombre d'itération du schéma d'Hamilton-Jacobi peut être interprété comme le "pas de descente" de la méthode de gradient proposée ici.

1.5 Existence de formes optimales

Dans tout ce qui suivra, nous considérerons que les domaines admissibles Ω doivent être contenus dans un domaine de référence D (cf équation (1.5)).

1.5.1 Les théorèmes d'existence pour la convergence de Hausdorff complémentaire

Nous ne visons pas ici à lister de manière exhaustive les techniques utilisées pour la résolution des problèmes d'optimisation de formes, comme le lecteur averti s'en aperçevra très rapidement. Nous introduisons simplement un des formalismes les plus utilisés. Parmi les topologies qui peuvent être mises sur l'ensemble des ouverts, une a plus particulièrement été étudiée, la topologie

de Hausdorff complémentaire. Il s'agit de la topologie induite par la distance suivante :

$$d(\Omega_1, \Omega_2) = \|d(\cdot, \Omega_1^c) - d(\cdot, \Omega_2^c)\|_{L^\infty(\mathbf{R}^d)}$$

Le principal avantage de cette topologie est que l'ensemble des ouverts contenus dans une boîte D donnée est compact. La semi-continuité inférieure de la fonctionnelle est facilitée par le fait que si une suite Ω_n converge vers Ω alors tout compact de Ω sera inclus, à partir d'un certain rang, dans les Ω_n. Par exemple, pour la fonctionnelle "énergie de Dirichlet" :

$$\mathcal{J}_{cp}(\Omega) = \max_{u \in H_0^1(\Omega)} E(u) = \max_{u \in H_0^1(\Omega)} -\int_\Omega \nabla u \cdot \nabla u + 2\int_\Omega fu$$

Lemme 1.5.1 *Si Ω_n tends vers Ω au sens Hausdorff-complémentaire alors* $\liminf \mathcal{J}_{cp}(\Omega_n) \geq \mathcal{J}_{cp}(\Omega)$

Preuve Quelque soit $\varepsilon > 0$, par densité de C_c^∞ dans H_0^1, soit $\phi \in C_c^\infty(\Omega)$ tel que $E(\phi) \geq E(u) - \varepsilon$. Il existe un n_0 tel que pour tout n plus grand que n_0, le support de ϕ soit dans Ω_n donc $\phi \in H_0^1(\Omega_n)$ puis $\mathcal{J}_{cp}(\Omega_n)$ est défini comme un maximum donc $\mathcal{J}_{cp}(\Omega_n) \geq E(\phi)$. On conclut en notant que ε est arbitraire. □

Avec la semi-continuité inférieure de $\mathcal{J}_{cp}$ par rapport à la convergence de Hausdorff et la compacité, on peut conclure que le problème de minimisation de l'énergie de Dirichlet admet une solution. Malheureusement, on ne la connaît que trop bien, c'est l'ensemble vide. De plus il ne sert à rien de rajouter des contraintes de volume sur les formes optimales du type : $|\Omega| \geq c$ car la mesure de Lebesgue n'est que semi-continue inférieurement.

Un problème plus intéressant est de mettre des conditions limites de Neumann au lieu de conditions aux limites de Dirichlet. Dans ce cas la fonctionnelle de la compliance est semi-continue supérieurement et Bucur et Varchon [BV02] ont montré que la semi-continuité inférieure pour le problème de Neumann du Laplacien en dimension 2 équivalait à la semi-continuité supérieure du problème de Dirichlet. Pour obtenir cette semi-continuité, une des hypothèses suivantes est suffisante :

- (i) Il existe une contrainte capacitaire uniforme (voir [BZ95])
- (ii) Les ouverts vérifient la condition du n-1 cône uniforme (voir [BZ95]), c'est un cas particulier de (i)
- (iii) En dimension 2 uniquement, le nombre de composantes connexes du complémentaire est borné (voir [Sve93] ou bien [BT98] où il est démontré que c'est un cas particulier de (i))

Ces problèmes ne règlent pas le cas de l'élasticité tridimensionnelle où la convergence de Mosco des espace $H^1(\Omega)$ n'entraîne pas forcément celle des espaces standards de l'élasticité :

$$\{u \in L^2(\Omega) \text{ tels que } e(u) \in L^2(\Omega)\}$$

Le cas de la dimension 2 ayant été résolu par Chambolle dans [Cha03].

Notons encore que certaines autres restrictions géométriques donnent de la régularité des ouverts et permettent l'existence d'ouverts optimaux. C'est le cas

par exemple si une contrainte sur le périmètre est forcée ([AB93], [CL03]) ou si l'ouvert vérifie la propriété du cône uniforme (voir [Che75]). La démonstration de ce dernier résultat est légèrement différente dans la mesure ou c'est la propriété du cône uniforme qui donne la compacité dans une topologie ou la fonctionnelle est continue, tandis que la contrainte capacitaire de Bucur donne la continuité de la fonctionnelle dans la topologie de Hausdorff complémentaire qui est "naturellement" compacte.

Il faut aussi se souvenir que les ouverts optimaux n'ont aucune raison d'avoir la régularité nécessaire pour permettre l'application des méthodes géométriques d'optimisation où on advecte la frontière comme nous allons voir dans l' exemple suivant.

1.5.2 Présence de cusps pour le Laplacien

Minimisons l'énergie interne du Laplacien pour un problème mixte en 2-d

$$\left\{\begin{array}{rcll} -\Delta u & = & f & \text{in } \Omega \\ u & = & 0 & \text{on } \Gamma_D \\ \partial_n u & = & 0 & \text{on } \Gamma_N. \end{array}\right. \tag{1.35}$$

L'énergie interne (l'équivalent de la compliance) étant définie par

$$\mathcal{L}_{cp}(\Omega) = \int_\Omega (\nabla u \cdot \nabla u) + \eta = \int_\Omega (fu) + \eta$$

Où η est un multiplicateur de Lagrange pour le volume. Pour avoir l'existence d'un minimum, bornons le nombre de composante connexes des complémentaires des ouverts admissibles

Supposons qu'il existe un "trou libre" régulier dans la forme optimale.

Définition 1.5.1 *Nous appellerons "trou libre" toute composante connexe du complémentaire de Ω dont la frontière Γ est une courbe fermée incluse dans Γ_N (définition d'un trou). De plus le support de f n'intersecte pas Γ (le trou est "libre", c-a-d il n'y a pas de termes sources à côté).*

Dans ce cas, pour toute forme optimale de la fonction objectif "compliance" pour le Laplacien 2-d,

Lemme 1.5.2 *Il n'existe pas de trou libre C^1. Si d'aventure il existait un trou libre C^1 sauf en un nombre fini de points, alors ces points ne seraient pas Lipschitz et seraient des cusps.*

Démonstration Supposons Γ Lipschitz. La normale n est définie presque partout sur Γ et sur un voisinage. La forme étant optimale pour la fonction objectif considérée, l'équation des points critiques est vérifiée pour tout champs de vecteur $\theta \in W^{1,\infty}(\mathbb{R}^2;\mathbb{R}^2)$:

$$0 = \mathcal{J}'_{cp}(\theta) = \int_\Gamma (\theta \cdot n)(\nabla u \colon \nabla u - \eta)$$

Ce qui entraîne l'équation d'Euler-Lagrange pour u, vérifiée presque partout sur Γ :

$$\|\nabla u\|^2 = \eta$$

Or la condition de Neumann $\partial_n u = 0$ implique que $\partial_\tau u = \pm\sqrt{\eta}$ où τ est le vecteur tangent à $\partial\Omega$.

Supposons Γ C^1, alors $\partial_\tau u = \pm\sqrt{\eta}$ partout et $\partial_\tau u$ doit changer de signe sur Γ puisque Γ est une courbe fermée.

Aux points où $\partial_\tau u$ change de signe, un blow-up permet de voir que Γ est plus irrégulière qu'un coin. Effectivement, posons nous sur un de ces points où $\partial_\tau u$ change de signe et supposons que nous sommes dans un coin d'ouverture ω. Dans un secteur autour de ce coin u vérifie $\Delta u = 0$ (le trou est "libre", voir définition 1.5.1) avec condition de Neumann homogènes. Les différents solutions fondamentales dans ce coin sont, en coordonnées polaires de type $r^{\frac{k\pi}{\omega}} cos(\frac{k\pi\theta}{\omega})$ avec $k \in \mathbb{N}$.

Selon le sens de la tangente, $\partial_\tau u = -\sqrt{\eta}$ sur un rayon et $\partial_\tau u = \sqrt{\eta}$ sur l'autre implique que u soit de la forme $u = \mu r$ pour $\theta = 0$ et $\theta = \omega$, avec μ une constante et $\mu \in \{-\sqrt{\eta}, \sqrt{\eta}\}$. Dans ce cas, il faut donc $\omega = 2\pi$ et $k = 2$. □

Sinon, on peut utiliser une transformation conforme pour ramener la partie de la frontière où Γ change de signe sur une droite et s'apercevoir que la condition $\partial_\tau u = \pm\sqrt{\eta}$ ainsi que l'étude des différentes solutions fondamentales de u sur une droite implique que la transformation conforme admet un développement caractéristique du cusp. Cette approche a l'avantage de considérer toutes les Γ qui peuvent localement se transformer de manière conforme à une droite et non toutes les Γ Lipschitz.

On peut conclure de cet exemple que les trous libres du Laplacien admettent au moins deux cusps car $\partial_\tau u$ doit changer deux fois de signe sur la courbe fermée Γ.

Si la forme optimale présente des trous libres, une méthode de type géométrique qui essaierait d'obtenir la forme optimale en bougeant la frontière d'ouverts Lipschitz ne peut pas converger. Donc si nous essayons des algorithmes qui restent dans la classe des ouverts Lipschitz (celle où la notion de dérivation par rapport au domaine existe), l'algorithme ne convergera pas.

1.5.3 Propriétés des formes optimales en élasticité

L'exemple-type est une forme à trouver dans un domaine plan 2×1 soumis à une force verticale unitaire localisée autour du point $(2, 0.5)$ et bloquée dans les deux directions sur l'axe $x = 0$. Le critère à optimiser est la compliance $\mathcal{J}_{cp}$ définie par (1.9). Nous supposerons la forme symétrique par rapport à l'axe $y = 0$, ce qui est le cas de la forme optimale obtenue par l'algorithme dans la figure 1.1 (droite).

La console est exactement la forme type pour laquelle Chambolle [Cha03] a montré qu'il y a existence d'une forme optimale pour la compliance sous la restriction du nombre de composantes connexes du complémentaire bornées.

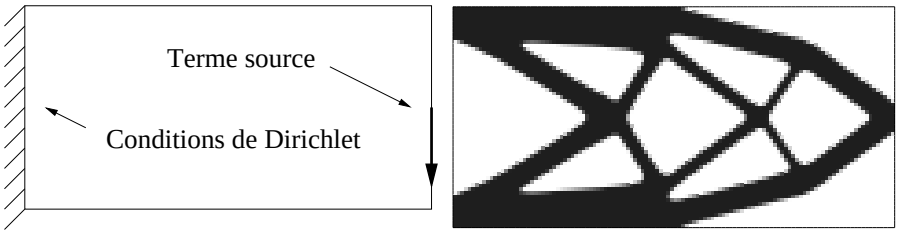

FIG. 1.1 – Le problème de la console et une des formes optimales standard

Nous voulons étudier dans ce paragraphe, quelques propriétés de la forme optimale. Nous arriverons à calculer, l'angle avec lequel, la frontière libre touche les conditions de Dirichlet et nous pouvons montrer par un argument de même nature que celui de la section 1.5.2 que si les frontières libres passent par l'axe de symétrie $y = 0$, alors il existe un coin.

Définition 1.5.2 *Par frontière libre, nous entendrons toutes les parties Lipschitz de Γ_N qui ne touchent pas le terme source.*

Les frontières libres vérifient donc, en tout point, l'équation d'Euler-Lagrange :

$$Ae(u) : e(u) = \eta$$

Comme ce sont des parties de Neumann, elles vérifient en plus l'équation $Ae(u) \cdot n = 0$. Posons $n = (a, b)$, et $\sigma = Ae(u)$, on a

$$a\sigma_{11} + b\sigma_{12} = 0 \quad \text{et } a\sigma_{12} + b\sigma_{22} = 0$$

Il existe donc k (qui dépend du point) tel que $\sigma = k \begin{pmatrix} b^2 & -ab \\ -ab & a^2 \end{pmatrix}$. On utilise $\sigma = Ae(u)$ pour obtenir $e(u) = \frac{k}{2\mu} \begin{pmatrix} b^2 - \lambda\alpha_0 & -ab \\ -ab & a^2 - \lambda\alpha_0 \end{pmatrix}$ avec $\alpha_0 = \frac{1}{2\lambda+2\mu}$ L'équation d'Euler donne :

$$\begin{aligned} \eta &= Ae(u) : e(u) = \sigma : e(u) = \frac{k^2}{2\mu}(b^4 + a^4 + 2a^2b^2 - \lambda\alpha_0) \\ &= \frac{k^2}{2\mu}(1 - \lambda\alpha_0) = \frac{k^2(\lambda + 2\mu)}{2\mu(2\lambda + 2\mu)} \end{aligned}$$

Le long des parties libres, $|k|$ est une constante et le déplacement vérifie les équations suivantes :

$$\left\{ \begin{array}{lcl} \partial_1 u^1 & = & \alpha + \beta b^2 \\ \partial_2 u^2 & = & \alpha + \beta a^2 \\ \partial_2 u^1 + \partial_1 u^2 & = & -2\beta ab \end{array} \right. \text{ avec } \left\{ \begin{array}{lcl} \alpha & = & \dfrac{-\lambda k}{(2\lambda + 2\mu)(2\mu)} \\ \beta & = & \dfrac{k}{2\mu} \end{array} \right. \tag{1.36}$$

Présence de coins

Nous supposerons que le multiplicateur de Lagrange η est non nul.

Lemme 1.5.3 *Si la forme optimale est symétrique par rapport à l'axe $y = 0.5$ alors toute frontière libre qui passe par cet axe présente un coin.*

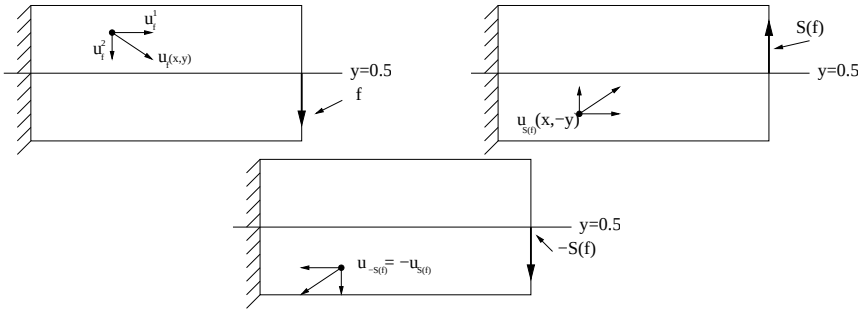

FIG. 1.2 – **Symétries du vecteur déplacement** : On applique d'abord la symétrie pour passer de la première forme à la seconde. On multiplie le terme source par -1 pour passer de la seconde forme à la troisième, par linéarité de l'équation , on multiplie aussi le déplacement par -1. On conclut en remarquant que le terme source ainsi obtenu $-S(f)$ est égal à f.

Démonstration Étudions d'abord les symétries de la forme et notons $S(u)$ le symétrique de u par la symétrie axiale $y = 0.5$ et $u_f(x, y)$ le déplacement correspondant au jeu de force f. Si $u = (u_1, u_2)$, nous avons $S(u) = (S(u^1), -S(u^2))$. En un point quelconque (x, y) de la forme par linéarité de l'équation $u_{-f}(x, y) = -u_f(x, y)$. Le jeu de force est antisymétrique par rapport à l'axe $y = 0$ donc $-S(f) = f$.

Par symétrie du domaine, linéarité de l'équation et antisymétrique du terme source : $S(u_f(x, y)) = u_{S(f)}(x, -y) = -u_{-S(f)}(x, -y) = -u_f(x, -y)$ (voir la Figure 1.2 pour les différentes étapes). On en déduit que u^2 est symétrique et u^1 est antisymétrique. En conséquence, $\partial_1 u^1$ et $\partial_2 u^2$ sont antisymétriques et $\partial_2 u^1$ et $\partial_1 u^2$ sont symétriques.

Nécessairement, si la frontière libre passe par $y = 0$ en un point où la normale est définie, les conditions de symétrie imposent, par l'équation (1.36) : $\alpha + \beta b^2 = 0 = \alpha + \beta a^2$.

L'équation précédente est impossible car la forme est symétrique par rapport à $y = 0.5$, donc la normale vaut $n = (\pm 1, 0)$, ce qui implique, avec l'équation précédente $k = 0$ donc $\eta = 0$.

On en déduit qu'en ce point, la normale n'est pas définie, donc il existe un coin (ou quelque chose de pire, un cusps...). □

Angle de la forme en $x = 0$

Nous pouvons aussi calculer l'angle avec lequel la forme optimale touche les conditions de Dirichlet (dans cet exemple l'axe $x = 0$).

Lemme 1.5.4 *Si la frontière libre touche l'axe $x = 0$, alors au point de contact, si u est régulier et si la normale est définie par $n = (a, b)$ en coordonnées cartésienne, on a :*

$$a^2 = \nu \quad et \quad a^2 + b^2 = 1$$

Démonstration En $x = 0$, on a : $\partial_2 u^2 = 0 = \partial_2 u^1$ sur cet axe. Supposons u régulier, alors cette condition se transmet jusqu'à la frontière. En réutilisant l'équation (1.36), on en déduit que $\alpha + \beta a^2 = 0$ d'oú

$$a = \pm\sqrt{\frac{\lambda}{2\lambda + 2\mu}} = \pm\sqrt{\nu}$$

Où ν est le coefficient de Poisson de l'opérateur d'élasticité. Connaissant a la composante suivant x de la normale, on peut calculer l'angle entre les conditions de Dirichlet et la forme. □

Si u n'est pas régulier, alors u excite une des solutions fondamentales non-régulière de l'élasticité. Or toutes ces solutions ont pour particularité d'avoir $\|\nabla u\| = +\infty$ au point de contact entre la forme et la condition de Dirichlet. Donc autour du point de contact, on peut trouver une partie de la frontière libre qui est assez régulière pour vérifier l'équation (1.36) mais où $\|\nabla u\|$ est assez grand pour violer cette condition. Une vérification détaillée de ces assertions est en cours.

On peut vérifier que l'angle de la forme optimale de la figure 1.1 (gauche) correspond bien à un facteur $\nu = 0.3$. De plus, quelque soit le coefficient de Poisson, l'angle entre les conditions de Dirichlet et la forme (celui qui est inscrit dans la forme) sera toujours strictement compris entre $\frac{\pi}{2}$ et $\frac{3\pi}{2}$ car $0 \leq \nu < \frac{1}{2}$.

1.6 Les problèmes SDP

Nous ne faisons ici qu'introduire les problèmes SDP qui reviendront de manière récurrente dans la thèse. Les problèmes SDP (ou Semi-definite Programming) sont des problèmes de la forme suivante :

Définition 1.6.1 *Soit $Y^0 \in \mathbb{R}^m$ un vecteur donné, appelons $Y \in \mathbb{R}^m$ l'inconnue. Soit une matrice $n \times n$ symétrique $E(Y)$ dont les coefficients dépendent affinement de Y. Le problème SDP est*

$$\begin{array}{rl} maximiser & Y^T Y^0 \\ tel\ que & E(Y) \geq 0 \end{array} \tag{1.37}$$

Où $E(Y) \geq 0$ signifie que toutes les valeurs propres de $E(Y)$ sont positives ou nulles.

L'ensemble des matrices $n \times n$ symétriques est noté S.
L'ensemble des matrices de S définies positives est noté S^+, c'est un cône.

Le dual d'un cône K est $K^* = \{y \text{ tel que } < x, y > \geq 0 \text{ pour tout } x \in K\}$. En considérant le produit scalaire de Froebenius $< X, Y >_F = tr(XY) = \sum X_{ij} Y_{ij}$, l'ensemble S^+ est son propre dual. Il existe donc une version duale d'un problème SDP qui est exprimée facilement à l'aide du produit de Froebenius.

Proposition 1.6.1 *Soit les matrices E_i définies par $E(Y) = E_0 + E_1 Y_1 + .. + E_m Y_m$ où Y_i est la i^e coordonnée de Y, le problème dual de (1.37) est :*

$$\begin{array}{rl} \textit{minimiser} & tr(E_0 Z) \\ \textit{tel que} & tr(E_i Z) + Y_i^0 = 0 \\ & Z \geq 0 \end{array} \tag{1.38}$$

Il existe une condition de Slater pour le problème SDP : Si il existe un point strictement admissible (ie Y tel que $E(Y) > 0$) alors il n'y a pas de saut de dualité entre les problèmes primaux et duaux.

Preuve Soit $\mathcal{L}(Y, Z)$ le Lagrangien défini par

$$\begin{aligned} \mathcal{L}(Y, Z) &= Y^0 Y^T + < E(Y), Z >_F & (1.39) \\ &= Y^0 Y^T + tr(E(Y)Z) \\ &= \sum_i Y_i^0 Y_i + tr\left(E_0 Z + \sum_i E_i Y_i Z \right) \\ &= tr(E_0 Z) + \sum_i Y_i tr(Y_i^0 Id + E_i Z) & (1.40) \end{aligned}$$

En utilisant le fait que S^+ est son propre cône dual et en utilisant la formulation (1.39), on trouve que

$$\mathcal{L}_Z = \min_{Z \geq 0} \mathcal{L}(Y, Z) = \begin{cases} Y^0 Y^T & \text{si } E(Y) \geq 0 \\ -\infty & \text{sinon} \end{cases}$$

En utilisant la formulation (1.40), on trouve que

$$\mathcal{L}_Y = \max_Y \mathcal{L}(Y, Z) = \begin{cases} tr(E_0 Z) & \text{si } tr(Y_i^0 Id + E_i Z) = 0 \text{ pour tout } i \\ +\infty & \text{sinon} \end{cases}$$

De tel sorte que $\min_{Z \geq 0} \mathcal{L}_Y$ et $\max_Y \mathcal{L}_Z$ sont bien des problèmes duaux. □

Les problèmes SDP sont ensuite facilement solubles par des méthodes duales de type "interior point" pour satisfaire les contraintes (voir [VB96]). Il est à noter que nous n'aurons besoin de problèmes SDP qu'en dimension très petite, ce qui rend ce problème facile à résoudre.

Chapitre 2

Structural optimization using topological and shape sensitivity via a level set method

Abstract

A numerical coupling of the level-set method with the bubble or topological gradient method is proposed. The level-set method does not allow the nucleation of new holes (at least in 2-d) and the bubble method is precisely designed for introducing new holes in the optimization process. Therefore, the coupling of these two method yields an efficient algorithm. The main advantage of our coupled algorithm is to make the resulting optimal design largely independent of the initial guess. This chapter is exactly the paper [AGJT05].

2.1 Introduction **24**
2.2 Setting of the problem **25**
2.3 Shape derivative **26**
2.4 Topological derivative **27**
2.5 Level set method for shape optimization **30**
2.6 Optimization algorithm **31**
2.7 Numerical examples in 2-d **33**
2.8 Numerical examples in 3-d **38**
2.9 Conclusion **41**

2.1 Introduction

This paper is a logical sequel of our previous work [AJT02], [AJT04] where we proposed a numerical method of shape optimization based on the level set method and on shape differentiation. Indeed, in [AJT02], [AJT04] we clearly indicated that, although the level set method makes possible topology changes during the optimization process, it does not solve the inherent problem of ill-posedness of shape optimization which manifests itself in the frequent existence of many local (non global) minima, usually having different topologies. The reason is that the level set method can easily remove holes but can not create new holes in the middle of a shape since the level set function obeys a maximum principle. In practice, this effect can be checked by varying the initialization which yields different optimal shapes with different topologies. To the best of our knowledge, other works on the level set method in shape optimization were also subject to this difficulty [OS01], [SW00], [WWG03]. This absence of a nucleation mechanism is an inconvenient mostly in 2-d : in 3-d, it is less important since holes can appear by pinching two boundaries (which can occur without destroying the connectivity of the structure).

In the present paper we propose as a remedy to couple our previous method with the topological gradient method of Schumacher, Masmoudi, Sokolowski and their co-workers [ES94], [Céa86], [GGM01], [SZ99], [SZ01]. Roughly speaking the topological gradient method amounts to decide whether or not it is favorable (for decreasing the objective function) to nucleate a small hole in a given shape. As a matter of fact, creating a hole changes the topology and is thus one way of escaping local minima (due to topological constraint). Our coupled method of topological and shape gradients in the level set framework is therefore a great improvement (at least in 2-d) with respect to previous methods and is much less prone to finding local, non global, optimal shapes. In particular, for most of our 2-d numerical examples of compliance minimization, the expected global minimum is attained from the trivial full domain initialization. Nevertheless there are some (relatively few) examples of local minima if we choose a different initialization. For 2-d mechanism design our coupled method is not fully independent of several parameters, including initialization, although it already produces excellent results with the trivial full domain initialization. To which extent the computed optimal shape depends on the initialization is presumably varying with the type of considered objective functions. As we already said, this improvement is far less important in 3-d where there is more geometrical freedom for the sole level set method, as confirmed by numerical experiments (see [AJT04] and the examples of Section 2.8). In practice, our 3-d numerical experiments for compliance minimization show that the optimal shapes are the same for the level set method with or without topological gradient (again, this may not be the case for other objective functions). In any case we do not claim that our coupled method is the ultimate one since local minima may still exist

(even in the class of shapes sharing the same topology) and the convergence speed can probably still be improved.

The main contribution of this paper is algorithmic and numeric. Actually, the theoretical tools used here have already been described (albeit separately) in the above quoted previous works. The novelty is in the coupling and in the robustness of the proposed numerical implementation. Our basic algorithm is to iteratively use the shape gradient or the topological gradient in a gradient-based descent algorithm. The tricks are to carefully monitor the decrease of the objective function (to avoid large changes in shape and topology) and to choose the right ratio of successive iterations in each method. We provide several 2-d and 3-d numerical examples for compliance minimization and mechanism design. In a slightly different context of inverse problems a different coupling of the shape and topological gradients (using the level set method too) has been proposed [BHR04]. There, the topological gradient was incorporated as a source term in the transport Hamilton-Jacobi equation used in the shape derivative algorithm for moving the shape. After this work was completed we learned that a similar method was developed independently in [WX04].

2.2 Setting of the problem

In this paper we restrict ourselves to linear elasticity although there is no conceptual difficulty in extending our work to non-linear elasticity (see [AJT04]). A shape is a bounded open set $\Omega \subset \mathbb{R}^d$ ($d = 2$ or 3) with a boundary made of two disjoint parts

$$\partial\Omega = \Gamma_N \cup \Gamma_D, \tag{2.1}$$

with Dirichlet boundary conditions on Γ_D, and Neumann boundary conditions on Γ_N. All admissible shapes Ω are required to be a subset of a working domain D (a bounded open set of $\mathbb{R}^d$). The shape Ω is occupied by a linear isotropic elastic material with Hooke's law A defined, for any symmetric matrix ξ, by

$$A\xi = 2\mu\xi + \lambda\big(\mathrm{Tr}\xi\big)\mathrm{Id},$$

where μ and λ are the Lamé moduli of the material. The displacement field u in Ω is the solution of the linearized elasticity system

$$\left\{\begin{array}{rcll} -div\,(A\,e(u)) & = & \mathbf{f_1} & \text{in } \Omega \\ u & = & 0 & \text{on } \Gamma_D \\ \big(A\,e(u)\big)n & = & \mathbf{f_2} & \text{on } \Gamma_N, \end{array}\right. \tag{2.2}$$

where $\mathbf{f_1} \in L^2(D)^d$ and $\mathbf{f_2} \in H^1(D)^d$ are the volume forces and the surface loads respectively. Assuming that $\Gamma_D \neq \emptyset$ (otherwise we should impose an equilibrium condition on $\mathbf{f_1}$ and $\mathbf{f_2}$), (2.2) admits a unique solution in $u \in H^1(\Omega)^d$.

The objective function is denoted by $\mathcal{J}(\Omega)$. A first classical example is the compliance (the work done by the load)

$$\mathcal{J}_{cp}(\Omega) = \int_\Omega \mathbf{f_1} \cdot u\,dx + \int_{\Gamma_N} \mathbf{f_2} \cdot u\,ds = \int_\Omega A\,e(u) \cdot e(u)\,dx, \tag{2.3}$$

which is very common in rigidity maximization. A second choice is a least square error between u and a target displacement

$$\mathcal{J}_{lse}(\Omega) = \left(\int_\Omega k(x)|u - u_0|^\alpha dx \right)^{1/\alpha}, \tag{2.4}$$

which is a useful criterion for the design of compliant mechanisms. We assume $\alpha \geq 2$, $u_0 \in L^\infty(D)$ and $k \in L^\infty(D)$, a non-negative given weighting factor. In both formulas (2.3) and (2.4), $u = u(\Omega)$ is the solution of (2.2). We define a set of admissible shapes that must be open sets contained in the working domain D and of fixed volume V

$$\mathcal{U}_{ad} = \Big\{ \Omega \subset D \text{ such that } |\Omega| = V \Big\}. \tag{2.5}$$

A model problem of shape optimization is

$$\inf_{\Omega \in \mathcal{U}_{ad}} \mathcal{J}(\Omega). \tag{2.6}$$

In practice we rather work with an unconstrained problem. Introducing a Lagrange multiplier η, we consider the Lagrangian minimization

$$\inf_{\Omega \subset D} \mathcal{L}(\Omega) = \mathcal{J}(\Omega) + \eta|\Omega|.$$

2.3 Shape derivative

In order to apply a gradient method to the minimization of (2.6) we recall the classical notion of shape derivative, going back to Hadamard (see e.g. [MS76], [Pir84], [Sim80], [SJP92]). Starting from a smooth reference open set Ω, we consider domains of the type

$$\Omega_\theta = \big(\mathrm{Id} + \theta\big)(\Omega), \tag{2.7}$$

with Id the identity mapping from $\mathbb{R}^d$ into $\mathbb{R}^d$ and θ a vector field in $W^{1,\infty}(\mathbb{R}^d, \mathbb{R}^d)$. It is well known that, for sufficiently small θ, $(\mathrm{Id} + \theta)$ is a diffeomorphism in $\mathbb{R}^d$. We remark that all admissible domains Ω_θ belong to the class of homotopy of the reference domain Ω (it implies that in 2-d the number of connected components of the boundary remains constant). In other words, no change of topology is possible with this method of shape variation.

Definition 2.3.1 *The shape derivative of $J(\Omega)$ at Ω is defined as the Fréchet derivative in $W^{1,\infty}(\mathbb{R}^d, \mathbb{R}^d)$ at 0 of the application $\theta \to J\big((\mathrm{Id} + \theta)(\Omega)\big)$, i.e.*

$$\mathcal{J}\big((\mathrm{Id} + \theta)(\Omega)\big) = \mathcal{J}(\Omega) + \mathcal{J}'(\Omega)(\theta) + o(\theta) \quad \textit{with} \quad \lim_{\theta \to 0} \frac{|o(\theta)|}{\|\theta\|} = 0 \,,$$

where $\mathcal{J}'(\Omega)$ is a continuous linear form on $W^{1,\infty}(\mathbb{R}^d, \mathbb{R}^d)$.

We recall the following classical result (see [AJT04] and references therein) about the shape derivatives for the two functionals under consideration : the compliance $\mathcal{J}_{cp}$ (see (2.3)) and the least square error $\mathcal{J}_{lse}$ (see (2.4)).

Theorem 2.3.2 *Let Ω be a smooth bounded open set and $\theta \in W^{1,\infty}(\mathbb{R}^d;\mathbb{R}^d)$. Assume that the data f and g as well as the solution u of (2.2) are smooth, say $\mathbf{f_1} \in H^1(\Omega)^d$, $\mathbf{f_2} \in H^2(\Omega)^d$, $u \in H^2(\Omega)^d$. The shape derivative of (2.3) is*

$$\begin{aligned}\mathcal{J}'_{cp}(\Omega)(\theta) = & \int_{\Gamma_N} \left(2\left[\frac{\partial(\mathbf{f_2}\cdot u)}{\partial n} + H\mathbf{f_2}\cdot u + \mathbf{f_1}\cdot u\right] - Ae(u)\cdot e(u)\right)\theta\cdot n\, ds \\ & + \int_{\Gamma_D} Ae(u)\cdot e(u)\,\theta\cdot n\, ds,\end{aligned} \tag{2.8}$$

where H is the mean curvature defined by $H = divn$. The shape derivative of (2.4) is

$$\begin{aligned}\mathcal{J}'_{lse}(\Omega)(\theta) = & \int_{\Gamma_N} \left(\frac{C_0}{\alpha}k|u-u_0|^\alpha + Ae(p)\cdot e(u) - \mathbf{f_1}\cdot p\right. \\ & \left. -\frac{\partial(\mathbf{f_2}\cdot p)}{\partial n} - H\mathbf{f_2}\cdot p\right)\theta\cdot n\, ds \\ & + \int_{\Gamma_D}\left(\frac{C_0}{\alpha}k|u-u_0|^\alpha - Ae(u)\cdot e(p)\right)\theta\cdot n\, ds.\end{aligned} \tag{2.9}$$

where p is the adjoint state, assumed to be smooth, i.e. $p \in H^2(\Omega)^d$, defined as the solution of

$$\left\{\begin{array}{rcll} -div\,(A\,e(p)) & = & -C_0k(x)|u-u_0|^{\alpha-2}(u-u_0) & in\ \Omega \\ p & = & 0 & on\ \Gamma_D \\ \big(Ae(p)\big)n & = & 0 & on\ \Gamma_N, \end{array}\right. \tag{2.10}$$

and C_0 is a constant given by

$$C_0 = \left(\int_\Omega k(x)|u(x)-u_0(x)|^\alpha dx\right)^{1/\alpha-1}. \tag{2.11}$$

Remark 2.3.3 *The shape derivative of the volume constraint is easily computed. The result is*

$$V(\Omega) = \int_\Omega dx \quad \Rightarrow \quad V'(\Omega)(\theta) = \int_{\partial\Omega}\theta\cdot n\, ds.$$

2.4 Topological derivative

One drawback of the previous method of shape derivative is that there is no change of topology in the parametrization Ω_θ. Numerical methods based on the shape derivative may therefore fall into a local minimum (corresponding to the

initial topology). Recently, a remedy to this inconveniency has been proposed as the bubble method, or topological asymptotic method, [ES94], [GGM01], [SZ01]. The main idea is to test the optimality of a domain to topology variations by removing a small hole with appropriate boundary conditions.

We give a brief review of this method that we shall call in the sequel topological gradient method. Consider an open set $\Omega \subset \mathbb{R}^d$ and a point $x_0 \in \Omega$. Introduce a fixed model hole $\omega \subset \mathbb{R}^d$, a smooth open bounded subset containing the origin. For $\rho > 0$ we define the translated and rescaled hole

$$\omega_\rho = x_0 + \rho\omega.$$

Then we define the perforated domain

$$\Omega_\rho = \Omega \setminus \bar{\omega}_\rho. \tag{2.12}$$

The goal is to study the variations of the objective function $\mathcal{J}(\Omega_\rho)$ as ρ goes to 0. By insertion of a hole, the class of homotopy of Ω_ρ is different from that of the limit domain Ω. In particular, in 2-d the number of connected components of the boundary varies. Therefore, this method, which performs topology variations, is very different from the previous approach of shape derivative where the class of homotopy of Ω_θ, defined by (2.7), is always the same. In this respect, the two methods of topology differentiation and shape differentiation are essentially distinct. The corresponding sets of admissible domains have actually an empty intersection, even though, both shape and topological derivatives rely on the adjoint method.

In the framework of structural optimization we put Neumann boundary conditions on $\partial\omega_\rho$. The objective function $\mathcal{J}(\Omega_\rho)$ is computed with the elastic displacement u_ρ, solution of the following elasticity problem

$$\left\{\begin{array}{rcll} -div\,(A\,e(u_\rho)) & = & \mathbf{f_1} & \text{in } \Omega_\rho \\ u_\rho & = & 0 & \text{on } \Gamma_D \\ \big(A\,e(u_\rho)\big)n & = & \mathbf{f_2} & \text{on } \Gamma_N \\ \big(A\,e(u_\rho)\big)n & = & 0 & \text{on } \partial\omega_\rho. \end{array}\right. \tag{2.13}$$

Definition 2.4.1 *If the objective function admits the following so-called topological asymptotic expansion for small $\rho > 0$*

$$\mathcal{J}(\Omega_\rho) = J(\Omega) + \rho^d D_T J(x_0) + o(\rho^d),$$

then $D_T\mathcal{J}(x_0)$ is called the topological derivative at point x_0.

Of course, since the topology of Ω_ρ and $\Omega = \Omega_0$ are different, the objective function is not differentiable with respect to ρ or ρ^d, in the sense of the previous section.

The following result gives the topological derivative of the volume (or weight) of the domain Ω. Note that this is a simple case where the functional does no depend on the state u.

Lemma 2.4.2 *The topological derivative of* $V(\Omega) = \int_\Omega dx$ *is*

$$D_T V(x) = -|\omega|.$$

From now on, we specify the model hole ω to be the unit ball. This simplifies greatly the computations of the topological derivatives. However, note that the shape of the model hole ω could also be optimized in order to find the "best" topological derivative, i.e. the smallest one if we minimize the objective function. The following two results give the expressions of the topological derivative for the compliance $\mathcal{J}_{cp}(\Omega)$ (see (2.3)) and for the least square error $\mathcal{J}_{lse}(\Omega)$ (see (2.4)) (for the proofs we refer to [GGM01], [SZ01]).

Theorem 2.4.3 *Take* ω *to be the unit ball of* $\mathbb{R}^d$*. Assume for simplicity that* $\mathbf{f_1} = 0$ *and that* $\mathbf{f_2}$ *as well as the solution* u *of (2.2) are smooth, say* $\mathbf{f_2} \in H^2(\Omega)^d$*,* $u \in H^2(\Omega)^d$*. For any* $x \in \Omega$ *the topological derivative of* $\mathcal{J}_{cp}$ *is, for* $d = 2$*,*

$$D_T \mathcal{J}_{cp}(x) = \frac{\pi(\lambda + 2\mu)}{2\mu(\lambda + \mu)} \big\{ 4\mu Ae(u) \cdot e(u) + (\lambda - \mu) tr(Ae(u)) tr(e(u)) \big\}(x), \tag{2.14}$$

and for $d = 3$*,*

$$D_T \mathcal{J}_{cp}(x) = \frac{\pi(\lambda + 2\mu)}{\mu(9\lambda + 14\mu)} \big\{ 20\mu Ae(u) \cdot e(u) + (3\lambda - 2\mu) tr(Ae(u)) tr(e(u)) \big\}(x). \tag{2.15}$$

A straightforward calculation shows that the topological derivatives in formulae (2.14) and (2.15) are nonnegative. This means that, for compliance minimization, there is no interest in nucleating holes if there is no volume constraint. However, if a volume constraint is imposed (see Lemma 2.4.2), the topological derivative may have negative values due to the addition of the term $-\eta|\omega|$, where η stands for the volume Lagrange multiplier.

Theorem 2.4.4 *Take* ω *to be the unit ball of* $\mathbb{R}^d$*. Assume for simplicity that* $\mathbf{f_1} = 0$ *and* $\mathbf{f_2}$ *as well as the solution* u *of (2.2) are smooth, say* $\mathbf{f_2} \in H^2(\Omega)^d$*,* $u \in H^2(\Omega)^d$*. For any* $x \in \Omega$ *the topological derivative of* $\mathcal{J}_{lse}$ *is, for* $d = 2$*,*

$$\begin{aligned} D_T \mathcal{J}_{lse}(x) \quad &= -\frac{\pi}{\alpha} C_0 k(x) |u(x) - u_0(x)|^\alpha - \\ &\frac{\pi(\lambda + 2\mu)}{2\mu(\lambda + \mu)} \big\{ 4\mu Ae(u) \cdot e(p) + (\lambda - \mu) tr(Ae(u)) tr(e(p)) \big\}(x), \end{aligned} \tag{2.16}$$

and for $d = 3$*,*

$$\begin{aligned} D_T \mathcal{J}_{lse}(x) \quad &= -\frac{4\pi}{3\alpha} C_0 k(x) |u(x) - u_0(x)|^\alpha - \\ &\frac{\pi(\lambda + 2\mu)}{\mu(9\lambda + 14\mu)} \big\{ 20\mu Ae(u) \cdot e(p) + (3\lambda - 2\mu) tr(Ae(u)) tr(e(p)) \big\}(x), \end{aligned} \tag{2.17}$$

where p *is the adjoint state, assumed to be smooth, i.e.* $p \in H^2(\Omega)^d$*, defined as the solution of (2.10), and* C_0 *is the constant defined by (2.11).*

The numerical application of the topological derivative is as follows. Consider the minimization of the Lagrangian

$$\mathcal{L}(\Omega) = \mathcal{J}(\Omega) + \eta|\Omega|,$$

where η is a given Lagrange multiplier. The corresponding topological gradient is

$$D_T\mathcal{L}(x) = D_T\mathcal{J}(x) - \eta|\omega|.$$

At the points x where $D_T\mathcal{L}(x)$ is negative, we introduce holes into the current domain Ω. Since this criterion applies for infinitesimal holes, we should not remove too much material. In practice it is better to nucleate holes only at the minimum (negative) points of this topological derivative. We remark that the application of the topological gradient can only decrease the volume of the current shape (see [NS04] for another criterion which amounts to add a thin ligament).

2.5 Level set method for shape optimization

Consider $D \subset \mathbb{R}^d$ a bounded domain in which all admissible shapes Ω are included, i.e. $\Omega \subset D$. In numerical practice, the domain D will be uniformly meshed once and for all. We parameterize the boundary of Ω by means of a level set function, following the idea of Osher and Sethian [OS88]. We define this level set function ψ in D such that

$$\left\{ \begin{array}{ll} \psi(x) = 0 & \Leftrightarrow x \in \partial\Omega \cap D, \\ \psi(x) < 0 & \Leftrightarrow x \in \Omega, \\ \psi(x) > 0 & \Leftrightarrow x \in \left(D \setminus \overline{\Omega}\right). \end{array} \right. \tag{2.18}$$

The normal n to the shape Ω is recovered as $\nabla\psi/|\nabla\psi|$ and the mean curvature H is given by the divergence of the normal $div\,(\nabla\psi/|\nabla\psi|)$ (these quantities are computed throughout the whole domain D).

During the optimization process, the shape $\Omega(t)$ is going to evolve according to a fictitious time parameter $t \in \mathbb{R}^+$ which corresponds to descent stepping. The evolution of the level set function is governed by the following Hamilton-Jacobi transport equation [OS88]

$$\frac{\partial\psi}{\partial t} + V|\nabla\psi| = 0 \quad \text{in} \quad D, \tag{2.19}$$

where $V(t,x)$ is the normal velocity of the shape's boundary. Equation (2.19) is simply obtained by differentiating the definition of a level set of ψ, $\psi\Big(t, x(t)\Big) =$ Cst, and replacing the velocity $\dot{x}(t)$ by Vn.

The choice of the normal velocity V is based on the shape derivative computed in Theorem 2.3.2

$$\mathcal{L}'(\Omega)(\theta) = \int_{\partial\Omega} v\,\theta \cdot n\,ds, \tag{2.20}$$

where the integrand $v(u, p, n, H)$ depends on the state u, adjoint state p, normal n and mean curvature H. The simplest choice is to take the steepest descent $\theta = -vn$. This yields a normal velocity for the shape's boundary $V = -v$ (remark that v is given everywhere in D and not only on the boundary $\partial\Omega$). Transporting ψ by (2.19) is equivalent to moving the boundary $\partial\Omega$ (the zero level set of ψ) along the descent gradient direction $-\mathcal{L}'(\Omega)$. The length of the time interval on which (2.19) is integrated corresponds to the descent step. It is not obvious that $\theta = -vn$ belongs to $W^{1,\infty}(\mathbb{R}^d, \mathbb{R}^d)$ in general (that depends on the regularity of Ω). This is one reason for choosing a different smoother velocity. Various formulas for V are possible and correspond to different choices of the inner product between $\mathcal{L}'(\Omega)$ and θ, or to a preconditioning of the gradient method (see e.g. [Bur03], [MP01]).

The main point is that the Lagrangian evolution of the boundary $\partial\Omega$ is replaced by the Eulerian solution of a transport equation in the whole fixed domain D. Likewise the elasticity equations for the state u (and for the adjoint state p) are extended to the whole domain D by using the so-called "ersatz material" approach. It amounts to fill the holes $D\backslash\Omega$ by a weak phase mimicking void but avoiding the singularity of the rigidity matrix. This is a well-known procedure in topology optimization which we already described in our previous work [AJT04]. In numerical practice, the weak material mimicking holes in $D\backslash\Omega$ is chosen as $10^{-3}A$.

The Hamilton-Jacobi equation (2.19) is solved by an explicit second order upwind scheme (see e.g. [Set99]) on a Cartesian grid. The boundary conditions for ψ are of Neumann type. Since this scheme is explicit in time, its time stepping must satisfy a CFL condition. In order to regularize the level set function (which may become too flat or too steep), we reinitialize it periodically by solving another Hamilton-Jacobi equation which admits as a stationary solution the signed distance to the initial interface [Set99]. In numerical practice, reinitialization is important because the level set function often becomes too steep which implies a bad approximation of the normal n or of the mean curvature H. For details of numerical implementation we refer to [AJT04].

2.6 Optimization algorithm

For the minimization problem (2.6) we propose an iterative coupling of the level set method and of the topological gradient method. Both methods are gradient-type algorithms, so our coupled method can be cast into the framework of alternate directions descent algorithms.

The level set method relies on the shape derivative $\mathcal{L}'(\Omega)(\theta)$ of Section 2.3, while the topological gradient method is based on the topological derivative $D_T\mathcal{L}(x)$ of Section 2.4. These two types of derivative define independent descent directions that we simply alternate as follows.

In a first step, the level set function ψ is advected according to the velocity $-v$ where v is the integrand in the shape derivative $\mathcal{L}'(\Omega)$, see (2.20). In a second step, holes are introduced into the current domain Ω where the topological

derivative $D_T\mathcal{L}(x)$ is minimum and negative. More precisely, at those points we change the negative sign of the level set function ψ into a positive sign, according to the parametrization (2.18).

In practice, it is better to perform more level set steps than topological gradient steps. Therefore, the main parameter of our coupled algorithm is an integer n_{opt} which is the number of gradient steps between two successive application of the topological gradient (typically, the value of n_{opt} is 5 which means that 4 level set steps are performed for each topological gradient step). Our proposed algorithm is an iterative method, structured as follows :

1. Initialization of the level set function ψ_0 corresponding to an initial guess Ω_0 (usually the full working domain D).
2. Iteration until convergence, for $k \geq 0$:
   (a) **Elasticity analysis.** Computation of the state u_k and adjoint state p_k through two problems of linear elasticity posed in Ω_k. This yields the values of the shape derivative and of the topological gradient.
   (b) **Shape gradient.** If $\mod(k, n_{top}) < n_{top}$, the current shape Ω_k, characterized by the level set function ψ_k, is deformed into a new shape Ω_{k+1}, characterized by ψ_{k+1} which is the solution of the transport Hamilton-Jacobi equation (2.19) after a time interval Δt_k with the initial condition ψ_k and a velocity $-v_k$ computed in terms of u_k and p_k. The time of integration Δt_k is chosen such that $\mathcal{L}(\Omega_{k+1}) \leq \mathcal{L}(\Omega_k)$.
   (c) **Topological gradient.** If $\mod(k, n_{top}) = 0$, we perform a nucleation step. We obtain a new shape Ω_{k+1} by inserting new holes into the current shape Ω_k. Namely, the sign of the level set function ψ_k is changed from negative to positive values (see (2.18)) in the regions of Ω_k where the topological derivative $D_T\mathcal{L}_k$, depending on u_k and p_k, has minimum negative values. If the objective function has increased, i.e. if $\mathcal{L}(\Omega_{k+1}) > \mathcal{L}(\Omega_k)$, then no holes are nucleated and we just take $\Omega_{k+1} = \Omega_k$.

For details about the shape gradient step, we refer to our previous work [AJT02], [AJT04]. Let us simply recall that the time interval Δt_k plays the role of the descent step in the minimization of $\mathcal{L}(\Omega)$, and is usually one order of magnitude bigger than the explicit time step used for solving the Hamilton-Jacobi equation (2.19) (which is limited by the CFL condition). Since one explicit time step for (2.19) is much cheaper, in terms of CPU time and memory requirement, than solving the state equation (2.2) or adjoint state equation (2.10), for each single evaluation of u_k and p_k (that we call iteration) we perform many explicit time steps for the Hamilton-Jacobi equation.

The topological gradient step is performed only if the topological gradient is negative. If an infinitesimal small hole is inserted where $D_T\mathcal{L}_k(x) < 0$, then, by Definition 2.4.1 of the topological asymptotic, the objective function must decrease. However, in numerical practice, a hole can not be smaller than a single mesh cell, which is not so infinitesimally small. Even more, if the topological

gradient $D_T\mathcal{L}_k$ is negative in several touching cells, it amounts to remove from the current shape a large zone which is not small at all. For this reason, our algorithm has two additional parameters. First we never remove more than a given proportion of the total volume (typically we impose a bound of 1% at most in the decrease of the volume). Second, even if only a few cells are removed, the objective function may increase because a single cell is too large. If it is the case, we do not accept the new nucleated holes and we simply keep the old shape, $\Omega_{k+1} = \Omega_k$. Nevertheless, such a decision may be too conservative : the shape of a cell (usually rectangular) is not optimal, the numerical evaluation of the topological gradient may be pessimistic because of discretization errors, and in any case, if a suboptimal hole is created the level set method will easily cancel it afterwards. Therefore, we accept the topological gradient step even if the objective function increases slightly. Introducing a threshold parameter ϵ_{gt} (typically 0.1), the new perforated shape is kept if

$$\mathcal{L}(\Omega_{k+1}) \leq (1 + \epsilon_{gt})\mathcal{L}(\Omega_k).$$

In our computer code, nucleating a hole in a cell means switching the sign of the level set function which has the effect of replacing in this cell the true material properties by those of the weak ersatz material. We always reinitialize the level set function after a hole nucleation in order that it becomes the signed distance to the shape boundary [Set99].

The choice of the coupling parameter n_{top} is more delicate since it has obviously some influence on the computed optimal shape. Recall that we perform n_{top} shape gradient steps between two topological gradient steps. If n_{top} is too small (say 1 or 2), then the objective function may not decrease smoothly and the resulting shape may be very irregular. If n_{top} is too large, the level set method may have already converged to a local minimum where it is difficult to nucleate a new hole while decreasing the objective function. In most of our numerical examples we choose $n_{top} = 5$, but a different choice may yield a different final result. This is clearly a limitation of the method.

Finally, if we had chosen $\epsilon_{gt} = 0$, the objective function would always decreases and our algorithm would converge to a (local) minimum. At convergence, stability is attained in both optimization processes (shape and topology). In practice, for efficiency reasons (already explained) we take $\epsilon_{gt} = 0.1$, so the objective does not always strictly decrease during a topological gradient step (in the hope to escape local minima) as can be checked on Figures 2.2 and 2.6.

2.7 Numerical examples in 2-d

We begin with single loads, minimal compliance problems, i.e. we minimize the Lagrangian

$$\inf_{\Omega \subset D} \mathcal{L}(\Omega) = \mathcal{J}_{cp}(\Omega) + \eta|\Omega|$$

for a fixed positive Lagrange multiplier $\eta > 0$, and $\mathcal{J}_{cp}$ being defined by (1.9). Our first example is the well-known cantilever problem which is fixed on the

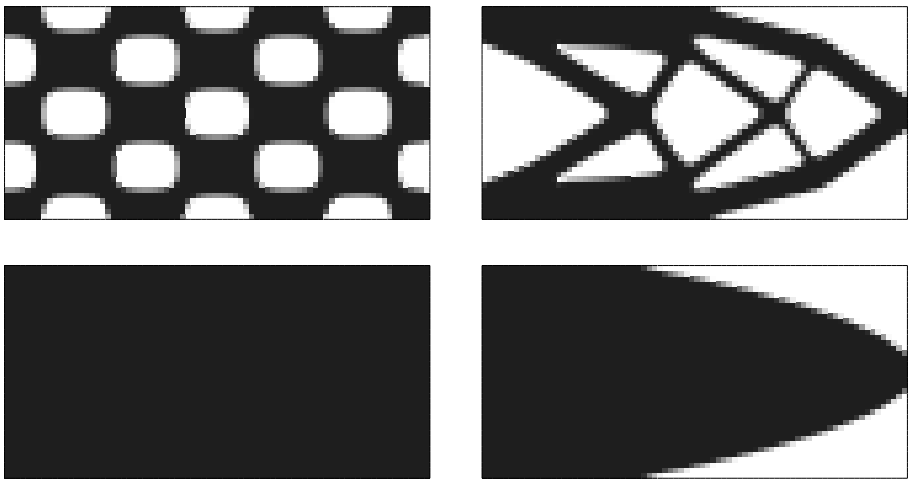

FIG. 2.1 – Shape gradient method (without topological derivative) for the cantilever problem : initializations (left) and optimal designs (right).

left wall and supports a unit vertical point load on the middle of the right wall. The working domain of size 2×1 is discretized by 3200 squared elements. The Lagrange multiplier for the volume constraint is $\eta = 100$. For the sake of comparison we recall the result of our previous level set method based on shape gradient **without** topological gradient in Figure 2.1 : we choose two different initializations : the "best" one (i.e. yielding the global minimum), and the trivial one (without holes). Then, we run our new method with coupling parameter $n_{top} = 5$: namely, every 5 iterations of the shape gradient method we compute the topological derivative and nucleate new holes accordingly. We start from the trivial initial design with no holes in the working domain and perform 50 iterations. The result displayed on Figure 2.2 is very similar to the best one in Figure 2.1 and the objective function takes the same value. As we explained in Section 2.6, the choice of the coupling parameter n_{top} is very important (which is a default of the method). On Figure 2.3 we obtain a suboptimal shape with less holes for a larger coupling parameter $n_{top} = 10$, and another suboptimal shape with irregular boundary for a smaller coupling parameter $n_{top} = 1$ (implying that we perform only topological gradient steps).

The working domain of the bridge problem is a 2×1.2 rectangle discretized with 3840 elements. The two lower corners have zero vertical displacement and a unit vertical load is applied at the middle of its bottom. The Lagrange multiplier is $\eta = 22$. The initialization is the full domain. The coupling parameter is $n_{top} = 5$. The final result as well as the intermediate results where new holes are nucleated by the topological gradient are displayed on Figure 2.4.

This bridge problem is an example where local minima still exist despite the use of the topological gradient (with fixed value of the coupling parameter

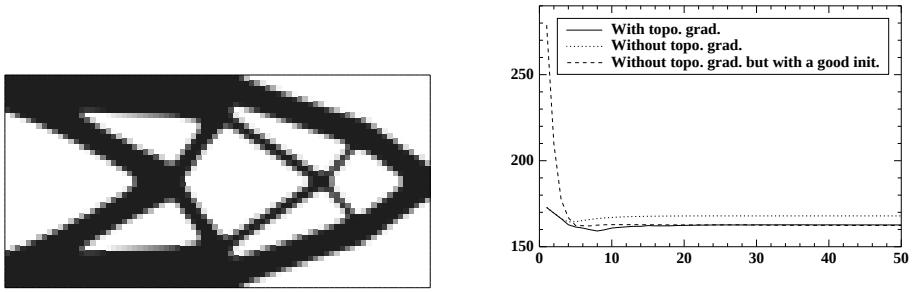

FIG. 2.2 – Coupled shape and topological gradient method for the cantilever : optimal design (left) and convergence history of the objective function (right).

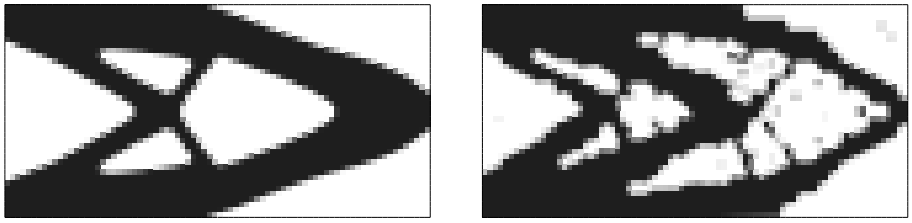

FIG. 2.3 – Optimal cantilever for the coupled shape and topological gradient method : $n_{top} = 10$ (left) and $n_{top} = 1$ (right).

n_{top}). Indeed, we run the same numerical example with a different initialization, namely the lower half of the domain. The resulting optimal shape, displayed on Figure 2.5, is better as can be checked on Figure 2.6.

For the optimal mast problem, we use a T-shaped working domain with height 6, width 2 at the bottom and 4 at the top. The two lower corners are fixed while two loads are applied at the lower corners of the horizontal branch of the T (see Figure 2.8). The quadrangular mesh is made of 3600 square cells. The Lagrange multiplier for the weight is equal to 15. The initialization is the full domain. We run 100 iterations of the level set method with coupling parameter $n_{opt} = 5$. The first topological gradient step occurs after iteration 5 where a hole is created in the upper part of the structure. Other holes are nucleated after iterations 10 and 15 and allow for a noticeable decrease of the objective function. However, the hole nucleated after iteration 20 is not so favorable and disappears in the final optimal result. The convergence is smooth except small peaks in the objective function after each topological gradient step (see Figure 2.7).

We now turn to mechanism design, i.e. we minimize the Lagrangian

$$\inf_{\Omega \subset D} \mathcal{L}(\Omega) = \mathcal{J}_{lse}(\Omega) + \eta |\Omega|$$

for a fixed Lagrange multiplier η, and $\mathcal{J}_{lse}$ being defined by (1.10) with the exponent $\alpha = 2$. The first example is a negative Poisson ratio mechanism :

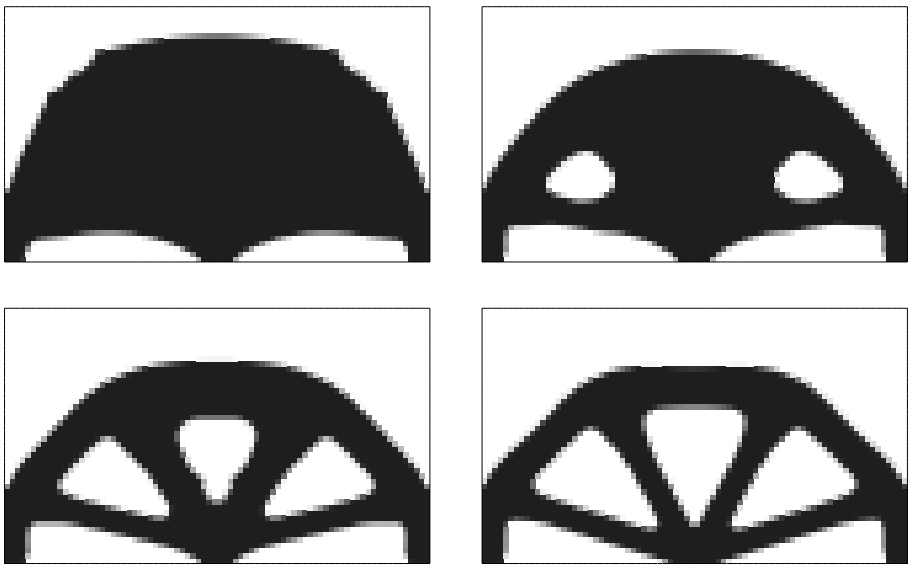

FIG. 2.4 – Optimal bridge in 2-d : iterations 6, 11, 16 and 100.

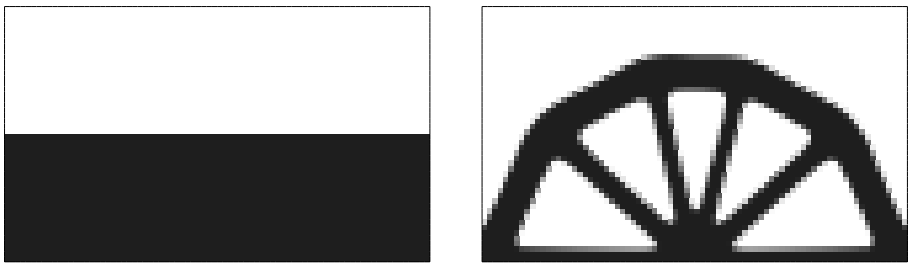

FIG. 2.5 – Optimal bridge in 2-d : half domain initialization and optimal shape after 100 iterations.

when we pull on the lateral sides it expands vertically. By symmetry, only 1/4 of the whole domain (of size 2×2) is meshed by 80×80 squared cells. All sides are made of a stiff material and excluded from optimization. In the formula for $\mathcal{J}_{lse}$, the localization coefficient $k(x)$ is non-zero (equal to 1) only at the boundary and the target displacement u_0 is $(0,1)$ on the top boundary, $(0,-1)$ on the bottom one and $(0,0)$ on the lateral ones. The Lagrange multiplier is $\eta = 0$. Starting from a full domain initialization we perform 500 iterations with the coupling parameter $n_{top} = 15$ (see Figure 2.9). As usual, the convergence is slower than for compliance minimization (see Figure 2.10). Furthermore, the computed optimal design is very sensitive to all parameters of the algorithm including the stiffness ratio between the weak ersatz material and the true material (which is here equal

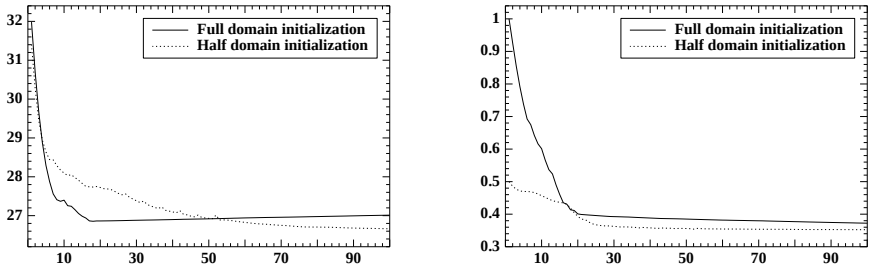

FIG. 2.6 – Convergence history of the objective function (left) and of the weight (right) for the 2-d optimal bridge.

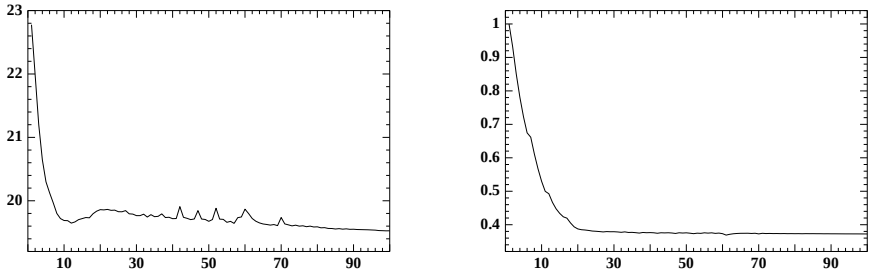

FIG. 2.7 – Convergence history of the objective function (left) and of the weight (right) for the 2-d optimal mast of Figure 2.8.

to 10^{-2}), the coupling parameter n_{top}, and the initialization. Different choices of these parameters lead to different topologies with similar performances.

Our second example is a gripping mechanism. Figure 2.11 shows the boundary conditions and the target displacement. A small force, parallel to the target displacement in the opposite direction, is also applied on the jaws of the mechanism in order to simulate a reaction force. We also add a constraint that the displacement of the location of the input forces are not too large. Starting from a full domain initialization we perform 300 iterations with the coupling parameter $n_{top} = 5$ (see Figure 2.12). The resulting optimal design is very similar to those obtained by the level set method [AJT04] or the homogenization method [All01].

Remark 2.7.1 *In all our examples the volume was not fixed. Rather, for a fixed Lagrange multiplier, we minimized the Lagrangian* $\mathcal{L}(\Omega) = \mathcal{J}(\Omega) + \eta|\Omega|$. *The reason is that we want to use a trivial initialization which do not bias the result. If we have to respect a volume constraint, the initial shape must include holes and the location and shapes of those holes may influence the result. Of course, it is not difficult to update the Lagrange multiplier* η *to satisfy a volume*

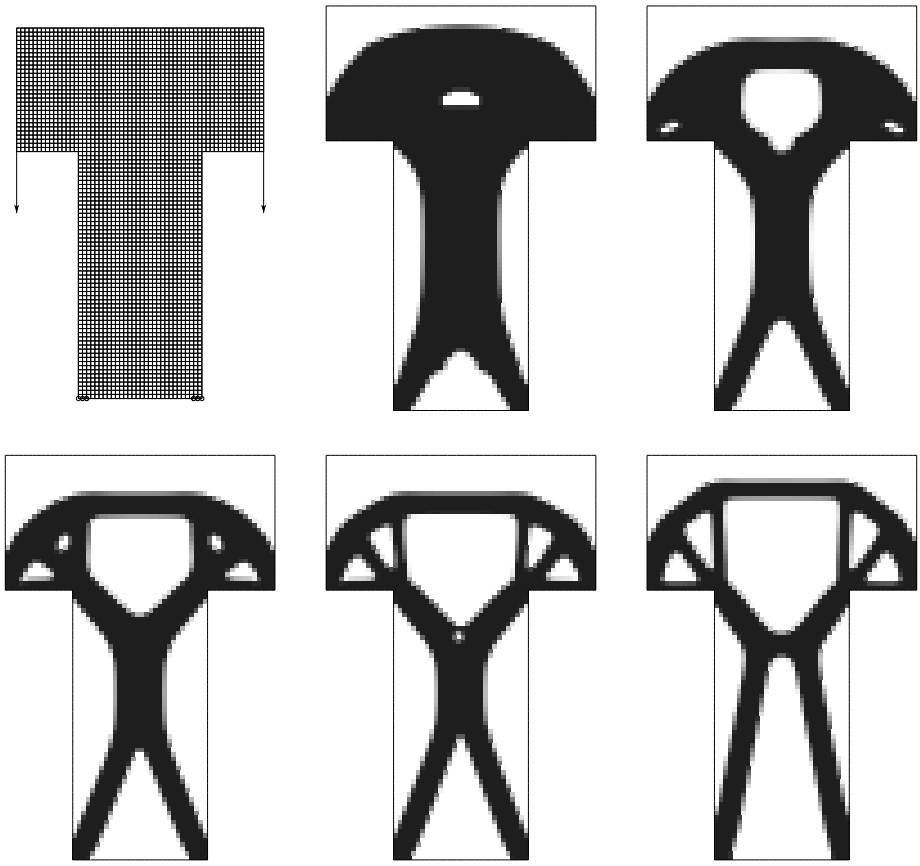

FIG. 2.8 – Optimal mast in 2-d : boundary conditions and iterations 6, 11, 16, 21 and 100.

constraint [AJ05].

2.8 Numerical examples in 3-d

As we already said the level set method works better in 3-d than in 2-d because holes are easier to create in 3-d [AJT04]. In all our 3-d numerical experiments, incorporating the topological gradient did not help in finding better optimal shapes. Of course, it may happen that the topological gradient speed up a little the convergence process but this effect is not striking and was not systematically studied here. We begin with compliance minimization problems.

We first optimize a 3-d cantilever where the right side is fixed and a horizontal unit point load is applied at the middle of the left side (see Figure 2.13). The working domain is of size $3 \times 2 \times 5$ and only half of it is discretized (by

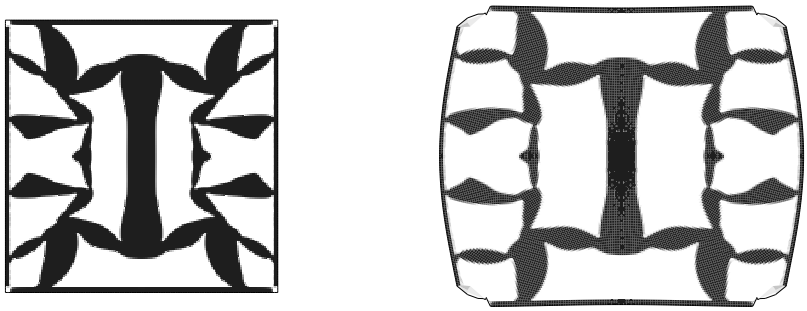

FIG. 2.9 – Optimal design (left) for the negative Poisson ratio mechanism, and deformed configuration (right).

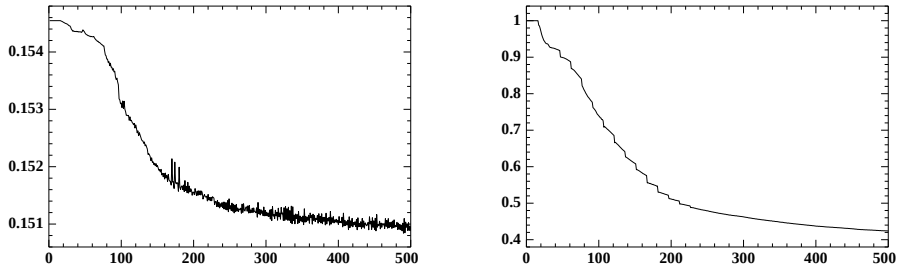

FIG. 2.10 – Convergence history of the objective function (left) and of the weight (right) for the negative Poisson ratio mechanism.

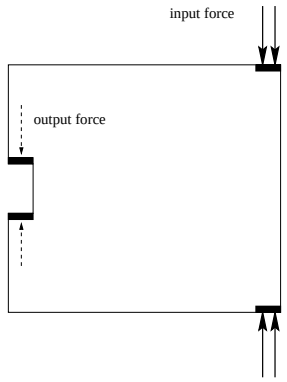

FIG. 2.11 – Boundary conditions and target displacement for the gripping mechanism.

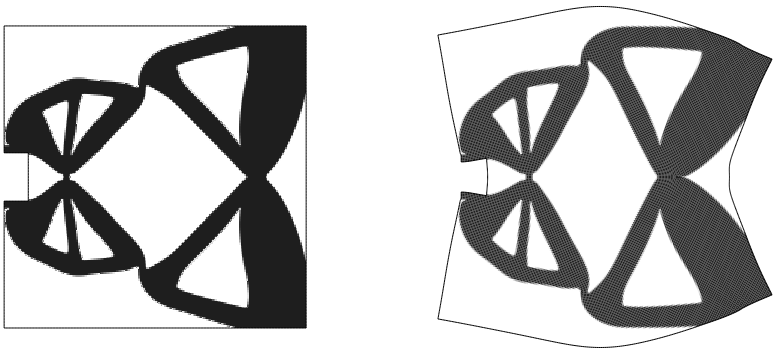

FIG. 2.12 – Optimal design (left) for the gripping mechanism, and deformed configuration (right).

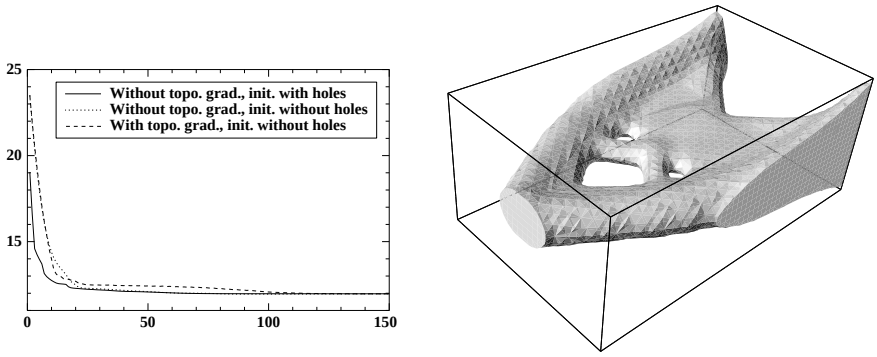

FIG. 2.13 – Optimal cantilever in 3-d (right). Convergence history of the objective function (left).

symmetry) using 15000 quadrilateral elements. The Lagrange multiplier for the weight constraint is $\eta = 20$. The coupling parameter is $n_{top} = 5$. We obtain precisely the same optimal shape with the level set method and our coupled method (incorporating the topological gradient). More than that, the result of the level set method was the same for two different initializations : either we start from the full working domain (without holes) or from a periodic collection holes as in [AJT04]. We believe that for any non-pathologic initialization we always get the same optimal shape. Finally, the result of our coupled method is also independent of the parameter n_{top} which characterizes the number of level set iterations between two evaluations of the topological gradient.

The same conclusions can be drawn from the 3-d optimal mast example (see Figure 2.14). Its result is independent of the method and of the initialization. We tried other simple examples in 3-d that confirm this behavior. Therefore, in view of this (limited) number of numerical experiments, we believe the level set

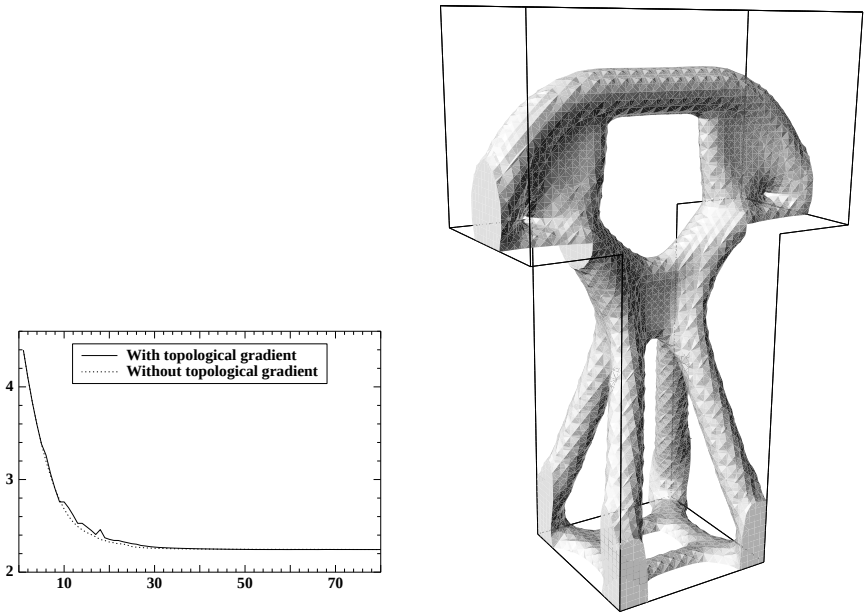

FIG. 2.14 – Optimal mast in 3-d (right). Convergence history of the objective function (left).

method alone in 3-d is as good as the coupled method (level set plus topological gradient).

2.9 Conclusion

We have proposed a coupled method of shape and topology differentiation in the level set framework. It is an iterative algorithm where repeatedly the shape boundary evolves smoothly and new small holes are nucleated. In 2-d numerical practice, this method is more insensitive to the initialization and is thus a great improvement over the previous level set method (at least for compliance minimization). In 3-d, our numerical experiments show that the improvement is not sensitive since the optimal shapes are the same than those obtained by the level set method (at least for compliance minimization).

There is still some room for improvement in the following directions : first, extend and test the robustness of our method for more general objective functions, second increase the speed of convergence, third implement a recent idea of Nazarov and Sokolowski [NS04] for another type of topology variations. Indeed, removing a hole in a shape is not the only possibility for changing the topology. Another issue, investigated in [NS04], is to add a thin ligament between two separated boundaries of the shape. It is somehow the opposite process of hole perforation, since it adds some material to the shape. Numerically this could be

an interesting process that may avoid, for example, the two different optimal shapes obtained for the 2-d bridge problem.

Finally, we remark that, for compliance minimization problems, the homogenization method [All01], [Ben95], [BS03] is still the most reliable method since it is the only one which is fully independent of the initialization and free of any important parameters.

Chapitre 3

Velocity extension for the Level-set method

Abstract

We study in this chapter the choice of the velocity for the underlying Hamilton-Jacobi of the level-set method. We comment on a new choice of velocity that regularize s and extend the original derivative that was only defined on the boundary of the shape. This method also endows a local Hilbertian structure for the shape optimization problem. We show that this new choice of velocity improves the algorithm and allows us to deal with new cases, namely the first eigenvalue maximization when it is multiple.

3.1 Introduction 44
3.2 Presentation of the problem 45
3.3 The weak material approximation and the natural extension method 46
3.4 Velocity regularization by the Hilbertian method 47
3.4.1 Definition of the Hilbertian method 47
3.4.2 Advantages of the method 47
3.4.3 Numerical example : Eigenvalues of a cantilever . . 49
3.4.4 Numerical example : The compliance of the cantilever 51
3.4.5 Numerical example : A 2-d gripping-mechanism . . 52
3.4.6 Numerical example : More 2-d mechanism 54
3.4.7 Numerical example : A 3-d gripping mechanism . . 57
3.5 Optimizing multiple eigenvalues 58
3.5.1 A general theorem about eigenvalue differentiation . 59
3.5.2 Calculus of the directional derivative of $\mathcal{L}_{vp}$ 60
3.5.3 Calculating V^* 64
3.6 Numerical results 66
3.6.1 The 3-d eigenvalue of a beam 66

3.6.2 The short cantilever 69

3.1 Introduction

Optimal design of elastic structures has been widely studied and many different numerical methods are used to solve this problem. Most of existing methods can be divided into two main classes : Topology optimization which optimizes a density of material in each cell and Geometric optimization which moves the boundary of the domain.

The most recent topology method, the homogeneization method and its variants (power-law method or SIMP method) may be considered quite classical in view of the number of publications (see e.g. [All01], [ABFJ97], [Ben95], [BS03], [BK88], [Che00]). The homogeneization method seems the most promising for its independence with respect to initialization and its strong mathematical result of existence of solution. Sadly it bears the difficulty of handling quite badly eigenvalue problems where apparitions of so-called fictitious-material modes prevents stable numerical calculus. Another problem is that topology methods generally end with non-classical domains but with composite optimal shape. Penalization methods allow to project the composite shape on a classical shape (a black-and-white design).

The problem of fictitious modes is naturally solved with the geometric methods where the shape is clearly identified and the void cannot generate fictitious modes.

The major drawback of geometric methods is their dependency with respect to initialization. Even the most recent level set method ([AJ05],[AJT04], [WWG03]) is very sensitive to initialization although the topology can change. In order to avoid this problem, a method of topology optimization, the bubble method, (or topological gradient method [ES94], [GGM01], [SJP92] [SZ01]) has been recently coupled with geometric optimization ([AGJT05], [BHR04]). Another recent advance in that field has been recently led by [NS04], but the numerical implementation of this method is still out of scope.

We wish here to correct the so-called void-problem that arises when using the level-set algorithm which is a geometric optimization method. This problem is generated by the weak material approximation that give rise to a null velocity for advecting the shape in the void. The void-problem slows down the algorithm when mesh is refined.

The void-problem is presented in **section 3.3** and the chosen solution is presented in **section 3.4**. The method mainly consists in applying the same inverse Laplacian operator to the velocity. It is a costless method to use because, this operator has to be inverted only once in the whole algorithm. This method allows to regularize, extend and endow an Hilbertian structure (see discussion of **section 3.4.2**). Numerical results are presented in **section 3.4.3** to **3.4.7**, they compare the new method with the previous one and show strong improvements of the level set algorithm.

It also has been made possible to deal with the problem of optimizing an eigenvalue when its multiplicity is greater than one. Theoretical differentiation of the eigenvalue is made in **section 3.5**. It is shown that, when the first eigenvalue is multiple, it is directionally differentiable with respect to shape variation. The algorithm that optimizes the first eigenvalue is detailed in **section 3.5.3**. It strongly relies on the endowment of a local Hilbertian structure made possible by velocity regularization. It is shown that the choice of the steepest descent is a Semi-Definite Program in low dimension that is easily solved. Some numerical results are presented in **section 3.6**.

The method used for optimizing multiple eigenvalues can be extended to other criteria that are not differentiable as the robust compliance criterion in the sense of [CC03]. The method of velocity regularization presented here is well-known in optimization processes ([Bur03], [PBH04], [MP01]).

3.2 Presentation of the problem

The setting is the maximization of the first eigenvalue, the Lagrangian to be minimized is given by (equation (1.7) and (1.11)) :

$$\mathcal{L}_{vp} = -\gamma_1(\Omega) + \eta$$

With derivative with respect to the domain equal to (proposition (1.3.4))

Proposition 3.2.1 *If the eigenvalue is simple, then $\mathcal{L}_{vp}$ is differentiable and*

$$\mathcal{L}'_{vp}(\theta) = \int_{\partial\Omega} (\theta \cdot n)\,(-v + \eta)$$

where $v = v(u,u)$ and $v(\cdot,\cdot)$ is the bilinear functional defined by :

$$\begin{aligned} v(u,w) &= Ae(u)\colon e(w) - \gamma_1(\Omega)\rho u \cdot w \quad \text{on } \Gamma_N \\ v(u,w) &= -Ae(u)\colon e(w) \quad \text{on } \Gamma_D \end{aligned}$$

and where u, the first eigenvector, has been renormalized by $\int_\Omega \rho u \cdot u = 1$

Recall that the level set method amounts to performing the following Hamilton-Jacobi method with gradient step T and descent direction V^* :

$$\begin{aligned} \phi(0) &= \phi_k \\ \frac{\partial \phi}{\partial t} + V^*|\nabla\phi| &= 0 \\ \phi_{k+1} &= \phi(T) \end{aligned} \tag{3.1}$$

Where ϕ_k is the level-set associated with the k^{th} domain of the optimization algorithm.

The standard choice of V^* is $V^* = v - \eta$ that is defined everywhere in the domain is called the "Natural extension method"

Remark 3.2.1 *In order to avoid multiple definition of V^* in the Natural extension method, it is supposed that the Dirichlet part of the boundary is fixed and that the v used everywhere in the domain is the one defined for Γ_N.*

3.3 The weak material approximation and the natural extension method

The stiffness matrix that corresponds to the linear operator of elasticity is not defined on the nodes that do not belong to Ω i.e. on $x \in D$ such that $\phi(x) > 0$. In other words, this matrix is not invertible. In order to avoid this problem, the so-called weak material (or ersatz material) approximation consists in fixing Hooke's law A and material density (a.k.a. mass matrix) ρ as :

$$\begin{array}{lllllll} A & = & A_0 & \text{and} & \rho & = & 1 \quad \text{in} \quad \Omega \\ A & = & \varepsilon A_0 & \text{and} & \rho & = & \varepsilon^\alpha \quad \text{outside} \quad \Omega \end{array}$$

with a small parameter ε and $\alpha \geq 1$. The fictitious modes are avoided by setting $\alpha = +\infty$. In the continuous case, it has been proved (see [SHSP89]) that the eigenvector $\tilde{u}$ calculated by using the ersatz material approximation is equal (at first order in ε) to the desired eigenvector u introduced in equation (1.6). In $D \setminus \Omega$ $\tilde{u}$ is the lifting of the Dirichlet condition $\tilde{u} = u$ on $\partial\Omega$ (at first order in ε).

Recalling that the Dirichlet part of the boundary of $\partial\Omega$ has been fixed (see remark 3.2.1), $v - \eta = Ae(u) : e(u) - \gamma_1 \rho u \cdot u - \eta$ is defined everywhere on D and the natural extension method consists in defining $V^* = Ae(u) : e(u) - \gamma_1 \rho u \cdot u - \eta$ on every cell.

This nevertheless raises a problem : since u is everywhere of order ε^0, then $Ae(u) : e(u)$ is of order ε outside Ω which means that the velocity extension is almost equal to $-\eta$ outside the domain, and makes it very difficult for the shape to increase its volume. Even if the descent step T is increased in order to speed up the method, the parts of the shape where there is a need to decrease the volume will move faster than the parts of the shape where there is a demand on increasing the volume. This difference of treatment leads to an higher ponderation of the velocity where it is negative, therefore the gradient that has been used is not the right one.

In numerical result, it can be seen that between each computation of the eigenvalue, the level-set method can not move $\partial\Omega$ more than one cell away from the original boundary when it wants to increase the volume. This leads to a drastically increasing computational time with mesh-refinement.

This remark is true, of course, for every objective function and not only for the minimization of the first eigenvalue.

3.4 Velocity regularization by the Hilbertian method

3.4.1 Definition of the Hilbertian method

We assume that the domain Ω has enough regularity so that $v(\cdot,\cdot)$ defined in proposition 3.2.1 belongs to $H^{-1/2}(\partial\Omega)$. Even if the optimal domain may possibly be irregular (see section 1.5.2), physical and numerical intelligence tells that throughout optimization $v(\cdot,\cdot)$ has the required regularity but mathematical proof of this fact is still lacking. Let us first define a scalar product :

Definition 3.4.1 *For $a \in \mathbb{R}^{*+}$, define the following scalar product on $H^1(D)$*

$$(u,w)_{H^1} = \int_D a\nabla u \cdot \nabla w + uw$$

With the associated norm $\|\cdot\|_{H^1}$.

The velocity V^* in the Hamilton-Jacobi equation (1.34) is chosen as the unique solution to

$$\int_{\partial\Omega} V^*(-v+\eta) = \min_{\substack{V\in H^1(D)\\ \|V\|_{H^1}=1}} \int_{\partial\Omega} V(-v+\eta) \tag{3.2}$$

Where v is the differential defined in proposition 3.2.1 and Ω is the actual shape.

3.4.2 Advantages of the method

$\diamond$ **Scalar versus vector :** We choose to extend the normal velocity which is a scalar field, i.e. : If θ is the vector field that advects the domain, its normal velocity is equal to $\theta \cdot n$ on the boundary of the domain. Seen as a distribution over D, the normal velocity is more regular than the vector velocity. A good example is when two parts of the boundary want to merge : $\theta \cdot n$ is positive on the two parts and θ changes orientation. This situation gets worst at the next step of the algorithm (see figure 3.1). That is why the normal velocity is extended and not the vector velocity.

$\diamond$ **How to compute V^* :** The problem of finding V^* is not difficult : Let $\bar{V}$ be the unique solution to

$$(\bar{V},X)_{H^1} = \int_{\partial\Omega} X(-v+\eta) \quad \forall X \in H^1(D)$$

Where $(\cdot,\cdot)_{H^1}$ is the scalar product of definition 3.4.1. Then $V^* = -\frac{\bar{V}}{\|\bar{V}\|_{H^1}}$ and the inversion of the matrix that corresponds to the scalar product $(\cdot,\cdot)_{H^1}$ has to be done only once in the optimization process.

$\diamond$ **Extension, Regularization and Hilbertian structure :** Three different goals are sought in the Hilbertian extension of the velocity.

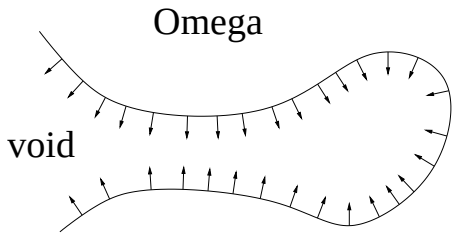

FIG. 3.1 – Two merging parts of the boundary leads to a non-regular vector field as seen as a distribution on D.

First, the formula for the differential of $\mathcal{L}$ gives a velocity that makes sense only on the boundary of the domain and the Hamilton-Jacobi equation (1.34) needs a speed defined everywhere on the domain or else the algorithm cannot move the boundary of more than one cell during optimization, this is the extension issue.

Secondly, the velocity is regularized by being diffused with the scalar product defined in definition 3.4.1. This is the regularization issue. It is expected to increase the accuracy of the algorithm and is a standard issue in optimization problems (see e.g. [PBH04], [Bur03],[MP01]).

Thirdly, the problem is endowed with an Hilbertian structure and we work with gradient-type methods, this issue will be developed later in section 3.5.

$\diamond$ **Hilbertian extension versus other extensions :** The most natural way to extend the velocity outside $\partial\Omega$ would have been to extend $v - \eta$ according to the normal of $\partial\Omega$ by a front-propagating type method as the fast-marching method described in [OS88]. This method does not endow the space with an Hilbertian structure. Neither does it regularize the velocity.

$\diamond$ V^* **is indeed an extension :** Because the scalar product diffuses the source term, the velocity is now defined everywhere on D and the typical problem of null velocity in the void that raises with the natural extension method is now cured .

$\diamond$ V^* **is indeed a regularization :** V^*, the speed used in the Hilbertian extension method is more regular than $v - \eta$ (the speed used in the Natural extension method) as can be seen in the following formal derivation :

If v belongs to an $H^s(D)$ then $X \mapsto \int_{\partial\Omega} X(-v + \eta)$ is a linear form on $H^{s-1/2}(D)$ and V^* belongs to an $H^{s+3/2}(D)$ by elliptic regularity on the very smooth domain D. Indeed V^* is obtained by multiplying the linear form $X \mapsto \int_{\partial\Omega} X(-v + \eta)$ by the inverse of an $H^1(D)$ scalar product and so gains two derivatives.

$\diamond$ **Consistency of the extension :** This extension would be consistent if for every $V \in H^1(D)$, there existed a vector field $\theta \in W^{1,\infty}(D; D)$ such that $\theta \cdot n = V$ on $\partial\Omega$. In this case we restrict ourselves to such θ and perform a steepest descent algorithm. Two hypotheses would then be needed to ensure the existence of such a vector field : a certain regularity on V and a certain regularity of the domain Ω through it's normal vector.

In order to ensure regularity of V^*, a scalar product on H^p, $p \geq 1$ could have been used instead of a scalar product on H^1 . But numerical computation of V^* may be quite difficult. Indeed, the computation of the matrix of the scalar product of H^p needs finite elements that are chosen accordingly to p.

$\diamond$ **The extension parameters :** The coefficient a characterize the diffusion of $v - \eta$ in the sense that setting it small compared to 1 will lead to a solution V^* which is point-wise almost equal to $v - \eta$ on $\partial\Omega$ on equal to zero outside $\partial\Omega$. It must be set small enough so that a big value of $|v - \eta|$ on one part of the boundary does not interfere too much with the values of $v - \eta$ on the other parts of the boundary. But it must be set big enough in order to diffuse the value of $v - \eta$ outside the boundary of Ω.

3.4.3 Numerical example : Eigenvalues of a cantilever

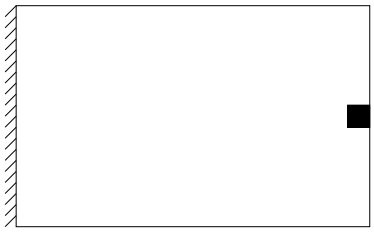

FIG. 3.2 – Boundary conditions for a 2-d cantilever (the black zone is heavier and not subject to optimization).

We study a medium-cantilever problem. The working domain is a 2×1 rectangle, with zero displacement condition on the left side and a small square region at the middle of the right side (see Figure 3.2) which is 500 times heavier and not subject to optimization. This heavier mass allows to avoid trivial shapes. The Young modulus of the material is set to 1, the Poisson ratio ν to 0.3 and the Lagrange multiplier to 7×10^{-2}. In the void, the ersatz material has a Young modulus set to 10^{-5} and a density ρ set to 0. The mesh is refined alternatively in each direction by a factor 2 and the number of transport iterations is adequately increased at each mesh refinement (see table below).

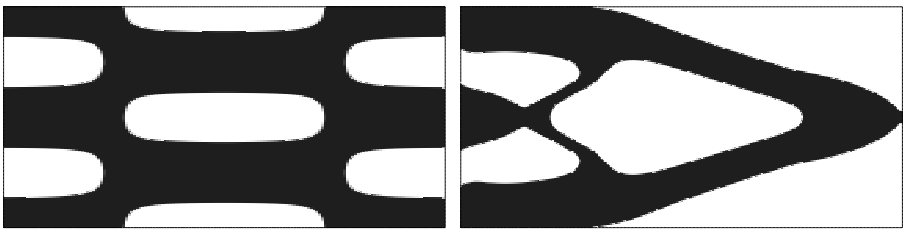

FIG. 3.3 – Initialization and optimal shape for the first eigenvalue of a cantilever.

Mesh	N^o of Transport	Time per iteration Hilbertian / Natural	Global time Hilbertian / Natural
81×41	16	1.46 / 1.62	30.68 / 50.13
161×81	32	9.35 / 11.37	233.87 / 330.01
321×161	64	72.17 / 94.91	2237.2 / 2657.63
41×41	14	0.74 / 0.84	13.26 / 22.6
81×81	28	4.46 / 6.19	120.62 / 136.1
161×161	56	38.50 / 46.61	1116.57 / 1771.44

TAB. 3.1 – Datas of the numerical test.

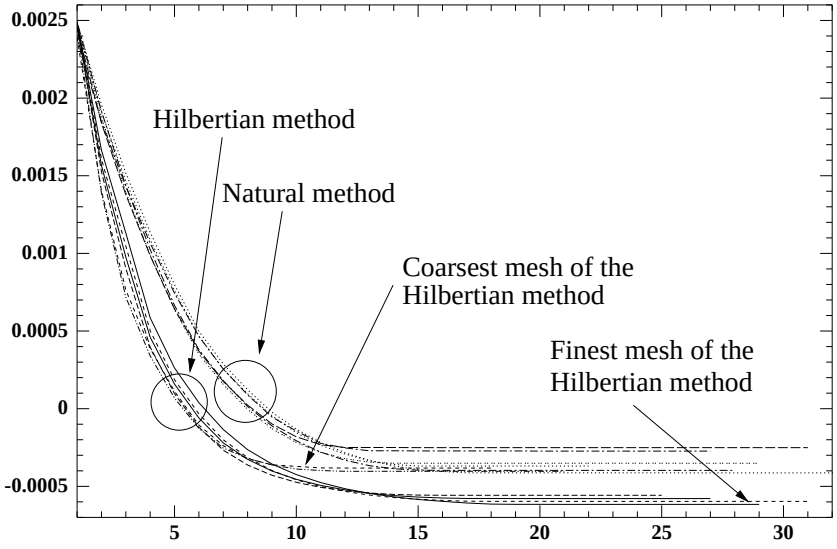

FIG. 3.4 – Mesh-refinement influence on the velocity for the Natural extension (left) and the Hilbertian extension (right).

◇ **Explanation of Table 3.4.3** That table lists, for different meshes, the number of transport iteration used for each optimization step in the Hamilton-Jacobi equation , the average computed time used per iteration step of the gradient method and the global computing time. The number of transport iteration is shown for the Hilbertian method only. The number of transport iterations for the natural method is 16 times the number of transport iterations of the Hilbertian method. This explains that the average time per iteration of the gradient algorithm is bigger for the Natural method than for the Hilbertian. The latest column is the global computing time for obtaining the optimal shape. The Hilbertian method takes the same amount of time than the Natural method to obtain the optimal shape, but only because it is more accurate : As can be seen

on figure 3.4, the convergence curves of the Hilbertian method are indeed better than the convergence curves of the Natural method. Time is given in seconds.

◇ **Explanation of Figure 3.4** There is two sets of curves in Figure 3.4. The better one are obtained with the Hilbertian method. It appears that the more the mesh is refined, the better the optimal shape is, even if , when mesh is refined, the decreasing of the smallest eigenvalue leads to an increase of the criterion. This is easily explained by a better accuracy on the optimal shape itself.

Remark 3.4.1 *In order to prove mesh-consistency of the algorithm and to have comparable curves in figure* 3.4*, the optimal shape have to be the same when the mesh is changed. Thus those examples are chosen so that there is no possibility for the algorithm to create thin structures when the mesh is refined. This explains why there are very few holes in the initialization. It is well known that the level-set algorithm can produce more complicated structures.*

3.4.4 Numerical example : The compliance of the cantilever

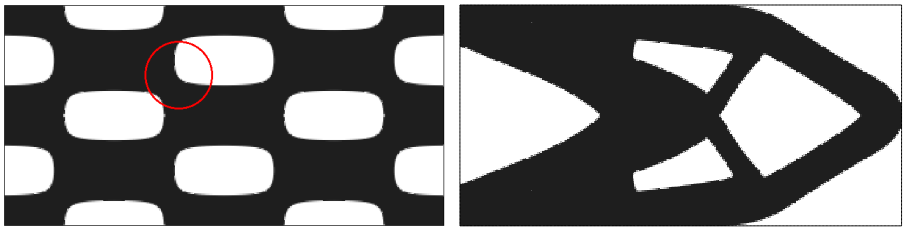

FIG. 3.5 – Initialization and optimal shape of the cantilever.

We performed our new velocity extension method on the well-known cantilever problem which is fixed on the left wall an supports a unit vertical point load in the middle of the right wall. The compliance $\mathcal{L}_{cp}$ as defined in equation (1.9) is optimized. The working domain size is 2×1. The Young modulus is set to 1 and the Poisson ratio to 0.3. The Lagrange multiplier is set to $\eta = 100$.

Optimization is performed for several finer meshes and the number of transport iteration is multiplied by 2 as each square of the mesh is cut into 4 squares. For the finest mesh (321×161) that corresponds to 51200 elements, the number of transport iterations is equal to 128 for the Natural extension and 16 for the Hilbertian. As a result, the Hilbertian extension is really quicker.

◇ **Mesh-refinement influence** The curves of figure 3.6 show that the Hilbertian method is less sensitive to mesh-refinement than the Natural method. Because there is parts of the boundary that have to increase the volume (one of them is encircled in figure 3.5) and that the Natural extension method have problems to improve these parts as was said in section 3.3, the Natural extension method is sensitive to mesh-refinement. In figure 3.4 there was no such demand

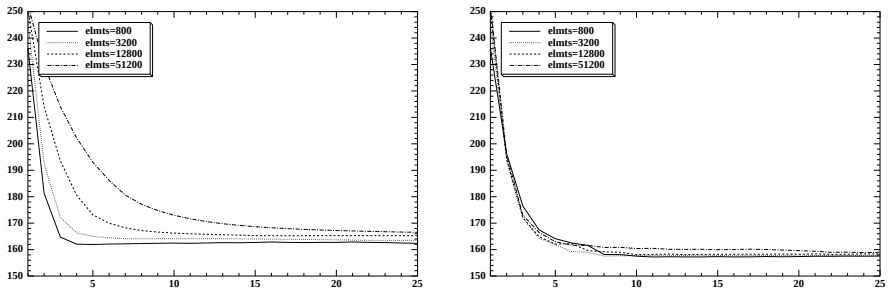

FIG. 3.6 – Mesh-refinement influence on the natural extension (left) and the Hilbertian extension (right).

on improving the volume and the mesh-independence of the Hilbertian method was less obvious.

3.4.5 Numerical example : A 2-d gripping-mechanism

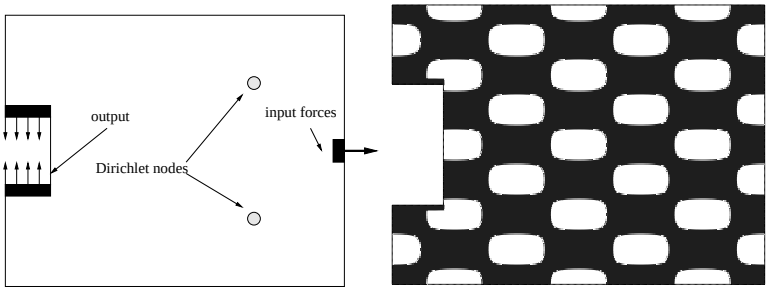

FIG. 3.7 – The definition of the 2-d gripping mechanism and its initialization.

On a 1.2×3.2 rectangle meshed with 241×641 nodes, we give a numerical example for minimizing the least square of a prescribed displacement. This example was given by the Commissariat à l'Energie Atomique for the design of a grip (see [Ber04]). The objective function is

$$\mathcal{J}_{lse}(\Omega) = \int_{\Omega} k(x)|u(x) - u_0(x)|^2 \tag{3.3}$$

where u is the displacement obtained by a given set of forces, u_0 is a prescribed given displacement and k is a scalar field that characterizes the zone of interest.

The ponderation k is equal to 10 on the left black box of figure 3.7 (left) ; is equal to 1 on the right black box and is equal to 0 elsewhere. The prescribed displacement u_0 is equal to $(0, \pm 1)$ on the left black box and $(0, 0)$ on the right box. Enforcing u to be close to zero where the force is input allows to ensure

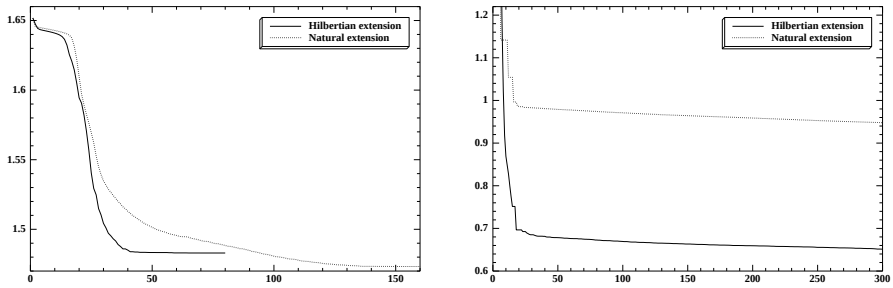

FIG. 3.8 – Evolution of the objective function for the first step (left) with a ratio for the weak material equal to 0.01 and the second step with a ratio of 10^{-5} (right).

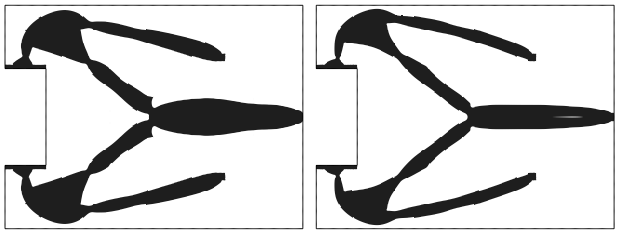

FIG. 3.9 – Optimal shape for the Hilbertian method (left) and the natural method (right) at the end of the first step of optimization.

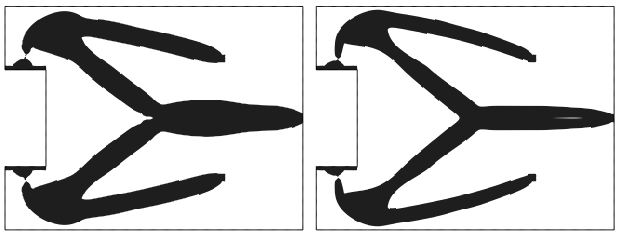

FIG. 3.10 – Optimal shape for the Hilbertian method (left) and the natural method (right) at the end of the second step of optimization.

the stiffness and the connectivity of the structure. These black boxes are not subject to optimization.

A force of modulus 1 N is applied in the x-direction on the middle of the left and a uniform pressure which represents a total force of modulus 5.10^{-2} N is applied between the jaws of the mechanism in order to enforce the mechanism to hold objects. The prescribed displacement is located on the black box on the left and shown in figure 3.7. The Young modulus is set to 1, the Poisson ratio to 0.3 and there is a small Lagrange multiplier of a volume constraint of value

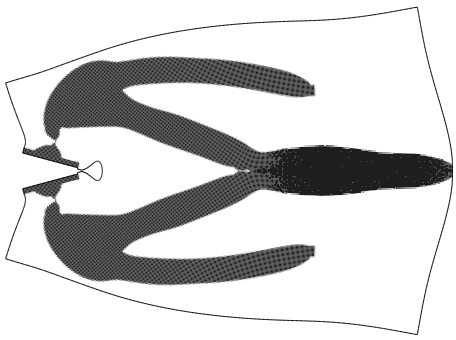

FIG. 3.11 – Optimal shape displacement.

0.05. This Lagrange multiplier helps removing parts of the boundary that are useless.

This is a typical problem where an adjoint is needed. For some incompletely understood reasons, the ratio of the weak material (the factor ε in section 3.3) cannot be set too low (typically it must be at least 1 percent of the strong material) or the algorithm won't work. One of the explanations that may be given is the tendency of the shape to create hinges. The algorithm then concentrate on the hinges only, ignoring the rest of the shape and it is believed it is then stuck in a local minimum. If the ratio of the weak material is high, hinges are less efficient and the previous problem is avoided.

Optimization must then be made in two steps. First the shape is optimized with a ratio of the weak material equal to 1 percent. The optimal shape is then re-optimized with a smaller ratio (10^{-5} in this numerical case). In the second optimization procedure, the displacement and the adjoint state are computed with a more accurate precision which leads to a better precision of the shape-derivative.

In figure 3.8 (left), it may seem that the Hilbertian method is less efficient than the Natural method. This is explained by the lack of precision in the computation of the shape derivative in the first step of the algorithm. But it is explained too by the lack of precision of the computation of the criterion during the first step of the algorithm. Indeed when the two shapes of figure 3.9 (obtained with $\varepsilon = 10^{-2}$) are computed using $\varepsilon = 10^{-5}$, the Hilbertian shape is the better one.

Remark 3.4.2 *The optimal shape for the natural extension method has less volume than the one for the Hilbertian extension, it is a numerical validation of the problem raised in section 3.3.*

3.4.6 Numerical example : More 2-d mechanism

We briefly present here some more 2-d mechanism, namely a negative Poisson modulus cell (figure 3.12 to 3.14) and a force inverter (figure 3.15 to 3.17). These

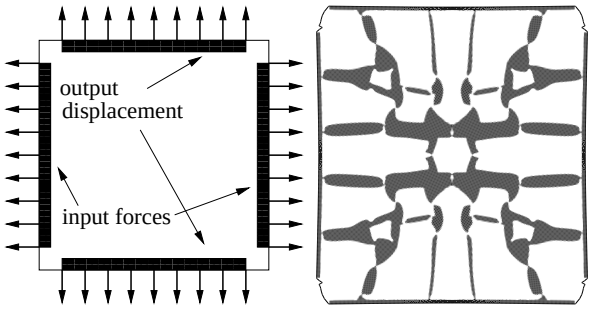

FIG. 3.12 – The Negative Poisson modulus problem and its deformed solution.

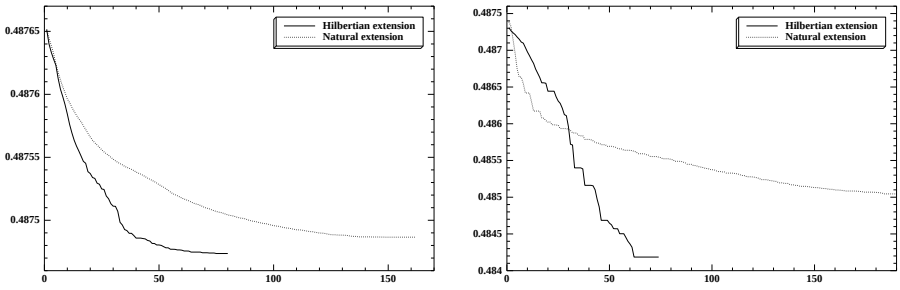

FIG. 3.13 – Negative Poisson modulus's evolution of the objective function at the first step (left) with a ratio for the weak material equal to 0.01 and the second step with a ratio of 10^{-5} (right).

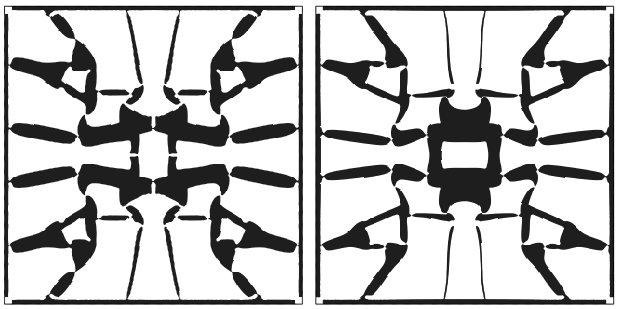

FIG. 3.14 – Negative Poisson modulus's optimal shape for the Hilbertian method (left) and the natural method (right) at the end of optimization.

examples are standards of shape optimization problems and their description can be found in [BS03]. In order to ensure stiffness of the structures, a small pressure load is applied where the displacement is optimized (on the right black box of Figure 3.15 for the force inverter and at the top and bottom of Figure

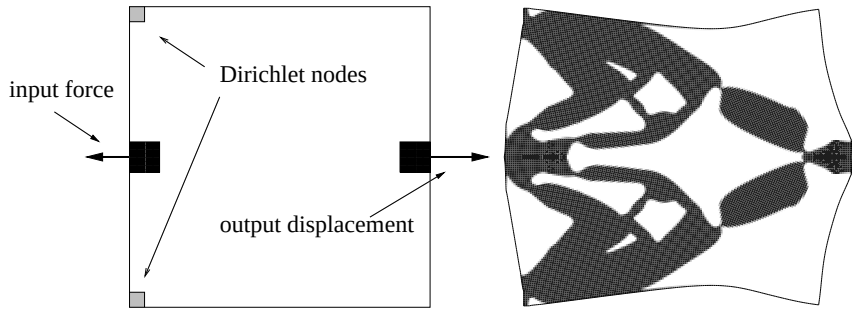

FIG. 3.15 – The Force inverter problem and its deformed solution.

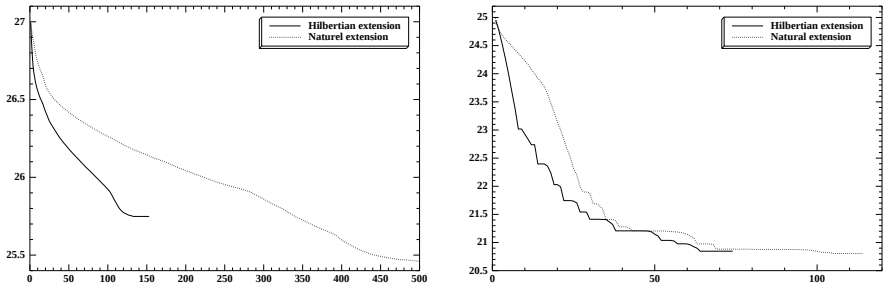

FIG. 3.16 – Force inverter's evolution of the objective function for the first step (left) with a ratio for the weak material equal to 0.01 and the second step with a ratio of 10^{-5} (right).

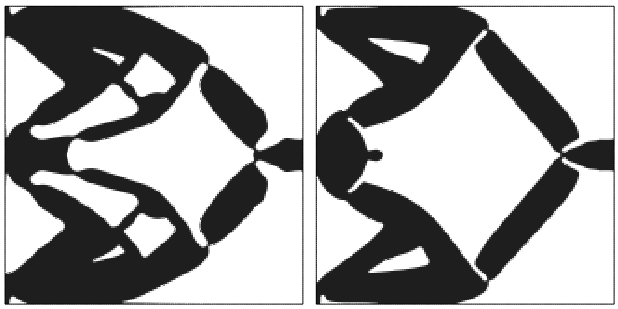

FIG. 3.17 – Force inverter's optimal shape for the Hilbertian method (left) and the natural method (right) at the end of optimization.

3.12 for the negative Poisson modulus mechanism). At the location of the input forces (left black box for the force inverter or the left and right walls for the negative Poisson modulus mechanism) the displacement is enforced to be close to zero in order to ensure connectivity of the shapes. Optimization is made in

two steps like the 2-d grip of section 3.4.5 and the behavior of the Hilbertian extension with respect to the natural extension is comparable.

3.4.7 Numerical example : A 3-d gripping mechanism

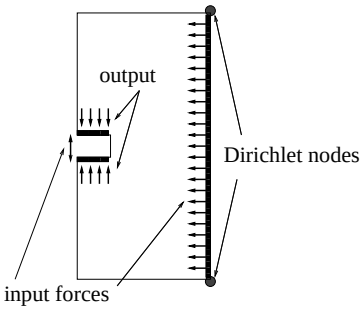

FIG. 3.18 – The problem of the 3-d gripping mechanism.

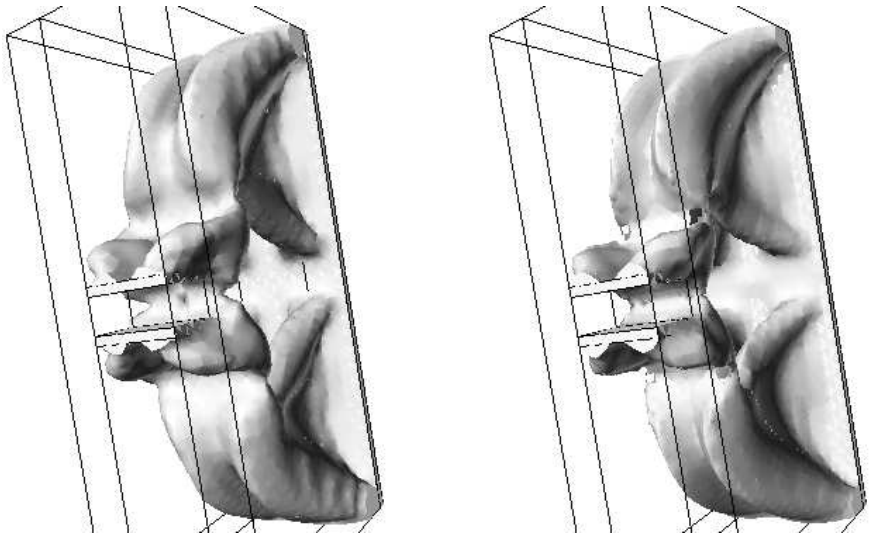

FIG. 3.19 – Optimal shape for the Hilbertian method (left) and the natural method (right) (isovalue 0 of the level-set is shown).

The objective function is defined by (3.3) in section 3.4.5. The working domain is a $3 \times 2 \times 6$ rectangle. A uniform pressure load is applied on the plane $x = 3$ and the prescribed displacement is localized on a box at the opposite side (see figure 3.18 where a cross-section at $y = 0$ is shown). A uniform pressure load (of order 60 percent of the one on the plane $x = 3$) is also imposed between the jaws of the mechanism so that this mechanism is designed to hold and grip.

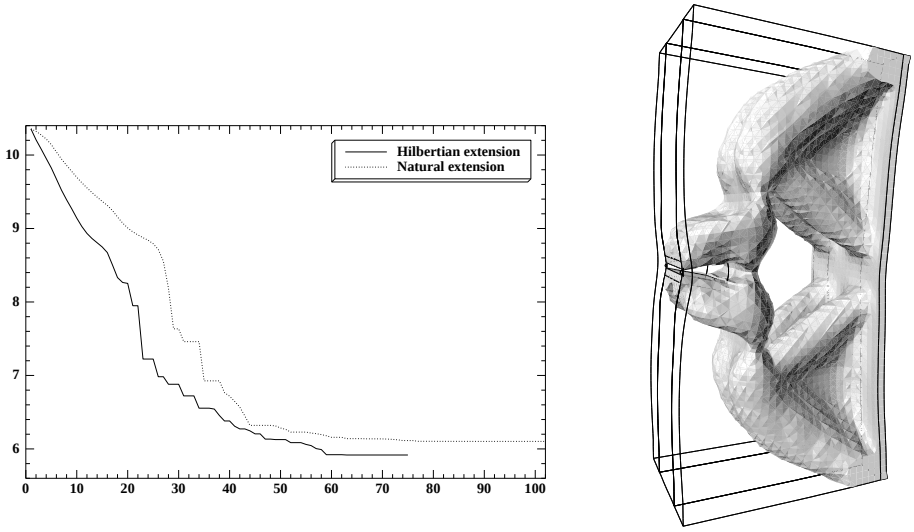

FIG. 3.20 – Objective function (left) and displacement of the Hilbertian shape (right) (density of material ≥ 0.3 is shown).

The Poisson ratio is 0.3 and the Young modulus is 1. The Lagrange multiplier is set to 3 and the mesh used is $31 \times 21 \times 61$. The ratio of the weak material is set to 10^{-5}. There is no need here to perform the two-step optimization of the section 3.4.5. The reason why things seems to be simpler in 3-d is that the changes of topology and the hinges are not of the same nature than in 2-d consequently it is believed that throughout the process of optimization, the objective function is more regular in 3-d.

3.5 Optimizing multiple eigenvalues

The development above for optimizing the first eigenvalue stands only when this eigenvalue is of multiplicity equal to 1. When this is not the case, there is no more differentiability of the first eigenvalue with respect to θ and the above method cannot be applied. Nevertheless it has been proven that $\mathcal{L}_{vp}$ is directionally differentiable. The velocity extension which endows the space with an Hilbertian structure allows to find a direction of descent. The used algorithm is now a sub-gradient type algorithm. The goal of this section is two-fold :

- Compute $\mathcal{L}'_{vp}(\theta) : W^{1,\infty}(D;D) \to \mathbb{R}$ the non-linear collection of directional derivative of $\mathcal{L}_{vp}$. Show that according to Hadamard's structure theorem $\mathcal{L}'_{vp}(\theta)$ depends only of the value of $\theta \cdot n$ on $\partial\Omega$. Let us denote $j(\theta \cdot n) = \mathcal{L}'_{vp}(\theta)$
- Compute V^* such that $j(V^*) = \min_{\|V\|=1} j(V)$ and advance the domain according to V^*.

It is in the computation of V^* that the Hilbertian structure is compulsory needed.

3.5.1 A general theorem about eigenvalue differentiation

Differentiating eigenvalues is nowadays quite standard, see [Kat76] for the foundations or [RC90] and [Lit00] for an extensive proof of the theorem 3.5.1 whose proof will only be sketched here. It must be emphasized that the derivation of eigenvalues is a corollary to the derivation of the robust compliance defined in chapter 4. As a result, the proof of the following theorem is just a consequence of the proof of theorem 3.5.1, given in Appendix B.

Define Ω_0 as the actual working domain.

Definition 3.5.1

$\diamond$ *Let $\alpha > 0$, $\beta_1 > 0$ be constants and $\mathbb{L}$ be the space of linear unbounded self-adjoint operators from $L^2(\Omega_0) \to L^2(\Omega_0)$ such that :*

$$\forall L \in \mathbb{L} \quad , \forall u \in H^1_D(\Omega_0) \quad \beta_1 \|u\|^2_{H^1_D(\Omega_0)} \geq (Lu, u)_{L^2} \geq \alpha \|u\|^2_{H^1_D(\Omega_0)}$$

i.e. : $\mathbb{L}$ is made of operators with 'uniformly' compact resolvent or 'uniformly' coercive with constant α and uniformly continuous with constant β_1

$\diamond$ *Let $\beta_2 > 0$ be a constant and $\mathbb{M}$ be the space of continuous linear self-adjoint operators from $L^2(\Omega_0) \to L^2(\Omega_0)$ uniformly continuous with constant β_2, ie :*

$$\forall M \in \mathbb{M} \quad , \forall u \in L^2(\Omega_0) \quad \beta_2 \|u\|^2_{L^2(\Omega_0)} \geq (Mu, u)_{L^2}$$

$\diamond$ *Define the norm in those two spaces as follows : If $N \in \mathbb{L}$ or $N \in \mathbb{M}$ then*

$$\|N\| = \max_{u \in H^1_D} \frac{(Nu, u)_{L^2}}{\|u\|^2_{H^1_D}}$$

ie, we endow $\mathbb{M}$ with the natural norm of $\mathbb{L}$

$\diamond$ *Let $W^{1,\infty}(D; D) \to \mathbb{L} \times \mathbb{M}$, $\theta \mapsto (L(\theta), M(\theta))$ be a Fréchet differentiable mapping with respect to the norm just defined. Define $L'(\theta_0)$ (resp $M'(\theta_0)$) the differential of $L(\theta)$ (resp $M(\theta)$) with respect to θ at the point $\theta = 0$ applied to θ_0.*

Theorem 3.5.1 *Define $\gamma_1(\theta)$ the smallest eigenvalue of the generalized eigenproblem $L(\theta)u = \gamma M(\theta)u$ and E_θ its eigenspace, $E_\theta = Ker(L(\theta) - \gamma_1 M(\theta))$. Then, for all $\theta_0 \in W^{1,\infty}(D; D)$, $\gamma_1(\theta)$ is directionally differentiable at the point $\theta = 0$ in the direction θ_0 and the value of the directional derivative is*

$$\gamma_1'(\theta_0) = \min_{\substack{u \in E_0 \\ (M(0)u, u) = 1}} \big(L'(\theta_0)u, u\big) - \gamma_1(0)\big(M'(\theta_0)u, u\big)$$

Sketch of the proof For a given direction θ_0 and for all $t \in \mathbb{R}^{*+}$, let $\tilde{\gamma_i}(t) = \gamma_i(t\theta_0)$ and suppose

$$\gamma_1 = \tilde{\gamma}_1(0) = \tilde{\gamma}_2(0) = ... = \tilde{\gamma}_d(0) \neq \tilde{\gamma}_{d+1}(0)$$

Identify H^1_D with its dual, and consider the operators $\tilde{L}(t)$ and $\tilde{M}(t)$ that are $H^1_D \to (H^1_D)' = H^1_D$ defined by :

$$\forall u \in H^1_D \quad (\tilde{L}(t)u, u)_{H^1_D} = (L(t\theta_0)u, u)_{L^2} \quad \text{and} \quad (\tilde{M}(t)u, u)_{H^1_D} = (M(t\theta_0)u, u)_{L^2}$$

For all t, $\tilde{L}(t)$ is a continuous coercive operator and $\tilde{M}(t)$ is a continuous compact operator.

Defining the self-adjoint compact operator $K(t) = \tilde{L}(t)^{-1/2}\tilde{M}(t)\tilde{L}(t)^{-1/2}$, and applying Kato's theory [Kat76] to the differentiable mapping $t \mapsto K(t)$, then the functions $\mathbb{R}^{*+} \to \mathbb{R}$, $t \mapsto \tilde{\gamma}_i(t)$ are -up to a reordering- differentiable in 0 and the derivatives are the eigenvalues of the generalized d-dimensional eigenproblem :

$$Pu = \gamma Mu \text{ where } P = \Pi \circ \big(L'(\theta_0) - \gamma_1(0)M'(\theta_0)\big) \circ \Pi^* \text{ and } M = \Pi \circ M(0) \circ \Pi^*$$

where $\Pi : L^2(\Omega_0) \to E_0$ denotes the projection onto the subspace E_0.

A good way to understand this result is to suppose that the mappings $\mathbb{R}^{*+} \to L^2(\Omega_0)$, $t \mapsto \tilde{u}_i(t)$ such that :

$$L(t\theta_0)\tilde{u}_i(t) = \tilde{\gamma}_i(t)M(t\theta_0)\tilde{u}_i(t) \quad \text{and} \quad \big(M(t\theta_0)\tilde{u}_i(t), \tilde{u}_i(t)\big) = \delta_{i,j} \tag{3.4}$$

are differentiable. In full generality, the eigenvectors are not even continuous. Performing a formal differentiation of the equations (3.4) gives

$$\big([L'(\theta_0) - \gamma_1(0)M'(\theta_0)]\tilde{u}_i(0), \tilde{u}_j(0)\big) = \tilde{\gamma}_i'\delta_{i,j} \tag{3.5}$$

where $\tilde{\gamma}_i'$ is the derivative of $t \mapsto \tilde{\gamma}_i(t)$ in 0.
Obtaining the formula of Theorem 3.5.1 is just expressing $\tilde{\gamma}_1'(\theta)$ as a Rayleigh quotient of the generalized eigenproblem (3.5). □

3.5.2 Calculus of the directional derivative of $\mathcal{L}_{vp}$

Let's apply Theorem 3.5.1 to the derivation of $\tilde{\mathcal{L}_{vp}}(\theta)$ defined as follows :

Definition 3.5.2
◇ *Let $T = Id + \theta$ and $\Omega_\theta = T \circ \Omega_0$*
◇ *Let $\tilde{M}(\theta)$ and $\tilde{L}(\theta)$ be defined as : for all u, v in $H^1_D(\Omega_\theta)$*

$$\begin{aligned} (\tilde{M}(\theta)u, v) &= \int_{\Omega_\theta} \rho u \cdot v \\ (\tilde{L}(\theta)u, v) &= \int_{\Omega_\theta} Ae(u) : e(v) \end{aligned}$$

$\diamond$ *Let* $\tilde{\gamma}_1(\theta)$ *be the smallest eigenvalue associated to the problem*

$$\tilde{L}(\theta)u = \tilde{\gamma}_1(\theta)\tilde{M}(\theta)u$$

$\diamond$ *Let* $\tilde{\mathcal{L}_{vp}}(\theta) = -\tilde{\gamma}_1(\theta) + \eta|\Omega_\theta|$

The $\tilde{\mathcal{L}_{vp}}(\theta)$ (respectively $\tilde{\gamma}_1(\theta)$) just defined corresponds to what has been denoted $\mathcal{L}_{vp}(\Omega_\theta)$ (respectively $\gamma_1(\Omega_\theta)$) in section 1.1.

Theorem 3.5.1 cannot be applied to $\tilde{\gamma}_1(\theta)$ because the the spaces where the operators $\tilde{L}(\theta)$ and $\tilde{M}(\theta)$ are defined changes with θ. That is why we consider :

Definition 3.5.3
$\diamond$ *Let* $M(\theta) \in \mathbb{M}$ *and* $L(\theta) \in \mathbb{L}$ *be defined as*

$$\begin{aligned}(M(\theta)u, v) &= (\tilde{M}(\theta)u \circ T^{-1}, v \circ T^{-1}) \\ (L(\theta)u, v) &= (\tilde{L}(\theta)u \circ T^{-1}, v \circ T^{-1})\end{aligned}$$

$\diamond$ *Let* $\bar{\gamma}(\theta)$ *be the smallest eigenvalue associated to the problem*

$$L(\theta)u = \bar{\gamma}(\theta)M(\theta)u$$

We shall work with those operators instead of the classical ones. They are defined on a domain independent of θ so that the first eigenvalue can be derivated in the sense of theorem 3.5.1. First it must be proven that the introduced eigenvalue $\bar{\gamma}$ is the same as γ_1 the first eigenvalue of the elasticity problem.

Lemma 3.5.2
$\diamond$ $L(\theta)$ *and* $M(\theta)$ *indeed belongs to* $\mathbb{L}$ *and* $\mathbb{M}$.
$\diamond$ $\bar{\gamma}(\theta)$ *and* $\tilde{\gamma}_1(\theta)$ *coincide, where* $\tilde{\gamma}_1$ *is defined in definition* 3.5.2.

We can now apply theorem 3.5.1 to $\bar{\gamma}(\theta) = \tilde{\gamma}_1(\theta)$ and end with the following result.

Theorem 3.5.3 *Recalling definition 3.5.2,* $\tilde{\mathcal{L}_{vp}}(\theta) = -\tilde{\gamma}_1(\theta) + \eta|\Omega_\theta|$ *is directionally differentiable with respect to* θ *and its directionally derivative at* $\theta = 0$ *in the direction* θ_0 *is given by*

$$\mathcal{L}'_{vp}(\theta_0) = \max_{\substack{u \in E_0 \\ \int_{\Omega_0} \rho u \cdot u = 1}} \int_{\partial\Omega_0} (\theta_0 \cdot n)\left(-v(u,u) + \eta\right)$$

where $v(\cdot,\cdot)$ *is a bilinear functional defined by*

$$\begin{aligned}v(u,w) &= Ae(u) : e(w) - \gamma_1\rho(\Omega_0)u \cdot w \quad \text{on } \Gamma_N \\ v(u,w) &= -Ae(u) : e(w) \quad \text{on } \Gamma_D\end{aligned}$$

and where E_0 *is the first eigenspace associated to* $\gamma_1(\Omega_0) = \tilde{\gamma}(0)$ *the smallest eigenvalue for* $\theta = 0$

One can of course verify that the formula when the dimension of the eigenspace is greater than one is the same that the formula when the dimension is equal to one.

Proof of lemma 3.5.2.
$\diamond$ Let us first prove that $\tilde{\gamma}_1(\theta) = \bar{\gamma}(\theta)$. Using $u \in H^1(\Omega_\theta) \Longleftrightarrow v = u \circ T^{-1} \in H^1(\Omega_0)$ we have :

$$\begin{aligned}\tilde{\gamma}_1(\theta)^{-1} &= \max_{u\in H^1(\Omega_\theta)} \frac{\left(\tilde{M}(\theta)u,u\right)}{\left(\tilde{L}(\theta)u,u\right)} = \max_{u\in H^1(\Omega_\theta)} \frac{\left(M(\theta)u\circ T,u\circ T\right)}{\left(L(\theta)u\circ T,u\circ T\right)} \\ &= \max_{v\in H^1(\Omega_0)} \frac{\left(M(\theta)v,v\right)}{\left(L(\theta)v,v\right)} = \bar{\gamma}(\theta)^{-1}\end{aligned}$$

$\diamond$ Let us now prove that $L(\theta)$ belongs to $\mathbb{L}$. The fact that $L(\theta)$ is coercive and bounded with respect to the $H^1_D(\Omega_0)$ norm comes from the fact that $\tilde{L}(\theta)$ is coercive and bounded in the $H^1_D(\Omega_\theta)$ norm. We have to show that these constant of coercivity and boundedness are uniform in θ. Let's introduce the tensor A which has the symmetries of the elasticity :

$$A^{ijkl} = A^{jikl} = A^{ijlk} = A^{klij}$$

such that $A^{ijkl}(\partial_j u^i)(\partial_l v^k) = Ae(u)\colon e(v)$. We have :

$$\begin{aligned}(L(\theta)u,v) &= \int_{\Omega_\theta} A^{ijkl}\partial_j(u\circ T^{-1})^i\partial_l(v\circ T^{-1})^k \\ &= \int_{\Omega_0} |det\nabla T|A^{ijkl}(\partial_s u^i)\left(\partial_j(T^{-1})^s\right)(\partial_m v^k)\left(\partial_l(T^{-1})^m\right) \\ &= \int_{\Omega_0} l(\theta)^{iskm}(\partial_s u^i)(\partial_m v^k)\end{aligned}$$

With

$$l(\theta)^{iskm} = A^{iskm} + (\partial_l\theta^l)A^{iskm} - A^{ijkm}(\partial_j\theta^s) - A^{iskl}(\partial_l\theta^m) + o(\|\theta\|_{W^{1,\infty}})$$

Such that at least for θ small L is indeed coercive with compact resolvent and that the coercivity constant is uniformly bounded from below. The same development applied to M shows that $M \in \mathbb{M}$. $\square$

Proof of theorem 3.5.3
We apply Theorem 3.5.1 to $\tilde{\gamma}_1(\theta) = \bar{\gamma}(\theta)$ in order to calculate $\mathcal{L}'_{vp}(\theta_0)$. The calculus above for L (and the same for M) shows that

$$\begin{aligned}(L'(\theta)u,v) = &\int_{\Omega_0} \left((\partial_l\theta^l)A^{iskm} - A^{ijkm}(\partial_j\theta^s) - A^{iskl}(\partial_l\theta^m)\right)(\partial_s u^i)(\partial_m v^k) \\ = &\int_{\Omega_0} A^{iskm}(\partial_l\theta^l)(\partial_s u^i)(\partial_m v^k) - A^{iskm}(\partial_s\theta^l)(\partial_l u^i)(\partial_m v^k) \\ &-A^{iskm}(\partial_m\theta^l)(\partial_s u^i)(\partial_l v^k) \\ (M'(\theta)u,v) = &\int_{\Omega_0} (\partial_l\theta^l)\rho u^i v^i\end{aligned}$$

Applying Theorem 3.5.1 gives

$$\mathcal{L}'_{vp} = \max_{\substack{u\in E_0 \\ \int_{\Omega_0}\rho u\cdot u=1}} -\int_{\Omega_0} A^{iskm}(\partial_l\theta^l)(\partial_s u^i)(\partial_m v^k) + \int_{\Omega_0} A^{iskm}(\partial_s\theta^l)(\partial_l u^i)(\partial_m v^k)$$
$$+\int_{\Omega_0} A^{iskm}(\partial_m\theta^l)(\partial_s u^i)(\partial_l v^k) + \int_{\Omega_0}(\partial_l\theta^l)\rho u^i v^i + \int_{\Omega_0}\eta(\partial_l\theta^l)$$

We perform an integration by part on θ , the term in $\int_{\Omega_0}$ is equal to :

$$\theta^l A^{iskm}\left[\partial_l(\partial_s u^i\partial_m u^k) - \partial_s(\partial_l u^i\partial_m u^k) - \partial_m(\partial_s u^i\partial_l u^k)\right] - \theta^l\gamma_1\rho\partial_l(u^i u^i)$$

Some algebra used in coordination with $\gamma_1\rho u = -divAe(u)$ allows us to conclude that this term is equal to zero. The remaining term is then equal to

$$\mathcal{L}'_{vp}(\theta) = \max \int_{\partial\Omega_0}(\theta\cdot n)[-A^{iskm}(\partial_s u^i)(\partial_m u^k) + \gamma_1\rho u\cdot u + \eta]$$
$$+ \int_{\partial\Omega_0} A^{iskm}\theta^l n^m(\partial_s u^i)(\partial_l u^k) + A^{iskm}\theta^l n^s(\partial_l u^i)(\partial_m u^k)$$

On the Neumann part of the boundary we use $Ae(u)\cdot n = 0$ and the definition of C to conclude that

$$A^{iskm}(\partial_s u^i)n^m = 0 = A^{iskm}(\partial_m u^k)n^s.$$

On the Dirichlet part of the boundary we use $u = 0$ so that $\nabla u = \frac{\partial u}{\partial n}\otimes n$ to conclude that

$$(\theta\cdot n)(\partial_m u^k) = \theta^l n^m(\partial_l u^k) \text{ and } (\theta\cdot n)(\partial_s u^i) = \theta^l n^s(\partial_l u^i)$$

So that

$$\mathcal{L}'_{vp}(\theta) = \max\int_{\partial\Omega_0}(\theta\cdot n)[-Ae(u)\colon e(u) + \gamma_1 u\cdot u + \eta] + 2\int_{\Gamma_D}(\theta\cdot n)Ae(u)\colon e(u)$$

□

Remark 3.5.1 *We did not use here the standard way of calculating shape sensitivity. The standard way (see [Sim80], [MS76]) would have been to first calculate the derivation of the eigenvector with respect to the domain. This leads to two difficulties : The first one relies on the non-derivability of the eigenvector with respect to domain variation. The second one relies in the fact that it is the Eulerian solution that is derivated (i.e. : if u_θ denotes the eigenvector it is $u_\theta\circ T$ that is derivated). This gives rise to the Lagrangian derivative Y, but Y has one less derivative than u. So that we need to ensure that u is H^2.*

In fact we do not need this trick for self-adjoint problems (like the compliance or the eigenvalue) which can be seen as a maximum and we do not need to verify that the maximizer is itself directionally differentiable. We gain this way an order of regularity because we do not have to perform the trick of Eulerian-Lagrangian point of view which makes us loose one derivative.

3.5.3 Calculating V^*

The goal of this subsection is to calculate V^* the minimizer to

$$\min_{\|V\|=1} \quad \max_{\substack{u \in E_0 \\ \int_{\Omega_0} u \cdot u = 1}} \quad \int_{\partial\Omega_0} V\left(-v(u,u) + \eta\right) \tag{3.6}$$

Where $v(\cdot,\cdot)$ is defined in Theorem 3.5.3. We will prove in this section that this is an semidefinite programming problem in low dimension that is easily solved. The use of SDP programming for eigenvalue optimization is classical, the goal of this section is to show that solving this SDP problem is a very easy task thanks to the Hilbertian structure endowed by the velocity regularization. A good introduction to SDP programming is [VB96] and the references therein. Only some basic facts about SDP problems have been recalled here

Definition 3.5.4

$\diamond$ *Let Y be an unknown vector , Give Y_0 a vector and $E(Y)$ a matrix whose coefficients depend linearly on Y. Let ≥ 0 stand for 'symmetric positive'. An SDP problem is of the form :*

$$\min_{E(Y)\geq 0} Y^T Y_0$$

$\diamond$ *SDP problems are efficiently solvable by duality methods. In order to insure that there is no gap of duality, a sufficient condition is to find Y_1 a strictly primal feasible point ,i.e. : such that $E(Y_1) > 0$ (definite positive).*

We now need to introduce the semidefinite programming problem we will work on.

Definition 3.5.5 *Recall definition 3.4.1 of the scalar product $(\cdot,\cdot)_{H^1}$*
$\diamond$ *Define $(e_i)_{i=1\ldots d}$ an orthonormal basis of the first eigenspace E_0 for the scalar product*

$$(u,w) = \int_{\Omega_0} \rho u \cdot w$$

$\diamond$ *Define $(a_{ij})_{i,j=1\ldots d}$ and c as*

$$(a_{ij}, X)_{H^1} = \int_{\partial\Omega_0} -Xv(e_i,e_j) \quad \textit{and} \quad (c,X)_{H^1} = \int_{\partial\Omega_0} X\eta$$

$\diamond$ *Define h_k an orthonormalized basis of $Span(a_{ij},c)_{i,j}$ for the scalar product $(,)_{H^1}$. Let m be the dimension of this space and let $(a_{ij}^k)_{k=1\ldots m}$ (resp $(c^k)_{k=1\ldots m}$) be the coordinates of a_{ij} (resp c) on the basis $(h_k)_{k=1\ldots m}$.*

$\diamond$ *For any* $X = (X_1, ..., X_m)$ *and* $(z, w) \in \mathbb{R}^2$, *let* $Y = [X, w, z]$.
$\diamond$ *Let* $A(X)$ *be the* $d \times d$ *matrix* $A(X)_{ij} = a_{ij}^k X_k$ *let* $C(X) = c^k X_k$ *and let*

$$D(Y) = \begin{bmatrix} -A(X) + z\mathbb{I}d & 0 \\ 0 & -C(X) - z + w \end{bmatrix} \quad E(Y) = \begin{bmatrix} D(Y) & 0 & 0 \\ 0 & \mathbb{I}d & X \\ 0 & X^T & 1 \end{bmatrix}$$

The coefficients of E *depend linearly on* $Y = [X, w, z]$
$\diamond$ *Let* $Y^* = [X^*, w^*, z^*]$ *be the solution of the following SDP problem :*

$$\min_{E(Y) \geq 0} w \tag{3.7}$$

Theorem 3.5.4
$\diamond$ V^*, *the minimizer of the problem* (3.6) *is given by*

$$V^* = \sum_{k=1}^{m} V_k h_k$$

where the vector $X^* = [V_1, ..., V_k]$ *is defined as a solution of the Semi-Definite problem* (3.7).
$\diamond$ *The problem* $\min_{E(Y) \geq 0} w$ *is strictly feasible, SDP programming can be applied.*
$\diamond$ V^* *(or equivalently* X^**) is attained.*

Proof
$\diamond$ We transform the problem (3.6) into (3.7) by using the fact that $v(\cdot, \cdot)$ is bilinear (see Theorem 3.5.3 for the definition of v)

$$\begin{aligned} & \min_{\|V\|_{H^1}=1} \max_{\substack{u \in E_0 \\ \int_{\Omega_0} \rho u \cdot u = 1}} \int_{\partial\Omega_0} V[-v(u,u) + \eta] \\ = & \min_{\|V\|_{H^1}=1} \max_{\sum_{i=1}^d \lambda_i^2 = 1} \int_{\partial\Omega_0} V[-\lambda_i \lambda_j v(e_i, e_j) + \eta] \\ = & \min_{\|V\|_{H^1}=1} \max_{\sum_{i=1}^d \lambda_i^2 = 1} \lambda_i \lambda_j (V, a_{ij})_{H^1} + (V, c)_{H^1} \\ = & \min_{\|V\|_{H^1}=1} \max_{\sum_{i=1}^d \lambda_i^2 = 1} (V, h_k)_{H^1} (\lambda_i \lambda_j a_{ij}^k + c^k) \end{aligned}$$

So that V^* is a minimizer of (3.6) if and only if $X_k^* = (V^*, h_k)$ are minimizer of the following problem

$$\min_{\sum X_k^2 \leq 1} \max_{\sum_{i=1}^d \lambda_i^2 = 1} \lambda_i \lambda_j a_{ij}^k X_k + c^k X_k \tag{3.8}$$

$\diamond$ Showing that (3.8) is equivalent to (3.7) is a standard issue of SDP programming : The condition $E([X, w, z]) \geq 0$ is equivalent to $(X, X) \leq 1$ and

$D([X,w,z]) \geq 0$. The condition $D([X,w,z]) \geq 0$ is equivalent to $zId \geq A(X)$ and $w \geq z + C(X)$. So that

$$E([X,w,z]) \geq 0 \Longleftrightarrow \sum_k X_k^2 \leq 1 \text{ and } w \geq z + X_k c^k \text{ and } z \geq \max_{\sum_{i=1}^d \lambda_i^2 = 1} \lambda_i \lambda_j a_{ij}^k X_k$$

So that minimizing w with the above condition is equivalent to finding X in the problem (3.8).
$\diamond$ Choosing $X = 0$, $z > 0$ and $w > z$ gives a $[X,w,z]$ for which $F([X,w,z]) > 0$ the problem is then strictly feasible, an extended Slater's condition holds and the dual problem (in term of semi-definite duality) have the same extremal value.
$\diamond$ The condition $\sum_k X_k^2 \leq 1$ ensures that X is bounded and that every minimizing sequence converges up to a subsequence. The maximum is indeed attained
$\square$

Remark 3.5.2 *The SDP problem is not difficult to solve , recall that d is the dimension of the first eigenspace, then* $[X,w,z]$ *is of dimension lower or equal to* $\frac{d(d+1)}{2} + 3$ *and the matrix E is a* $\frac{d(d+3)}{2} + 3$ *square matrix.*

3.6 Numerical results

3.6.1 The 3-d eigenvalue of a beam

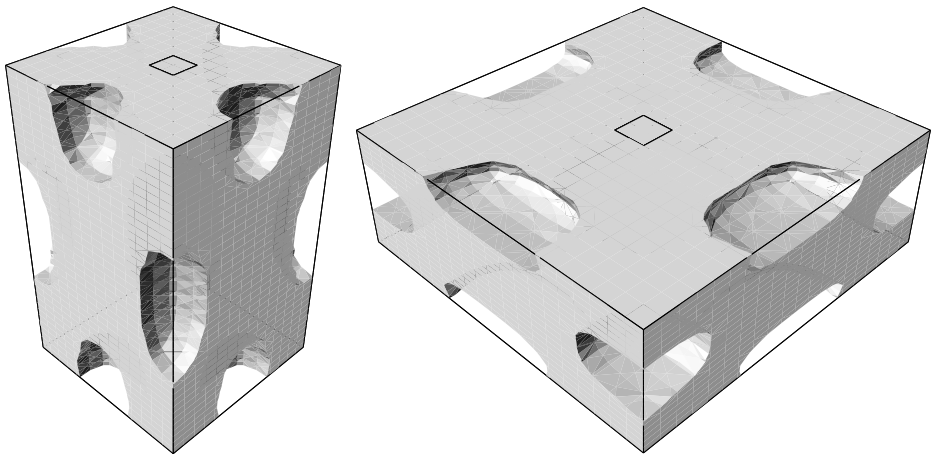

FIG. 3.21 – Initialization for narrow domain (left) and for the big domain (right).

We naturally set our problem in 3-d with symmetries, where we are sure to obtain a multiplicity of the first eigenvalue greater than one. The first example which will be called the 'big domain' problem is a $3 \times 3 \times 1$ rectangle discretized with a $21 \times 21 \times 23$ mesh. A zero displacement boundary condition is imposed on

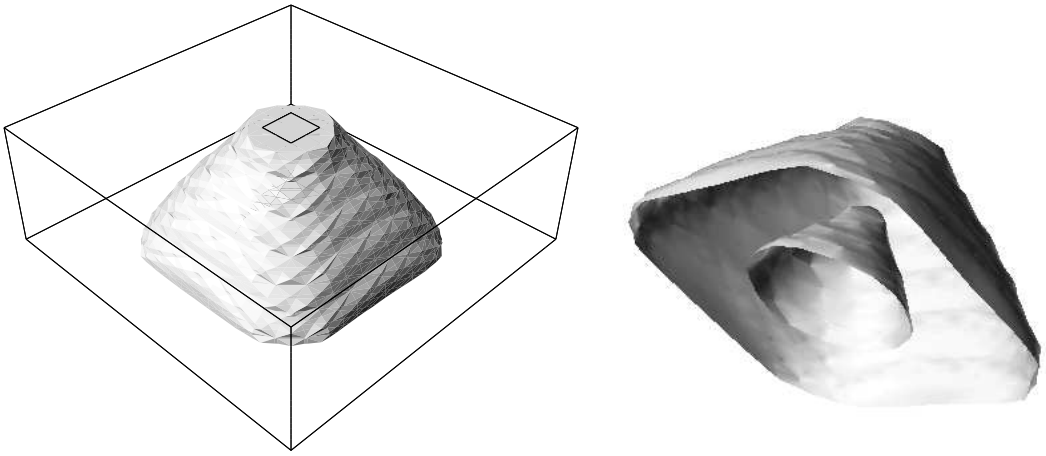

FIG. 3.22 – The optimal shape for the first eigenvalue in a big domain (left) and its boundary (right).

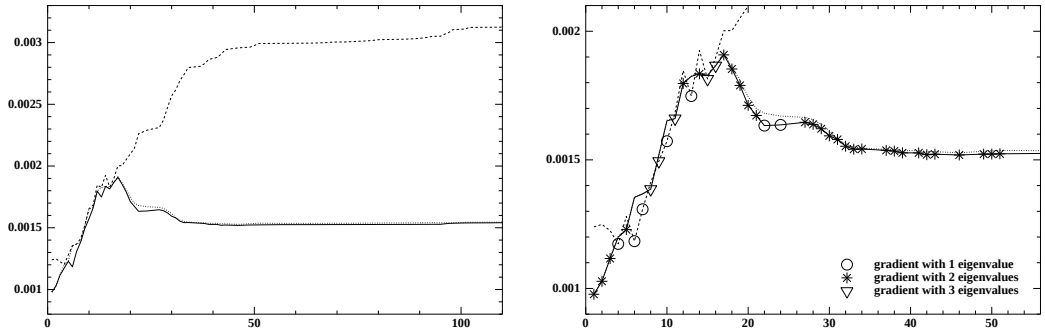

FIG. 3.23 – Evolution of the three smallest eigenvalue (left) and an interpretation (right) for the big domain.

the plane $z = 0$ and four cells on the middle of the plane $z = 1$ are not subject to optimization and are 50 times heavier (see figure 3.21). Since the domain is symmetric, the shapes are expected to keep a first eigenvalue of dimension at least 2 along the iterations. The Young's modulus is set to 1 and Poisson ratio to 0.3. In the void, the density ρ is set to 0 and the parameter ε is equal to 10^{-5}. The second problem is the same than the first except that the rectangle is of dimension $0.6 \times 0.6 \times 1$ (discretized by a $15 \times 15 \times 43$ mesh) with a mass tip that is 200 times heavier . The second problem will be called in this section the 'narrow domain' problem.

$\diamond$ **Discussion about the big domain problem** The Lagrange multiplier being set to 5.3×10^{-8}, figure 3.23 is a display of the evolution of the three

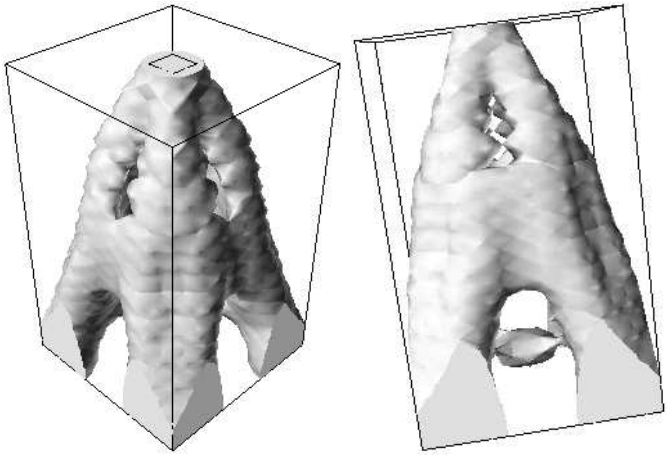

FIG. 3.24 – The optimal shape for the first eigenvalue in a narrow domain (isovalue 0.2 of the density is drawn).

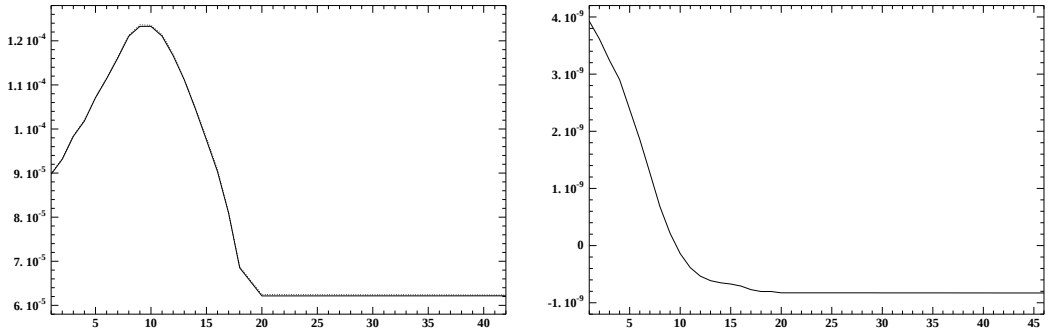

FIG. 3.25 – Evolution of the two smallest eigenvalue (left) and the objective function (right) for the narrow domain.

smallest eigenvalues. There is one eigenvalue that is always (except on iterations 22 to 28) of multiplicity two and one which is of multiplicity one. The eigenvalue of multiplicity one corresponds to an eigenvector which is localized on the heavy cells and that interfere in the optimization process. The figure on the left of figure 3.23 shows the evolution of the eigenvalues. On each iteration, the value of d the dimension of the subspace of the first eigenvalue is shown. The expected behavior of the algorithm can be verified.

◇ **Discussion about the narrow domain problem** As can be seen on figure 3.25 (left), the global evolution of the algorithm is as follows : First reinforce the structure so that the first eigenvalue raises and then optimize the weight of the structure. The Lagrange multiplier is set to 10^{-8} for this example.

◇ **Discussion about the symmetries** None of the two problems give rise to radially-symmetrical shapes. For the narrow-domain problem it can be easily understood by the fact that the shape is constrained into a box. For the big-domain problem one can advance an explanation based on a mesh-effect. But it is known that there exist symmetric problem whose solutions do not respect the symmetries. We still do not know if the optimal shape is or is not radially-symmetric for this problem.

3.6.2 The short cantilever

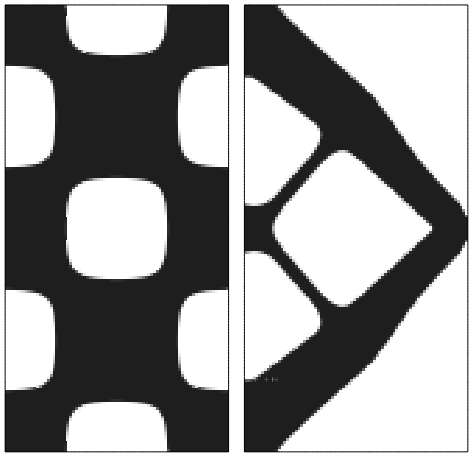

FIG. 3.26 – Initialization and optimal shape for the first eigenvalue of a short cantilever.

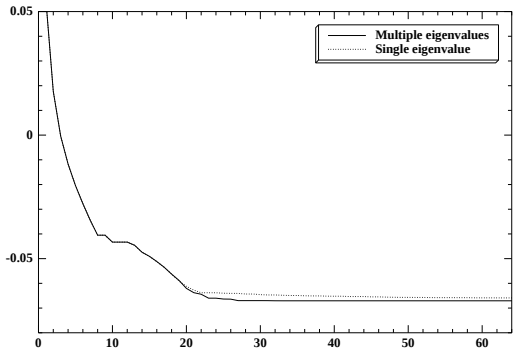

FIG. 3.27 – Evolution of the objective function for the two different methods.

We run our algorithm on a vibrating cantilever that is the same test case than

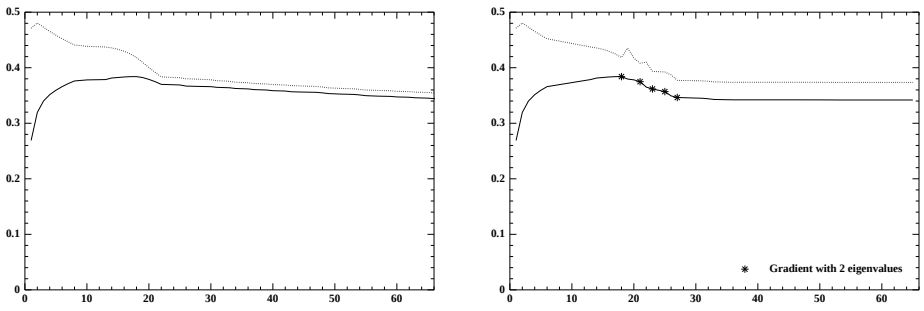

FIG. 3.28 – Evolution of the two smallest eigenvalues for the Single eigenvalue optimization (left) and the Multiple eigenvalue optimization (right).

the one of section 3.4.3 except that the working domain is of size 1×2 discretized with a regular 80×160 mesh. The other parameters that have changed are the Lagrange multiplier which is set to 0.3 and the heavier mass which has a density 80 times heavier. This test case was introduced in [AJ05] where the authors pointed out the appearance of multiple eigenvalues. It is not the exact same test, because when the test of [AJ05] has been run, the improvement of the multiple eigenvalue method were not as obvious as in the test presented here.

The test is run with the standard single eigenvalue optimization (only one eigenvalue is taken in account during optimization) and the multiple eigenvalue optimization processes. Figure 3.27 shows the evolution of the objectives functions for the two different processes.

At iteration n, the algorithm considers an eigenvalue to be of multiplicity d if and only if the relative differences $\gamma_d/\gamma_1 - 1 \leq \epsilon_0 < \gamma_{d+1}/\gamma_1 - 1$. Where ε_0 is a user-defined criterion. If the shape computed at iteration $n+1$ is not better than the shape computed at iteration n and if the eigenvalue at iteration n is multiple then the parameter ε_0 is decreased. The parameter ε_0 is set to 10 percent at the beginning of the optimization process. This explains the behavior of the algorithm in Figure 3.28 (right).

It can be seen in Figure 3.28 (left) that when the first eigenvalue is considered to be always of multiplicity one, the two first eigenvalues have a tendency to merge and the algorithm cannot improve the shape. If we follow the branches of eigenvalues according to the modes, we would see that the smallest eigenvalue does not correspond to the same modes during optimization. ie, the algorithm optimizes one mode at iteration n and an other one at iteration $n+1$. This is standard of optimization with respect to a maximum of a function when the maximum is multiple and it is well-known to slow down the algorithm.

Chapitre 4

The direct problem of the robust compliance

Abstract

We define and study in this chapter the problem of the robust compliance when the domain is fixed. The existence of a worst perturbation is proved, a characterization of the set of worst perturbations is given and a stable algorithm based on a Newton method that computes that set is proposed.

4.1 Motivation 72
4.2 The problem 73
4.2.1 Setting 73
4.2.2 Equivalent formulation 74
4.2.3 An overview of chapter 4 75
4.3 The maximum is a critical value 76
4.3.1 The maximum is attained 77
4.3.2 The maximum is a critical value 77
4.4 The critical point problem 78
4.4.1 The Fredholm alternative 78
4.4.2 The set of critical points 80
4.5 Finding ρ^* 81
4.5.1 Restriction on the maximizers 81
4.5.2 The function g 82
4.6 An algorithm 85
4.6.1 A stable algorithm 85
4.6.2 Bounds on s 86
4.7 Numerical results 88
4.7.1 Monotonic properties 88
4.7.2 Non-dependency of the bounds with respect to the mesh 90

4.1 Motivation

We set our model problem in linearized elasticity. Let $\Omega \subset \mathbb{R}^d$ ($d = 2$ or 3) be a bounded open set occupied by a linear isotropic elastic material with Hooke's law A. Recall that, for any symmetric matrix ξ, A is defined by

$$A\xi = 2\mu\xi + \lambda\big(\mathrm{Tr}\xi\big)\mathbb{I}\mathrm{d},$$

where μ and λ are the Lamé moduli of the material.

According to variational theory, u is also a maximizer over $H^1_D(\Omega)^d$ of the functional

$$v \mapsto E_\Omega(v, \mathbf{f}) = -\int_\Omega A\, e(v) \cdot e(v)\, dx + 2\int_\Omega \mathbf{f_1} \cdot v\, dx + 2\int_{\Gamma_N} \mathbf{f_2} \cdot v\, ds \qquad (4.1)$$

Where $\mathbf{f}$ denotes $(\mathbf{f_1}, \mathbf{f_2})$ the set of source terms. The value of the latest maximum $C_\Omega(\mathbf{f}) = \max_u E_\Omega(u, \mathbf{f})$ is called the compliance. The compliance $C_\Omega(\mathbf{f})$ is a good measurement of the stiffness of the structure Ω submitted to the loads $\mathbf{f}$. Thus a classical problem in shape optimization is to find the domain Ω_0 that minimizes $C_\Omega(\mathbf{f})$ with a volume constraint.

But if a shape is optimized with respect to one load, it has no reason to be stable with respect to perturbation of that load, as can be seen in the following example : For a structure fixed on its bottom part, and a vertical load at the top, the optimal shape is a beam but it has no engineering interest because a small perturbation would drastically increase the energy. See figure 4.1 (left) for the a-priori design of the optimal shape and figure 4.1 (right) for the a-priori worst perturbation.

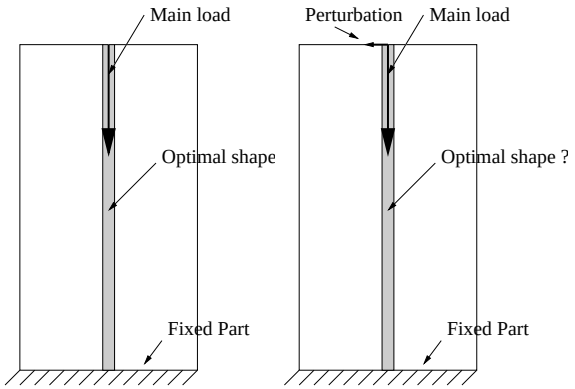

FIG. 4.1 – The model example

We thus propose to optimize with respect to the domain the so-called "robust compliance" or "worst-case problem". It reads

$$\mathcal{J}_{rob}(\Omega) = \sup_{g \text{ perturbation}} C_\Omega(\mathbf{f} + g) \qquad (4.2)$$

The set of admissible perturbations must be made precise, as an example we consider $g = (g_1, g_2)$ with $g_1 = \chi s$, $g_2 = 0$ and $\|s\|_{L^2(\Omega)^d} \leq m$ where χ is the characteristic function of a smooth subset U of Ω. Other choices are of course possible.

This problem is solved in two steps, first the direct problem is studied, ie : we study, characterize the maximizers of (4.2) and we compute $\sup_g C_\Omega(\mathbf{f} + g)$ when Ω is fixed. This is done in chapter 4. Then we will be able to perform shape optimization with respect to this criteria in chapter 5

The most advanced result in this field is [CC03] and the references therein where the authors introduced the term "principal compliance" for what we denote here "robust compliance". In [CC03], the authors proved the existence of a worst perturbation for a broader class of type of perturbation, but their result are, naturally, less sharp than those presented here.

4.2 The problem

4.2.1 Setting

At first, notations are introduced for the sake of generality and conciseness.
$\diamond$ Let V and H be two Hilbert spaces such that V is compactly and densely embedded in H. We denote as $(\cdot, \cdot)$ the dual product on V and V'. Because H is identified with its dual, the scalar product of H is also denoted $(\cdot, \cdot)$. The norm in V is denoted by $\|\cdot\|_V$ and the subscript is dropped for the norm of H.
$\diamond$ Let $\mathbf{A} : V \to V'$ be a linear coercive, bounded symmetric operator, $\mathbf{f} \in V'$ and define the energy as : $E(v, \mathbf{f}) = -(\mathbf{A}v, v) + 2(\mathbf{f}, v)$
$\diamond$ Let $\mathbf{B} : H \to H$ be a continuous linear operator that characterizes the location of the perturbation and $\mathbf{B}^*$ its adjoint. The condition for $\mathbf{g}$ to be a perturbation is $\mathbf{g} = \mathbf{B}^* s$ with $\|s\| \leq m$.

Definition 4.2.1 *The robust compliance $\mathcal{J}_{rob}$ is equal to*

$$\mathcal{J}_{rob} = \sup_{\substack{\mathbf{g}=\mathbf{B}^* s \\ \|s\| \leq m}} \max_u E(u, \mathbf{f} + \mathbf{g})$$

The link with the Introduction of chapter 4.1 is the following :

$$V = H^1_D(\Omega)^d \quad H = L^2(\Omega)^d \quad V' = H^{-1}(\Omega)^d \times H^{-1/2}(\Gamma_N)^d$$

$\diamond$ $\mathbf{A}$ is the operator such that $(\mathbf{A}v, w) = \int_\Omega A\, e(v) \cdot e(w)\, dx$
$\diamond$ $\mathbf{f}$ is the element of V' such that $(\mathbf{f}, v) = \int_\Omega \mathbf{f_1} \cdot v\, dx + \int_{\Gamma_N} \mathbf{f_2} \cdot v\, ds$
$\diamond$ $\mathbf{B} = \mathbf{B}^*$ is the multiplication by the characteristic function χ

Remark 4.2.1 $\mathbf{B}$ *could have been chosen in a different way : Let S be an arbitrary Hilbert space and $\mathbf{B}^* : S \mapsto V'$ so that $\mathbf{B} : V \mapsto S'$. As long as $\mathbf{B}^*\mathbf{B} : V \mapsto V'$ is continuous and compact, then the following development*

stands with obvious changes. In this case, the perturbation are defined as $\mathbf{g} = \mathbf{B}^* s$ *with* $\|s\|_S \leq m$. *In the elasticity setting, it allows to deal with perturbations of the form* $\mathbf{g} = s|_\Gamma$ *with* $\|s\|_{L^2(\Gamma)} \leq m$, *where* Γ *denotes a smooth subset of the boundary of* Ω.

4.2.2 Equivalent formulation

The functional $\mathcal{J}_{rob}$ is defined as two maximums, one on the u variable and one on the s variable. They can be inverted and solved in one of the variables to give rise to a non-linear problem in the other variable. There is thus several equivalent formulations of the same problem, we can work with the s or with the u variable :

Proposition 4.2.1
Let $F(u) = -(\mathbf{A}u, u) + 2(\mathbf{f}, u) + m\|\mathbf{B}u\|$ *and* $G(s) = (\mathbf{f} + \mathbf{B}^* s, \mathbf{A}^{-1}(\mathbf{f} + \mathbf{B}^* s))$ *we have :*

$$\sup_{u \in V} F(u) = \mathcal{J}_{rob} = \sup_{\|s\| \leq m} G(s)$$

Proof (Of the formulation in u)

$$\begin{aligned} \sup_{\substack{\mathbf{g}=\mathbf{B}^* s \\ \|s\| \leq m}} \max_u E(u, \mathbf{f} + \mathbf{g}) &= \sup_u \sup_{\substack{\mathbf{g}=\mathbf{B}^* s \\ \|s\| \leq m}} E(u, \mathbf{f} + \mathbf{g}) \\ &= \sup_u -(\mathbf{A}u, u) + 2(\mathbf{f}, u) + 2 \sup_{\substack{\mathbf{g}=\mathbf{B}^* s \\ \|s\| \leq m}} (\mathbf{g}, u) \end{aligned}$$

The latest supremum is then equal to

$$\sup_{\|s\| \leq m} (\mathbf{B}^* s, u) = \sup_{\|s\| \leq m} (s, \mathbf{B}u)$$

Thanks to Cauchy-Schwarz, this maximum is attained by $s = \frac{m}{\|\mathbf{B}u\|}\mathbf{B}u$. The problem to study is then

$$\sup_{u \in V} F(u) \quad \text{where} \quad F(u) = -(\mathbf{A}u, u) + 2(\mathbf{f}, u) + 2m\|\mathbf{B}u\| \tag{4.3}$$

The formulation in s is done the same way, by finding the optimal $u = \mathbf{A}^{-1}(\mathbf{f} + \mathbf{B}^* s)$ for any given s. □

The problem : $\sup_{\|s\| \leq m} (\mathbf{f} + \mathbf{B}^* s, \mathbf{A}^{-1}(\mathbf{f} + \mathbf{B}^* s))$ is a quadratic problem in s with norm-constraints, ie a trust-region problem. Despite the impressive literature on trust-region problems, the proof of existence of the maximizers for the infinite dimensional case does not seem to exist. Indeed the proof of existence and computation of the maximizers of a trust-region problem relies on a duality approach for which there is no gap of duality. The proof of absence of gap relies on the so-called S procedure which is a pure finite-dimensional method (see [VB96] for this approach an all the references herein). In all the papers

dealing with trust-region problems it does not seem that an infinite-dimensional technique could be applied.

In the trust-region setting, it also does not seem easy to calculate the bounds of section 4.6.2 and the algorithm for calculating the maximizers is harder to put in place. Essentially because, in numerical programming, we never get access to the matrix $\mathbf{A}^{-1}$ but only to the product $\mathbf{A}^{-1}v$ for any v (see [Bri98] for trust-region algorithms).

That is why the formulation in u is chosen here. The problem reads :

$$\text{Solve} \quad \sup_{u\in V} F(u) \quad \text{with} \quad F(u) = -(\mathbf{A}u, u) + 2(\mathbf{f}, u) + 2m\|\mathbf{B}u\| \tag{4.4}$$

Nevertheless, there is a correspondence between trust-region problems and the robust compliance problem. The results advanced in papers dealing with trust-region problems will match the result proven here.

Remark 4.2.2 *Setting $m = 0$ in problem 4.4 leads to the standard problem of compliance and setting $\mathbf{f} = 0$ leads to an eigenvalue problem (the so-called Auchmuty variational principle [Auc89]). There is uniqueness of the maximizers in the first case but not in the second. This difference will be seen in the characterization of the maximizers. The problem of robust optimization can be interpreted as a mix between the standard linear equation and the eigenvalue problem.*

4.2.3 An overview of chapter 4

It must be born in mind that the functional F may admit local maximizers (see appendix A). Thus the need for a special technique in order to characterize (and compute) the global maximizers. Indeed, usual techniques as fixed point methods will not allow stable calculation of the maximum. The approach chosen here is the following :

◇ **Prove that the maximum is a critical point :** The first thing that has to be done in studying this maximum problem is to prove that the maximum is attained (section 4.3.1) and attained by points where $F(u) = -(\mathbf{A}u, u) + 2(\mathbf{f}, u) + 2m\|\mathbf{B}u\|$ is differentiable (ie $\mathbf{B}u \neq 0$) (section 4.3.2). The critical point equation will then be :

$$\mathbf{A}u = \mathbf{f} + \rho\mathbf{B}^*\mathbf{B}u \tag{4.5}$$

$$\rho\|\mathbf{B}u\| = m \tag{4.6}$$

Throughout the paper, the critical points of F are understood as a couple (u, ρ) that obeys to equation (4.5) and (4.6)

◇ **Characterize the critical points :** When ρ is given, Section 4.4.1 solves problem (4.5) and (4.6) by finding -if they exist- every corresponding u. Section 4.4.2, characterizes $Y_1 \cup Y_2$ the set of ρ for which such a u exists

◇ **Amongst the critical points, choose the ones that can be maximizers :** Section 4.5 is devoted to finding the ρ in $Y_1 \cup Y_2$ that gives rise to a

u that is a maximizer of F and not only a critical point. In fact such a ρ is to be proved unique and the smallest element of $Y_1 \cup Y_2$ (in section 4.5.1). Section 4.5.2 is devoted to characterizing $\min Y_1 \cup Y_2$

Statement of the result

Each implicit assertion of this section is to be demonstrated later

Definition 4.2.2 *Consider the generalized eigenproblem* $\mathbf{A}u = \rho\mathbf{B}^*\mathbf{B}u$
$\diamond$ *Let* $E_\rho = ker(\mathbf{A} - \rho\mathbf{B}^*\mathbf{B})$ *be the eigenspaces*
$\diamond$ *Let* $Sp(\mathbf{A}, \mathbf{B}) = \{\rho \text{ st } E_\rho \neq \{0\}\}$ *be the set of eigenvalues*
$\diamond$ *Let* $\lambda_1 = min\{\lambda \in Sp(\mathbf{A}, \mathbf{B})\}$ *be the smallest eigenvalue*

Definition 4.2.3 (cf Fredholm alternative) *For a given* ρ *such that* $\mathbf{f} \perp E_\rho$, *let* u_ρ *be the unique solution to*

$$\begin{aligned} \mathbf{A}u_\rho &= \mathbf{f} + \rho\mathbf{B}^*\mathbf{B}u_\rho \\ \mathbf{A}u_\rho &\in (E_\rho)^\perp \end{aligned}$$

Theorem 4.2.2 (Robust optimization) *Define the functional* F *as*

$$F(u) = -(\mathbf{A}u, u) + 2(\mathbf{f}, u) + 2m\|\mathbf{B}u\|$$

- *If* $\mathbf{f} \perp E_{\lambda_1}$ *and if* $\lambda_1\|\mathbf{B}u_{\lambda_1}\| \leq m$, *then the set of maximizers of* F *over* V *is exactly*

$$\{u_{\lambda_1} + v \text{ s.t. } v \in E_{\lambda_1} \text{ and } \lambda_1(\|\mathbf{B}v\| + \|\mathbf{B}u_{\lambda_1}\|) = m\}$$

- *If the above conditions are not met then the set of maximizers of* F *is exactly* $\{u_s\}$. *Where*
  - s *is the unique real* $\in]0, \lambda_1[$ *such that* $s\|\mathbf{B}u_s\| = m$
  - s *is the only critical point on* $]0, \lambda_1[$ *of the convex function*

$$\rho \mapsto (\mathbf{f}, u_\rho) + \frac{m^2}{\rho}$$

4.3 The maximum is a critical value

Before working on the critical point problem, it must be shown that the maximum is indeed attained (section 4.3.1) and that the maximum cannot be attained by a point where F is not differentiable, ie on the kernel of $\mathbf{B}^*\mathbf{B}$ (section 4.3.2).

4.3.1 The maximum is attained

Proposition 4.3.1
◇ *There exist* $u^* \in V$ *such that* $F(u^*) = \sup_{u \in V} F(u)$
◇ *Any maximizer* u^* *of* F *on* V *satisfies* $\|u\|_V < 2\frac{\|f\|+m\|\mathbf{B}\|}{\nu}$ *where* ν *is the coercivity constant of* $\mathbf{A}$

Proof
◇ **Coercivity of** $-F$ **:** Because of the coercivity of $\mathbf{A}$, $\exists \nu$ s.t $(\mathbf{A}u, u) \geq \nu \|u\|_V^2$ and then

$$F(u) \leq -\nu \|u\|_V{}^2 + 2\|\mathbf{f}\|_{V'}\|u\|_V + 2m\|\mathbf{B}\|\|u\|_V$$

Therefore there exists $\gamma = 2\frac{\|\mathbf{f}\|+m\|\mathbf{B}\|}{\nu} > 0$ such that $F(u)$ is negative outside the ball $B(0,\gamma)$, the ball centered in 0 of radius γ. Because $F(0) = 0$ then the maximum is attained inside this very ball.
◇ **Upper semi-continuity of** F **:** Let $(u_n)_n$ be a sequence that weakly converges to u^* for the V topology. Because of the compact inclusion from V to H , $(u_n)_n$ is strongly convergent in H. We then have

- $(\mathbf{f}, u_n)_{(V',V)} \mapsto (\mathbf{f}, u^*)$ because $u_n \rightharpoonup u^*$ in V
- $\|\mathbf{B}u_n\| \mapsto \|\mathbf{B}u^*\|$ because $\mathbf{B} : H \to H$ is continuous and $u_n \mapsto u^*$ in H
- $\liminf(\mathbf{A}u_n, u_n) \geq (\mathbf{A}u^*, u^*)$ because $u_n \rightharpoonup u^*$ in V and $(\mathbf{A}\cdot, \cdot)$ is equivalent to a norm in V

So that $\limsup F(u_n) \leq F(u^*)$
◇ **Conclusion :** It is now classical to show that the maximum is attained, let $(u_n)_n$ be a maximizing sequence of F, ie $F(u_n) \to \max_{u \in H} F(u)$. Let $\varepsilon > 0$. Because of the coercivity, it can be assumed that up to a subsequence $\|u_n\|_V < \gamma + \varepsilon$ for all n. So $(u_n)_n$ is bounded in the V-norm, is (up to a subsequence) weakly convergent to an u^* in the V-topology. Because of the upper semi-continuity, $\limsup F(u_n) \leq F(u^*)$ And because u_n is a maximizing sequence, then u^* is a maximizer. So the maximum is attained □

4.3.2 The maximum is a critical value

The functional $F(u) = -(\mathbf{A}u, u) + 2(\mathbf{f}, u) + 2m\|\mathbf{B}u\|$ is differentiable on $V \setminus Ker(\mathbf{B}^*\mathbf{B})$. The set of critical values is given by the equation

$$\mathbf{A}u = \mathbf{f} + \frac{m}{\|\mathbf{B}u\|}\mathbf{B}^*\mathbf{B}u \tag{4.7}$$

It must now be shown that the maximum cannot be attained by a point where F is non-differentiable, ie on $Ker(\mathbf{B}^*\mathbf{B})$.

Proposition 4.3.2 *If* $\mathbf{B}$ *is not equal to* 0 *on* V*, then there is no maximizer of* F *on* $Ker(\mathbf{B}^*\mathbf{B})$

Proof If $r \in Ker(\mathbf{B}^*\mathbf{B})$ is a maximizer of F then

$$F(r) = -(\mathbf{A}r, r) + 2(\mathbf{f}, r) \leq (\mathbf{f}, \mathbf{A}^{-1}\mathbf{f}) \leq (\mathbf{f}, \mathbf{A}^{-1}\mathbf{f}) + 2m\|\mathbf{B}\mathbf{A}^{-1}\mathbf{f}\| = F(\mathbf{A}^{-1}\mathbf{f})$$

Because r is a maximizer of F, the inequalities are in fact equalities and $r = \mathbf{A}^{-1}\mathbf{f} \in Ker(\mathbf{B}^*\mathbf{B})$

In order to construct an u such that $F(u) > F(r)$, recall that when $\mathbf{B}$ is not equal to 0 on V, then $Ker(\mathbf{B}^*\mathbf{B}) \cap V$ is a closed proper subset of V and there exists an $u^\perp \in [Ker(\mathbf{B}^*\mathbf{B}) \cap V]^\perp$ which is not equal to 0. Let $u = r + tu^\perp$, with $r = \mathbf{A}^{-1}\mathbf{f} \in Ker(\mathbf{B}^*\mathbf{B}) \cap V$ then

$$F(u) = F(r) + 2m|t|\|\mathbf{B}u^\perp\| - t^2(u^\perp, \mathbf{A}u^\perp)$$

With t being small enough , and because $u^\perp \in [Ker(\mathbf{B}^*\mathbf{B}) \cap V]^\perp \Rightarrow \|\mathbf{B}u^\perp\| \neq 0$, there exists an u st $F(u) > F(r)$ which is a contradiction □

Remark 4.3.1 *It will be useful later to remark that for every critical point*

$$F(u) = (\mathbf{f}, u) + m\|\mathbf{B}u\|$$

4.4 The critical point problem

This section is devoted to the computation of the set of critical points of F, ie the set of (u, ρ) solution to equations (4.5) and (4.6)

4.4.1 The Fredholm alternative

For a given ρ, solving equation (4.5) is quite classical. The problem of finding u such that $\mathbf{A}u = \mathbf{f} + \rho\mathbf{B}^*\mathbf{B}u$ is a quite straightforward application of the Fredholm alternative, the result reads :

Proposition 4.4.1 *Define the eigenspaces as $E_\lambda = ker(\mathbf{A} - \lambda\mathbf{B}^*\mathbf{B})$ and the spectrum as $Sp(\mathbf{A}, \mathbf{B}) = \{\lambda \in \mathbb{R} \text{ s.t. } E_\lambda \neq \{0\}\}$*

For any $\mathbf{f} \in V'$ and $\rho \in \mathbb{R}$, consider the following equation in u :

$$(\mathbf{A} - \rho\mathbf{B}^*\mathbf{B})u = \mathbf{f}$$

The set of solutions is given by Fredholm alternative which reads

-if $\rho \notin Sp(\mathbf{A}, \mathbf{B})$ then *there exist a unique solution $\{u_\rho\}$*
-if $\rho \in Sp(\mathbf{A}, \mathbf{B})$ then *· if $\mathbf{f} \not\perp E_\rho$ then there is no solution*
· if $\mathbf{f} \perp E_\rho$ then the set of solutions is $\{u_\rho\} + E_\rho$

Where in the last case u_ρ is chosen as the unique normalized solution, ie $\mathbf{A}u_\rho \in (E_\rho)^\perp$

Proof The trick is to shift the problem into finding $\mathbf{A}^{1/2}u$ such that

$$(1 - \rho\mathbf{A}^{-1/2}\mathbf{B}^*\mathbf{B}\mathbf{A}^{-1/2})\mathbf{A}^{1/2}u = \mathbf{A}^{-1/2}\mathbf{f}$$

which is a problem posed in the Hilbert space H.

Because $\Lambda = \mathbf{A}^{-1/2}\mathbf{B}^*\mathbf{B}\mathbf{A}^{-1/2}$ is a compact self-adjoint operator from H onto H, Λ admits an orthonormalized eigenbasis of H. This eigenbasis is orthogonal for Λ and the corresponding eigenvalues is a denumerable sequence that converge to 0. Each eigenspace (except maybe for the kernel of Λ) is of finite dimension. Once shifted, the solution to equation (4.5) obeys the Fredholm alternative which is proposition 4.4.1. □

Remark 4.4.1 *The definition of* $\mathbf{A}^{1/2}$ *may be quite subtle if* $\mathbf{A}$ *is considered as an operator* $V \to V'$*. It is easier to understand* $\mathbf{A}$ *as an unbounded operator form* $H \to H$ *and to take* $\mathbf{f} \in H$*.*

The decomposition of Λ into its eigenspaces will come in handy. Shifted back in terms of $\mathbf{A}$ and $\mathbf{B}$ this decomposition is stated in proposition 4.4.2. On the base of eigenvectors of Λ, u_ρ can be expressed as in proposition 4.4.3. This analytical expression of u_ρ will be helpful in section 4.5.2

Proposition 4.4.2 *There exist* I_1 *and* I_2 *two complementary subsets of* $\mathbb{N}$ *and there exist* $(\lambda_i)_{i\in I_1}$ *an increasing sequence of real positive numbers and there exist* $(e_i)_{i\in\mathbf{N}}$ *a base of* V *such that*

$$\begin{array}{rcccc}
\mathbf{A}e_i & = & \lambda_i\mathbf{B}^*\mathbf{B}e_i & & \forall i \in I_1 \\
\mathbf{B}^*\mathbf{B}e_i & = & 0 & & \forall i \in I_2 \\
(\mathbf{A}e_i, e_j) & = & \delta_{i,j} & & \forall i,j \\
(\mathbf{B}e_i, \mathbf{B}e_j) & = & 0 & \text{if } i \neq j & \forall i,j \\
\mathbf{f} & = & \displaystyle\sum_{i\in\mathbf{N}} \mathbf{f}_i\mathbf{A}e_i & \text{where } \mathbf{f}_i =< \mathbf{f}, e_i >_{<V',V>} & \forall \mathbf{f} \in V'
\end{array}$$

Proposition 4.4.3 *If* $\mathbf{f}_i =< \mathbf{f}, e_i >_{<V',V>}$

$$u_\rho = \sum_{i\in I_1} \frac{\lambda_i \mathbf{f}_i}{\lambda_i - \rho} e_i + \sum_{i\in I_2} \mathbf{f}_i e_i$$

With the convention that if there exist an i *such that* $\rho = \lambda_i$ *then* $\mathbf{f}_i = 0$ *(or else* u_ρ *do not exist) and the corresponding term* $\frac{\lambda_i \mathbf{f}_i}{\lambda_i - \rho}$ *is equal to* 0*.*

Finally, the choice of orthogonalization of u_ρ in the case $\rho \in Sp(\mathbf{A}, \mathbf{B})$ and $\mathbf{f} \perp E_\rho$ of proposition 4.4.1 is driven by the following property :

Lemma 4.4.4 *If* $\rho \in Sp(\mathbf{A}, \mathbf{B})$ *and* $\mathbf{f} \perp E_\rho$ *then* $\forall v \in E_\rho$ *we have*

$$\|\mathbf{B}u_\rho + \mathbf{B}v\| = \|\mathbf{B}u_\rho\| + \|\mathbf{B}v\| \tag{4.8}$$

Proof If $v \in E_\rho$ then $\mathbf{B}^*\mathbf{B}v = \mathbf{A}v/\rho \in \mathbf{A}(E_\rho)$ and the orthogonalization of u_ρ which is $\mathbf{A}u_\rho \in (E_\rho)^\perp$ or equivalently $u_\rho \in \big(\mathbf{A}(E_\rho)\big)^\perp$ leads to

$$0 = (\mathbf{B}^*\mathbf{B}v, u_\rho) = (\mathbf{B}v, \mathbf{B}u_\rho)$$

□

4.4.2 The set of critical points

The goal of this section is to characterize the set of (u, ρ) which satisfies equation (4.5) and (4.6). It shall be born in mind that for a given ρ, the set of u solution to equation (4.5) has been calculated in proposition 4.4.1.

Definition 4.4.1 *Recall the definition of u_ρ in proposition 4.4.1 and let Y_1 and Y_2 be the following two subsets of $\mathbb{R}$*

$$\begin{aligned} Y_1 &= \{\rho \in \mathbb{R} \text{ s.t. } \rho\|\mathbf{B}u_\rho\| = m\} \\ Y_2 &= \{\rho \in Sp(\mathbf{A},\mathbf{B}) \text{ s.t. } \mathbf{f} \perp E_\rho \text{ and } \rho\|\mathbf{B}u_\rho\| \leq m\} \end{aligned}$$

Proposition 4.4.5 *(u, ρ) is a critical point (ie a solution to equations* (4.5) *and* (4.6) *) if and only if*

$$\begin{aligned} u = u_\rho \qquad & \text{and } \rho \in Y_1 \\ \text{or} & \\ u \in \{u_\rho + v \text{ with } v \in E_\rho \text{ and } \rho(\|\mathbf{B}v\| + \|\mathbf{B}u_\rho\|) = m\} \qquad & \text{and } \rho \in Y_2 \end{aligned}$$

Where u_ρ is defined by proposition 4.4.1 *(and recalled in proposition 4.2.3)*

Proof

$\diamond$**Necessary condition :** Let (u, ρ) be a critical point of F ie : $\rho\|\mathbf{B}u\| = m$ (4.6) and $\mathbf{A}u = \mathbf{f} + \rho\mathbf{B}^*\mathbf{B}u$ (4.5)
-If $\rho \notin Sp(\mathbf{A},\mathbf{B})$, then the solution to (4.5) is unique and $u = u_\rho$ (prop 4.4.1) so that $m = \rho\|\mathbf{B}u\| = \rho\|\mathbf{B}u_\rho\|$ and therefore $\rho \in Y_1$
-If $\rho \in Sp(\mathbf{A},\mathbf{B})$, then because u is a solution of (4.5) then $\mathbf{f} \perp E_\rho$ and $\exists v \in E_\rho$ such that $u = u_\rho + v$ (prop 4.4.1). According to proposition 4.4.4, $\|\mathbf{B}u\| = \|\mathbf{B}u_\rho\| + \|\mathbf{B}v\|$. So that equation 4.6, $\rho\|\mathbf{B}u\| = m$ implies $\rho\|\mathbf{B}u_\rho\| \leq m$ and therefore ρ belongs to Y_2.

$\diamond$ **Sufficient condition :**
-If $\rho \in Y_2$, let $u = u_\rho + v$ where $v \in E_\rho$ and $\|\mathbf{B}v\| = m/\rho - \|\mathbf{B}u_\rho\|$ then $\mathbf{A}u = \mathbf{f} + \rho u$ and $\rho = m/(\|\mathbf{B}u_\rho\| + \|\mathbf{B}v\|) = m/\|\mathbf{B}u\|$. So that u is a solution to equation (4.5) and $\rho\|\mathbf{B}u\| = m$.
-Finally if $\rho \in Y_1$ the demonstration is straightforward $\square$

We can now state a corollary which shows that if (u, ρ) is a critical point of F, then the value of $F(u)$ only depends on ρ

Corollary 4.4.6 *If (u, ρ) is a critical point of F, then the value of $F(u)$ depends only on ρ by*

$$F(u) = (\mathbf{f}, u_\rho) + m^2/\rho$$

Where u_ρ is defined by ρ in proposition 4.4.1

Proof If (u, ρ) is a critical point of F then equation (4.5) gives $F(u) = -(\mathbf{A}u, u) + 2(\mathbf{f}, u) + 2m\|\mathbf{B}u\| = (\mathbf{f}, u) + m\|\mathbf{B}u\|$. Using the characterization

of the critical points in proposition 4.4.5
$\diamond$ If $u = u_\rho$ and $\rho \in Y_1$ then $\rho\|\mathbf{B}u\| = m$ so that

$$F(u) = (\mathbf{f}, u) + m\|\mathbf{B}u\| = (\mathbf{f}, u_\rho) + m^2/\rho$$

$\diamond$ If $u = u_\rho + v$ with $v \in E_\rho$ and $\|\mathbf{B}u\| = m/\rho$ and $\rho \in Y_2$ then

$$F(u) = (\mathbf{f}, u) + m\|\mathbf{B}u\| = (\mathbf{f}, u_\rho + v) + m\|\mathbf{B}u\| = (\mathbf{f}, u_\rho) + m^2/\rho$$

because $\mathbf{f} \perp E_\rho$ (proposition 4.4.1) $\square$

4.5 Finding ρ^*

4.5.1 Restriction on the maximizers

By corollary 4.4.6 it is known that the value of F on a critical point (u, ρ) only depends of the value of ρ. This section shows that ρ must be taken the smallest possible.

Proposition 4.5.1 *For all (u_1, ρ_1) and (u_2, ρ_2) critical points of F we have*

$$F(u_1) \geq F(u_2) \Longleftrightarrow \rho_1 \leq \rho_2$$

and equality in one of the inequalities implies equality in the other.
Therefore the only possible maximizers are the (u, ρ^*) critical points such that $\rho^* = \min Y_1 \cup Y_2$. Once ρ^* is found, proposition 4.4.5 gives the adequate u

Proof Let u_1 and u_2 be two critical points of F. The following equations hold :

$$\mathbf{A}u_i = \mathbf{f} + \frac{m}{\|\mathbf{B}u_i\|}\mathbf{B}^*\mathbf{B}u_i \tag{4.9}$$

$$F(u_i) = (\mathbf{f}, u_i) + m\|\mathbf{B}u_i\| \tag{4.10}$$

Using the symmetry of the $\mathbf{A}$ and $\mathbf{B}^*\mathbf{B}$ operators and equation (4.9) we obtain

$$(\mathbf{f}, u_2) + \frac{m}{\|\mathbf{B}u_1\|}(\mathbf{B}^*\mathbf{B}u_1, u_2) = (\mathbf{A}u_2, u_1) = (\mathbf{f}, u_1) + \frac{m}{\|\mathbf{B}u_2\|}(\mathbf{B}^*\mathbf{B}u_2, u_1) \tag{4.11}$$

ie :

$$(\mathbf{f}, u_1 - u_2) = m\frac{\|\mathbf{B}u_2\| - \|\mathbf{B}u_1\|}{\|\mathbf{B}u_1\|\|\mathbf{B}u_2\|}(\mathbf{B}^*\mathbf{B}u_1, u_2) \tag{4.12}$$

Using equations (4.12) and (4.10)

$$\begin{aligned} F(u_1) - F(u_2) &= (\mathbf{f}, u_1 - u_2) + m\|\mathbf{B}u_1\| - m\|\mathbf{B}u_2\| \\ &= m\frac{\|\mathbf{B}u_2\| - \|\mathbf{B}u_1\|}{\|\mathbf{B}u_1\|\|\mathbf{B}u_2\|}[(\mathbf{B}u_1, \mathbf{B}u_2) - \|\mathbf{B}u_1\|\|\mathbf{B}u_2\|] \end{aligned}$$

Thanks to Cauchy-Schwarz inequality , $(\mathbf{B}u_1, \mathbf{B}u_2) - \|\mathbf{B}u_1\|\|\mathbf{B}u_2\| \leq 0$ and is equal to 0 if and only if $\exists \alpha > 0$ such that $\mathbf{B}u_1 = \alpha \mathbf{B}u_2$ (the case $\alpha = 0$ is forbidden by proposition 4.3.2) . In this case using equations (4.9) :

$$\mathbf{A}(u_1 - u_2) = \frac{m}{\alpha \|\mathbf{B}u_2\|} \alpha \mathbf{B}^* \mathbf{B}u_2 - \frac{m}{\|\mathbf{B}u_2\|} \mathbf{B}^* \mathbf{B}u_2 = 0$$

Thus $u_1 = u_2$ and $\alpha = 1$ so that the term $(\mathbf{B}u_1, \mathbf{B}u_2) - \|\mathbf{B}u_1\|\|\mathbf{B}u_2\|$ is equal to 0 if and only if $u_1 = u_2$. We therefore have proved that

$$F(u_1) > F(u_2) \Longleftrightarrow \|\mathbf{B}u_1\| > \|\mathbf{B}u_2\| \text{ and } F(u_1) = F(u_2) \Longleftrightarrow \|\mathbf{B}u_1\| = \|\mathbf{B}u_2\|$$

To conclude, it is sufficient to recall that $\rho_1 \|\mathbf{B}u_1\| = m = \rho_2 \|\mathbf{B}u_2\|$ (see equation (4.6))

□

4.5.2 The function g

Recalling proposition 4.5.1, we now want to characterize $\rho^* = \min Y_1 \cup Y_2$, the only value of ρ which can give rise to a maximizer. For that purpose, we use an auxiliary function g

Definition 4.5.1 *Define Z, the set of ρ for which the Fredholm alternative 4.4.1 does not admit solutions, i.e.*

$$Z = \{\rho \in Sp(\mathbf{A}, \mathbf{B}) \text{ such that } \mathbf{f} \not\perp E_\rho\} \tag{4.13}$$

and call $\bar{\lambda}$ the smallest element of Z.
Define the auxiliary function g on $\mathbb{R}_+^* \setminus Z$ by

$$g(\rho) = (\mathbf{f}, u_\rho) + m^2/\rho \tag{4.14}$$

Where u_ρ is defined in proposition 4.4.1.

Before achieving the main result (proposition 4.5.3), the following lemma has to be demonstrated

Lemma 4.5.2 *The auxiliary function g is a $C^\infty(\mathbb{R}_+^* \setminus Z)$ function which is convex on $]0, \bar{\lambda}[$. This function g tends to $+\infty$ in 0^+ and $\bar{\lambda}^-$. Its derivative is equal to*

$$g'(\rho) = \|\mathbf{B}u_\rho\|^2 - m^2/\rho^2 \tag{4.15}$$

Proposition 4.5.3 *Define $\rho^* = min Y_1 \cup Y_2$ and s the only critical point of the convex function g on $]0, \bar{\lambda}[$. The following alternative holds*

$$\begin{array}{lll} \textit{IF} & (\mathbf{f} \perp E_{\lambda_1} \textit{ and } g'(\lambda_1) \leq 0) & \textit{THEN} \quad \rho^* = \lambda_1 \\ \textit{ELSE} & \rho^* = s & \end{array}$$

Where $\lambda_1 = \min Sp(\mathbf{A}, \mathbf{B})$ is the smallest eigenvalue of the spectrum as defined in proposition 4.4.1

Proof [Of lemma 4.5.2] Recall the analytical expressions of $\mathbf{f}$ and u_ρ (proposition 4.4.2 and 4.4.3)

$$\mathbf{f} = \sum_{i\in\mathbf{N}} \mathbf{f}_i \mathbf{A} e_i \quad \text{and} \quad u_\rho = \sum_{i\in I_1} \frac{\lambda_i \mathbf{f}_i}{\lambda_i - \rho} e_i + \sum_{i\in I_2} \mathbf{f}_i e_i$$

Using $(\mathbf{A}e_i, e_j) = \delta_{i,j}$ and equation 4.14 for the definition of g, we have

$$g(\rho) = \sum_{i\in I_1} \frac{\lambda_i (\mathbf{f}_i)^2}{\lambda_i - \rho} + \sum_{i\in I_2} (\mathbf{f}_i)^2 + m^2/\rho \tag{4.16}$$

Equation (4.16) then proves the smoothness of g and its behavior as ρ tends to 0^+ or $\bar{\lambda}^-$. Differentiating twice g when given as in equation (4.16) yields :

$$g'(\rho) = \sum_{i\in I_1} \frac{\lambda_i (\mathbf{f}_i)^2}{(\lambda_i - \rho)^2} - m^2/\rho^2 \tag{4.17}$$

$$g''(\rho) = 2\sum_{i\in I_1} \frac{\lambda_i (\mathbf{f}_i)^2}{(\lambda_i - \rho)^3} + 2m^2/\rho^3 \tag{4.18}$$

The convexity on $]0, \bar{\lambda}[$ comes from $\bar{\lambda} = min\{\lambda \in Z\}$ and $\mathbf{f}_i = 0$ if $\lambda_i \notin Z$ (see equation (4.13) of Z).

Expression (4.15) of g' is a simple consequence of equation (4.17) and the following equation which can be obtained from proposition 4.4.2.

$$\mathbf{B}^*\mathbf{B}u_\rho = \sum_{i\in I_1} \frac{\mathbf{f}_i}{\lambda_i - \rho} \mathbf{A} e_i \quad \Rightarrow \|\mathbf{B}u_\rho\|^2 = \sum_{i\in I_1} \frac{\lambda_i (\mathbf{f}_i)^2}{(\lambda_i - \rho)^2}$$

□

Proof [Of proposition 4.5.3] Using $g'(\rho) = \|\mathbf{B}u_\rho\|^2 - m^2/\rho^2$ (equation (4.15)) and the definition 4.4.1 of Y_1 and Y_2 the following characterization of the set $Y_1 \cup Y_2$ holds

$$\begin{aligned} \rho \in Y_1 &\iff g'(\rho) = 0 \\ \rho \in Y_2 &\iff g'(\rho) \leq 0 \text{ and } \rho \in Sp(\mathbf{A}, \mathbf{B}) \setminus Z \end{aligned}$$

Using the convexity of g on $]0, \bar{\lambda}[$, we then have $\min Y_1 = s$.
Due to the convexity of g, any $0 < \rho < s$ verifies $g'(\rho) < 0$. So that $\rho^* = \min Y_1 \cup Y_2$ is not equal to s if and only if $\rho^* = \min Y_2 = \min Sp(\mathbf{A}, \mathbf{B}) \setminus Z$ and $\rho^* < s$. In this case $\min Sp(\mathbf{A}, \mathbf{B}) \setminus Z < s < \bar{\lambda}$. Recall that $\bar{\lambda} = \min Z$ so that ρ^* is not equal to s if and only if $\rho^* = \lambda_1 = \min Sp(\mathbf{A}, \mathbf{B}) \notin Z$ and $\lambda_1 < s$. The condition $\lambda_1 = \min Sp(\mathbf{A}, \mathbf{B}) \notin Z$ is by definition of Z, equivalent to $\mathbf{f} \perp E_{\lambda_1}$
Then ρ^* is not equal to s if and only if $\rho^* = \lambda_1$ and $\lambda_1 < s$ (ie $g'(\lambda_1) < 0$ by convexity) and $\mathbf{f} \perp E_{\lambda_1}$ □

We can now state the theorem advanced in section 4.2.3

Theorem 4.5.4 (Robust optimization) *Define $\rho^* = min Y_1 \cup Y_2$, we have*

– *If* $\mathbf{f} \perp E_{\lambda_1}$ *and* $\lambda_1 \|\mathbf{B}u_{\lambda_1}\| \leq m$ *then* $\rho^* = \lambda_1$ *and the set of maximizer of* F *is exactly*

$$\{u_{\lambda_1} + v \ s.t. \ v \in E_{\lambda_1} \ \text{and} \ \lambda_1 \|\mathbf{B}v\| + \lambda_1 \|\mathbf{B}u_{\lambda_1}\| = m\}$$

– *Else* $\rho^* = s$ *and the set of maximizers of* F *is* $\{u_s\}$

Proof The result is obtained by using proposition 4.5.1 to state that the maximizers of F are the critical point corresponding to $\rho^* = \min Y_1 \cup Y_2$, by using proposition 4.5.3 that characterize ρ^*,by using lemma 4.5.2 to change the condition $g'(\lambda_1) \leq 0$ of proposition 4.5.3 into the condition $\|\mathbf{B}u_{\lambda_1}\| \leq m/\lambda_1$ and finally by using proposition 4.4.5 that characterize the set of critical points of F when ρ^* is given. □

Remark 4.5.1 *It can be seen that* ρ^* *is also equal to the minimum of* g *over* $]0, \lambda_1]$. *For any* $\rho \in]0, \lambda_1]$, *the operator* $\mathbf{A} - \rho \mathbf{B}^*\mathbf{B}$ *being self-adjoint positive, we have :*

$$(\mathbf{A} - \rho \mathbf{B}^*\mathbf{B})u_\rho = \mathbf{f} \Rightarrow (\mathbf{f}, u_\rho) = \max_{u \in V} -(\mathbf{A}u, u) + 2(\mathbf{f}, u) + \rho(\mathbf{B}u, \mathbf{B}u)$$

and $g(\rho) = (\mathbf{f}, u_\rho) + \frac{m^2}{\rho} = \max_{u \in V} -(\mathbf{A}u, u) + 2(\mathbf{f}, u) + \rho(\mathbf{B}u, \mathbf{B}u) + \dfrac{m^2}{\rho}$ *so that*

$$\begin{aligned}
& \min_{\rho \in]0, \lambda_1]} \max_u -(\mathbf{A}u, u) + 2(\mathbf{f}, u) + \rho(\mathbf{B}u, \mathbf{B}u) + \frac{m^2}{\rho} = \min_{\rho \in]0, \lambda_1]} g(\rho) = g(\rho^*) \\
= \ & (\mathbf{f}, u_\rho^*) + \frac{m^2}{\rho^*} = \max_{u \in V} F(u) = \max_{u \in V} -(\mathbf{A}u, u) + 2(\mathbf{f}, u) + \|\mathbf{B}u\| \\
= \ & \max_{u \in V} [-(\mathbf{A}u, u) + 2(\mathbf{f}, u) + \min_{\rho \in \mathbf{R}} [\rho(\mathbf{B}u, \mathbf{B}u) + \frac{m^2}{\rho}]] \\
= \ & \max_{u \in V} \min_{\rho \in \mathbf{R}} -(\mathbf{A}u, u) + 2(\mathbf{f}, u) + \rho(\mathbf{B}u, \mathbf{B}u) + \frac{m^2}{\rho}
\end{aligned}$$

And the theorem is mainly an inversion of a max *and a* min. *Which is in this case a priori forbidden by the lack of concavity in the variable* u.

Remark 4.5.2 $\frac{1}{\rho}$ *is the Lagrange multiplier for the condition* $\|s\| \leq m$. *Indeed*

$$\begin{aligned}
F(u) &= \max_{u \in V} \max_s \min_{\mu \geq 0} -(\mathbf{A}u, u) + 2(\mathbf{f}, u) + 2(\mathbf{B}^*s, u) + \mu[m^2 - (s, s)] \\
&= \max_{u \in V} \min_{\mu \geq 0} -(\mathbf{A}u, u) + 2(\mathbf{f}, u) + \mu m^2 + \max_s [-(s, s)\mu + 2(s, \mathbf{B}u)] \\
&= \max_{u \in V} \min_{\mu \geq 0} -(\mathbf{A}u, u) + 2(\mathbf{f}, u) + \mu m^2 + \frac{(\mathbf{B}u, \mathbf{B}u)}{\mu}
\end{aligned}$$

Which is exactly one of the last line of the remark 4.5.1 with $\mu = \rho^{-1}$. *The fact that* μ *is never equal to* 0 *implies that the condition* $\|s\| \leq m$ *is always qualified.*

Which seems normal a posteriori. The function g is the dual Lagrangian function of the function G defined in proposition 4.2.1. Thus the convexity of g is not a surprise (even if Lagrangian duality cannot be applied here). The fact that $g'(s) = 0 \Longleftrightarrow \rho\|\mathbf{B}u_\rho\| = m$ *is also a standard of Lagrangian duality result.*

4.6 An algorithm

It must be kept in mind that ρ^* may only take two values s (as defined in proposition 4.5.3 as the only critical point on $]0, \bar{\lambda}[$ of the convex function g) and λ_1 (as defined in proposition 4.2.2 as the smallest eigenvalue). So that it is difficult to calculate ρ^* if and only if $\rho^* \neq \lambda_1$ and it is quite hard to think of an algorithm that does not calculate the first eigenvalue in order to check in which case we are.

The standard idea would be to calculate the maximizer of (4.3) by using a standard gradient or fixed-point algorithms. Sadly we can exhibit simple cases where there exists local maxima that are not global (Appendix A). That is why we propose here a stable algorithm that minimize g (a convex function) over the bounded set $]0, \lambda_1[$. We will also come with more accurate bounds on ρ^* than 0 and λ_1.

4.6.1 A stable algorithm

The first thing that has to be done is to compute numerically λ_1, the minimum of $Sp(\mathbf{A}, \mathbf{B})$, it can be done by an inverse power algorithm. It also yields E_{λ_1}, the eigenspace associated to λ_1.
If $\mathbf{f}$ does belong to $(E_{\lambda_1})^\perp$, one has to compute u_{λ_1}, the unique solution to $(\mathbf{A} - \lambda_1\mathbf{B}^*\mathbf{B})u_{\lambda_1} = \mathbf{f}$ and $\mathbf{A}u_{\lambda_1} \in (E_{\lambda_1})^\perp$. A program like SYMMLQ in FORTRAN will do fine. If $\|\mathbf{B}u_{\lambda_1}\| \leq m/\lambda_1$ then the set of maximizer has been found. If those conditions are not met we have to find s which is the minimizer of g on $]0, \lambda_1[$. Recall that g is convex on this interval and is given by :

$$\begin{aligned} u_\rho &= (\mathbf{A} - \rho\mathbf{B}^*\mathbf{B})^{-1}\mathbf{f} \\ g(\rho) &= (\mathbf{f}, u_\rho) + m^2/\rho \\ g'(\rho) &= \|\mathbf{B}u_\rho\| - m^2/\rho^2 \\ v_\rho &= \mathbf{A}^{-1}\mathbf{B}^*\mathbf{B}(\mathbf{A} - \rho\mathbf{B}^*\mathbf{B})^{-1}\mathbf{A}u_\rho \\ g''(\rho) &= 2(\mathbf{B}^*\mathbf{B}u_\rho, \mathbf{B}^*\mathbf{B}v_\rho) + 2m^2/\rho^3 \end{aligned}$$

Where the last equation is obtained by writing g'' analytically and using proposition 4.4.3

Remark 4.6.1 $v_\rho = \mathbf{A}^{-1}\mathbf{B}^*\mathbf{B}(\mathbf{A} - \rho\mathbf{B}^*\mathbf{B})^{-1}\mathbf{A}u_\rho$ *seems difficult to calculate a priori. Nevertheless,it is useful to gain information on the second derivative of g. If the computation* $(\mathbf{A} - \rho\mathbf{B}^*\mathbf{B})^{-1}$ *has already been done by a direct method when calculating* u_ρ*, then it is costless to reuse the result. The inverse power*

algorithm that computes λ_1 already calculated $\mathbf{A}^{-1}$ and we just have to store it along the iterations.

So that the second derivative of g can be computed and a Newton method can be applied to compute s. Theorem 4.5.4 gives then the set of maximizers.

4.6.2 Bounds on s

Because each iteration of the Newton method costs a lot, it would be a good idea to find bounds on $\rho^* = s$. These bounds will be called s_m and s_M such that $s_m \leq s \leq s_M$

Suppose n eigenvectors $(e_i)_{i\in I}$ and n eigenvalues $(\lambda_i)_{i\in I} \in Sp(\mathbf{A}, \mathbf{B})$ were computed. Compute $\mathbf{f}_i = (\mathbf{f}, e_i)$ where e_i are normalized as $(\mathbf{A}e_i, e_j) = \delta_{i,j}$.

It must be kept in mind that $I \subset I_1$ where I_1 is defined as in proposition 4.4.2

Remark 4.6.2 *The normalization is not a difficult process because as soon as the e_i belongs to different eigenspaces E_{λ_i}, then they are automatically orthogonal. So we only have to perform an orthogonalization into the eigenspaces associated to the same eigenvalue which is generally done by the algorithm which computes the eigenvectors.*

Proposition 4.6.1 *Recall that $I = \{i_k\}_{k=1..n}$ denotes the set of n eigenvectors/eigenvalues already computed and define as $\lambda_M = \max_{i\in I} \lambda_i$. Let (s_M, s_m) be the solutions to*

$$0 \leq s_M \leq \lambda_1 \text{ and } \quad \Sigma_{i\in I} \frac{\lambda_i {\mathbf{f}_i}^2}{(\lambda_i - s_M)^2} = m^2/s_M$$

$$0 \leq s_m \leq \lambda_1 \text{ and } \quad \frac{\lambda_M \alpha}{(\lambda_M - s_m)^2} + \Sigma_{i\in I} \frac{\lambda_i {\mathbf{f}_i}^2}{(\lambda_i - s_m)^2} = m^2/s_m$$

Where α is defined as

$$\alpha = \min\left\{(\mathbf{A}^{-1}\mathbf{f}, \mathbf{f}) - \sum_{i\in I} (\mathbf{f}_i)^2 \quad , \quad \lambda_M(\mathbf{B}^*\mathbf{B}\mathbf{A}^{-1}\mathbf{f}, \mathbf{A}^{-1}\mathbf{f}) - \sum_{i\in I} (\mathbf{f}_i)^2 \frac{\lambda_M}{\lambda_i}\right\}$$

Then $s_m \leq s \leq s_M$ with an equality if and only if $Sp(\mathbf{A}, \mathbf{B}) \setminus Z \subset \{\lambda_i, i \in I\}$

Computing s_M and s_m is not a difficult process. Indeed arrange $I = \{i_k\}_{k=1..n}$ is in increasing order, define $\mathbf{A} = diag(\lambda_{i_k})_{k=1..n}$, define $\mathbf{B}$ the matrix identity of rank n, then s_M and s_m are respectively the solutions to the robust optimization problem with a source term equal to

$$\begin{aligned}
\mathbf{f}_m &= [\sqrt{\lambda_{i_1}}\mathbf{f}_{i_1} \quad \sqrt{\lambda_{i_2}}\mathbf{f}_{i_2} \quad .. \quad \sqrt{\lambda_{i_{n-1}}}\mathbf{f}_{i_{n-1}} \quad \sqrt{\lambda_{i_n}}\mathbf{f}_{i_n}] \\
\mathbf{f}_M &= [\sqrt{\lambda_{i_1}}\mathbf{f}_{i_1} \quad \sqrt{\lambda_{i_2}}\mathbf{f}_{i_2} \quad ... \quad \sqrt{\lambda_{i_{n-1}}}\mathbf{f}_{i_{n-1}} \quad \sqrt{\lambda_{i_n}(\alpha + \mathbf{f}_{i_n})}]
\end{aligned}$$

And there is no extra computation for $Sp(\mathbf{A},\mathbf{B})$ and $(\mathbf{A}-\lambda\mathbf{B}^*\mathbf{B})^{-1}$.
The explicit formulation of s_M and s_n for $n=1$ is

$$s_M = \frac{\lambda_M m}{m+\sqrt{\lambda_M}|\mathbf{f}_1|} \text{ and } s_m = \frac{\lambda_M m}{m+\sqrt{\lambda_M \alpha}}$$

Proof *Of proposition 4.6.1, for $s_M \geq s$*
Recall that $\mathbf{f}_i = (\mathbf{f}, e_i)$ and $g'(\rho) = \sum_{i\in I_1} \frac{\lambda_i(\mathbf{f}_i)^2}{(\lambda_i-\rho)^2} - m^2/\rho^2$ (cf proof of the lemma 4.5.2)

$$\sum_{i\in I_1} \frac{\lambda_i(\mathbf{f}_i)^2}{(\lambda_i - s_M)^2} \geq \sum_{i\in I} \frac{\lambda_i(\mathbf{f}_i)^2}{(\lambda_i - s_M)^2} = m^2/s_M$$

so that $g'(s_M) \geq 0$. We have $\lambda_1 \geq s_M \geq 0$ and g is convex on $]0,\lambda_1[$ and $g'(s) = 0$ so that $s_M \geq s$ □

Proof *Of proposition 4.6.1, for $s_m \leq s$*
This demonstration is a little bit harder. Following the previous idea, we must first find a good majoration of the term

$$K = \sum_{i\in I_1\setminus I} \frac{(\mathbf{f}_i)^2}{({\lambda_i}^{1/2} - {\lambda_i}^{-1/2} s_m)^2} = \sum_{i\in I_1\setminus I} \frac{(\mathbf{f}_i)^2/\lambda_i}{(1-{\lambda_i}^{-1} s_m)^2}$$

We will first rely on the following identities

$$\begin{aligned}
\sum_{i\in I_1\setminus I} (\mathbf{f}_i)^2 &= (\mathbf{A}^{-1}\mathbf{f},\mathbf{f}) - \sum_{i\in I}(\mathbf{f}_i)^2 - \sum_{i\in I_2}(\mathbf{f}_i)^2 \\
\sum_{i\in I_1\setminus I} (\mathbf{f}_i)^2/\lambda_i &= (\mathbf{B}^*\mathbf{B}\mathbf{A}^{-1}\mathbf{f}, \mathbf{A}^{-1}\mathbf{f}) - \sum_{i\in I}(\mathbf{f}_i)^2/\lambda_i
\end{aligned}$$

So that the two following majoration are available

$$\begin{aligned}
K &= \sum_{i\in I_1\setminus I} \frac{(\mathbf{f}_i)^2}{({\lambda_i}^{\frac{1}{2}} - {\lambda_i}^{-\frac{1}{2}} s_m)^2} \leq \frac{\sum_{i\in I_1\setminus I}(\mathbf{f}_i)^2}{({\lambda_M}^{\frac{1}{2}} - {\lambda_M}^{-\frac{1}{2}} s_m)^2} \\
&\leq \lambda_M \frac{(\mathbf{A}^{-1}\mathbf{f},\mathbf{f}) - \sum_{i\in I}\mathbf{f}_i^2}{(\lambda_M - s_m)^2} \\
K &= \sum_{i\in I_1\setminus I} \frac{(\mathbf{f}_i)^2/\lambda_i}{(1-s_m/\lambda_i)^2} \leq \frac{\sum_{i\in I_1\setminus I}(\mathbf{f}_i)^2/\lambda_i}{(1-s_m/\lambda_M)^2} \\
&= {\lambda_M}^2 \frac{(\mathbf{B}^*\mathbf{B}\mathbf{A}^{-1}\mathbf{f}, \mathbf{A}^{-1}\mathbf{f}) - \sum_{i\in I}\mathbf{f}_i^2/\lambda_i}{(\lambda_M - s_m)^2}
\end{aligned}$$

We can now conclude that

$$\begin{aligned}\sum_{i\in I_1}\frac{\lambda_i(\mathbf{f}_i)^2}{(\lambda_i-s_m)^2} &= \sum_{i\in I}\frac{\lambda_i(\mathbf{f}_i)^2}{(\lambda_i-s_m)^2}+\sum_{i\in I_1\setminus I}\frac{\lambda_i(\mathbf{f}_i)^2}{(\lambda_i-s_m)^2}\\ &= \sum_{i\in I}\frac{\lambda_i(\mathbf{f}_i)^2}{(\lambda_i-s_m)^2}+K\\ &\leq \sum_{i\in I}\frac{\lambda_i(\mathbf{f}_i)^2}{(\lambda_i-s_m)^2}+\frac{\lambda_M\alpha}{(\lambda_n-s_m)^2}=m^2/s_m\end{aligned}$$

so that $g'(s_m)=\sum_{i\in I_1}\frac{\lambda_i(\mathbf{f}_i)^2}{(\lambda_i-s_m)^2}-m^2/s_m\leq 0$ and therefore $s_m\leq s$

□

4.7 Numerical results

4.7.1 Monotonic properties

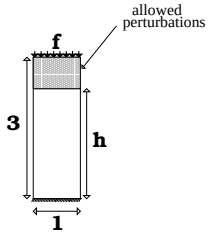

FIG. 4.2 – The model problem.

The model problem is a 2-d rectangular elastic beam which is clamped in its bottom part. The dimension of the beam are $[0,1]\times[0,3]$. The main source term is a downward directed pressure force of total L^2-norm 3 which is located on the upper part of the boundary. The perturbation are located on the rectangle $[0,1]\times[h,3]$ and are allowed in the horizontal and vertical direction.

We wish in this section to numerically verify some expected monotonic properties of the robust compliance $\mathcal{J}_{rob}=\max_{u\in V}-(\mathbf{A}u,u)+2(\mathbf{f},u)+2m\|\mathbf{B}u\|$ with respect to the following criteria :

- $\mathcal{J}_{rob}$ is increasing with respect to m
- $\mathcal{J}_{rob}$ is decreasing with respect to h
- $\mathcal{J}_{rob}$ is (slowly) increasing with respect to mesh-refinement

The analysis of the numerical result is as follows

- Figure 4.3 ($h=0$) : When m increases, the norm of the allowed perturbation increases, the energy must therefore increase. The asymptotic behavior of $\mathcal{J}_{rob}$ when m goes to ∞ must be $\frac{m^2}{\lambda}$, ($\lambda=1.2.10^{-2}$ here)

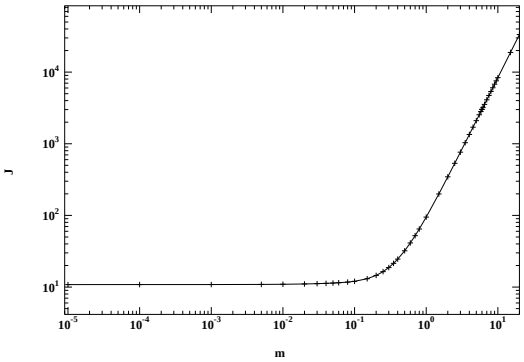

FIG. 4.3 – Compliance as a function of m (log scale).

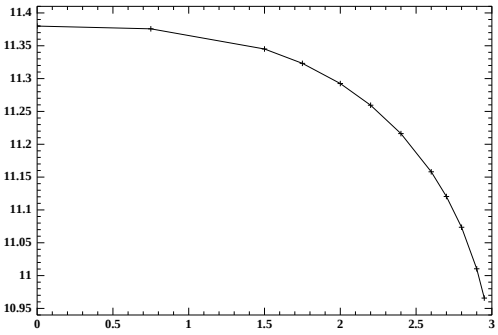

FIG. 4.4 – Compliance as a function of h.

essentially because $\mathbf{f}$ is negligible in the equation and setting $\mathbf{f} = 0$ in the equation (4.3) leads to the Auchmuty problem. The value of the maximum is in this case $\frac{m^2}{\lambda}$.

– Figure 4.4 ($m = 5.10^{-2}$) : When h decreases, the set of allowed perturbation increases thus $\mathcal{J}_{rob}$ must increase
– Figure 4.5 ($h = 0$,$m = 5.10^{-2}$) : When the mesh is refined, there is more degrees of freedom in the rectangle that defines the perturbation, and because the set of allowed perturbation increases, then $\mathcal{J}_{rob}$ increases. Figure 4.5 is obtained by alternatively cutting every square of the mesh in the y then in the x direction . The x-coordinate of this figure is equal to the decimal logarithmic of the number of degrees of freedom.The mesh that is used for the other calculation is the one with 9922 degrees of freedom. Sadly, mesh-refinement increases efficiency of numerical approximation and it is known to increase the value of the compliance. There does not seem to exist a way to distinguish the two effects.

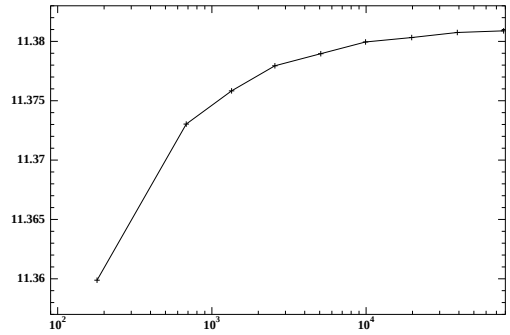

FIG. 4.5 – Compliance as a function of the mesh.

4.7.2 Non-dependency of the bounds with respect to the mesh

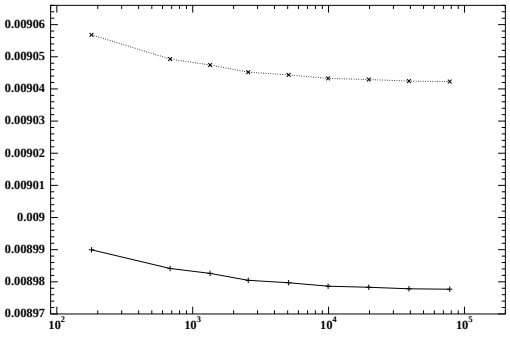

FIG. 4.6 – Dependency of s_M and s_m with respect to the mesh.

On the accuracy of the two bounds (s_M, s_m) as defined in definition 4.6.1 depends the quality of the algorithm. The upper-bound s_M on ρ^* is obtained by identifying $\mathbf{f}$ with its orthonormal projection in the n-first eigenspaces (n=4 in our numerical case) . The lower-bound s_m on ρ^* is mainly obtained by identifying every eigenvalue that is greater to the n^{th} with the n^{th}. The error made on the bounds depends essentially on those identifications which do not depend (too much) on the mesh. Figure 4.6 is an example of the evolution of the bounds with respect to mesh-refinement. The test is the same that in section 4.7.1 with parameters $h = 0$ and $m = 5.10^{-2}$ As a result the calculation of the robust compliance always needs the same number of Newton iteration on g (3 or 4 in our case) in order to achieve a 10^{-8} accuracy on ρ^*. The global cost of the Newton method is (in our case) one half of the calculation of the eigenvalues. This ratio of calculus time does depend of the problem of course but not on the

mesh. In any other problem treated, it did not seem that more than 15 Newton iteration were needed to solve the problem.

Remark 4.7.1 *Robust compliance analysis gives rise to an interesting criterion. Recall notations of section 4.2.1 and 4.2.3. Given an operator* $\mathbf{A}$*, a source term* $\mathbf{f}$ *and a set of admissible perturbations (that defines* $\mathbf{B}$*), then if* $\mathbf{f} \perp E_{\lambda_1}$*, let* $\varepsilon_0 = \|\mathbf{B}u_{\lambda_1}\|/\|\mathbf{f}\|$*. As a function of* $\mathbf{f}$*,* ε_0 *is homogeneous of degree* 0*.*

If $m \leq \|\mathbf{f}\|\varepsilon_0$*, there is only one worst perturbation (it is* $\mathbf{A}u_{\lambda_1}$*) and if* $m > \|\mathbf{f}\|\varepsilon_0$ *there is multiples perturbation, ie a whole sphere centered in* $\mathbf{A}u_{\lambda_1}$*, inscribed in* $\mathbf{A}E_{\lambda_1}$ *and of radius* $m - \|\mathbf{f}\|\varepsilon_0$*.*

ε_0 *is a good indication of the stability of a linear operator submitted to a given source term.*

Chapitre 5

Shape optimization of the robust compliance

Abstract

According to the setting of chapter 4, we study in this chapter the shape derivative of the robust compliance. The directional derivative is shown to exist and calculated. A gradient-type algorithm that relies on an SDP problem can be performed thanks to the Hilbertian structure endowed by the work of chapter 3. Some numerical results are provided

5.1 Shape optimization setting 94
5.2 Shape differentiability 94
5.2.1 Introduction : Lagrange derivation 95
5.2.2 A general theorem about robust derivation 96
5.2.3 Application of theorem 5.2.1 to shape optimization . 98
5.3 An algorithm of shape optimization 100
5.3.1 The SDP problem 101
5.3.2 The choice of descent direction 102
5.4 Numerical results 104
5.4.1 From the beam to a cantilever 104
5.4.2 The Wheel-bridge 105
5.4.3 The 2-d mast 106
5.4.4 The 3-d beam 109
5.4.5 The 3-d bridge 110
5.4.6 The 3-d chair 111
5.5 Conclusion 111

We now want to optimize the criterion of the robust compliance with respect to the domain.

5.1 Shape optimization setting

Use the direct problem and Theorem 4.2.2 with the following definitions

Definition 5.1.1

$$V = H^1_D(\Omega)^d \quad H = L^2(\Omega)^d \quad V' = H^{-1}(\Omega)^d \times H^{-1/2}(\Gamma_N)^d$$

$\diamond$ $\mathbf{A}$ *is the operator such that* $(\mathbf{A}v, w) = \int_\Omega A\, e(v) \cdot e(w)\, dx$
$\diamond$ $\mathbf{f}$ *is the element of* V' *such that* $(\mathbf{f}, v) = \int_\Omega \mathbf{f_1} \cdot v\, dx + \int_{\Gamma_N} \mathbf{f_2} \cdot v\, ds$
$\diamond$ $B = B^*$ *is the multiplication by the characteristic function* χ

For different domains Ω, the functional $\mathcal{J}_{rob}(\Omega)$ depends on Ω and is defined as (in the formulation in u) :

Definition 5.1.2

$$\mathcal{J}_{rob}(\Omega) = \max_{u \in H^1_D(\Omega)} -\int_\Omega A\, e(u) \cdot e(u) + 2\mathbf{f_1} \cdot u\, dx + 2\int_{\Gamma_N} \mathbf{f_2} \cdot u\, ds + m\Big(\int_\Omega \chi u \cdot u\, dx\Big)^{1/2}$$

We are interested in the following problem

$$\min_\Omega \mathcal{L}_{rob}(\Omega) \text{ where } \mathcal{L}_{rob}(\Omega) = \mathcal{J}_{rob}(\Omega) + \eta|\Omega|$$

Where η is a Lagrange multiplier for a volume constraint. Introduce a big domain D and add the constraint that $\Omega \subset D$.

We reinterpret Theorem 4.2.2 into :

Proposition 5.1.1 *Define* $\mathcal{M}$ *the set of maximizers of* $\mathcal{J}_{rob}$*, then* $\mathcal{M}$ *is given by :*

$$\begin{aligned} \mathcal{M} = \quad & \{u_{\rho^*} + rv \text{ st } v \in E_{\lambda_1} \text{ and } \|Bv\| = 1\} \\ \text{With} \quad & (\rho^*, r) = (s, 0) \text{ when the maximizer is unique} \\ & (\rho^*, r) = (\lambda_1, \frac{m}{\lambda_1} - \|Bu_{\rho^*}\|) \text{ when there are multiple maximizers} \end{aligned}$$

Where u_ρ*,* s*,* λ_1 *and* E_{λ_1} *are defined in definition 4.2.2;* u_ρ *is defined for any* ρ *by definition 4.2.3 and* s *is defined in Theorem 4.2.2*

5.2 Shape differentiability

We briefly recall the notion of shape differentiability that is defined in Section 1.2

Definition 5.2.1 *Define*

$$\Omega_\theta = (Id + \theta) \circ \Omega = \{x + \theta(x) \text{ such that } x \in \Omega\}$$

For any functional $\mathcal{J}_{rob}(\Omega)$, its shape derivative $\mathcal{J}'_{rob}(\theta)$ is defined as (when it exists) the derivative of the functional $W^{1,\infty}(D;D) \to \mathbb{R}$; $\theta \mapsto \mathcal{J}_{rob}(\Omega_\theta)$ at 0. When this functional admits a Fréchet derivative, then $\theta \mapsto \mathcal{J}'_{rob}(\theta)$ is a linear continuous form on $W^{1,\infty}(D;D)$.

In order to simplify the notations, the diffeomorphism $Id + \theta$ will be denoted by T

5.2.1 Introduction : Lagrange derivation

For the sake of simplicity, we suppose that $f = (\mathbf{f_1}, \mathbf{f_2})$, the set of loads is a volume load (ie $\mathbf{f_2} = 0$). This simplifies the calculus but does not change the result. Shape derivative is obtained very easily when the solution to the robust compliance problem is unique. The method is originally due to [Céa86] and has been widely used a posteriori (see [AJ05]). Suppose that the set of maximizers of $\mathcal{J}_{rob}$ consists of the singleton $\{u_{\rho^*}\}$ and that u^*_ρ is shape-differentiable. The solution verifies the following Eulerian equations :

$$\begin{aligned}
\int_\Omega A\, e(u_{\rho^*}) \colon e(X)\, dx &= \int_\Omega \mathbf{f_1} \cdot X\, dx + \rho^* \int_\Omega \chi u_{\rho^*} \cdot X\, dx \quad \forall X & (5.1)\\
\rho^* \big(\int_\Omega \chi u_{\rho^*} \cdot u_{\rho^*} \big)^{1/2} &= m & (5.2)\\
\rho^* &= s \text{ Where } s \text{ is defined in Theorem 4.5.4}
\end{aligned}$$

Introduce the Lagrangian defined for any $(v, q) \in H^1(\mathbb{R}^d;\mathbb{R}^d)^2$ by

$$\mathcal{L}^c(\Omega, v, q) = -\int_\Omega Ae(v) \colon e(v) + 2\int_\Omega \mathbf{f_1} \cdot v + 2m\big(\int_\Omega \chi v \cdot v\big)^{1/2} + 2\int_{\Gamma_D} q \cdot v$$

Where q is a Lagrange multiplier for the Dirichlet boundary condition on Γ_D. It is worth noticing that v and q belong to a functional space that does not depend on Ω, so we can apply the usual differentiation rule to the Lagrangian $\mathcal{L}^c$. $\mathcal{J}_{rob}(\Omega)$ is the value at the saddle-point (u, p)

$$\mathcal{J}_{rob}(\Omega) = \max_{v \in H^1(\mathbb{R}^d;\mathbb{R}^d)} \min_{q \in H^1(\mathbb{R}^d;\mathbb{R}^d)} \mathcal{L}^c(\Omega, v, q)$$

(minimizing first in q we recover the Dirichlet boundary condition for v on Γ_D) The stationarity of the Lagrangian gives the optimality conditions. The partial derivative of $\mathcal{L}^c$ with respect to q in the direction ϕ gives

$$\big(\frac{\partial \mathcal{L}^c}{\partial q}(\Omega, u, p), \phi\big) = 2\int_{\Gamma_D} \phi \cdot u$$

Varying the trace function ϕ on Γ_D gives the Dirichlet condition on u.

The partial derivative of $\mathcal{L}^c$ with respect to v in the direction ϕ gives

$$(\frac{\partial \mathcal{L}^c}{\partial v}(\Omega,u,p),\phi) = -2\int_\Omega Ae(u)\colon e(\phi) + 2\int_\Omega \mathbf{f_1}\cdot\phi + \frac{2m}{\|\chi u\|_{L^2}}\int_\Omega \chi u\cdot\phi + 2\int_{\Gamma_D} p\cdot\phi$$

Since $\frac{\partial \mathcal{L}^c}{\partial v}(\Omega,u,p)=0$, taking ϕ with compact support in Ω gives, after integration by parts,

$$-div(Ae(u)) = \mathbf{f_1} + \frac{m}{\|\chi u\|}\chi u$$

which is nothing but the Eulerian equation (5.1) and (5.2). Then, varying the trace function ϕ on Γ_N gives the Neumann boundary condition, while varying the trace function ϕ on Γ_D gives the value of the Lagrange multiplier $p = Ae(u)\cdot n$. The shape derivative of the objective function is obtained by differentiating

$$\mathcal{J}_{rob}(\Omega) = \mathcal{L}^c(\Omega, u(\Omega), p(\Omega))$$

which, by the chain rule theorem, reduces to the partial derivative of $\mathcal{L}^c$ with respect to Ω in the direction θ

$$\begin{aligned}(\frac{\partial \mathcal{L}^c}{\partial \Omega}(\Omega,u,p),\theta) &= -\int_{\partial\Omega}(\theta\cdot n)Ae(u)\cdot e(u) + 2\int_{\partial\Omega}(\theta\cdot n)\mathbf{f_1}\cdot u \\ &+ \frac{m}{\|\chi u\|}\int_{\partial\Omega}(\theta\cdot n)\chi u\cdot u + 2\int_{\Gamma_D}(\theta\cdot n)[\frac{\partial p\cdot u}{\partial n} + Hp\cdot u]\end{aligned}$$

taking in account the boundary condition $u=0$ on Γ_D and $p = Ae(u)\cdot n$ on Γ_D which also simplifies $Ae(u)\cdot e(u) = Ae(u)\cdot\frac{\partial u}{\partial n}n = p\partial_n u = \partial_n(p\cdot u)$ on Γ_D, we deduce

$$\mathcal{J}'_{rob}(\theta) = \int_{\Gamma_N}(\theta\cdot n)[-Ae(u)\cdot e(u) + 2\mathbf{f_1}\cdot u + \frac{m}{\|\chi u\|}\chi u\cdot u] + \int_{\Gamma_D}(\theta\cdot n)Ae(u)\cdot e(u)$$

5.2.2 A general theorem about robust derivation

The development of section 5.2.1 stands only when the maximizer of F is unique. We need a more general theorem that is able to handle the case where there is multiple maximizers of F.

Definition 5.2.2

$\diamond$ *Let $\alpha > 0$, $\beta_1 > 0$ be constants and $\mathbb{L}$ be the space of linear unbounded self-adjoint operators from $H \to H$ such that :*

$$\forall L\in\mathbb{L} \quad ,\forall u\in V \quad \beta_1\|u\|_V^2 \geq (Lu,u)_H \geq \alpha\|u\|_V^2$$

ie : $\mathbb{L}$ is made of operator with 'uniformly' compact resolvent or 'uniformly' coercive with constant α and uniformly continuous with constant β_1

$\diamond$ *Let $\beta_2 > 0$ be a constant and $\mathbb{M}$ be the space of continuous linear self-adjoint operators from $H \to H$ uniformly continuous with constant β_2, ie :*

$$\forall M\in\mathbb{M} \quad ,\forall u\in H \quad \beta_2\|u\|_H^2 \geq (Mu,u)_H$$

$\diamond$ *Define the norm in those two spaces as follows : If* $N \in \mathbb{L}$ *or* $N \in \mathbb{M}$ *then*

$$\|N\| = \max_{u \in V} \frac{(Nu, u)_H}{\|u\|_V^2}$$

ie, we endow $\mathbb{M}$ *with the natural norm of* $\mathbb{L}$

$\diamond$ *Let* X *be a given Banach space* $X \to \mathbb{L} \times \mathbb{M} \times V'$, $\theta \mapsto (\mathbf{A}(\theta), B^*B(\theta), \mathbf{f}(\theta))$ *be a Fréchet differentiable mapping (for* $\mathbf{A}$ *and* B*, the differentiability is understood with respect to the norm just defined). Define* $\mathbf{A}'(\theta_0)$ *(resp* $B^*B'(\theta_0)$*,* $\mathbf{f}'(\theta_0)$*) the differential of* $\mathbf{A}(\theta)$ *(resp* $B^*B(\theta)$*,* $\mathbf{f}(\theta)$*) with respect to* θ *at the point* $\theta = 0$ *applied to* θ_0*.*

Before working on the main theorem, let us briefly give a simple definition of the directional derivative, which is the easiest derivative one can achieve

Definition 5.2.3 *The functional* $\theta \mapsto \mathcal{J}_{rob}(\theta)$ *is said to be directional derivable at* $\theta = 0$ *if and only if, for every direction* θ_0*, the following limit is achieved :*

$$\lim_{t \to 0 \ , \ t>0} \frac{\mathcal{J}_{rob}(t\theta_0) - \mathcal{J}_{rob}(0)}{t} = \mathcal{J}'_{rob}(\theta_0)$$

The collection of $\mathcal{J}'_{rob}(\theta_0)$ *when* θ_0 *is the directional derivative, it may be a non-linear mapping, as is for instance the derivative of the absolute value at the point* 0*.*

Let us state the main theorem about shape-derivative of the robust compliance.

Theorem 5.2.1 *Define* $\mathcal{J}_{rob}(\theta)$ *the robust compliance*

$$\mathcal{J}_{rob}(\theta) = \max_{u \in V} -(\mathbf{A}(\theta)u, u) + 2(\mathbf{f}(\theta), u) + m(B^*B(\theta)u, u)$$

and let $\mathcal{M}_0$ *be the set of maximizers of* $\mathcal{J}_{rob}(0)$

Then, for all $\theta_0 \in X$*,* $\mathcal{J}_{rob}(\theta)$ *is directionally derivable at the point* $\theta = 0$ *in the direction* θ_0 *and the value of the directional derivative is*

$$\mathcal{J}'_{rob}(\theta_0) = \max_{u \in \mathcal{M}_0} -\big(\mathbf{A}'(\theta_0)u, u\big) + 2(\mathbf{f}'(\theta_0), u) + \rho^*\big(B^*B'(\theta_0)u, u\big)$$

Where $\rho^* = \lambda_1$ *the smallest eigenvalue of* $Sp(\mathbf{A}, B)$ *when there is multiple maximizers and where* $\rho^* = s = \frac{m}{\|Bu_s\|}$ *when there is a single maximizer*

Proof (sketch) The entire proof is postponed to Appendix B. The main idea is that if $\mathcal{J}_{rob}$ is defined as $\mathcal{J}_{rob}(\theta) = \max_u F(\theta, u)$ then $\mathcal{J}_{rob}$ is directionally derivable in $\theta = 0$ and

$$\mathcal{J}'_{rob}(\theta_0) = \max_{u \text{ maximizer of } F(0,u)} \frac{\partial F}{\partial \theta}(0, u).\theta_0 \tag{5.3}$$

$\diamond$ This is easily understood if we suppose the maximizers to be continuous. In this case in $t\theta_0$ with t small, the maximum of $F(t\theta_0, u)$ may only emerge from a point u_t close to u_0 a maximum of $F(0, u)$. We note $u_t = u_0 + tu' + o(t)$.

The value of $\mathcal{J}_{rob}(t\theta_0)$ is then equal to $F(u_0)+t\partial_\theta F(0,u_0).\theta_0+t\partial_u F(0,u_0).u'+O(t)$. Recalling that u_0 is a maximizer of F, we have $\partial_u F(0,u_0)=0$.

Every maximizer of $F(0,u)$ is in competition to give rise to the maximum of $F(t\theta_0,u)$, the one who won is the one with the biggest derivative $\partial_\theta F(0,u_0).\theta_0$. So that $\mathcal{J}'_{rob}(\theta_0)=\partial_\theta F(0,u^*).\theta_0$ for u^* a maximizer of $\partial_\theta F(0,u_0).\theta_0$ over the set of maximizers of $F(0,u)$.

$\diamond$ In order to prove (5.3), Clarke's subgradient theory [Cla90] has to be used. Let $S\subset V$ that does not depend on θ such that S contains $\mathcal{M}(\theta)$ for every θ small.The set S can be chosen bounded in V, compact in V and such that for every θ the function $F_\theta : u\mapsto F(\theta,u)$ are differentiable on S. The construction of S is allowed by the uniform conditions of coercivity and continuity of the space $\mathbb{L}$ and $\mathbb{M}$

The set of function $F_u : \theta\mapsto F(\theta,u)$ are uniformly Lipschitz (on S) and then the subgradient of $\mathcal{J}_{rob}$ can be computed. The directional derivative of $\mathcal{J}_{rob}$ is just obtained by taking the supremum on the subgradient. $\square$

5.2.3 Application of theorem 5.2.1 to shape optimization

The goal of this section is to compute the directional derivative of the robust compliance. In order to simplify the notations, only volume forces are considered (ie $\mathbf{f_2}=0$ in section 4.2.1). And as usual, for any θ in $W^{1,\infty}(D;D)$, we define $\Omega_\theta=(\mathbb{Id}+\theta)\circ\Omega$, and we differentiate the robust compliance with respect to θ. The theorem to be proved is the following.

Theorem 5.2.2 *The mapping of the robust compliance $\theta\mapsto\mathcal{J}_{rob}(\Omega_\theta)$ is directionally derivable and the value of the directional derivative in the direction θ is given by*

$$\mathcal{J}'_{rob}(\theta)=\max_{u\in\mathcal{M}_0}\int_{\partial\Omega}(\theta\cdot n)[v(u,u)+2\mathbf{f_1}\cdot u] \tag{5.4}$$

Where $\mathcal{M}_0$ is the set of maximizers of $\mathcal{J}_{rob}(\Omega)$ and v is defined by

$$\begin{aligned} v(u,w) &= -Ae(u)\cdot e(w)+\rho^*\chi u\cdot w \text{ on } \Gamma_N \\ v(u,w) &= Ae(u)\cdot e(w) \text{ on } \Gamma_D \end{aligned}$$

Where ρ^* is the common value of $\frac{m}{\|\chi u\|}$ for every u in $\mathcal{M}_0$

Theorem 5.2.1 cannot be directly applied here, because the spaces $\mathbb{L}$ and $\mathbb{M}$ defined in definition 5.2.2 deal with operators whose definition space $L^2(\Omega)$ do not change with θ. This is not the case with shape optimization problems. Indeed the operator of elasticity $\mathbf{A}$ is defined from $H^1_D(\Omega)\to H^{-1}(\Omega)\times H^{-1/2}(\Gamma_N)$. When Ω is changed into Ω_θ, the spaces on which $\mathbf{A}$ is defined changes. That is why we consider,

Definition 5.2.4 *Let $(\cdot,\cdot)$ denotes the scalar product of $L^2(\Omega)$*

For every θ in $W^{1,\infty}(D;D)$ close enough to $\theta=0$, recall that $T\in W^{1,\infty}(D;D)$ is defined as $T=\mathbb{Id}+\theta$

$\diamond$ *let* $\tilde{\mathbf{A}}(\theta) \in \mathbb{L}$ *such that* $(\tilde{\mathbf{A}}(\theta)v, w) = \int_{\Omega_\theta} A\, e(v \circ T^{-1}) \cdot e(w \circ T^{-1})\, dx$
$\diamond$ *Let* $\tilde{B^*B}(\theta) \in \mathbb{M}$ *such that* $(\tilde{B^*B}(\theta)v, w) = \int_{\Omega_\theta} \chi(v \circ T^{-1}) \cdot (w \circ T^{-1})$
$\diamond$ *Let* $\tilde{\mathbf{f}}(\theta) \in V'$ *such that* $(\tilde{\mathbf{f}}(\theta), v) = \int_{\Omega_\theta} \mathbf{f_1} \cdot (v \circ T^{-1})\, dx$
$\diamond$ *Let*

$$\tilde{\mathcal{J}_{rob}}(\theta) = \max_{u \in V} -(\tilde{\mathbf{A}}(\theta)u, u) + 2(\tilde{\mathbf{f}}(\theta), u) + m(\tilde{B^*B}(\theta)u, u)^{1/2}$$

Proposition 5.2.3
$\diamond$ *If* θ *is close enough to* 0, *then* $\tilde{\mathbf{A}}(\theta) \in \mathbb{L}$ *and* $\tilde{B^*B}(\theta) \in \mathbb{M}$ *and* $\tilde{\mathbf{f}}(\theta) \in V'$
$\diamond$ *For every* θ *close to* 0, $\tilde{\mathcal{J}_{rob}}(\theta) = \mathcal{J}_{rob}(\Omega_\theta)$ *where* $\mathcal{J}_{rob}(\Omega_\theta)$ *is defined in definition 5.1.2*

Proof Let's first prove that $\tilde{\mathcal{J}_{rob}}(\theta) = \mathcal{J}_{rob}(\Omega_\theta)$. Relying on the following proposition : If T and T^{-1} are in $W^{1,\infty}(D; D)$ then

$$u \circ T^{-1} \in H^1(\Omega_\theta) \Longleftrightarrow u \in H^1(\Omega)$$

$$\begin{aligned}
\tilde{\mathcal{J}_{rob}}(\theta) &= \max_{u \in H^1(\Omega)} -(\tilde{\mathbf{A}}(\theta)u, u) + 2(\tilde{\mathbf{f}}(\theta), u) + 2m(\tilde{B^*B}(\theta)u, u)^{1/2} \\
&= \max_{u \in H^1(\Omega_\theta)} -(\tilde{\mathbf{A}}(\theta)u \circ T, u \circ T) + 2(\tilde{\mathbf{f}}(\theta), u \circ T) + 2m(\tilde{B^*B}(\theta)u \circ T, u \circ T)^{1/2} \\
&= \max_{u \in H^1(\Omega_\theta)} -\int_{\Omega_\theta} A\, e(u) \cdot e(u)\, dx + 2\int_{\Omega_\theta} \mathbf{f_1} \cdot u\, dx + 2m\Big(\int_{\Omega_\theta} \chi u \cdot u\, dx\Big)^{1/2} \\
&= \mathcal{J}_{rob}(\Omega_\theta)
\end{aligned}$$

$\diamond$ We will just prove that $\tilde{\mathbf{A}}(\theta)$ belongs to $\mathbb{L}$ for small θ, the other assumptions of proposition 5.2.3 being proved the same way. Let's introduce the tensor A which has the symmetries of elasticity :

$$A^{ijkl} = A^{jikl} = A^{ijlk} = A^{klij}$$

such that $A^{ijkl}(\partial_j u^i)(\partial_l v^k) = Ae(u) \colon e(v)$. We have :

$$\begin{aligned}
(\tilde{\mathbf{A}}(\theta)v, w) &= \int_{\Omega_\theta} A^{ijkl} \partial_j (v \circ T^{-1})^i \partial_l (w \circ T^{-1})^k\, dx \\
&= \int_{\Omega_0} |det \nabla T| A^{ijkl} \partial_j (v \circ T^{-1})^i \circ T \partial_l (w \circ T^{-1})^k \circ T\, dx \\
&= \int_{\Omega_0} |det \nabla T| A^{ijkl} (\partial_s v^i \partial_j (T^{-1})^s)(\partial_m w^l \partial_k (T^{-1})^m)\, dx \\
&= \int_{\Omega_0} C^{iskm}(\theta) \partial_s v^j \partial_m w^l\, dx
\end{aligned}$$

With

$$\begin{aligned}
C^{iskm}(\theta) &= A^{iskm} + C_\theta^{iskm} + o(\|\theta\|_{W^{1,\infty}}) \\
C_\theta^{iskm} &= (\partial_l \theta^l) A^{iskm} - A^{ijkm}(\partial_j \theta^s) - A^{iskl}(\partial_l \theta^m)
\end{aligned}$$

The coefficients are then uniformly derivable with respect to θ, this proves that the operator $\tilde{\mathbf{A}}(\theta)$ is, at least for θ small, uniformly coercive and bounded with respect to θ. $\square$

The development above gives also the value of $\tilde{\mathbf{A}}'(\theta)$ which is :

$$(\mathbf{A}'(\theta)v, w) = \int_{\Omega_0} C_\theta^{iskm} \partial_s v^j \partial_m w^l \, dx$$

The value of $\tilde{\mathbf{f}}'$ and $\tilde{B^*B'}$ is given by

$$\begin{aligned} (\tilde{\mathbf{f}}'(\theta), v) &= \int_{\Omega_0} div(\theta)\mathbf{f_1} \cdot v + \mathbf{f_1} \cdot (\nabla v \theta) \\ (\tilde{B^*B'}(\theta)v, w) &= \int_{\Omega_0} \chi[div(\theta)v \cdot w + (\nabla v\theta) \cdot w + v \cdot (\nabla w \nabla \theta)] \end{aligned}$$

Proof of theorem 5.2.2 Theorem 5.2.1 can be applied to $\tilde{\mathcal{J}_{rob}}$ which is locally equal to $\mathcal{J}_{rob}(\Omega_\theta)$, in order to prove theorem 5.2.2, it is sufficient to prove that :

$$-\big(\mathbf{A}'(\theta)u, u\big) + 2(\mathbf{f}'(\theta), u) + \rho^*\big([B^*B]'(\theta)u, u\big) = \int_{\partial\Omega} (\theta \cdot n)[v(u,u) + 2\mathbf{f_1} \cdot u] \quad (5.5)$$

where $v(\cdot,\cdot)$ is defined in Theorem 5.2.2. This is a pure algebraic proof, first perform an integration by part on θ on the left-hand term of (5.5). There are two terms, the one in $\int_\Omega$ and the one in $\int_{\partial\Omega}$. The terms in $\int_\Omega$ are equal to zero because u verify the Eulerian equations (5.1) and (5.2). The terms in $\int_{\partial\Omega}$ are equal to :

$$\int_{\partial\Omega} (\theta \cdot n)[-Ae(u) \cdot e(u) + \rho^* \chi u \cdot u + 2\mathbf{f_1} \cdot u] + 2C^{ijkl} \partial_s u^i \theta^s n^j \partial_l u^k \quad (5.6)$$

The last term is treated differently on the Neumann part and on the Dirichlet part of the boundary.
$\diamond$ On the Neumann part of the boundary, the homogeneous condition $Ae(u) \cdot n = 0$ means that $C^{ijkl}\partial_l u^k n^j = 0$, therefore this term is equal to 0.
$\diamond$ On the Dirichlet part of the boundary, using that $\nabla u = \frac{\partial u}{\partial n} n$, we have

$$\partial_s u^i \theta^s n^j = \frac{\partial u^i}{\partial n} n^s \theta^s n^j = \partial_j u^i (\theta \cdot n)$$

so that the last term in the integrand of (5.6) is equal to $2(\theta \cdot n) Ae(u) \cdot e(u)$ $\square$

5.3 An algorithm of shape optimization

The function $\theta \mapsto \mathcal{J}_{rob}(\Omega_\theta)$ ($\mathcal{J}_{rob}$ being defined in definition 5.1.2) admits a directional derivative with respect to $\theta \in W^{1,\infty}(D; D)$. So does $\mathcal{L}_{rob}(\Omega_\theta) = \mathcal{J}_{rob}(\Omega_\theta) + \eta|\Omega_\theta|$ The goal of this section is to develop an algorithm that minimize

$\mathcal{L}_{rob}(\Omega_\theta)$. This algorithm is in two steps : the choice of a particular descent direction and a level-set method that changes the domain.

We do not develop the level-set theory here, we refer the reader to section 1.4 and to [OS01], [Set99] or [AJT02] for an extensive explanation of this method applied to shape-optimization.

The choice of descent direction will then be made according to chapter 3 -Notice that the value of $\mathcal{L}'_{rob}(\theta)$, the directional derivative in the direction θ only depends on the value of $(\theta \cdot n)$ on the boundary of Ω. It has the form $\mathcal{L}'_{rob}(\theta) = g(\theta \cdot n)$. The value of g is given by Theorem 5.2.2 and is equal to

$$g(V) = \max_{u \in \mathcal{M}_0} \int_{\partial\Omega} V[v(u,u) + 2\mathbf{f_1} \cdot u + \eta] \tag{5.7}$$

-Introduce an Hilbertian scalar-space K (see chapter 3 for choices of the space K, we work with $H^1(D)$ usually). Perform a steepest-descent algorithm on the space K, ie find $V^* \in K$ solution of the following problem

$$g(V^*) = \min_{\|V\|_K = 1} g(V) \tag{5.8}$$

This problem is an SDP problem in low dimension that is easily solved.

5.3.1 The SDP problem

Recall that the set of maximizers is given by

Proposition 5.3.1

$$\begin{aligned} \mathcal{M}_0 = \quad & \{u_{\rho^*} + rv \ st \ v \in E_{\lambda_1} \ and \ \|Bv\| = 1\} \\ With \quad & (\rho^*, r) = (s, 0) \ when \ the \ maximizer \ is \ unique \\ & (\rho^*, r) = (\lambda_1, \frac{m}{\lambda_1} - \|Bu_{\rho^*}\|) \ when \ there \ is \ multiple \ maximizer \end{aligned}$$

Where u_ρ, s and λ_1 are defined in Theorem 4.5.4. The next definition is used to introduce the SDP problem.We refer the reader to section 1.6 or to [VB96] for an introduction to SDP problems. We shall only recall here that an SDP problem is of the following form : given a matrix $E(Y)$ whose coefficient depends linearly on the vector Y and a given vector Y_0, find the vector Y^* which realizes the minimum

$$\min_{E(Y) \geq 0} Y^T Y_0$$

where $\geq$ stands for 'symmetric positive'.

We will state here that the problem introduced in equation (5.9) is easily solved and that its computational time is negligible compared to the computational time of the robust-compliance.

Definition 5.3.1 (Definition of the SDP-problem) *Each time there is reference to a scalar product it is implicitly assumed that it is the scalar product of K*
$\diamond$ *Define $(e_i)_{i=1...d}$ an orthonormal basis of E_{λ_1}*
$\diamond$ *Define $(a_{ij})_{i,j=1...d}$,$(b_i)_{i=1...d}$ and c in K*

$$\begin{aligned}(a_{ij},X) &= \int_{\partial\Omega_0} Xr^2 v(e_i,e_j)\\ (b_i,X) &= \int_{\partial\Omega_0} Xr[v(u_\rho^*,e_i)+\mathbf{f_1}\cdot e_i]\\ (c,X) &= \int_{\partial\Omega_0} X[v(u_\rho^*,u_\rho^*)+2\mathbf{f_1}\cdot u_\rho^*+\eta]\end{aligned}$$

Where $v(\cdot,\cdot)$ is defined in Theorem 5.2.2 as the bilinear part of the directional derivative.
$\diamond$ *Define h_k an orthonormalized basis of $Span(a_{ij},b_i,c)_{i,j}$, let m be the dimension of this space and for any i,j let $(a_{ij}^k)_{k=1...m}$ (resp $(b_i^k)_{k=1...m}$ and $(c^k)_{k=1...m}$) be the coordinates of a_{ij} (resp b_i and c) on the basis $(h_k)_{k=1...m}$*
$\diamond$ *For any $X=(X_1,...,X_m)$ and $(z,w)\in\mathbb{R}^2$, Let $Y=[X,w,z]$*
$\diamond$ *Let $A(X)$ be the $d\times d$ matrix $A(X)_{ij}=a_{ij}^kX_k$ let $B(X)$ be the $d\times 1$ matrix $B(X)_i=b_i^kX_k$ and let $C(X)$ be the scalar $C(X)=c^kX_k$ and let*

$$D(Y)=\begin{bmatrix}-A(X)+z\mathbb{I}d & B(X)\\ B^*(X) & -C(X)-z+w\end{bmatrix}\quad E(Y)=\begin{bmatrix}D(Y) & 0 & 0\\ 0 & \mathbb{I}d & X\\ 0 & X^T & 1\end{bmatrix}$$

The coefficient of E depends linearly on $Y=[X,w,z]$
$\diamond$ *Let $Y^*=[X^*,w^*,z^*]$ be the solution of the following SDP problem :*

$$\min_{E(Y)\geq 0} w \tag{5.9}$$

5.3.2 The choice of descent direction

The goal here is to make the link between the descent direction V^*, solution to equation (5.8) and the SDP problem introduced in section 5.3.1.

Proposition 5.3.2 *The descent direction V^*, solution to* (5.8) *is given by*

$$V^*=\sum_{k=1}^m X_k h_k$$

where h_k is defined in definition 5.3.1 *and X_k are the coordinates in the basis $(h_k)_k$ of X^* and where $Y^*=[X^*,w^*,z^*]$ is the solution of the SDP problem* (5.9)

In order to prove this result, one has to recall the very special shape of g, the directional derivative of equation (5.8) (see Theorem 5.2.2)

$$g(V) = \max_{u \in \mathcal{M}_0} \int_{\partial\Omega} V[v(u,u) + 2\mathbf{f_1} \cdot u - \eta]$$

Where v is bilinear. We now use the characterization of $\mathcal{M}_0$ given by proposition 5.3.1 to make the following development :

$$\begin{aligned} g(V) &= \max_{\substack{w \in E_{\lambda_1} \\ \|Bw\|=r}} \int_{\partial\Omega} V[v(u_{\rho^*} + w, u_{\rho^*} + w) + 2\mathbf{f_1} \cdot u_{\rho^*} + 2\mathbf{f_1} \cdot w - \eta] \\ &= \max_{\sum_i \lambda_i^2 = 1} \lambda_i \lambda_j (a_{ij}, V) + 2\lambda_i (b_i, V) + (c, V) \end{aligned}$$

Decomposing the descent direction in $V^* = \sum_{k=1}^m X_k h_k + V^\perp$, then the X^k are solution to :

$$\begin{aligned} & \min_{\sum_k (X_k)^2 \leq 1} \max_{\sum_i (\lambda_i)^2 = 1} \lambda_i \lambda_j a_{ij}^k X_k + 2\lambda_i b_i^k X_k + c^k X_k \\ = & \min_{X^T X \leq 1} \max_{\lambda^T \lambda = 1} \lambda^T A(X) \lambda + 2\lambda^T D(X) + C(X) \end{aligned}$$

Let us drop the X dependence for a moment. For any matrix A and vector B, the following trust-region problems are equivalent

$$\max_{\lambda^T \lambda = 1} \lambda^T A \lambda + 2\lambda^T B = \min_{-A + z\mathrm{Id} \geq 0} B^T (-A + z\mathrm{Id})^{-1} B + z$$

With the convention that B must belongs to the range of $(-A + z\mathrm{Id})$. See for instance [VB96] (page 229). A good idea of the proof of such a result is :

$$\begin{aligned} & \max_{\lambda^T \lambda = 1} \lambda^T A \lambda + 2\lambda^T B = \max_{\lambda^T \lambda = 1} \min_z \lambda^T (A - z\mathrm{Id}) \lambda + 2\lambda^T B + z \\ = & \min_z \max_{\lambda^T \lambda = 1} \lambda^T (A - z\mathrm{Id}) \lambda + 2\lambda^T B + z = \min_{A - z\mathrm{Id} \leq 0} -B^T (A - z\mathrm{Id})^{-1} B + z \end{aligned}$$

The only difficult point being the inversion of the min and the max which can be done here because we have a problem which is quadratic in one of its variable and linear in the other. So that the following problems are equivalents :

$$\begin{aligned} & \max_{\lambda^T \lambda \leq 1} \lambda^T A \lambda + 2\lambda^T B + C = \min_{-A + z\mathrm{Id} \geq 0} B^T (-A + z\mathrm{Id})^{-1} B + z + C \\ = & \min_{\substack{-A + z\mathrm{Id} \geq 0 \\ -C - z + w \geq B^T (-A + z\mathrm{Id})^{-1} B}} w = \min_{D \geq 0} w \end{aligned} \tag{5.10}$$

When D is defined through $D = \begin{bmatrix} -A + z\mathrm{Id} & B \\ B^T & -C - z + w \end{bmatrix}$

Returning to the SDP problem (5.9), the condition $E(Y) \geq 0$ is equivalent to $X^T X \leq 1$ and $D(Y) \geq 0$. So that problem (5.9) is equivalent to

$$\min_{X^T X \leq 1} \min_{D(Y) \geq 0} w$$

Which is equivalent to (5.8), thanks to the development made in equation (5.10)

5.4 Numerical results

5.4.1 From the beam to a cantilever

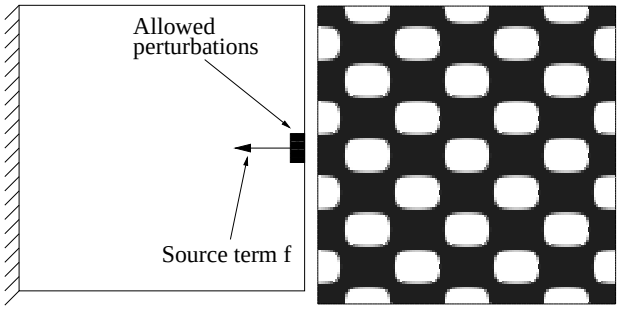

FIG. 5.1 – The beam-to-cantilever problem and its initialization.

The working domain is a 1×1 square meshed with 121×121 nodes. The shape is clamped on the right wall and a unit horizontal load is applied in the middle of the left wall.Vertical perturbations are allowed in an unoptimizable box (the black box of figure 5.1 left) in the middle of the right wall. We perform several test with an increasing parameter m, ie perturbations of bigger norm are allowed. For each of the nine following tests, the same initialization is used (figure 5.1 right), A different Lagrange multiplier is used so that the optimal shape have a volume approximatively equal to 0.2. The other parameters are the same for each test and are set to 1 for the Young modulus, to 0.3 for the Poisson modulus. The weak-material approximation is used to mimick the void, its Young modulus is set to 10^{-4}.

Figure 5.2 is a display of the solutions for increasing m (m increases from left to right and then from the top to the bottom).The different values of m, of the volume and of the Lagrange multiplier η are listed in Table 5.1.

m	=	10^{-3}	5.10^{-3}	7.10^{-3}	$8,5.10^{-3}$	10^{-2}	2.10^{-2}	10^{-1}	1	4
Vol	=	20.3	21.3	21.6	20.2	18.5	19.3	20	24.7	21.8
η	=	.45	.6	.7	.85	1	1.8	20	10^3	2.10^4

TAB. 5.1 – The value of the different parameters for the beam problem.

It can be seen that the upper-left shape is close to a beam (m is the smallest) and the lower-right shape is close to a cantilever (m is the biggest). When m is equal to 0 the robust-compliance problem is a standard compliance problem whose solution is a beam. When m is big, the source term is negligible and the problem turns to be an eigenvalue problem (see remark 4.2.2), the solution is then a cantilever.

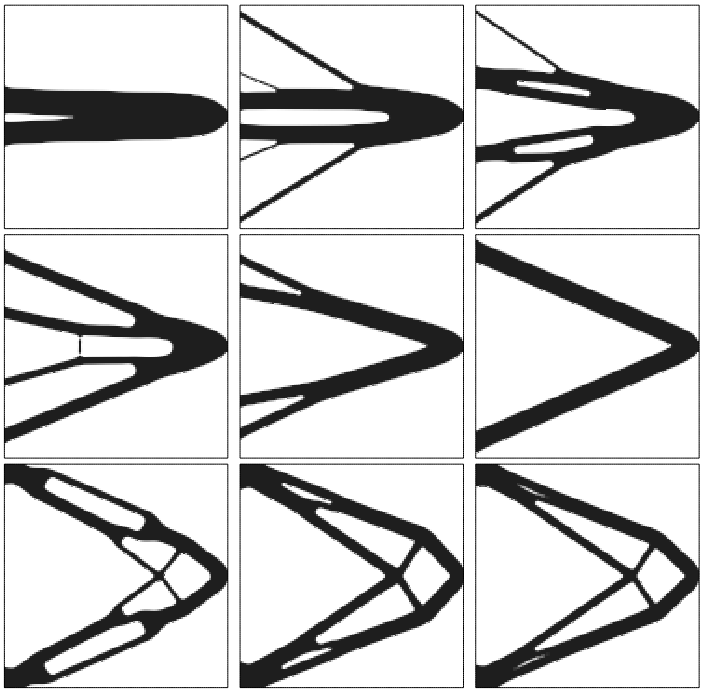

FIG. 5.2 – Increasing values of m in the beam-to-cantilever problem.

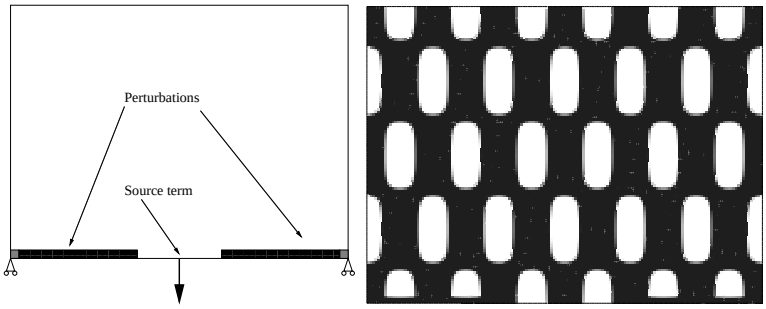

FIG. 5.3 – The Wheel-bridge problem and its initialization.

5.4.2 The Wheel-bridge

On a 16×12 rectangle meshed with 161×121 nodes, we study the case of the wheel-bridge. Namely, a unit vertical load is applied on the middle of the bottom of the bridge and the shape is only constrained by a null vertical displacement on the two sides of the bottom of the bridge (the gray boxes of figure 5.3 (right)). Vertical perturbation are located on the black boxes of Figure 5.3 (right).In order to deal with the problem of rigid displacement that are still allowed in this setting, we enforce the nodes close to where the load is applied to have null

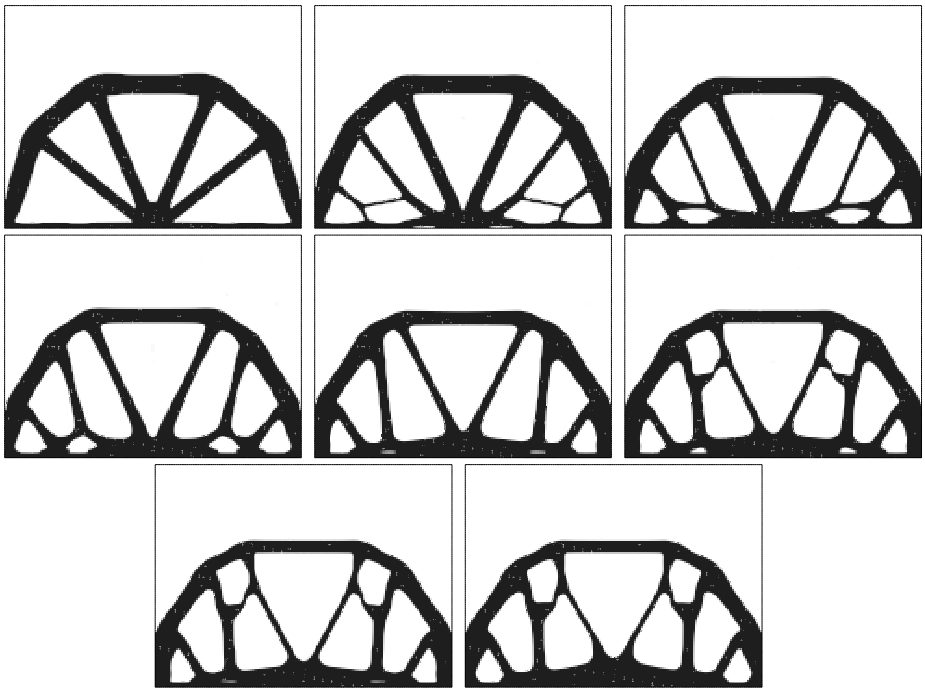

FIG. 5.4 – Increasing values of m in the wheel-bridge problem.

horizontal displacement. As in the above section, the test was run for several different values of the parameter m (see Table 5.2), the same initialization has been used for the different tests, optimal shape are displayed in figure 5.4.

m	=	0.001	0.1	0.3	0.5	1.3	1.5	2.3	6
Volume	=	25.5	25.4	25.5	25.7	25.7	25.5	25.1	25.8
η	=	2.7	4	8	15	55	70	140	800

TAB. 5.2 – The value of the different parameters for the wheel-bridge problem.

5.4.3 The 2-d mast

The optimal mast problem is a T-shaped working domain meshed with 3600 square cell. The T shape has an height 6, a width 2 at the bottom and 4 at the top. The bottom of the shape is fixed while two loads are applied at the lower corner of the horizontal branch of the T (see Figure 5.5). This test was run in chapter 2 with a slight difference, ie the Dirichlet nodes were located only at the two lower corner. It was done so because the optimal shape for the compliance of this problem (seen in Figure 5.6 (left)) has only one branch at the bottom and is less interesting from an engineering point of view than the one in chapter 2.

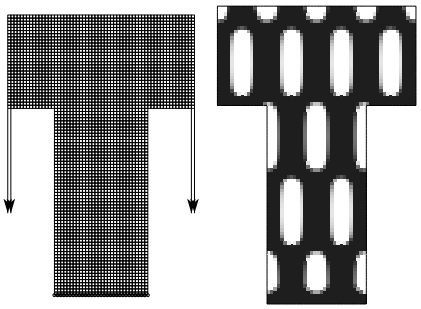

FIG. 5.5 – Mesh and initialization of the 2-d mast problem.

The solution to the compliance problem is not stable. Vertical perturbations are allowed were the loads are sets. Figure 5.6 is a display of the different optimal shapes for different parameters that are shown in Table 5.3.

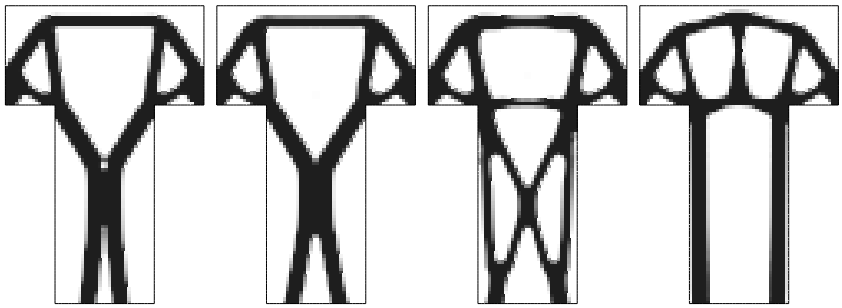

FIG. 5.6 – Increasing values of m for the 2d-mast problem (vertical perturbations).

m	=	0	0.01	0.05	0.1
Volume	=	0.34	0.33	0.37	0.34
η	=	3	3.5	4	6

TAB. 5.3 – The value of the different parameters for the mast problem with vertical perturbations.

The 2-d mast test has also been performed with perturbations both horizontal and vertical. Figure 5.7 is a display of the solutions for increasing values of m and the value of the different parameters is shown in table 5.4

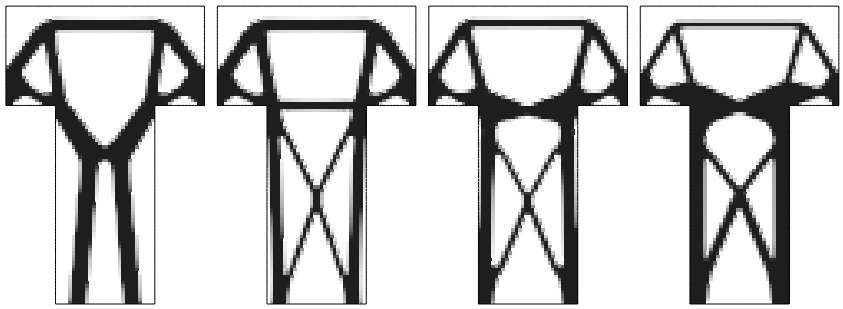

FIG. 5.7 – Increasing values of m for the 2d-mast problem (vertical and horizontal perturbations).

m	=	0.02	0.03	0.1	0.2
Volume	=	0.345	0.335	0.347	0.376
Lagrange	=	3.6	4	8	14

TAB. 5.4 – The value of the different parameters for the mast problem with vertical and horizontal perturbations.

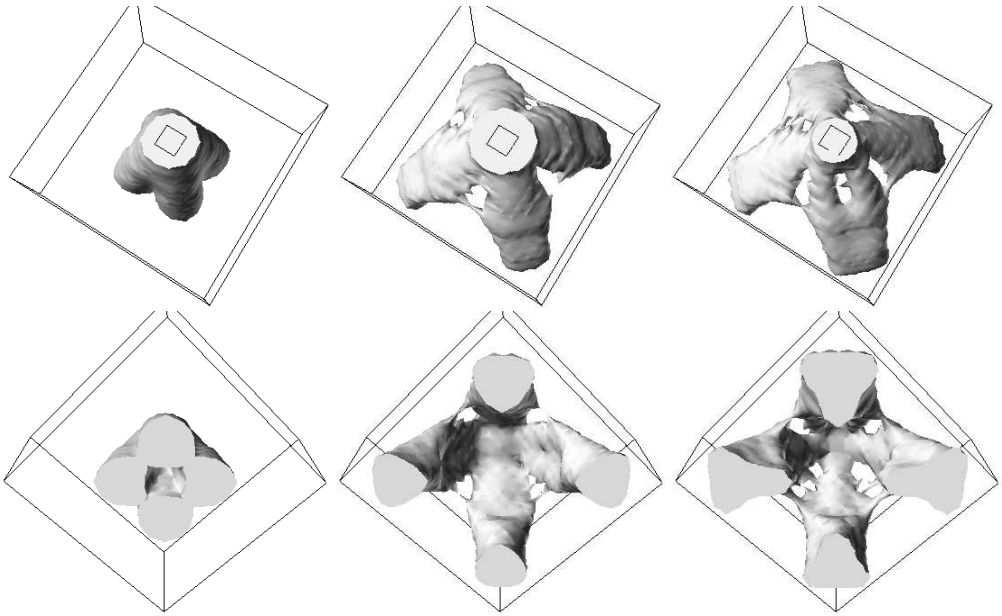

FIG. 5.8 – Upper and bottom view of the optimal shapes for $m = 10^{-2}, 3\times10^{-2}$ and 5×10^{-2} for a volume of 10 percent.

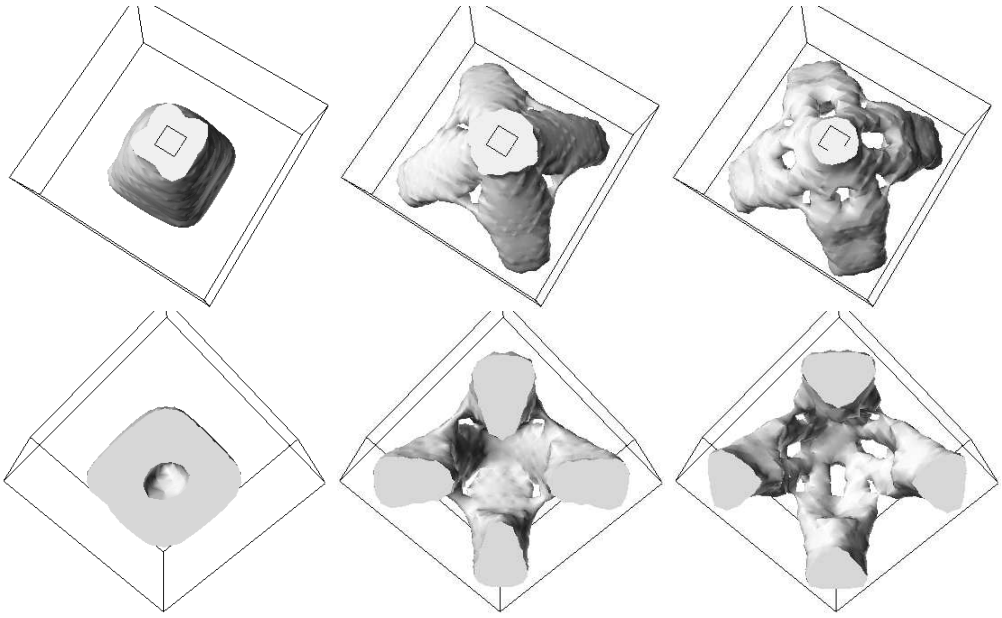

FIG. 5.9 – Upper and bottom view of the optimal shapes for $m = 10^{-2}, 3 \times 10^{-2}$ and 5×10^{-2} for a volume of 14 percent.

5.4.4 The 3-d beam

A $40 \times 40 \times 21$ domain is meshed with a $21 \times 21 \times 22$ grid. The plane $z = 0$ corresponds to Dirichlet nodes and a vertical unit load is applied on the middle of the plane $z = 21$. Perturbations are allowed everywhere and in every direction. The Young modulus is set to 1 in the shape and to 10^{-3} in the void. The Poisson ratio is set to 0.3 everywhere. As for every test, the same initialization is used and the Lagrange multiplier is set so that the different shapes have approximatively a volume of 10 percent for Figure 5.8 and 14 percent for Figure 5.9

It is interesting to notice that if the value of m is increased too much then the algorithm will have the tendency to remove the upper part of the shape. This behavior of the algorithm is well-known in optimization of the first eigenvalue (see chapter 3 for the same test with eigenvalue optimization). A common way to avoid this problem is to put an heavier mass-tip at the top. This test was designed so that we could avoid this trick of the mass-tip by imposing a balance between the optimization of the first eigenvalue and the optimization with respect to the load. When the value of m is set too high, this balance is lost and the algorithm removes the upper part of the shape . Figure 5.10 is a display of the optimal shape when m is set to 7×10^{-2}. The shape is not symmetric because the algorithm concentrates on removing the top of the shape. It must be born in mind that in Figure 5.10, it is the isovalue 0 of the level-set that is shown and not the isovalue 0.3 of the density like in Figures 5.8 and 5.9 and

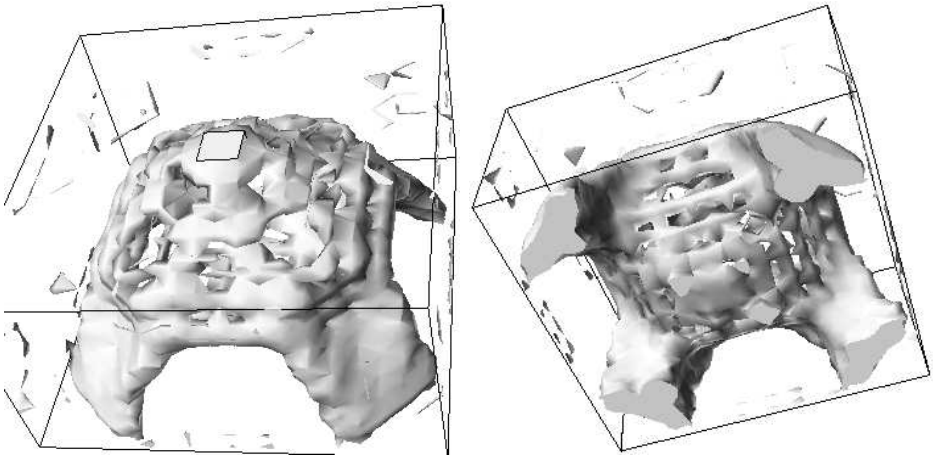

FIG. 5.10 – Optimal shape for $m = 7\times10^{-2}$ and a volume of 11 percent (isovalue 0 of the level-set is shown).

that the top of the shape is indeed almost disconnected (in numerical sense) to the bottom part.

5.4.5 The 3-d bridge

This problem has been introduced in [AJ05] where the authors compared the single load and the multiple load optimization. The 3-d bridge is made of a non-optimizable roadway and two lateral vertical boxes where reinforcements can be applied. A single load is applied on the roadway that corresponds to the weight of the bridge. The perturbations are allowed on the vertical direction everywhere on the roadway. On contrario to the results advanced in [AJ05], the

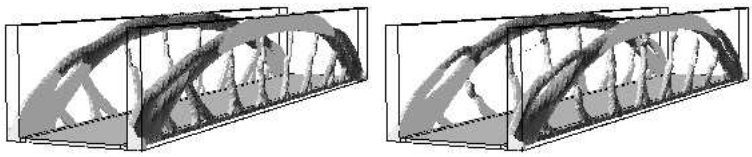

FIG. 5.11 – Optimal shape of the bridge for $m = 0$ (left) and $m = 1$ (right).

optimal shape is the same whatever the size of the perturbations and is of same nature than the optimal shape for the multiple load of [AJ05] (see figure 5.11). In order to be able to perform the SDP algorithm, the technique of Hilbertian embedding of the velocity was used (see chapter 3), thus the gradient algorithm used is not the same than the one used in [AJ05]. That is why the results for $m = 0$ (single-load optimization of the compliance) are not the same than in [AJ05]. Numerical comparison of the two optimal shapes shows that the one

advanced here is better than the one advanced in [AJ05]. This shows that the design and hence the single load problem of figure 5.11 (left) is very stable.

5.4.6 The 3-d chair

This problem has also been studied in [AJ05]. The four bottom corners are fixed while the back and the seat of the chair are not subject to optimization and support the pressure loads. The pressure applied on the back of the chair is 5 times smaller than the pressure applied on the seat. Perturbations are allowed both on the back and on the seat and are of the following type :

$$g = \chi_S s_3 e_3 + 0.2\chi_B s_1 e_1 \quad \text{with } \|s\|_{L^2(D)} \leq m$$

Where e_i is the i^{th} vector of the Cartesian coordinate and s_i is the i^{th} coordinate of s. χ_S denotes the characteristic function of the seat while χ_B is the one of the back. The two optimal shapes are displayed in figure 5.12. The robust-

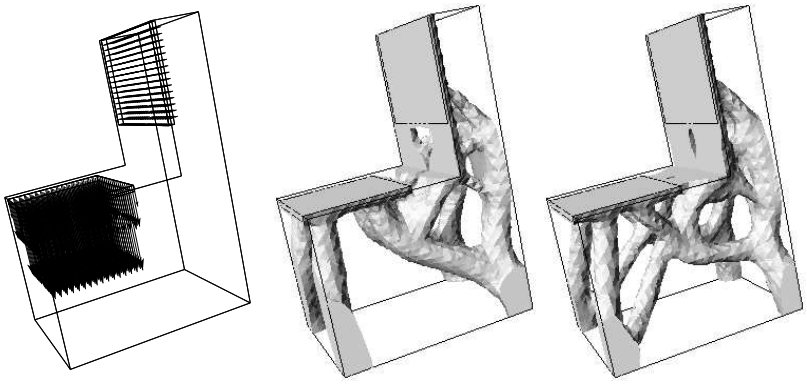

FIG. 5.12 – Loading and optimal shape of the chair for $m = 0$ (left) and $m = .1$ (right).

compliance optimal chair has a more complex topology and is more stable. The topology of the robust-compliance optimal chair is not the same than the topology of the multiple load optimal chair (see [AJ05]), the robust chair seems more stable than the multiple load chair.

5.5 Conclusion

We gave the proof of existence of a worst perturbation to a given set of loads $\mathbf{f}$, we gave the characterization of the set of the perturbation that are the worst.

We gave a stable algorithm that calculates the set of worst perturbations and the robust compliance, this algorithm relies on a Newton type method and we gave performing bounds on the critical point of the Newton method. Thanks to those bounds, in every test made, we did not need more than a small number

of iterations (± 15) inside the Newton method. Each iteration costs no more than a direct inversion of a matrix, as a result, we claim that finding the worst perturbation of a given load is of same difficulty than finding the energy of that load.

We then proved the existence of a shape directional derivative for the robust compliance problem and used a local SDP problem in order to perform the regularized level-set method. Taking in account the standard drawback of the level-set method (ie falling into local minima), the algorithm successfully find optimal shapes that are stable with respect to unknown perturbations. Optimal designs are new and cannot be compared to the kind of design obtained by the multiple load optimization which are known to be more stable than the single load problem.

Because the problem of the robust compliance is an self-adjoint problem that can be considered as a mix between the standard compliance and a generalized eigenvalue problem, it may have chances to behave well with respect to the homogeneization theory. This relaxation theory bears the advantage of proving the existence of a global minimizer in a broader class of admissible set and of avoiding the local minimizer problem. A full investigation of this issue is to be performed.

Chapitre 6

Shape optimization of the buckling load

Abstract

We wish to study and to optimize the buckling of a loaded shape. The buckling criterion is defined as the limit load of the linear response of an elastic structure. Although not-well posed, this criterion is the simplest guess of the non-linear response of a structure.

6.1 The direct problem 113
6.1.1 Definition of the linearized buckling load 113
6.2 Shape sensitivity of the buckling load 116
6.2.1 Multiplicity equal to one 116
6.2.2 Multiplicity greater than one 119
6.2.3 The algorithm 120
6.3 Numerical example 121
6.3.1 The loaded beam 121
6.3.2 The two beams reinforcement 123
6.3.3 The compliant bridge 125
6.3.4 The buckling of a grip 126
6.4 Conclusion 129

6.1 The direct problem

6.1.1 Definition of the linearized buckling load

In the setting of the non-linear elasticity, the strains are defined by :

Definition 6.1.1 *For a given displacement u, let $e(u)$ be the non-linear strain, defined as $e(u) = \varepsilon(u) + \frac{1}{2}Q(u,u)$, with*

$$\varepsilon(u) = \frac{1}{2}(\nabla u + \nabla u^*) \quad Q(u,v) = \frac{1}{2}(\nabla u \nabla v^* + \nabla v \nabla u^*)$$

Given a shape Ω and a set of loads f, let u_f be the solution to the non-linear elasticity system, ie :

Definition 6.1.2 *Let $E(u,f)$ the functional of the non-linear elasticity, ie :*

$$E(u,f) = \int_\Omega Ae(u) : e(u) - 2\int_\Omega f_1 \cdot u - 2\int_{\partial\Omega} f_2 \cdot u$$

Then u_f the displacement is given by :

$$E(u_f, f) = \min_u E(u,f)$$

Formal proof of the buckling criterion. The following formal development leads to the introduction of the equation of the buckling load criterion : *For small f, the displacement u_f is supposed to be small. In this case, the linearization of the non-linear elasticity system is the standard elasticity system (see equation (1.6)). If u_f is supposed to be small enough, then it exists and is unique.*

The buckling load λ is defined as the smallest positive real such that $u_{\lambda f}$ ceases to be unique. If λ exists, it is then defined as the first bifurcation point of the curve $t \mapsto u_{tf}$ (given $u_0 = 0$). Standard bifurcation theory imposes to find the first occurrence in t such that $\partial^2_{uu} E(u_{tf}, tf)$ is not positive definite. Dropping the rest of the standard bifurcation theory discussion, we define λ the buckling load criterion as the smallest t such that this Hessian is not definite positive. This Hessian is defined as :

Definition 6.1.3 *Define the trilinear symmetric application C as :*

$$C(u; v, w) = A\varepsilon(u) : Q(v,w) + A\varepsilon(w) : Q(u,v) + A\varepsilon(v) : Q(w,u)$$

The Hessian of the energy is given by

$$\partial^2_{uu} E(u_{tf}, tf).(v,w) = \int_\Omega A\varepsilon(v) : \varepsilon(w) + \int_\Omega C(u_{tf}; v, w) + \int_\Omega AQ(u_{tf}, u_{tf}) : Q(v,w)$$

The first occurrence in t when the Hessian begins to be degenerate is written as :

$$\min_{t>0} \min_v \partial^2_{uu} E(u_{tf}, tf).(v,v) \leq 0$$

We define the linearized buckling load γ as the minimizer (in t) of the linearization of the above equation around the point $t = 0$. The development at first

order in t of u_{tf} is $u_{tf} = tu_0 + O(t^2)$ where u_0 is the solution to the problem of linearized elasticity :

$$\int_\Omega A\varepsilon(u_0) : \varepsilon(w) = \int_\Omega f_1 \cdot w + \int_{\partial\Omega} f_2 \cdot w \quad \forall w \in H^1_D(\Omega) \tag{6.1}$$

The equation for the linearized buckling load γ is then

Proposition 6.1.1 *Find the smallest γ positive such that there exist an $u_1 \in H^1_D(\Omega) \setminus \{0\}$ such that :*

$$\int_\Omega A\varepsilon(u_1) : \varepsilon(u_1) = -\gamma \int_\Omega C(u_0; u_1, u_1) \tag{6.2}$$

Where u_0 is given in equation (6.1)

The linearized buckling load is then defined through a Rayleigh quotient as an eigenvalue of a generalized eigenproblem. The Rayleigh formulation of the problem is :

$$\gamma^{-1} = \max_v - \frac{\int_\Omega C(u_0; v, v)}{\int_\Omega A\varepsilon(v) : \varepsilon(v)} \tag{6.3}$$

The definition of γ^{-1} as a biggest eigenvalue only makes sense if this biggest eigenvalue is positive. If not, the shape will not be considered to buckle and γ will be set to infinity.

There is no gap of derivative between the two sides of the generalized

eigenproblem, so that there is a priori no compactness. It is still unknown if γ is or is not attained. That is why, we will assume in the sequel that the set of admissible modes u_1 is sought in a **finite dimensional** vector space V included in $H^1_D(\Omega)$. The maximum of the Rayleigh quotient (6.3) is then defined over V. This will allow us to get rid of compactness problems and to be able to perform the mathematical analysis of shape derivation. Define γ^{-1} as :

Definition 6.1.4 *The linearized buckling load γ is such that γ^{-1} is the biggest eigenvalue of the eigenproblem :*

$$\int_\Omega A\varepsilon(u_1) : \varepsilon(w) = -\gamma \int_\Omega C(u_0; u_1, w) \quad \forall w \in V \tag{6.4}$$

The vector space V being, of course, the vector space spanned by the basis function of the mesh that will be used. It is true that in numerical sense, we do not have to bother about the compactness problem because vectors and matrix are finite-dimensional but this does not solve the problem. It is well known that a lack of compactness may result in great numerical difficulties, especially if mesh is refined.

In physical models of the linearized buckling load, engineers and physicist do not work with definition (6.4) of γ. Their equation is obtained if C is replaced by :

$$C(u; v, w) = A\varepsilon(u) : Q(v, w) \tag{6.5}$$

The approximation that is made to obtain this equation is not consistent ! Indeed, there is a development in powers of t where for unknown reasons the two last terms in definition of C is omitted (see [Nov53], [NSB02],[NRG95]). Nevertheless, the following still holds true for such a C and numerical test has been performed with both models.

Definition 6.1.5 *In equation* (6.2) *of proposition 6.1.1 of the definition of the buckling mode, if the C used is the one of equation* (6.5) *:*

$$C(u; v, w) = A\varepsilon(u) : Q(v, w)$$

then γ will be called "the standard buckling load".

If the C used is the one of definition 6.1.3 :

$$C(u; v, w) = A\varepsilon(u) : Q(v, w) + A\varepsilon(w) : Q(u, v) + A\varepsilon(v) : Q(w, u)$$

then γ will be called "the extended buckling load".

6.2 Shape sensitivity of the buckling load

6.2.1 Multiplicity equal to one

We first suppose that the multiplicity of the buckling eigenvalue is equal to one, In this case, if Ω is sufficiently smooth, the eigenvalue is differentiable and so is u_0 the solution to the linear problem.

Theorem 6.2.1
$\diamond$ *Assume that $u_1 \in V \subset H^1_D(\Omega)$, the mode defined by* (6.4) *is normalized by $\int_\Omega C(u_0; u_1, u_1) = -1$ and define the adjoint state $p \in H^1_D(\mathbb{R}^d)$ as the unique solution to*

$$\int_\Omega A\varepsilon(\phi) : \varepsilon(p) = \gamma \int_\Omega C(\phi; u_1, u_1) \quad \forall \phi \in H^1_D(\Omega) \tag{6.6}$$

$\diamond$ *The buckling load $\gamma(\Omega)$ is then derivable with respect to the domain and its derivative is given by*

$$\gamma'(\theta) = \int_{\partial\Omega} \big(\theta \cdot n\big) v(u_1, u_1)$$

Where $v(u_1, u_1)$ is defined as

$$\left.\begin{array}{rcll} v(u_1,u_1) & = & A\varepsilon(u_1) : \varepsilon(u_1) + \gamma C(u_0; u_1, u_1) & \\ & - & A\varepsilon(u_0) : \varepsilon(p) + f_1 \cdot p + \partial_n(f_2 \cdot p) + Hf_2 \cdot p & \text{on } \Gamma_N \\ v(u_1,u_1) & = & -A\varepsilon(u_1) : \varepsilon(u_1) - 2\gamma C(u_1; u_0, u_1) & \\ & + & A\varepsilon(u_0) : \varepsilon(p) & \text{on } \Gamma_D \end{array}\right\} \tag{6.7}$$

The simplest way to compute the shape sensitivity is to apply the Lagrangian derivation originally introduced by Céa [Céa86] and that was also used in section 5.2.1. We just need an additional notation for the following integration by parts

Definition 6.2.1 *For any v, w, define $D(v,w)$ such that for any u, $C(u;v,w) = D(v,w)\colon \nabla u$, where C is defined in definition 6.1.3. The following integration by parts is available :*

$$\int_\Omega C(u;v,w) = \int_\Omega -div(D(v,w))u + \int_{\partial\Omega} (D(v,w)\cdot n)u \tag{6.8}$$

For the extended buckling load, D is given by :

$$D(v,w)^l_j = AQ(v,w)^l_j + \big(A\varepsilon(w)\big)^k_j \partial_k v^l + \big(A\varepsilon(v)\big)^k_j \partial_k w^l \tag{6.9}$$

Proof of Theorem 6.2.1 This proof is formal only, we hereby assume that the first mode is shape-differentiable. Define the following Lagrangian $\mathcal{L}^c$

$$\begin{aligned}
\mathcal{L}^c(\Omega,v,u,q,r) &= \frac{-\int_\Omega C(u;v,v) + 2\int_{\Gamma_D} rv}{\int_\Omega A\varepsilon(v)\colon\varepsilon(v)} + \int_\Omega A\varepsilon(u)\colon\varepsilon(q) \\
&- \int_\Omega f_1\cdot q - \int_{\Gamma_N} f_2\cdot q \\
&- \int_{\Gamma_D} \big(A\varepsilon(u)\cdot n\big)q + \big(A\varepsilon(q)\cdot n\big)u \\
&+ \frac{\int_{\Gamma_D}\big(D(v,v)\cdot n\big)u}{\int_\Omega A\varepsilon(v)\colon\varepsilon(v)}
\end{aligned}$$

Where q is a Lagrange multiplier for the state equation of u_0 and r is a Lagrange multiplier for the Dirichlet condition of u_1. We denote by $(u_1, u_0, \tilde{p}, s)$ the min-max or saddle points of $\mathcal{L}^c$ for :

$$\max_{(u,v)\in H^1(\mathbf{R}^d;\mathbf{R}^d)}\ \min_{(q,r)\in H^1(\mathbf{R}^d;\mathbf{R}^d)} \mathcal{L}^c(\Omega,v,u,q,r)$$

The stationarity of the Lagrangian gives the optimality conditions. The partial derivative of $\mathcal{L}^c$ with with respect to q in the direction $\phi \in H^1(\mathbb{R}^d;\mathbb{R}^d)$ is

$$\begin{aligned}
\Big(\frac{\partial\mathcal{L}^c}{\partial q}(\Omega,u_1,u_0,\tilde{p},s),\phi\Big) &= \int_\Omega \big(-divA\varepsilon(u_0) - f_1\big)\phi + \int_{\Gamma_N}(A\varepsilon(u_0)\cdot n - f_2)\phi \\
&- \int_{\Gamma_D}\big(A\varepsilon(\phi)\cdot n\big)u
\end{aligned}$$

Varying ϕ on Ω gives us the state equation, varying the trace function ϕ on Γ_N gives us the Neumann boundary condition on u_0. And varying $A\varepsilon(\phi)\cdot n$ on Γ_D yields the Dirichlet condition $u = 0$ on Γ_D.

The optimality condition on r of $\mathcal{L}^c$ is the Dirichlet condition $u_1 = 0$ on Γ_D. It follows that the saddle point is just the Rayleigh quotient that gives the eigenvalue γ^{-1}.

$$\gamma^{-1}(\Omega) = \max_{(u,v)\in H^1(\mathbf{R}^d;\mathbf{R}^d)} \min_{(q,r)\in H^1(\mathbf{R}^d;\mathbf{R}^d)} \mathcal{L}^c(\Omega, v, u, q, r)$$

In order to simplify notations, let's denote α as

$$\int_\Omega A\varepsilon(u_1) : \varepsilon(u_1) = \alpha \tag{6.10}$$

The partial derivative of $\mathcal{L}^c$ with respect to u in the direction $\phi \in H^1(\mathbb{R}^d;\mathbb{R}^d)$ gives the equation for the adjoint which is, after an integration by part :

$$\begin{aligned}\Big(\frac{\partial \mathcal{L}^c}{\partial u}(\Omega, u_1, u_0, \tilde{p}, s), \phi\Big) &= \int_\Omega \big(\alpha^{-1} div D(u_1,u_1) - div A\varepsilon(\tilde{p})\big)\phi \\ &+ \int_{\Gamma_N} \big(A\varepsilon(\tilde{p})\cdot n - \alpha^{-1} D(u_1,u_1)\cdot n\big)\phi - \int_{\Gamma_D} \big(A\varepsilon(\phi)\cdot n\big)\tilde{p}\end{aligned}$$

Where D is defined in equation (6.8) and α is defined in equation (6.10) .Varying ϕ gives the equations for $\tilde{p}$ which are :

$$\left.\begin{array}{rcll} div A\varepsilon(\tilde{p}) = & \alpha^{-1} div D(u_1,u_1) & \text{on } \Omega \\ A\varepsilon(\tilde{p})\cdot n = & \alpha^{-1} D(u_1,u_1)\cdot n & \text{on } \Gamma_N \\ \tilde{p} = & 0 & \text{on } \Gamma_D \end{array}\right\} \tag{6.11}$$

The partial derivative of $\mathcal{L}^c$ with respect to v in the direction ϕ is equal to :

$$\begin{aligned}\Big(\frac{\partial \mathcal{L}^c}{\partial v}(\Omega, u_1, u_0, \tilde{p}, s), \phi\Big) &= -2\alpha^{-1}\int_\Omega C(u_0; u_1, \phi) - 2\alpha^{-1}\gamma^{-1}\int_\Omega A\varepsilon(u_1) : \varepsilon(\phi) \\ &+ 2\alpha^{-1}\int_{\Gamma_D} s\phi + 2\alpha^{-1}\int_{\Gamma_D}\big(D(u_1,\phi)\cdot n\big)u_0 \\ &+ 2\alpha^{-2}\left(\int_{\Gamma_D}\big(D(u_1,u_1)\cdot n\big)u_0\right)\int_\Omega A\varepsilon(u_1) : \varepsilon(\phi)\end{aligned}$$

Setting this partial derivative to zero and recalling that $u_0 = 0$ on Γ_D, we perform an integration by part which gives :

$$\begin{aligned}0 = \Big(\frac{\partial \mathcal{L}^c}{\partial v}(\Omega, u_1, u_0, \tilde{p}, s), \phi\Big) &= 2\alpha^{-1}\int_\Omega \big(div D(u_0;u_1) + \gamma^{-1} div A\varepsilon(u_1)\big)\,\phi \\ &- 2\alpha^{-1}\int_{\Gamma_N}\big(D(u_0,u_1)\cdot n + \gamma^{-1}A\varepsilon(u_1)\cdot n\big)\phi \\ &- 2\alpha^{-1}\int_{\Gamma_D}\big(D(u_0,u_1)\cdot n + \gamma^{-1}A\varepsilon(u_1)\cdot n - s\big)\phi\end{aligned}$$

Varying ϕ on Ω and on Γ_N gives the state equation for u_1 and varying ϕ on Γ_D gives the equation for s. Using that Γ_D is a level-set of u_1, we have : $\partial_n u_1 n = \nabla u_1$ so that the definition of D, definition 6.2.1 implies

$$s\partial_n u_1 = \gamma^{-1} A\varepsilon(u_1) : \varepsilon(u_1) + C(u_1; u_0, u_1) \tag{6.12}$$

The shape derivative of γ^{-1} is obtained by differentiating $\mathcal{L}^c(\Omega)$ which by the chain rule theorem reduces to the partial derivative of $\mathcal{L}^c$ with respect to Ω in the direction θ which is :

$$\begin{aligned}
(\frac{\partial \mathcal{L}^c}{\partial \Omega}(\Omega, u_1, u_0, \tilde{p}, s), \theta) &= -\int_{\Gamma_N} \frac{\partial (f_2 \cdot \tilde{p})}{\partial n} + H f_2 \cdot \tilde{p} + f_1 \cdot \tilde{p} \\
+ &\int_{\partial\Omega} -\alpha^{-1} C(u_0; u_1, u_1) - \alpha^{-1}\gamma^{-1} A\varepsilon(u_1) \colon \varepsilon(u_1) + A\varepsilon(u_0) \colon \varepsilon(\tilde{p}) \\
+ &\int_{\Gamma_D} \alpha^{-1} 2s \partial_n u_1 - \big(A\varepsilon(u_0) \cdot n\big)\partial_n \tilde{p} - \big(A\varepsilon(\tilde{p}) \cdot n\big)\partial_n u_0 \\
+ &\int_{\Gamma_D} \alpha^{-1} \big(D(u_1, u_1) \cdot n\big)\partial_n u_0
\end{aligned}$$

Where we used $u_1 = u_0 = \tilde{p} = 0$ on Γ_D to simplify the equations. Using the fact that Γ_D is a level-set of $\tilde{p}$ and u_0 we have

$$\big(A\varepsilon(u_0) \cdot n\big)\partial_n \tilde{p} = A\varepsilon(\tilde{p}) \colon \varepsilon(u_0) = \big(A\varepsilon(\tilde{p}) \cdot n\big)\partial_n u_0$$

$$\big(D(u_1, u_1) \cdot n\big)\partial_n u_0 = C(u_0; u_1, u_1)$$

Using property (6.12) of s, then the derivative of $\mathcal{L}^c$ becomes

$$\begin{aligned}
(\frac{\partial \mathcal{L}^c}{\partial \Omega}(\Omega, u_1, u_0, \tilde{p}, s), \theta) &= -\int_{\Gamma_N} \frac{\partial (f_2 \cdot \tilde{p})}{\partial n} + H f_2 \cdot \tilde{p} + f_1 \cdot \tilde{p} \\
- &\int_{\Gamma_N} \gamma^{-1}\alpha^{-1} A\varepsilon(u_1) \colon \varepsilon(u_1) - A\varepsilon(u_0) \colon \varepsilon(\tilde{p}) + \alpha^{-1} C(u_0; u_1, u_1) \\
+ &\int_{\Gamma_D} \alpha^{-1}\gamma^{-1} A\varepsilon(u_1) \colon \varepsilon(u_1) - A\varepsilon(u_0) \colon \varepsilon(\tilde{p}) + 2\alpha^{-1} C(u_1; u_0, u_1)
\end{aligned}$$

This equation is homogeneous in u_1, we set $\alpha = \gamma$, we also set $p = \gamma^2 \tilde{p}$. Then u_1 is normalized by $\int_\Omega C(u_0; u_1, u_1) = -1$ and the adjoint state p obeys equation (6.6). Recalling that the saddle point of the Lagrangian is equal to γ^{-1} the partial derivative of γ in the direction θ is given by :

$$(\gamma)'(\theta) = -\gamma^2 (\frac{\partial \mathcal{L}^c}{\partial \Omega}(\Omega, u_1, u_0, \tilde{p}, s), \theta) = \int_{\partial\Omega} (\theta \cdot n) v(u_1, u_1) \tag{6.13}$$

Where $v(\cdot, \cdot)$ is defined in (6.7) □

6.2.2 Multiplicity greater than one

When the multiplicity of γ is greater than one, γ is no more differentiable but only directionally differentiable. In order to compute the directional derivative of γ, we express

γ^{-1} as a maximum :

$$\gamma^{-1} = \max_{v \in V} F(v, \Omega) \tag{6.14}$$

Where F is given by the Rayleigh quotient or equivalently

$$F(v,\Omega) = \max_{u\in H^1(\mathbf{R}^d;\mathbf{R}^d)} \min_{(q,s)\in H^1(\mathbf{R}^d;\mathbf{R}^d)} \mathcal{L}^c(\Omega,v,u,q,s)$$

F is Lipschitz with respect to v and with some compactness hypothesis that are insured by the fact v is sought in the finite dimensional space V, we can calculate the sub-gradient of γ^{-1} and its directional derivative. It is given by (see [FR98]) :

$$\big(\frac{\partial\gamma^{-1}}{\partial\Omega},\theta\big) = \max_{u\in\mathcal{M}} \big(\frac{\partial F}{\partial\Omega}(u,\Omega),\theta\big)$$

Where $\mathcal{M}$, the first eigenspace, is the set of v which realizes the maximum in (6.14). The derivative of F with respect to Ω at a point $u \in \mathcal{M}$ has been calculated in section 6.2.1. The directional derivative of γ is given by :

$$\gamma'(\theta) = \max_{\substack{u\in\mathcal{M}\\ \|u\|=1}} \int_{\partial\Omega} (\theta\cdot n) v(u,u) \tag{6.15}$$

Where $v(\cdot,\cdot)$ is defined in (6.7) and $\|u\| = 1$ means that the eigenvectors are normalized by $\int_\Omega A\varepsilon(u)\colon\varepsilon(u) = \gamma$.

6.2.3 The algorithm

The first objective function to be considered is

$$\min_{\Omega\in\mathcal{U}_{ad}} \mathcal{J}_{bu}(\Omega) \quad \text{Where} \quad \mathcal{J}_{bu}(\Omega) = -\gamma(\Omega) \tag{6.16}$$

and $\mathcal{U}_{ad}$ is defined in equation (1.5). Using a Lagrange multiplier η for the volume constraint, the objective function to be minimized is given by

$$\mathcal{L}_{bu}(\Omega) = -\gamma(\Omega) + \eta|\Omega|$$

This objective function is directionally shape-differentiable and its derivative is given by :

$$\mathcal{L}'_{bu}(\theta) = \max_{\substack{u\in\mathcal{M}\\ \|u\|=1}} \int_{\partial\Omega} (\theta\cdot n)(v(u,u)+\eta) \tag{6.17}$$

Where $v(\cdot,\cdot)$ is defined in (6.7). the term η is independent of u and $v(\cdot,\cdot)$ is bilinear in u. The set $u \in \mathcal{M}$ such that $\|u\| = 1$ is a sphere of dimension the dimension equal to that of the first eigenspace. A development like the one in section 3.5.3 shows that this problem is solvable by an SDP algorithm. We then apply the standard technique of shape optimization already developed in chapter 3 for the optimization of multiple eigenvalues.

6.3 Numerical example

Computing the linearized buckling load is quite a standard issue. In this section only, matrices are written in capital letters and vectors in lower-case letters. Furthermore, the terms "biggest one" and "smallest one" refer to the natural order of $\mathbb{R}$ (where a negative real is always smaller than a positive one). The term "biggest one in absolute value" refers to the norm of $\mathbb{R}$, when a negative is bigger than a positive one granted that it's absolute value is bigger. The confusion may come from the fact that, for power algorithms, the eigenvalue computed is the "biggest one in absolute value" and we are interested in the "biggest one".
$\diamond$ Compute the stiffness matrix K.
$\diamond$ Find u_0 the linearized displacement solution to $u_0 = K^{-1}f$, where f is the source loads.
$\diamond$ Compute the geometric matrix $G(u_0)$. The problem is to find γ the smallest positive eigenvalue of the generalized eigenproblem :

$$Ku_1 = -\gamma G(u_0)u_1 \tag{6.18}$$

The problem can be restated into : let λ_M be the biggest eigenvalue of the matrix $-K^{-1}G(u_0)$. If λ_M is positive, then $\lambda_M = \gamma^{-1}$, if it is negative then there is no positive eigenvalue solution to the eigenproblem (6.18), the shape do not buckle.
$\diamond$ Perform a power algorithm on the matrix $-K^{-1}G(u_0)$ in order to find λ the biggest eigenvalue in absolute value. If λ is positive, then it is equal to λ_M and therefore to γ^{-1} and stop the algorithm. If λ is negative, it is equal to λ_m, the smallest eigenvalue of $K^{-1}G(u_0)$.
$\diamond$ If λ is negative, let $\alpha < \lambda < 0$ be a shifting parameter and perform a power algorithm on the matrix $(-K^{-1}G(u_0) - \alpha\mathrm{Id})$, every eigenvalue of this matrix is strictly positive so that the biggest one in absolute value is equal to the biggest one, which in turn is equal to $\lambda_M - \alpha$. If λ_M is negative then stop, the shape do not buckle. If λ_M is positive, then it is equal to γ^{-1}.

Once this is done, the level-set method can be run.

6.3.1 The loaded beam

A 60×80 rectangle meshed with 61×81 nodes is forced with Dirichlet condition on its bottom. A force of norm 1 is applied at the top of the rectangle on the middle of it. The nearby cells of the node where the force is applied are not subject to optimization. The Young modulus of the material is set to 1, the Poisson ratio ν to 0.3 and the Lagrange multiplier to 8×10^{-6}. Figure 6.3 is a convergence history of the criterion. As in section 3.4.5, the higher the ratio of the weak material is, the smoother the objective function with respect to domain variation. So that we optimize the shape with a ratio of the weak material equal to 10^{-2}. But we need to re-optimize it afterward because if the ratio ε is too high, then the adjoint is not computed with enough accuracy. So that we re-optimize the optimal shape with a ration equal to 10^{-5}. The

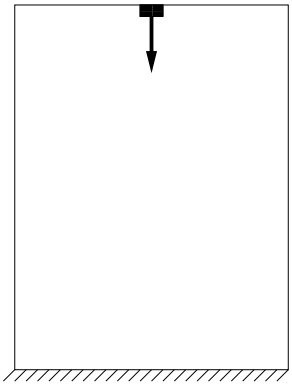

FIG. 6.1 – The beam problem.

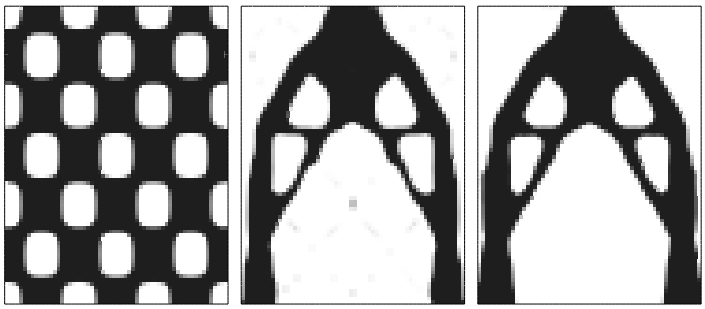

FIG. 6.2 – Initialization (right) and the solutions for a ratio of the weak material equal to 10^{-2} (center) and then equal to 10^{-5} (left).

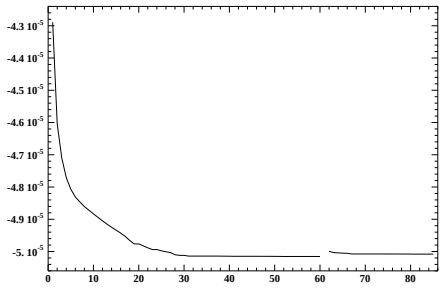

FIG. 6.3 – Evolution of the objective function for the beam problem.

two successive optimal shapes are displayed on Figure 6.2. The discontinuity at iteration 60 corresponds to the change of ratio for the weak material.

6.3.2 The two beams reinforcement

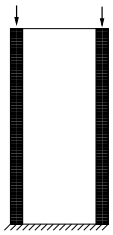

FIG. 6.4 – The two-beams problem.

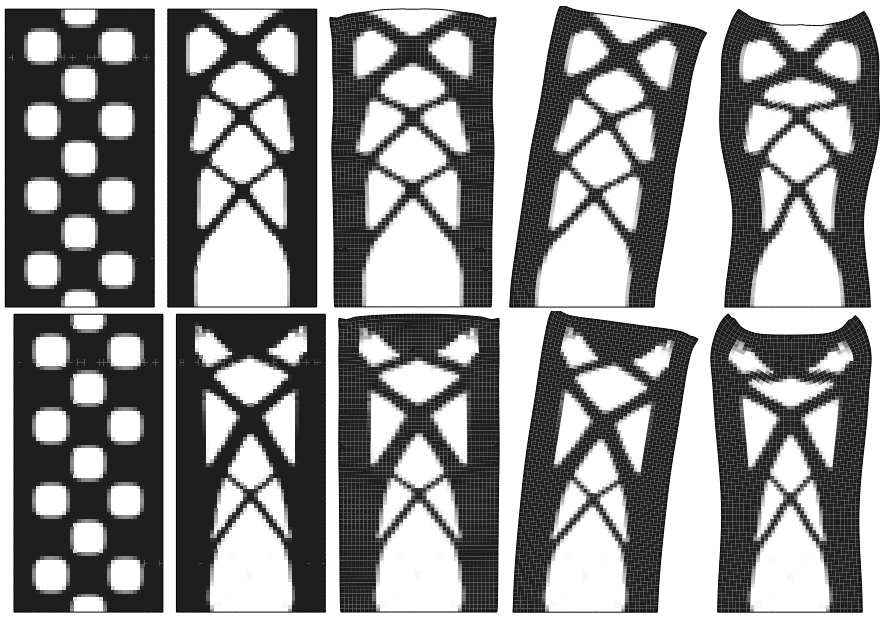

FIG. 6.5 – **The two beam reinforcement problem** Top : The standard buckling, Bottom : The extended buckling. From left to right : Initialization, optimal shape, linearized displacement at the buckling point and the two first modes that correspond to the buckling eigenvalue which is always of multiplicity 2.

The working domain is a 40×80 rectangle with a 41×81 mesh. At $x = 0$ and $x = 40$ there are two non-optimizable zones with a pressure force directed downwards at $y = 80$. At $y = 0$ there is Dirichlet homogeneous conditions (see figure 6.4). The Young modulus of the material is set to 1, the Poisson ratio ν to 0.3 and the Lagrange multiplier to 6×10^{-5} for the standard case and to 3×10^{-5} for the second case. We performed optimization with the two different

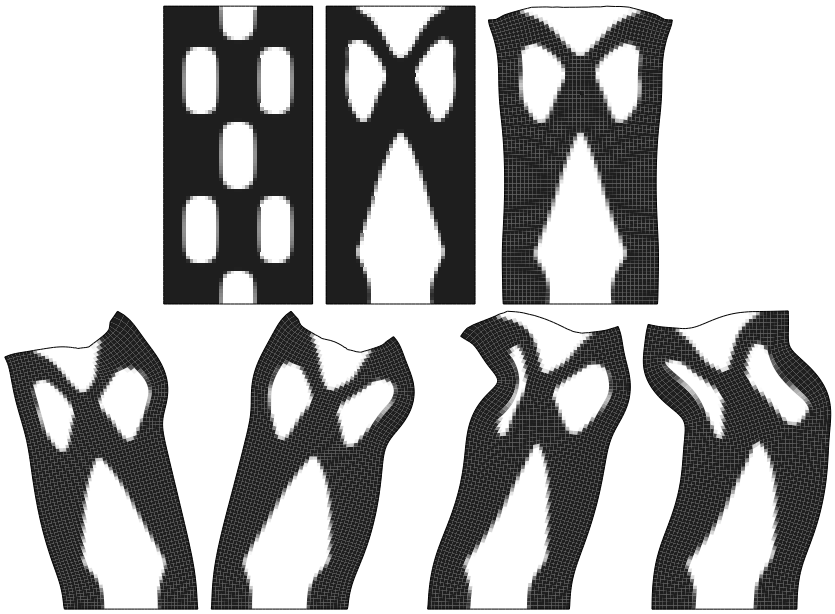

FIG. 6.6 – Top : From left to right : The initialization, The optimal shape and the linearized displacement at the buckling point of the two beam reinforcement in the standard case. Bottom : The first four buckling modes.

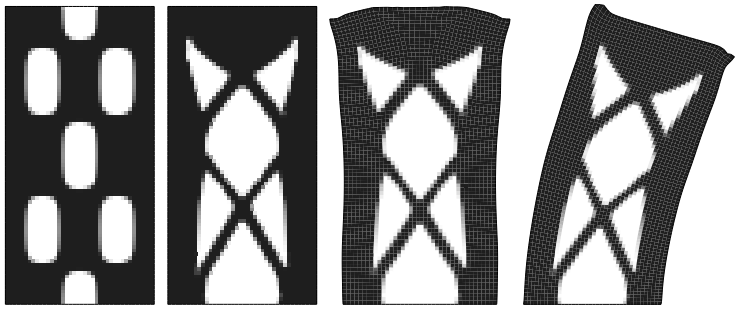

FIG. 6.7 – From left to right : Initialization, The optimal shape, The linearized displacement at the buckling point and the buckling mode of the two beam reinforcement in the extended case.

ways of calculating the buckling. The two different geometric matrices lead to two different solutions. The main idea, however is to link the two beams in order to prevent them from buckling separately. The buckling load will then be a buckling of the whole structure (like if the material was everywhere). In the standard buckling case however the algorithm computes a first buckling mode that is always multiple. See Figure 6.5 (top line) where the buckling eigenvalue

is of multiplicity 2 and Figure 6.6 where the buckling eigenvalue is of multiplicity 4. Not only do the structure buckle like if the material where everywhere but the two beams buckle also at their upper half.

In the extended buckling case for the initialization of Figure 6.5 (bottom line) the buckling eigenvalue of the optimal shape is indeed of multiplicity 2 but in Figure 6.7, only the structure as a whole is considered to buckle.

We emphasize the fact that multiplicity of the buckling load at the optimal point is **not** due to the lack of compactness in the buckling problem. Indeed, the buckling modes are *global* and *not oscillatory*, meaning that they are unlikely to be the limit of a subsequence that converges weakly but not strongly. The first eigenmodes are unlikely to be the numerical representation of a sequence of Weyl's-like eigenvectors. Furthermore, the accumulation of multiple modes at optimal shape is well-known in optimization and is even an indicator of optimality.

6.3.3 The compliant bridge

The working domain is a 40×10 rectangle with a 81×21 mesh. A vertical load of norm 1 is applied at the middle of the top of the domain. The left and right side are endowed with Dirichlet homogeneous conditions (see Figure 6.8 (left)). The Young modulus of the material is set to 1, The Poisson ratio ν to 0.3 and the Lagrange multiplier to 16×10^{-6}. Here, we choose to optimize $C(\mathbf{f})/\gamma^2$ where $(C\mathbf{f})$ is the compliance. This means that we want to decrease the compliance and increase the buckling load at the same time. Optimizing the compliance stabilizes the shapes and prevents disconnected shapes to appear.

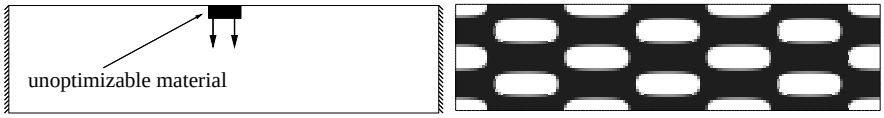

FIG. 6.8 – The compliant bridge problem (left) and its initialization (right).

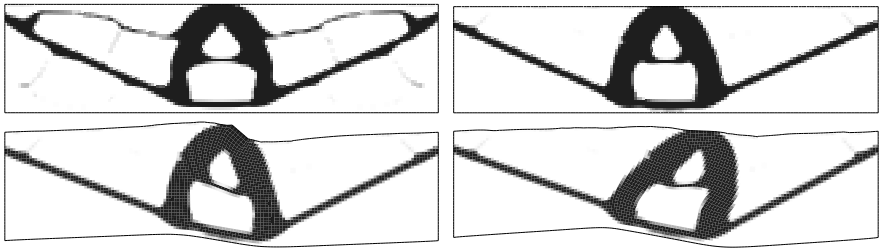

FIG. 6.9 – Top : The compliant bridge problem optimal shapes. Bottom : The compliant bridge problem buckling modes.

Figure 6.9 (top, left) is a display of the optimal shape for a ratio of the weak

material equal to 10^{-3}. We see thin bars appearing, the algorithm cannot remove them because they would be the cause of the buckling if they were made thiner. That is why the thin bars have been removed using a diffusion process in the Hamilton-Jacobi equation and the shape has been then re-optimized in order to give rise to the optimal shape of Figure 6.9 (top, right). Figure 6.9 (bottom) shows the two first buckling eigenspace which is of multiplicity 2. Figure 6.10 shows the history of the objective function. On this figure, the curve named "First optimization" is the history from the initialization to the first optimal shape of Figure 6.9 (top, left), the curve named "Second optimization" is the history of the objective function from the shape of Figure 6.9 (top, left) to the shape of Figure 6.9 (top, right). As can be seen on those curves, there is indeed a huge gap between the last iteration of the curve "First optimization" and the first iteration of the curve "Second optimization". This gap is due to the disappearance of the thin bars which means that those thin bars made the optimal shape of 6.9 (top, left) a local minimizer -at least in numerical sense-.

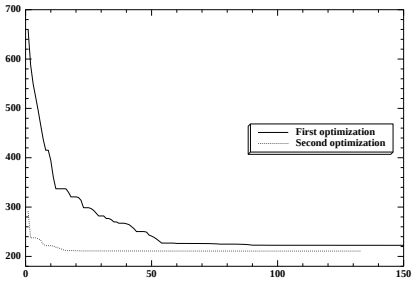

FIG. 6.10 – Convergence history of the compliant bridge objective function.

6.3.4 The buckling of a grip

We mix the optimization of the buckling with mechanism design. The main idea is that mechanism design involves hinges and that these hinges easily buckle. So that we may try to minimize the appearance of hinges by forcing the shape not to buckle too easily. The standard example is a grip introduced in section 2.7 for which the optimal shape involves an hinge. See Figure 6.11 for the definition of the problem and a standard optimal solution as well as its first buckling mode.

The objective function is given by

$$\mathcal{J}^2 = \int_\Omega h|\gamma u_0 - v_0|^2 + k|u_0 - v_0|^2$$

Where u_0 is the computed linear displacement, γ is the buckling eigenvalue, v_0 is a target displacement and h and k are two localization functions.

$\diamond$ Suppose $k = 0$ everywhere and h is non-zero between the jaws while $v_0 = \pm 10$. The objective function $\mathcal{J}$ taken in consideration may be considered

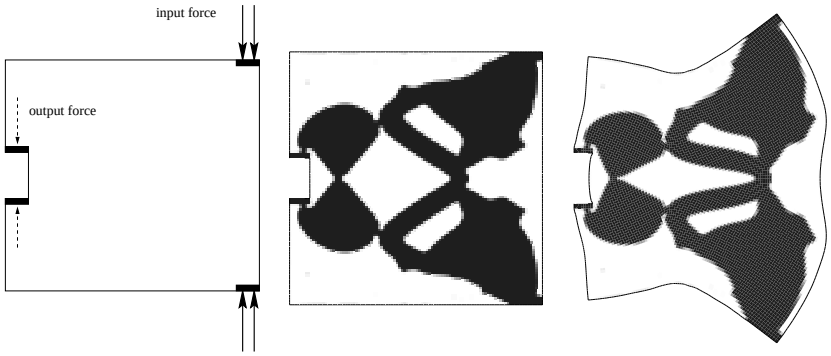

FIG. 6.11 – From left to right : Definition of the gripping mechanism problem, a standard optimal solution and its buckling mode.

as : "The mechanism must grip and must stay in the linear mode as long as possible".

$\diamond$ It is well known that we need to enforce the displacement to be close to zero where forces are input. That is why near this area, k is equal to 2 while $v_0 = 0$. We enforce the displacement to be close to zero by using k and not h because if we had used h, it may have given the tendency to reduce γ so that γu_0 is the closer possible to 0.

Remark 6.3.1 *At the very beginning of the algorithm, because the jaws of the grips are open and then $h(u_0, \gamma u_0 - v_0) < 0$ then the algorithm has the tendency to reduce γ (so that γu_0 is the smallest possible, ie it is better to have γu_0 close to 0 than γu_0 in the opposite direction of v_0). At the beginning of the algorithm, γ is then reduced (see Figure 6.13 (right)). This brings huge problems because :*

- *The algorithm is very sensitive to parameters. For some of them, the algorithm will not converge. For instance the algorithm may (and did) disconnect the shape in order to reduce the buckling eigenvalue ; It will never be able to reconnect the shapes.*
- *Due to this sensitivity to parameters, Lagrange multiplier for a volume constraint cannot be applied at the beginning of the optimization. They are used in mechanism design in order to remove the useless parts of the boundary. But they have the tendency, of course, to reduce the shape's volume. Because the beginning is a critical phase were the algorithm wants to reduce the first buckling load and hence to make the shape thinner, it is really not a good idea to add a constraint that would also reduce the volume of the shape. That is why we do not use Lagrange multiplier.* **As a result optimal shapes have a lot useless parts**.

An example of grip optimization is given in Figure 6.12 while its convergence history is given in Figure 6.13 . This grip is made of material with a Young modulus equal to 1 and a Poisson ratio equal to 0.3. There is a material of

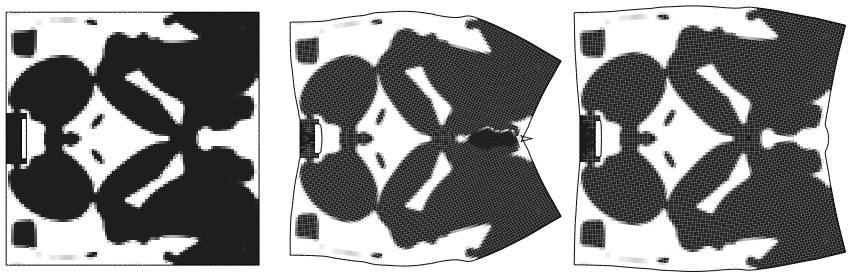

FIG. 6.12 – From left to right : Optimal shape, the displacement at the buckling point and the buckling mode of the buckling grip.

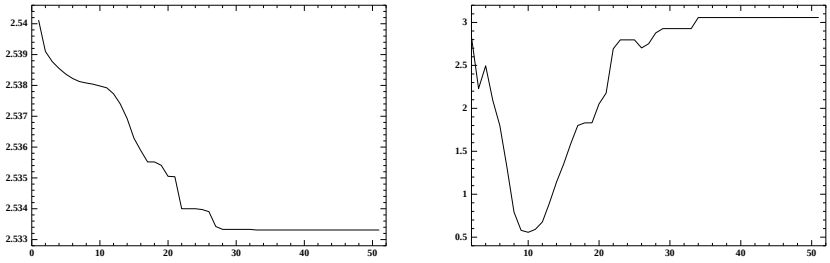

FIG. 6.13 – Convergence history (left) and buckling eigenvalue history (right) for the buckling grip.

Young modulus equal 0.1 and a Poisson ratio equal to 0 in between the jaws so that the grip is physically designed to hold objects. In order to remove the useless part of the shape, we re-optimize this shape using a small Lagrange multiplier. When used as a new initialization, because this grip actually works, the algorithm do not have the tendency to reduce the buckling load. The remark 6.3.1 do not apply during the second optimization.

The resulting optimal shape is the one presented in Figure 6.11 (middle). As a conclusion concerning application of the buckling load to mechanism design, we have to admit that it only brings more complication and that it does not solve the hinge problem. Used with any initialization, the algorithm behaves badly (see remark 6.3.1).

We can use the buckling load optimization as a post-processing tool. We optimize a shape with a standard target displacement objective function and then we re-optimize the shape with introducing the buckling load. It is very efficient but *do not* remove hinges. It is perhaps an indication that hinges may be the only way out of creating some mechanism.

As an other example, we give two grips, one which is obtained by mixing the buckling load with mechanism design, its optimal buckling load being equal

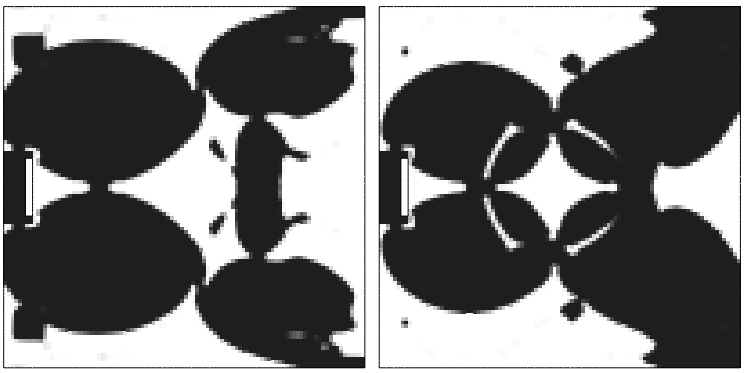

FIG. 6.14 – Left : A grip calculated by the standard method. Right : A grip computed by using the buckling load with a final buckling eigenvalue equal to 1.

to 1. The other grip is optimized without taking in account the buckling load, its optimal shape buckling load being equal to 0.57. The two optimal shapes are given in Figure 6.14. The one on the right is the one optimized without buckling and the one on the left is the one optimized with the buckling load. They both present useless parts because no Lagrange multiplier was used (see remark 6.3.1). As can be seen on the comparison of these two optimal shapes, even if the one which is optimized with the buckling load has an hinge, its hinge is "stronger" than the one optimized without the buckling load.

6.4 Conclusion

We computed the derivative of the buckling load with respect to domain variation. We showed that when the first buckling mode is of multiplicity greater than one, then the problem of finding the steepest-descent of the gradient of the buckling load is of the same nature than the problem of optimizing the first eigenvalue of elasticity. It is an easy-to-solve SDP problem. Nevertheless, on a pure theoretical approach we still do not know if the direct problem addresses a solution due to the lack of compactness.

We wanted to implement buckling optimization with mechanism design in order to prevent apparitions of hinges, we saw that hinges still occur, it is an indication that they are compulsory to the design of mechanism.

We also showed some of the main problems encountered when optimizing the buckling load :
◇ In section 6.3.1 the weak material approximation was discussed. An high ratio of the weak material leads to a smoother function with respect to domain variation. But the higher the ratio is, the worst is the calculation of the derivative. This issue is well-known in mechanism design (see section 3.4.5) where the

so-called two-steps optimization is used. One step with an high ratio (typically 10^{-2}) and one step with a lower ratio (10^{-5}).
$\diamond$ Thin bars problem occur, we will address this problem in section 8.1.1 of chapter 8. This problem is due to a topology change. The reload method of section 8.1.4 has been here applied. This problem has been addressed in section 6.3.3.
$\diamond$ The Lagrange multiplier trick for removing useless parts of a mechanism cannot be applied here. This leads to "ugly" mechanism (a lot of useless material), nevertheless the mechanisms still work. This problem was shown in section 6.3.4.

As a conclusion we claim that buckling optimization condenses the different numerical issues that appears in the standard level-set method for shape optimization of stationary problems.

Chapitre 7

D'autres résultats numériques

Résumé
Nous montrons d'autres résultats numériques dans ce chapitre.

7.1 Compliance robuste de la console courte 131
7.2 Valeur propre de la console courte 133
7.3 La pince du CEA 135
7.4 Une autre pince 138
7.5 Le mécanisme à coefficient de Poisson négatif . . 139

7.1 Compliance robuste de la console courte

Nous utilisons le formalisme du chapitre 4 et du chapitre 5 pour étudier un problème d'optimisation robuste. Le domaine de travail est un rectangle de taille 1×2 avec un maillage 40×80. En $x = 0$, on impose des conditions de Dirichlet et une force verticale unitaire est appliquée au milieu de $x = 1$. C'est une console courte pour laquelle, tout d'abord les perturbations ne sont autorisées que horizontalement et autour de l'endroit où est appliquée la force. Les différentes formes obtenues sont résumées dans la figure 7.1 et les paramètres sont dans la table 7.1. On rappelle que m désigne la taille des perturbations admissibles et $\mathcal{J}_{rob}$ la valeur de la compliance robuste. Le Lagrangien $\mathcal{L}_{rob} = \mathcal{J}_{rob} + \eta|\Omega|$ est utilisé pour satisfaire la contrainte de volume. Le multiplicateur de Lagrange η est augmenté quand m varie pour que les formes optimales soient toutes de même volume.

Dans la Figure 7.1, on voit que la forme optimale passe de la console courte classique à une poutre qui supporte bien mieux les forces horizontales quand m augmente.

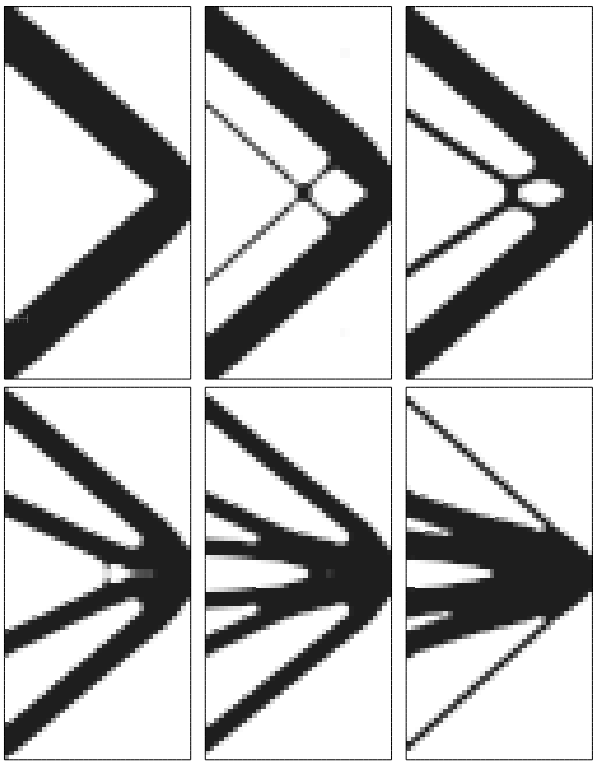

FIG. 7.1 – La console courte avec perturbations horizontales.

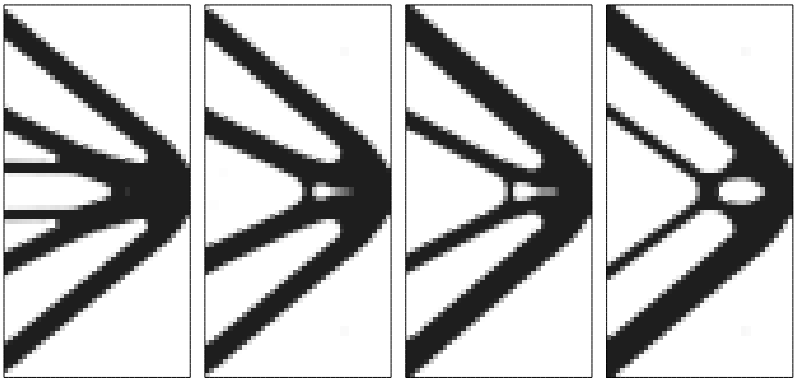

FIG. 7.2 – La console courte avec perturbations mixtes.

Pour $m = 0.5$, on change l'ensemble des perturbations admissibles. Une perturbation g sera un terme source volumique de la forme $g_1 = s_1$ et $g_2 = \chi s_2$, où g_1 est la composante horizontale de g et g_2 sa composante verticale. On pose

m	=	0.1	0.15	0.2	0.3	0.5	1
Volume	=	30.72	30.03	30.86	29.83	30.66	29.90
Lagrange	=	7.5	8.5	10	14	20	43
$\mathcal{J}_{rob}$	=	3.93	4.60	5.02	6.33	9.39	22.34
$\mathcal{L}_{rob}$	=	6.21	7.15	8.10	10.51	15.52	35.20

TAB. 7.1 – Paramètres de la console courte avec perturbations horizontales.

χ	=	0.05	0.1	0.2	0.3
Volume	=	31.29	31.84	30.02	29.99
Lagrange	=	21	27	30	35

TAB. 7.2 – Paramètres de la console courte avec perturbations mixtes.

$s = (s_1, s_2)$ un champs de vecteur localisé autour du point d'application de la force et $\|s\|_L^2(\Omega) \leq m$. Ainsi, les perturbations g sont autorisées dans une ellipse d'axe horizontal de taille 1 et d'axe vertical de taille χ. Les différentes figures obtenues pour différents χ sont résumées dans la Figure 7.2 et les paramètres dans la table 7.2. Le paramètre χ a le sens physique suivant : Une perturbation "coûte" 1 dans la direction horizontale et $1/\chi$ dans la direction verticale. Ainsi plus χ est grand, plus les perturbations verticales sont favorisées par rapport aux pertubations horizontales. Ceci est vérifié dans la Figure 7.2 où l'algorithme passe d'une forme résistant bien à des forces horizontales à une sorte de console qui resiste mieux aux forces verticales.

7.2 Valeur propre de la console courte

On reprend le test de la section 3.6.2 avec les changements suivants : La densité est 50 fois plus grande dans la boîte noire (le mass-tip) au lieu de 80 fois. Le multiplicateur de Lagrange passe de $\eta = 0.3$ à $\eta = 1$.

Deux types d'optimisation sont fait : On optimise par rapport à la première valeur propre en la considérant comme toujours simple ou en la considérant comme possiblement multiple. Dans le cas de l'optimisation possiblement multiple, le paramètre ε_0 introduit dans la section 3.6.2 pour considérer la première valeur propre comme multiple est fixé à 10% et est diminué par un facteur 2/3 si plus de deux réduction du pas de descente sont effectuées. L'optimisation avec une première valeur propre toujours simple est obtenue en fixant ce paramètre ε_0 à 0. On rapelle que si les valeurs propres sont classées par ordre croissant $\gamma_1 \leq \gamma_2 \leq ..$ et que si d est définit par :

$$\frac{\gamma_d}{\gamma_1} - 1 \leq \varepsilon_0 < \frac{\gamma_{d+1}}{\gamma_1} - 1$$

Alors le premier espace propre est considéré comme étant de dimension d.

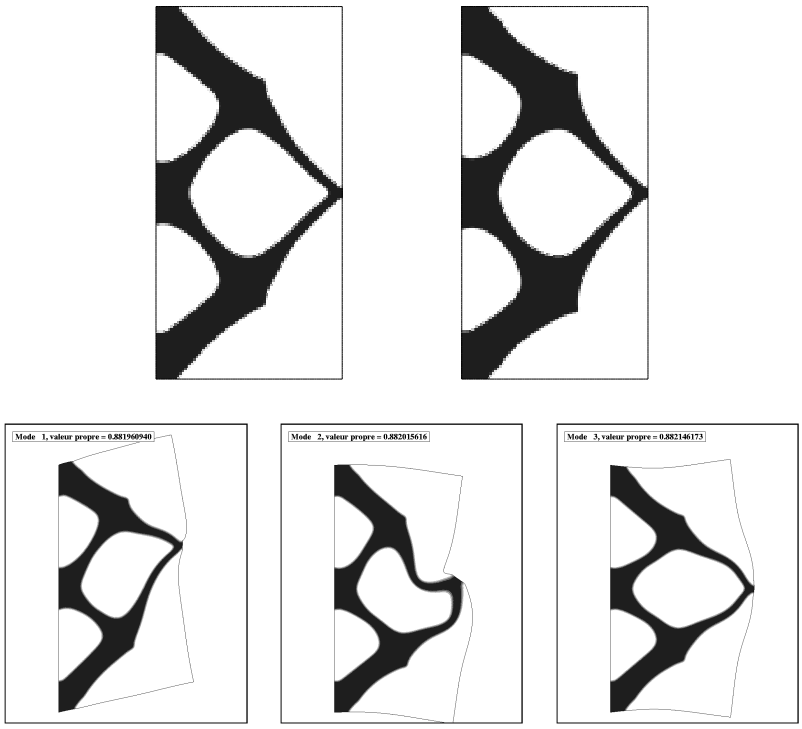

FIG. 7.3 – En haut, formes optimales pour la première valeur propre de la console courte possiblement multiple (gauche) ou toujours simple (droite). En bas, les trois premiers modes pour la forme optimale de gauche.

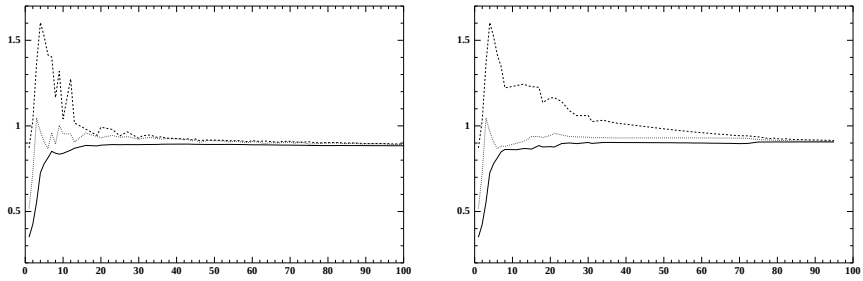

FIG. 7.4 – Evolution des trois premières valeurs propres de la console courte possiblement multiple (gauche) ou toujours simple (droite).

La Figure 7.3 montre les formes optimales obtenues pour les deux tests, on s'aperçoit que les formes n'ont pas exactement convergé (à cause des deux cornes qui n'ont pas de réel sens physique). Cependant ce test est intéressant dans la

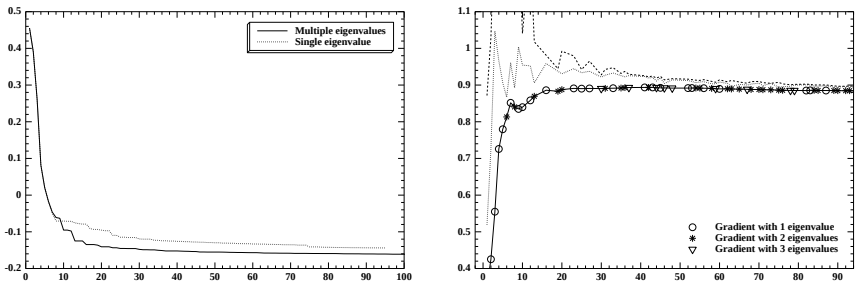

FIG. 7.5 – A gauche, comparaison de l'évolution des fonctions objectifs. A droite, évolution des valeurs propres et du nombre de valeurs propres considérées comme multiples au cours des itérations.

mesure où il y a agglutination de 3 valeurs propres à l'optimum (voir la figure 7.4). Ceci s'explique par le choix précis qui a été fait entre le facteur de poids de la masse plus lourde (50 ici) et le multiplicateur de Lagrange. En effet, un mode parasite (le deuxième de la figure 7.3 (bas)) qui correspond à un mode localisé dans la masse plus lourde est venu s'ajouter aux modes existant. C'est parce que il y a 3 modes et que nous sommes proches de l'optimum que l'algorithme ne peux plus converger, en tout cas pour ce maillage. La Figure 7.5 (gauche) montre l'évolution des deux fonctions objectifs au cours de l'optimisation. La Figure 7.5 (droite) montre la multiplicité de la première valeur propre au cours de l'optimisation. Les itérations où la multiplicité de la première valeur propre n'est pas mentionné correspond à un avancement qui ne décroît pas la fonction objectif et conséquemment à une réduction du pas de descente. Ces itérations correspondent aux paliers de la Figure 7.5 (gauche). Comme il est dit plus haut, si deux itérations successives de ce genre apparaissent, le facteur ε_0 est multiplié par 2/3.

7.3 La pince du CEA

On reprend la pince de la section 3.4.5 avec la même initialisation et les paramètres suivants. Le module d'Young vaut 1 et le coefficient de Poisson 0.3. Dans le vide le paramètre ε vaut 10^{-2} . On ne fait que la première étape de l'optimisation en deux temps proposée dans la section 3.4.5. Une pression de $-1N$ est appliquée en bas de la pince et la pression appliquée entre les mâchoires de la pince vaut pN. On rapelle que la fonction coût

est donnée par :

$$\mathcal{J}_{lse}(\Omega) = \left(\int_{\Omega} k(x)|u(x) - u_0(x)|^2 \right)^{1/2} \qquad \mathcal{L}_{lse}(\Omega) = \mathcal{J}_{lse}(\Omega) + \eta|\Omega|$$

La fonction $k(x)$ qui caractérise la zone d'intérêt du déplacement cible peut avoir deux valeurs k_0 au niveau de la zone d'application de la force et 1 au

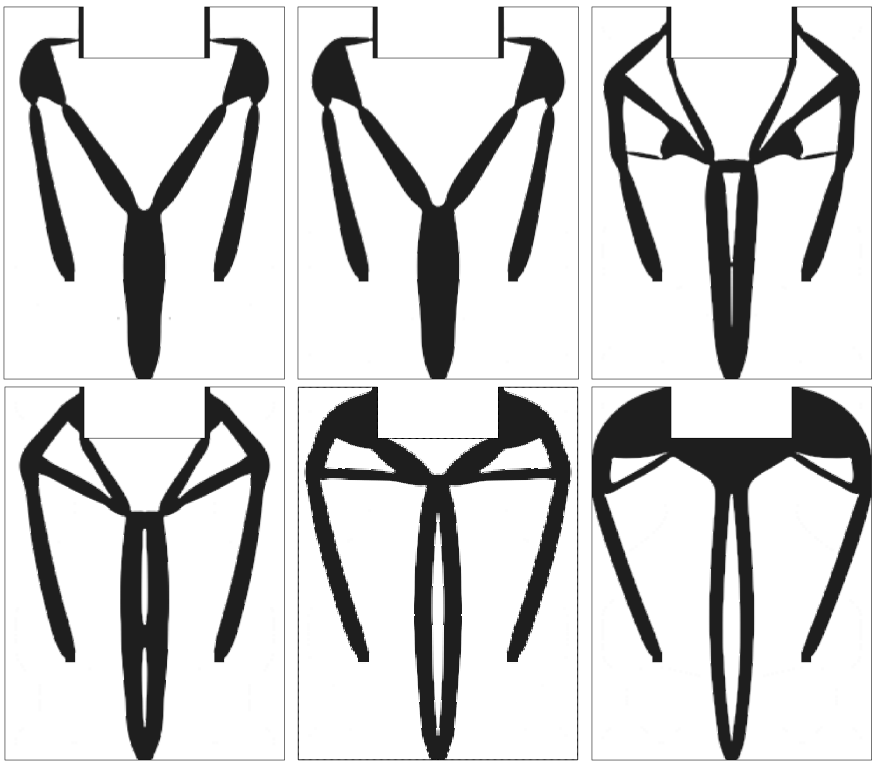

FIG. 7.6 – La pince du CEA avec une pression p entre les mâchoires de plus en plus fortes.

niveau des mâchoires. Le déplacement cible u_0 vaut toujours $(0,0)$ dans la zone d'application de la force et vaut $(\pm 10, 0)$ entre les mâchoires. On peut aussi décomposer $\mathcal{J}_{lse}$ en $\mathcal{J}^2_{lse}(\Omega) = \mathcal{J}_0(\Omega) + \mathcal{J}_1(\Omega)$ avec

$$\mathcal{J}_0(\Omega) = \int_\Omega k_0(x)|u(x)|^2 \quad \mathcal{J}_1(\Omega) = \int_\Omega |u(x) - u_0(x)|^2$$

$\mathcal{J}_0$ dénote à quel point le déplacement est important au niveau de la zone d'application des forces et $\mathcal{J}_1(\Omega)$ dénote à quel point le mécanisme pince bien.

Dans un premier temps, on fait évoluer p, la pression entre les mâchoires de la pince. La Figure 7.6 montre l'évolution de la forme optimale quand p varie et la table 7.3 résume les valeurs de p pour un multiplicateur de Lagrange $\eta = 0.2$. Il est à noter que la dernière forme, celle pour $p = 1N$ ne pince plus,

la pression étant trop grande. Pour donner un sens à la Table 7.4, on rappelle que le mesure du support de k_0 (zone d'application des forces) est 21 fois inférieure à la mesure du support de la zone d'intérêt entre les mâchoires (i.e. $supp(k = 1)$). Dans la Table 7.4 est aussi listé la valeur de $Vol = |\Omega|$.

Dans un deuxième temps, on fait évoluer k_0, la pondération qui permet de

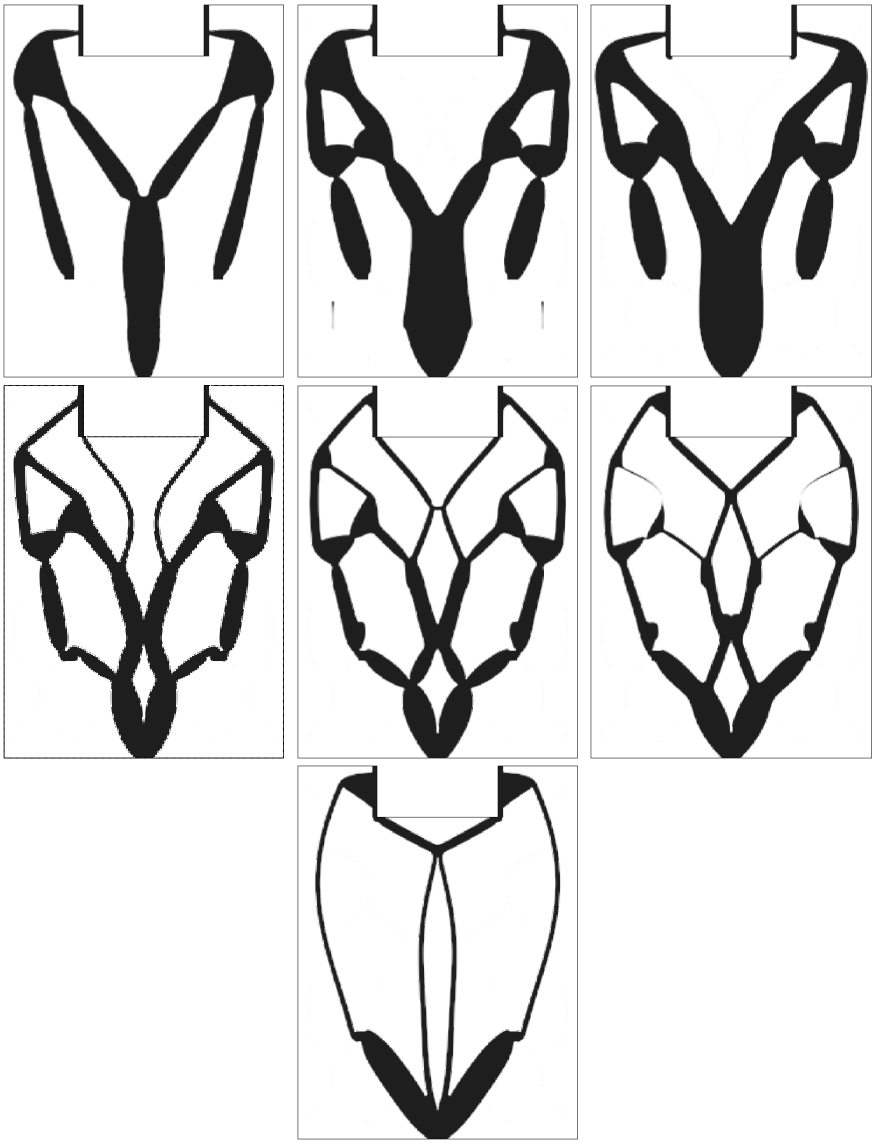

FIG. 7.7 – D'une pince à un amplificateur de déplacement.

p	=	0.	0.01	0.1	0.2	0.5	1
$\mathcal{J}_0$	=	0.00312	0.00314	0.00294	0.00254	0.00211	0.00041
$\mathcal{J}_1$	=	0.19170	0.19342	0.20758	0.21622	0.22842	0.24251
$\mathcal{J}_{lse}$	=	0.46455	0.46661	0.48290	0.49225	0.50533	0.51253
$\mathcal{L}_{lse}$	=	0.46870	0.47087	0.48764	0.49700	0.51051	0.51806
Vol	=	20.76	21.27	23.68	23.73	25.89	27.63

TAB. 7.3 – Les différents paramètres pour les différentes pinces optimales de la Figure 7.6 avec $\eta = 0.02$ et $k_0 = 60$.

k_0	=	60	400	800	900	10^3	$1,5.10^3$	2.10^3
$\mathcal{J}_0$	=	0.0031	0.0086	0.0103	0.0064	0.0045	0.0028	0.0021
$\mathcal{J}_1$	=	0.1993	0.2091	0.2147	0.2232	0.2274	0.2319	0.2332
$\mathcal{J}_{lse}$	=	0.4736	0.4912	0.4993	0.5044	0.5069	0.5100	0.5107
$\mathcal{L}_{lse}$	=	0.4785	0.4979	0.5061	0.5096	0.5117	0.5140	0.5139
Vol	=	22.18	30.51	31.20	23.79	21.69	18.29	14.74

TAB. 7.4 – Les différents paramètres pour les différentes pinces optimales de la Figure 7.7 avec $p = 0.05$ et $\eta = 0.022$.

faire en sorte que le déplacement reste petit là où les forces sont appliquées. Dans la Figure 7.6 k_0 était fixé à 60 et la Figure 7.7 montre l'évolution des formes optimales

quand k_0 varie avec une pression pN fixée entre les mâchoires de $0.05N$, les différents paramètres sont rappelés dans la table 7.4. La table 7.4 et la figure 7.7 montrent que, en faisant varier k_0, on passe d'une pince classique à un amplificateur de déplacement, i.e. quand k_0 est augmenté, l'algorithme a plus intérêt à restreindre le déplacement au niveau de la zone d'application des forces. Il est à noter que la dernière forme, celle pour $k_0 = 2000$ ne pince plus, l'algorithme préfère se concentrer à éviter que la zone

d'application des forces bouge et la pression p a tendance à ouvrir les mâchoires de la pince.

7.4 Une autre pince

Nous appliquons la régularisation de la vitesse à une autre pince, celle abordée dans la section 2.7 (Voir la figure 2.11). La Figure 7.8 montre la forme optimale obtenue pour un multiplicateur de Lagrange $\eta = 1,85.10^{-3}$. Ce test a aussi été fait avec l'extension naturelle, cependant cette dernière donne une forme optimale égale au vide pour ce multiplicateur de Lagrange. Il sera discuté dans la section 8.4.3 de ce problème.

Au lieu de mettre des pressions entre les mâchoires pour assurer que la pince puisse aggriper, on peut aussi mettre une petite barre qui fait office de ressort

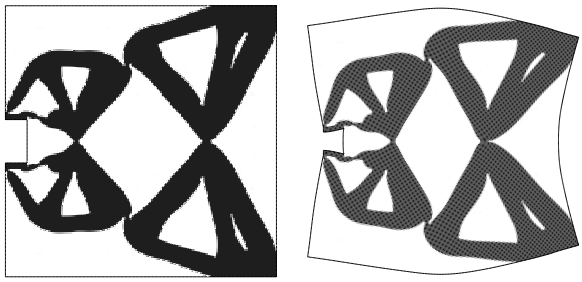

FIG. 7.8 – Une autre pince pour la méthode hilbertienne (gauche) et sa déformée (droite).

entre les mâchoires. Les tests de la Figure 7.9 sont faits avec une barre de module d'Young égal à 0.3 pour les deux premières et égal à 0.5 pour les deux dernières pinces. Dans tous les cas, le coefficient de Poisson du ressort entre les mâchoires a été fixé à zéro. On rappelle que le module d'Young de la pince est de 1. Deux type d'initialisations sont utilisées pour les pinces optimales de la Figure 7.9 (gauche), les pinces 1 et 3 (resp 2 et 4) sont obtenues avec la même initialisation.

7.5 Le mécanisme à coefficient de Poisson négatif

On revient sur le test de la section 3.4.6. Dans une boîte de taille 2×2 maillée avec 241×241 noeuds, on essaie de construire un mécanisme à coefficient de Poisson negatif. Le materiau a un coefficient de Poisson $\nu = 0.3$ et un module d'Young $\lambda = 1$. Le matériau mou a un module d'Young égal à $\lambda = 10^{-2}$. Une pression $p = -10^{-3}N/m$ est appliquée sur les deux côtés de la boîte et une pression $q = 10^{-4}N/m$ est appliquée en haut et en bas. Le déplacement cible vaut $(0, 0)$ sur les côtés avec un facteur de ponderation k_0 et le déplacement cible vaut $(0, \pm 0.5)$ en haut

et en bas avec un facteur de ponderation $k_1 = 20$. Pour stabiliser le processus, les barres noires de la figure 7.10 (gauche) ont un module d'Young égal à $\lambda = 10^3$. Plusieurs test sont effectués en changeant la valeur de k_0. L'initialisation est toujours la même et est la figure 7.10 (droite). Le multiplicateur de Lagrange vaut $\eta = 2.10^{-3}$. Comme dans l'exemple de la section 7.3, la fonction coût $\mathcal{J}_{lse}$ est décomposée en sa partie selon k_0 et k_1 respectivement appellées $\mathcal{J}_0$ et $\mathcal{J}_1$ avec $\mathcal{J}_{lse}^2 = \mathcal{J}_0 + \mathcal{J}_1$.Ces valeurs ainsi que la valeur $Vol = |\Omega|$ et la valeur de $\mathcal{L}_{lse} = \mathcal{J}_{lse} + \eta|\Omega|$ sont données dans la Table 7.5. La dernière forme, celle pour $k_0 = 10^4$ n'est plus une cellulle à coefficient de Poisson négatif. La pression mise en haut et en bas suffit à comprimer la cellulle. Cela peut se voir dans la Figure 7.11 (en bas à droite). L'algorithme a crée des renforts au niveau des coins de la cellulle qui empêchent les barres supérieures de descendre. En effet, si ces barres n'étaient pas en train de descendre, les renforts seraient essentiellement contre-productifs. En fait la figure optimale correspondant à ce test précis et en

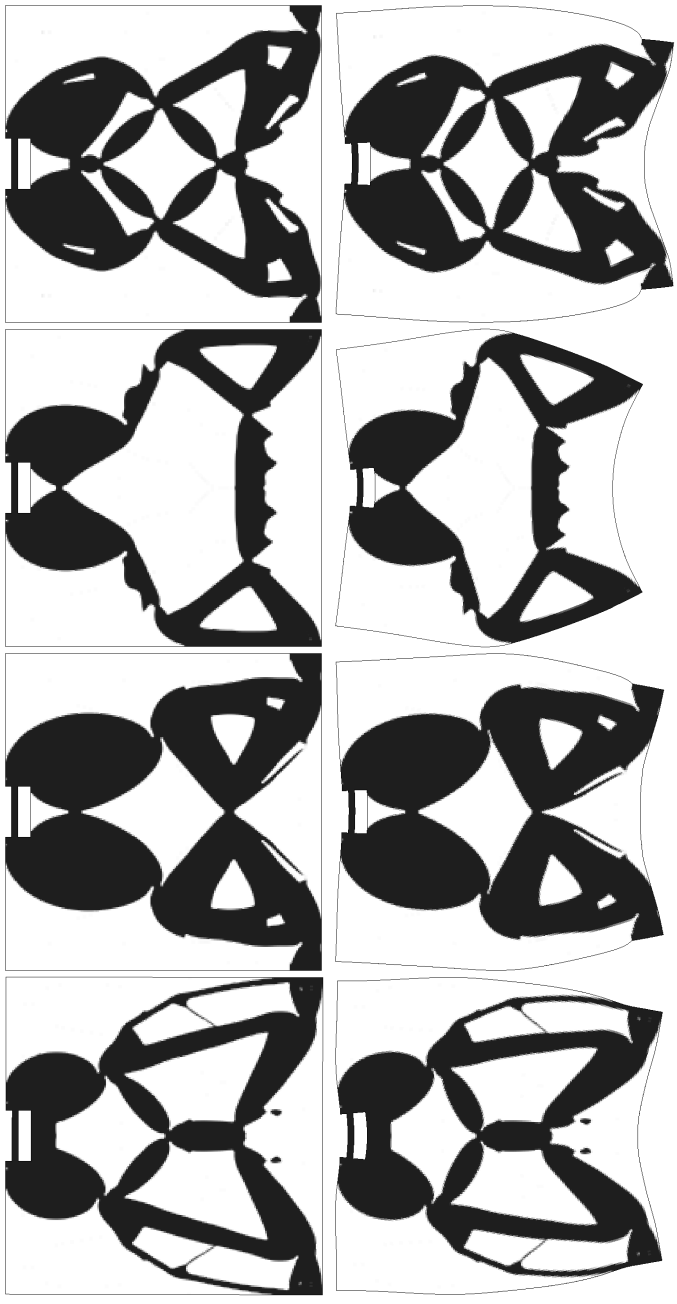

FIG. 7.9 – Différentes topologies de pinces optimales avec un ressort entre les mâchoires.

k_0	=	10^2	10^3	3.10^3	10^4
$\mathcal{J}_0$	=	0.000155	0.000190	0.000321	0.000310
$\mathcal{J}_1$	=	0.11816	0.11869	0.11872	0.11896
$\mathcal{J}_{lse}$	=	0.34397	0.34480	0.34502	0.34536
$\mathcal{L}_{lse}$	=	0.34483	0.34572	0.34595	0.34648
Vol	=	43.02	46.16	46.60	56.06

TAB. 7.5 – Table des différents paramètres du mécanisme à coefficient de Poisson négatif.

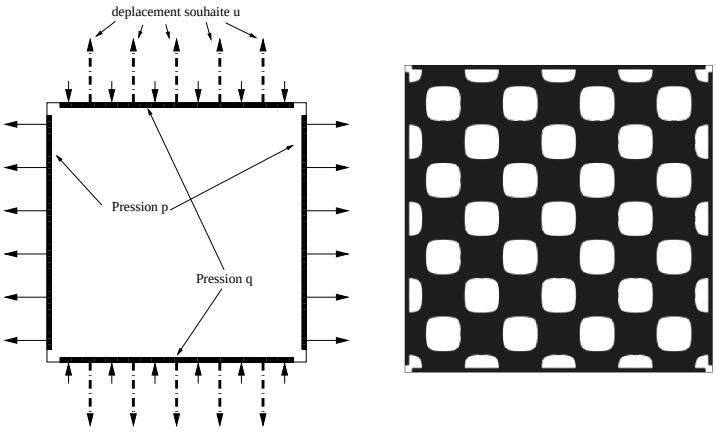

FIG. 7.10 – Le problème du mécanisme à coefficient de Poisson négatif (gauche) et son initialisation (droite).

l'absence de multiplicateur de Lagrange est la cellulle entièrement remplie de matériau.

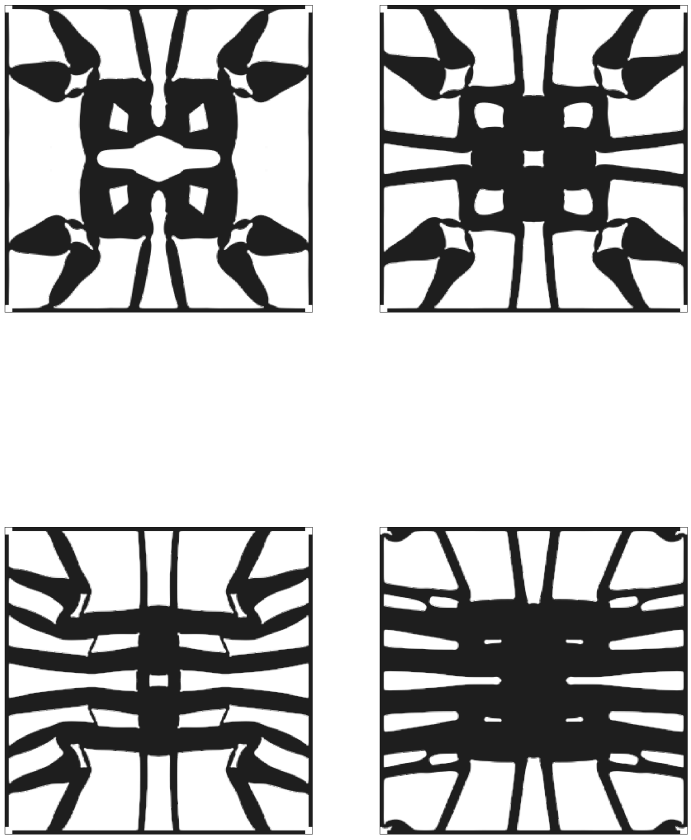

FIG. 7.11 – Différentes formes optimales du mécanisme à coefficient de Poisson négatif pour un coefficient k_0 augmentant.

Chapitre 8

Numerical results : beyond the mirror

Abstract

In this chapter we discuss some of the main numerical problems that arise in shape optimization by the level-set method and the argumented solution that has been chosen. Despite common decency, the term "optimal shape" will refer throughout this chapter to any ending shape of the algorithm.

8.1 2-d issues for the compliance and the robust compliance 144

8.1.1 The thin bar problem 144

8.1.2 The tolerance parameter solution is not available for the robust compliance 145

8.1.3 Topological gradient as a solution to the thin bar problem 146

8.1.4 The reload method as the chosen solution for the robust compliance 147

8.2 The fiber problem in 3-d compliance 147

8.3 Modes in disconnected parts of the shape 148

8.4 Mechanism design 151

8.4.1 The Hinges and Horn's problem 151

8.4.2 Disconnection of the mechanism 153

8.4.3 The Natural extension method and the Lagrange multiplier 154

8.5 Conclusion 156

8.1 2-d issues for the compliance and the robust compliance

8.1.1 The thin bar problem

In papers dealing with the level-set method, it has been constantly said that this method is not capable of nucleation of new holes. The first attempt that has been made to correct this problem was to initiate the algorithm with a shape that has many holes. In 2-d, a new topological problem arises : the apparition of thin bars. The model problem is the wheel bridge of section 5.4.2 (for the robust

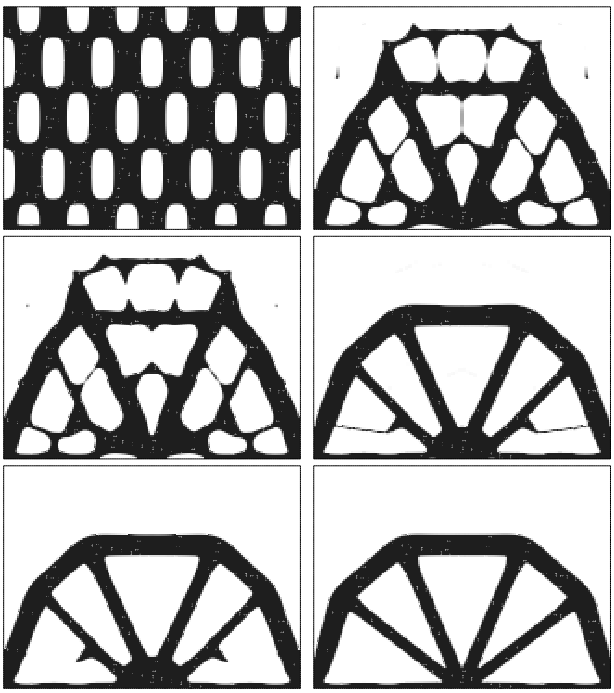

FIG. 8.1 – Three different initialisation (left) and three different optimal shapes (right).

compliance problem, setting $m = 0$ leads to the standard compliance problem). Figure 8.1 is a display of the optimal shapes (right) obtained for three different corresponding initialisation (left). It can be seen that the two first initialisation lead to optimal shapes who have thin bars and the algorithm concentrate on adjusting the size of the thin bars without being concerned at all with the rest of the shape. In fact removing those thin bars leads to an increasing of the objective function.

8.1.2 The tolerance parameter solution is not available for the robust compliance

The standard way to avoid the problem of thin bars is to set a tolerance parameter Tol greater than 1, ie if the objective function $\mathcal{J}_{cp}^{k+1}$ at the step $k+1$ is strictly lower than $Tol \times \mathcal{J}_{cp}^{k}$, then the algorithm accepts the new shape as better.

In the robust compliance setting, the factor Tol must be set equal to 1. The reason is that the solution to the problem of the robust compliance may not be unique. A good example is the beam-to-cantilever problem of section 5.4.1. During the algorithm process, the algorithm looses the original symmetry of the shape. In this case, a worst perturbation is isolated and the algorithm optimizes with respect to that perturbation only. The shape is moved accordingly, a new perturbation is isolated and the algorithm enters a cycle.

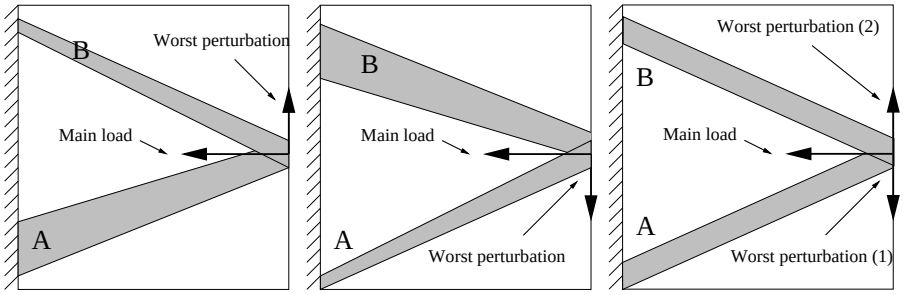

FIG. 8.2 – Entering a cycle when loosing symmetry if the tolerance parameter is not equal to 1.

To make things clear, suppose that during the computation, the algorithm works on the shape of Figure 8.2 (left) that is made of two bars named A and B. If A is larger than B then the worst perturbation (shown in Figure 8.2 (left)) is unique and tends to improve B while decrease the size of A. The algorithm then finds the new shape of Figure 8.2 (middle) and by the same argument enters a cycle between the two shapes. If the tolerance Tol is set to 1, then the step of the algorithm is decreased until the algorithm finds a more symmetric shape. When arriving to a symmetric shape, the algorithm computes a set of perturbation that is no more a singleton (see Figure 8.2 (right)) and completely change the descent direction, allowing to continue the optimization process.

Remark 8.1.1 *The entering a cycle could be a problem for the compliance itself, but numerically it never happens. A three-steps explanation could be that :*

1- For the case of the compliance, the objective function can admit an Hessian with respect to topology changes. For the robust compliance problem, the algorithm can switch between the case were there is a single perturbation and

the one where there is multiple perturbations. Hence, the descent direction cannot even be continuous.

2- Near the optimum, the velocity is higher on the parts of the $\partial\Omega$ that touches the boundary of D and the one that touches where forces are applied. So that the CFL condition turns out to force the descent direction to decrease when the derivative decreases. The step of the gradient algorithm is then smaller when the derivative is smaller.

3- Now the difference of treatment between the compliance and the robust compliance is of the same nature than when one tries to minimize $y^2 + x^2$ or $y^2 + |x|$ when the step of the gradient algorithm depends on the norm of the gradient. In the first case he will surely end in the point $(0, 0)$ even if he a admits a Tolerance parameter greater than one. In the second case, he will surely never be able to end in the point $(0, 0)$ with a Tolerance parameter greater than one. He will more likely end in a loop between $(0, x_1 < 0)$ and $(0, x_2 > 0)$.

In this analogy, the line $x = 0$ represents the line of multiple perturbations. When we get away from this line, we want to come back to it. But the "non-continuity" of the differential prevent us from coming back to this line. The only way to do it is to set the Tolerance parameter to 1.

8.1.3 Topological gradient as a solution to the thin bar problem

Recall that the shapes are initialised with a great number of holes because the level-set cannot nucleate them. When two holes want to coalesce, they create thin bars. Those thin bars create problems in 2-d. The solution is then to initiate the shape without any holes and to create the holes one at a time when needed.

For this reason, the bubble method has been coupled with the level-set method in chapter 2. But this theory is not available for the robust compliance problem when there is multiple perturbations.

First we don't know if there exist a topological "directional derivative" to the robust compliance problem and what would make sense. More than that there would be no convenient way to choose the steepest descent direction with an SDP problem.

Indeed the criterion that is interesting is to nucleate some hole with a bound on the measure of the material that is removed. This is clearly not an Hilbertian bound and SDP programming cannot be applied. Recall that SDP programming relies on the problem "find the direction **of given Hilbertian norm 1** that minimizes the directional derivative".

In order to have consistent results with the change of different parameters, the bubble method has not been used in simple compliance problem that were to be compared with robust compliance problems.

8.1.4 The reload method as the chosen solution for the robust compliance

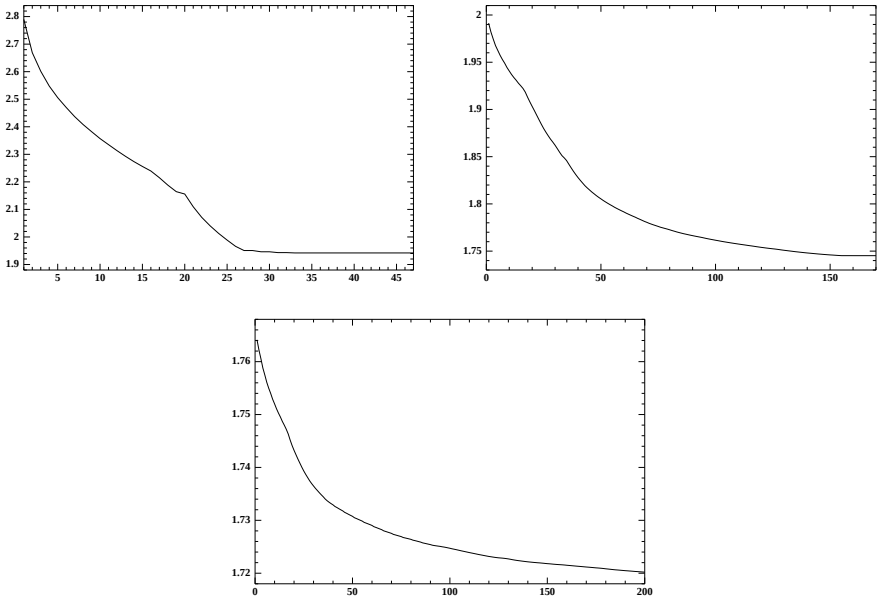

FIG. 8.3 – History of the objective functions for the three steps of optimization for the Figure 8.1.

The choice that has been made is to let the level-set method converge. If the shape is not satisfying, we perform an other optimization process. We choose for the new initialisation the old solution where thin structures are removed. Figure 8.1 shows the three steps of the whole optimization for the problem of the compliant wheel bridge of section 5.4.2. Three algorithm were successively launched, each with the optimal shape of the previous one where the thin bars has been removed. Figure 8.3 is a display of the objective function for the three steps of the process. It can be checked that the objective function is indeed higher at the beginning of one step than at the end of the previous one. This is due to the disappearance of the thin bars that lead to an increase of the objective functions. The thin bars were indeed needed but locked the algorithm into a local minimum.

8.2 The fiber problem in 3-d compliance

The fiber (or leaf) problem is the 3-d equivalent of the 2-d thin bar problem. Sometimes, in the 3-d setting setting, the algorithm may be locked into a local minimum that involves a fiber. A fiber is a thin shell, an example is given in

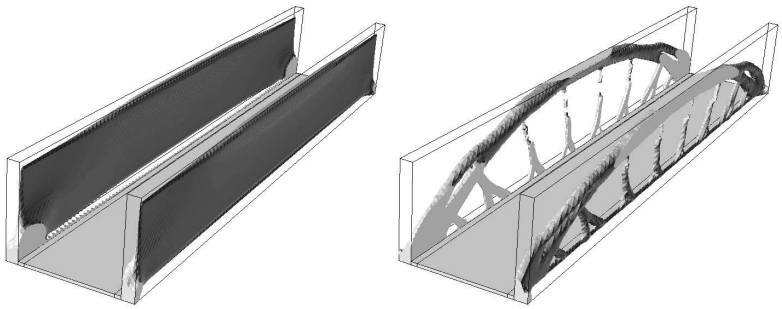

FIG. 8.4 – The fiber local optimum (left) and the global optimum (right) for the 3-d bridge problem.

Figure 8.4 (left). It is believed that the lack of precision of the computation of the elasticity solution forbids the algorithm to have enough accurate precision on the velocity in order to create the needed hole in the fiber. The few times fibers ever appeared were when the initialization was material in the whole domain. Initializing the shape with some hole prevent the apparition of fibers as well as the use of the topological gradient of chapter 2. That is why we claim the fiber problem not to be a real issue but an epiphenomenon that may occur.

8.3 Modes in disconnected parts of the shape

An other issue that is related with the change of topologies in 2-d and in eigenvalue optimization is the apparition of modes when the parts of the shapes are disconnected. Indeed, during optimization, it happens that the level-set method remove some part of the shapes and turn them into islands of material. In the setting of the optimization of the first eigenvalue, theses islands can generate a first eigenvalue that is almost equal to 0.

An example of "island" is given by Figure 8.5 (left). For this shape, the first three modes are shown in Figure 8.6, It can be seen that it is indeed the two islands that give rise to the first mode.

Indeed, in the continuous sense, because the island does not have connections with the rest of the shape and especially connection with a Dirichlet node, the first eigenvector is a mode located on the island, equal to a rigid-displacement and with eigenvalue equal to 0. In numerical sense, the island will still see the Dirichlet nodes, thanks to the ersatz material, but the first eigenvalue will nevertheless be close to 0.

An example of this problem is the optimization of the first eigenvalue of the short cantilever of section 3.6.2. Every parameter is the same except the initialisation shown in figure 8.5 (left) and the number of transport iteration that is set to 1 (ie we slow down the algorithm by reducing the descent step). The algorithm do not converge and end with figure 8.5 (right). On Figure 8.6 (left), we show the pressure $X \mapsto \int_\Omega (X)(-v + \eta)$, ie the derivative of the first

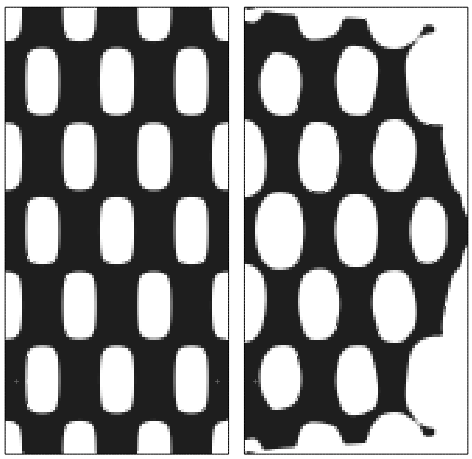

FIG. 8.5 – Initialization and optimal shape for the first eigenvalue of a short cantilever with islands.

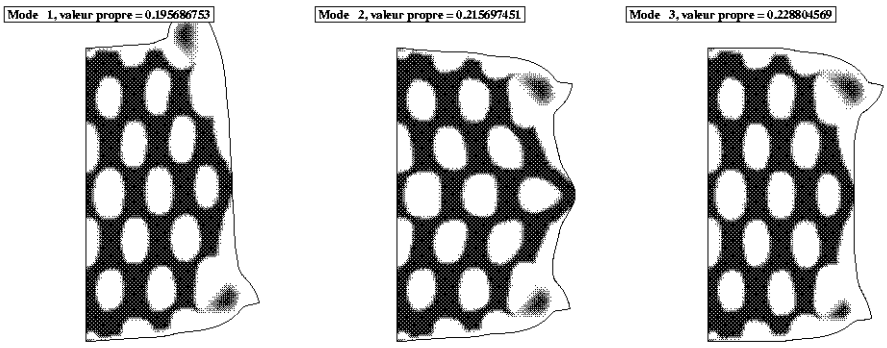

FIG. 8.6 – The first three modes of the short cantilever with islands.

eigenvalue seen as a pressure. When this pressure is negative, the shape wants to increase its volume, when it is positive, the shape want to decrease it. As can be seen the island is indeed a local minima in numerical sense. The island itself want to decrease its volume and the isthmus that connects the island to the rest of the shape wants to increase it. We can force the convergence for this initialization by four ways . The first one relies on an increase of the descent step, so that the algorithm will not pass by the local minimum of the islands. But unfortunately, the algorithm will be stuck in an other local minima involving thin bars (see Figure 8.8 (leftmost)). An other choice will be to accept a tolerance parameter Tol greater than 1. The problem raised in section 8.1.1 about the loosing of symmetry could happen here but is not present here on this special test, mainly because the first eigenvalue of the optimal shape is of multiplicity one. The algorithm is also stuck on the shape involving thin bars

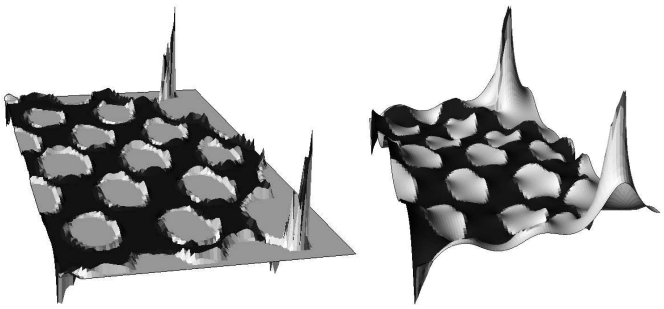

FIG. 8.7 – The velocity (left) and it's regularization (right) in the local minima induced by islands.

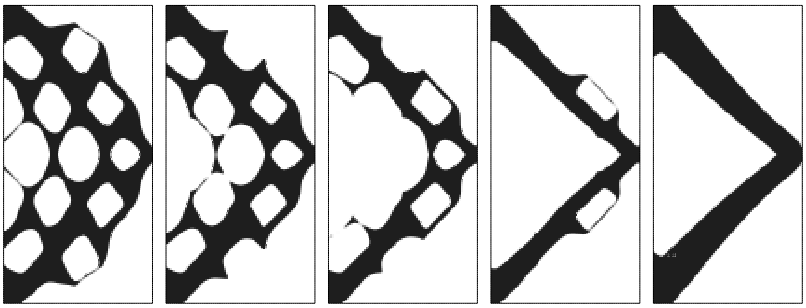

FIG. 8.8 – Different successive optimal shapes for the reload operation.

of Figure 8.8 (leftmost). The third solution is then to fix the ersatz material to an higher ratio. In this case, the changes of topology will be smoother, but the shape will also be stuck on the shape of Figure 8.8 (leftmost) that involves thin bars. The last solution is to perform the reload operation of section 8.1.4, i.e. to re-optimize the shape with removing the bars (see Figure 8.8 for the different successive optimal shapes). The best bet is still not to work with this special initialization or to use a topological gradient method.

An other example of the island problem is given by Figure 8.9. This Figure displays the third eigenvalue of the buckling generalized eigenproblem with a given set of forces that is given accordingly to section 6.3.2.

The arrows represent the eigenvector and in the center of the vortex, there is a small island of the material which receive, through the ersatz material, strains. This problem is not related to the so-called "fictitious mode" when the void itself buckles. We emphasized enough the fact that we avoid them. Here, there is indeed a small island of material in the center of the vortex. It is this island which buckle, and not the void.

There seem to be no way to deal with this problem if such an island located buckling mode is the first buckling eigenvalue. Except by using the reload method which will remove "manually" the small island.

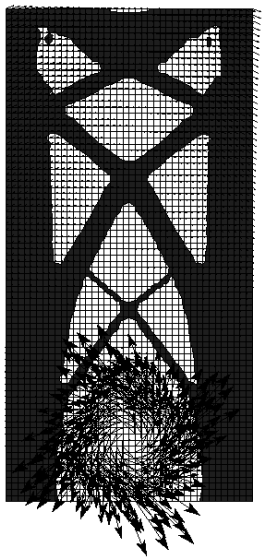

FIG. 8.9 – A buckling mode localized on an island.

8.4 Mechanism design

8.4.1 The Hinges and Horn's problem

An "horn" is a useless part of a mechanism that is still present at the end of the optimization process. It bears this name because this useless parts sometimes looks like a protuberance or a nodulus-like protrusion. The term Horns will also denote the some islands of useless material. The horn's problem is generally avoided by setting a Lagrange multiplier for a volume constraint that is going to remove the unwanted parts. We will see here that horns can be an issue as a direct consequence to the hinge problem. As was advanced in section 3.4.5, 2-d mechanism design is a real issue for the level-set method because the shape has a tendency to create hinges. An example of hinges is given in Figure 8.10 (left), where the problem is the grip of section 2.7 with a ratio of the weak material $\varepsilon_0 = 10^{-5}$. Figure 8.10 (left) is the optimal shape given by the algorithm and Figure 8.10 (right) is a display of the velocity (before regularization). As can be seen on Figure 8.10 (right), because the velocity is highly irregular, there is a need of a lot of precision in order to adjust an hinge. Meanwhile, the rest of the shape do not converge. As was said in section 3.4.5, the trick lies into setting ε_0 big enough (typically $\varepsilon_0 = 0.01$) so that hinges are no longer efficient.

Raising the ratio of the weak material allows to remove the majority of the hinges, but even if the ratio of the weak material is set big enough, hinges can be annoying.

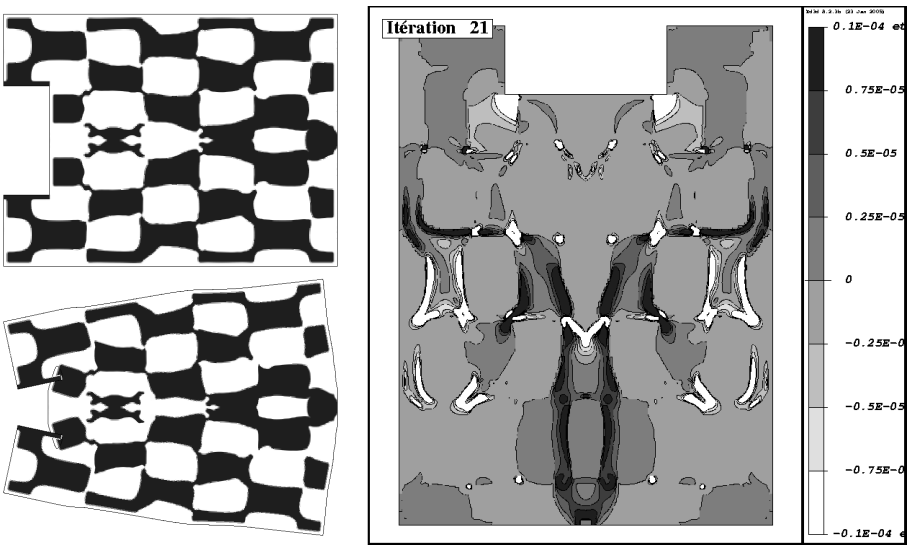

FIG. 8.10 – A locally optimal shape for the CEA grip, its deformed configuration and the value of the velocity on its boundary.

Take for instance the shapes of Figure 8.11 (only the upper part is shown) that represent the grip of Figure 8.12 (right) during optimization process. Figure 8.11 is a display of the working shapes at iteration 12 to 14 and of the "optimal" shape at iteration 54 when the parameter Tol is set to one. As can be seen on this figure, the algorithm concentrate on the hinge (the one at the center) only and do not converge. On Figure 8.12 (left) there is a display of

the convergence history of this test (the one with the legend "Tolerance equal to one"). As can be seen on this Figure, the algorithm stops advancing soon after iteration 14 (iterations of the algorithm that do not decrease the criterion and lead to a reducing of the step of descent are counted and represent the horizontal bars of Figure 8.12 (left)). There is a small Lagrange multiplier in order to remove the islands, but the algorithm do not even bore about them and let the islands in the optimal shape of Figure 8.11 (iteration 52).

The solution is to let the parameter Tol be higher than one, the algorithm will then converge to the shape of Figure 8.12 (right). The price to pay is, of course, the somewhat chaotic look of the convergence history. The display of the convergence history in such a case is given in Figure 8.12 under the legend "Tolerance greater than one". Sometimes, fine tuning of the different parameters, allows to avoid this problem (see for instance the 2-d mechanism of chapter 3 and their convergence history).

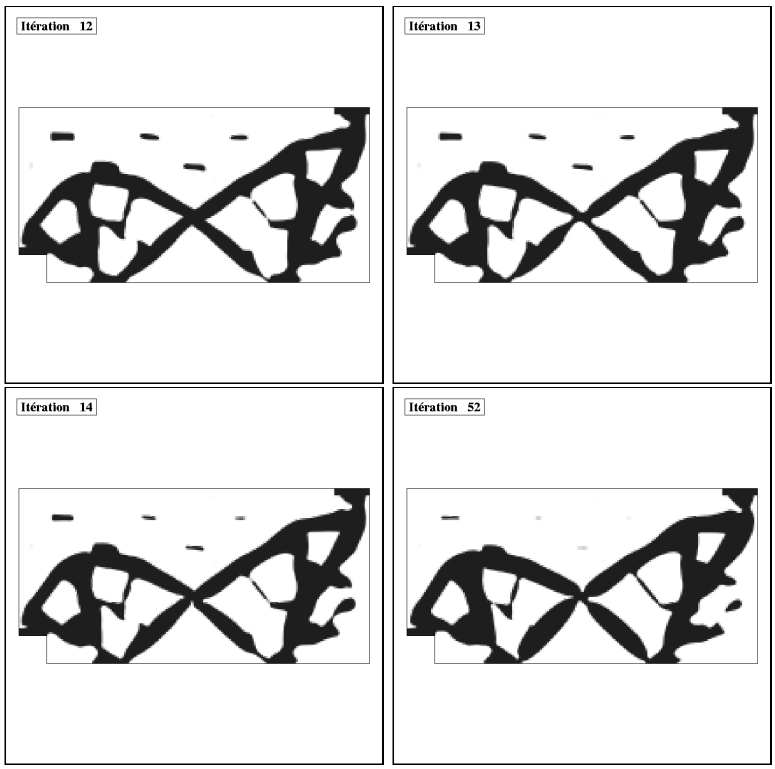

FIG. 8.11 – An hinge forbids the algorithm to converge to a grip.

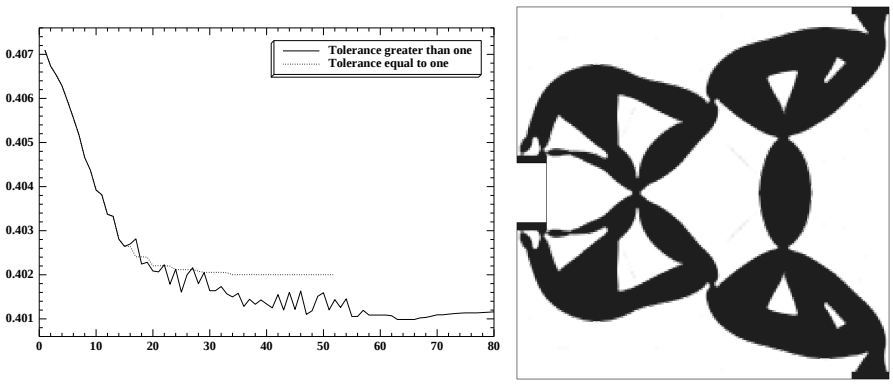

FIG. 8.12 – History of convergence rate for the two methods and optimal shape obtained with a Tol parameter greater than one.

8.4.2 Disconnection of the mechanism

A problem raised by the weak material approximation for mechanism design is that the mechanism may use the void in order to transmit strains. A good

example is the 'optimal' grip of Figure 8.13 (left), its displacement is shown in Figure 8.13 (right) and a close-up of the displacement is shown in Figure 8.14. If the algorithm ended with such a shape, it is almost incapable of continuing

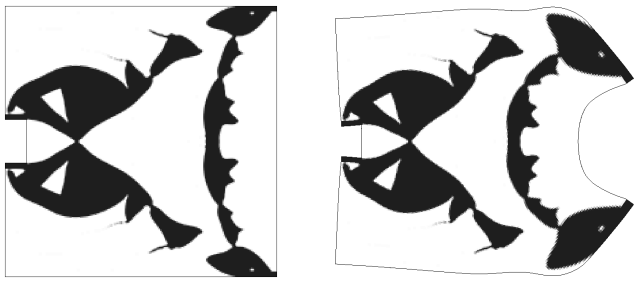

FIG. 8.13 – The disconnected 'optimal shape' and it's displacement.

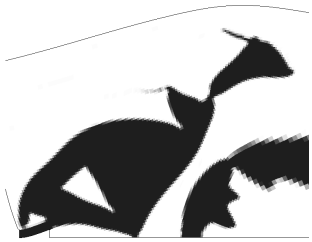

FIG. 8.14 – A close-up on the displacement of the disconnected "optimal shape".

and -for example- to reconnect the shape. this is mainly due to the fact that we use formula based on the continuous setting and the formula for the derivative do not take the weak-material approximation into account. A very few things can be done to solve this problem if it arises which hopefully scarcely happens. Still, when it does, one can try to enforce the displacement where the force is input to be close to zero which is well-known for forcing connectivity.

8.4.3 The Natural extension method and the Lagrange multiplier

As was previously said, even in the mechanism design setting, we use a small Lagrange multiplier in order to remove some useless parts of the shape and to end with nice design of the mechanism. The first issue is that mechanism design is very sensitive to the Lagrange multiplier and very fine tuning of this parameter is required. The second issue is that, for not completely understood reason, the Natural extension method and the Hilbertian extension method are not sensitive to the same Lagrange multiplier. The optimal shapes for the

Natural extension method has always less volume than the one for the Hilbertian extension method. Take for instance, the optimal shapes of figure 8.15 or any optimal shape of chapter 3. Figure 8.15 is a display of some optimal shapes

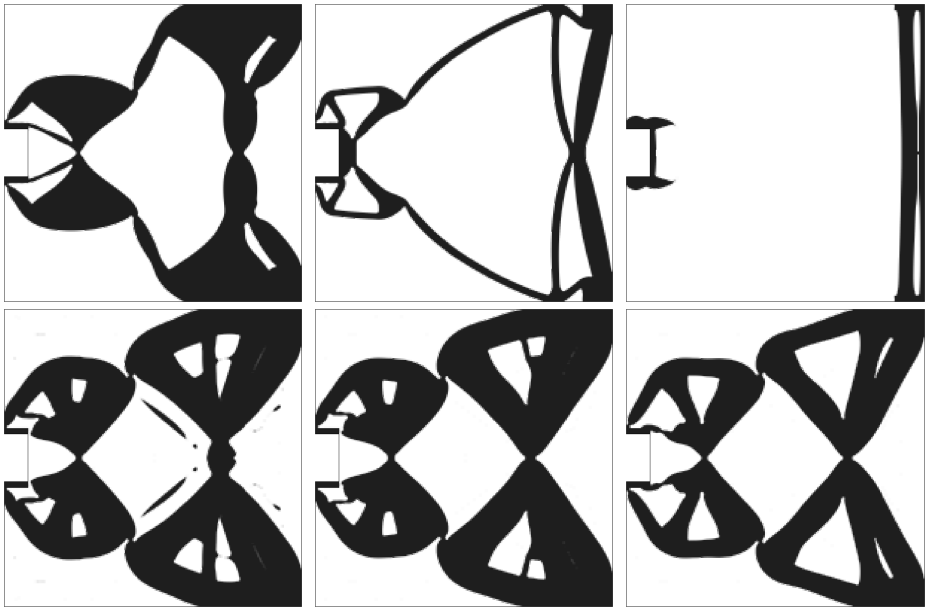

FIG. 8.15 – Up : The optimal grips of the natural extension method. Down : The optimal grips for the Hilbertian extension method.

η	=	10^{-2}	$1,2.10^{-2}$	$1,85..10^{-2}$
$\mathcal{L}_{lse}$	=	0.40293 / 0.40270	0.40296 / 0.40525	0.40302 / 0.40560
$\mathcal{J}_{lse}$	=	0.40241 / 0.40235	0.40234 / 0.40504	0.40221 / 0.40545
vol	=	51.8862 / 37.4452	51.8240 / 18.3182	43.6645 / 8.4543

TAB. 8.1 – Optimal criteria of the Lagrange grips (Hilbertian/Natural).

found for the grip of section 2.7. The upper shapes are obtained for the Natural extension method and the lower shapes are obtained for the Hilbertian extension method. the Lagrange multiplier increases from left to right. Table 8.1 lists the value of the objective function $\mathcal{J}_{lse}$ and the objective function added with the Lagrange multiplier $\mathcal{L}_{lse}$ for every Lagrange multiplier η and for the Hilbertian (on the left) and the Natural (on the right) method.

The main reasons that may be advanced for this difference of reaction of the algorithm towards the Lagrange multiplier are :
$\diamond$ As was said in section 3.3, the velocity for the natural extension method is equal to $-\eta$ everywhere in the void, this is not the case for the Hilbertian extension method. It may be a good example of the 'higher ponderation of the

gradient' discussed in section 3.3.
⋄ Recall that mechanism are very sensitive to the Lagrange multiplier, this is a catalytic effect of the previous remark.

We still do not fully understand the extraordinary high differences of treatment in Figure 8.15 between the Natural and the Hilbertian method. Nevertheless, recall that in chapter 3, we were able to find some tests where the two methods converged with comparable history of convergence and optimal shape. But this few tests were really very hard to exhume.

8.5 Conclusion

We showed some still unsolved problems that arises when numerically using shape optimization by the level-set method. The bubble method helped a lot in solving previous issues but the problems are still solved by the mean of tricks and await for better methods. Most of these problem are deeply related to the very nature of geometric method who roughly speaking "are only concerned in local regions of the boundary of the domain". No matter if this boundary is close to another one (the thin bar problem) ; No matter if this boundary is relevant (disconnection of the shape). But still geometric methods are very efficient for the wideness of the problems they address and the fact that the material is always clearly identified (avoiding e.g. the fictitious modes). Sadly they don't have the global point of view that is the strength of topology methods.

Annexe A

Existence of a local maximum for the direct problem of the robust compliance

We wish to exhibit a local maximum that is not a global maximum. Let x be a parameter that will be chosen big. Let $m = 3\sqrt{x^2+1}$

$$\mathbf{A} = \begin{bmatrix} 1 & 0 \\ 0 & 2 \end{bmatrix} \quad B = \begin{bmatrix} 1 & 0 \\ 0 & 1 \end{bmatrix} \quad f = \begin{bmatrix} x \\ 1 \end{bmatrix} \quad u = \begin{bmatrix} -2x \\ 2 \end{bmatrix}$$

It is easy to check that u is indeed a critical point of $F(u) = -(\mathbf{A}u, u) + 2(f, u) + 2m\|u\|$, in the sense that $D_u F = -\mathbf{A}u + f + \frac{m}{\|u\|}u = 0$.

In order to prove that u is a local maximum, we have to prove that the Hessian of F is definite negative this matrix is given by :

$$D_u^2 F(v, w) = -(\mathbf{A}v, w) + \frac{m}{\|u\|}(v, w) - \frac{m}{\|u\|}^3 (v, u)(w, u)$$

which as a matrix is

$$D_u^2 F = \frac{1}{2(x^2+1)} \begin{bmatrix} (x^2+1) - 3x^2 & 3x \\ 3x & -(x^2+1) - 3 \end{bmatrix}$$

The trace of $D_u^2 F$ is equal to $-3/2$ and setting x big enough can allow us to have $det(D_u^2 F) > 0$ which means that the two eigenvalues of the matrix are strictly negative and that u is a local maximum. But u can not be a global maximum because we know that for the globals maxima : $\frac{m}{\|u\|} \leq \lambda_1$. where in our case $\frac{m}{\|u\|} = \frac{3}{2}$ and λ_1 the smallest eigenvalue of $\mathbf{A}$ is equal to 1. Or for a quicker approach,

$$F(2x, 2) = 12x^2 + 8 > 4x^2 + 8 = F(-2x, 2) = F(u)$$

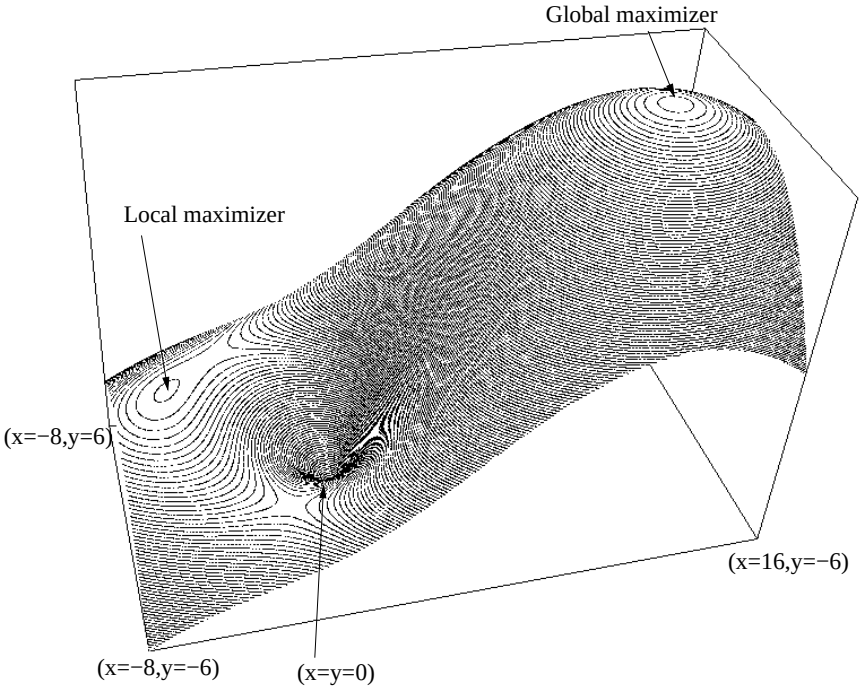

FIG. A.1 – The functional F for $x = 3$.

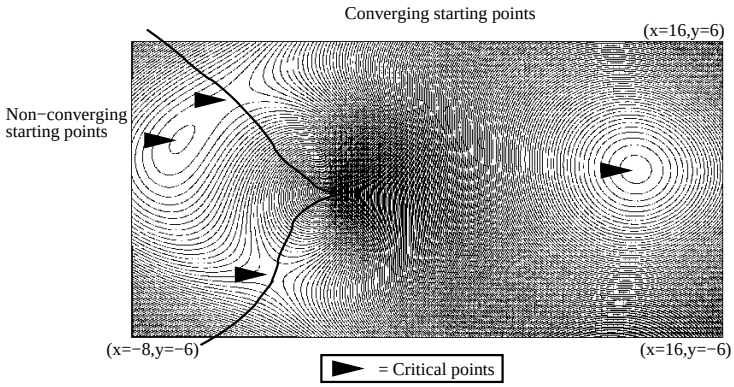

FIG. A.2 – The functional F for $x = 3$ (seen from above).

Figure A.1 displays the functional F for $x = 3$. The equation $g'(s) = 0$ is a polynomial of s of order 4 and the two eigenvalues of $\mathbf{A}$ does belong to Z (ie, $f \not\perp E_1$ and $f \not\perp E_2$) so that F has a maximum of 4 critical points which are

shown on figure A.1. Figure $A.2$ shows the level-sets of this function. Roughly speaking, a standard gradient algorithm would stop at the local maximizer for any starting point located at the left of figure $A.2$.

Annexe B

Proof of Theorem 5.2.1

B.1 The subgradient of $\mathcal{J}_{rob}$ 161
B.2 The directional derivative 163

Let X be a Banach space and suppose that there exist an application

$$\begin{array}{rcl} X & \rightarrow & \mathbb{L} \times \mathbb{M} \times V' \\ \theta & \mapsto & (\mathbf{A}(\theta), C(\theta), f(\theta)) \end{array}$$

That is continuously differentiable in $\theta = 0$.

B.1 The subgradient of $\mathcal{J}_{rob}$

We will use the Theorem (2.8.2) of [Cla90]. Let X be a Banach space and applications $\theta \mapsto (\mathbf{A}(\theta), C(\theta), f(\theta))$ that are continuously differentiable on U a neighbourhood of $\theta = 0$.

Theorem B.1.1 *Define $\mathcal{J}_{rob}$ as*

$$\mathcal{J}_{rob}(\theta) = \max_{u \in S} -(\mathbf{A}(\theta)u, u) + 2(f(\theta), u) + 2m(C(\theta)u, u)^{1/2}$$

There exist a subgradient of $\mathcal{J}_{rob}$ in the point $\theta = 0$ which is a subset of X^*

$$\partial \mathcal{J}_{rob}(0) = \{ \int_S DF_u(0)\mu(du) \ st \ \mu \in P[\mathcal{M}(0)] \} \tag{B.1}$$

where the following notations are used

- $F_u(\theta) = -(\mathbf{A}(\theta)u, u) + 2(f(\theta), u) + 2m(C(\theta)u, u)^{1/2}$
- $DF_u(\theta_0) \in X^*$ is the differential of $\theta \mapsto F_u(\theta)$ at the point θ_0
- $\mathcal{M}(\theta) = \{u \in S \text{ st } F_u(\theta) = \mathcal{J}_{rob}(\theta)\}$ ie : the set of maximizers
- $P[\mathcal{M}(\theta)]$ is the set of Radon probability measures supported by $\mathcal{M}(\theta)$
- $< \int_S DF_u(\theta)\mu(du), v >_{<X^*,X>} = \int_S < DF_u(\theta), v >_{<X^*,X>} \mu(du)$

The conditions for Theorem $B.1.1$ to stand are :

Proposition B.1.2
- S is sequentially compact and metrisable
- $\forall \theta \in U$ the mapping $u \mapsto F_u(\theta)$ is upper semi-continuous
- There exist $K > 0$ independent of u such that for each $u \in S$, the mapping $\theta \mapsto F_u(\theta)$ is Lipschitz of rank K.
- For each $\theta \in U$, the set $\{F_u(\theta) : u \in S\}$ is bounded
- For every $(\theta_0, u) \in U \times S$, $DF_u(\theta_0)$ the differential of $\theta \mapsto F_u(\theta)$ at the point θ_0 exists.
-The mapping $U \times S \to X^*$ defined by $(\theta, u) \mapsto DF_u(\theta)$ is continuous.

Proof B.1.2.1 (construction of S) *Recall that in definition 5.1.2, the maximum of $\mathcal{J}_{rob}$ is taken over the set H. In order to prove proposition $B.1.2$, it is sufficient to build a set S that have the following properties*
- For all θ in U and for all u maximizer over H of $F_u(\theta)$, then $u \in S$
- There exists constants γ, β such that for all $u \in S$ and for all $\theta \in U$ $\|u\|_V \leq \gamma$ and $(C(\theta)u, u) \geq \beta$
$\diamond$ Uniform bound on $\|u\|_V$: For all θ and for all u maximizer over H of $F_u(\theta)$, we have $F_u(\theta) \geq F_0(\theta) = 0$. Thus

$$-(\mathbf{A}(\theta)u, u) + 2(f(\theta), u) + 2m(C(\theta)u, u)^{1/2} \geq 0$$

Using the uniform properties of $\mathbb{L}$ and $\mathbb{M}$, we have :

$$\alpha\|u\|_V^2 \leq 2\|f(\theta)\|_{V'}\|u\|_V + 2m\sqrt{\beta_2}\|u\|_H$$

Using the continuous injection of V into H, and a uniform bound on $\|f(\theta)\|_{V'}$ for all $\theta \in U$. There exist $\gamma > 0$ independent of θ such that for every $\theta \in U$ and $u \in \mathcal{M}(\theta)$ then $\|u\|_V \leq \gamma$
$\diamond$ Uniform bound on $(C(\theta)u, u)$: For each $\theta \in U$ and u maximizer of $F_u(\theta)$ over H, u verifies the Eulerian equation which gives :

$$(C(\theta)u, u)^{1/2} = \frac{m}{\rho_\theta}$$

Where ρ_θ is always smaller than the first eigenvalue of the generalized eigenproblem $\mathbf{A}(\theta)u = \lambda C(\theta)u$. Expressing the first eigenvalue as a Rayleigh quotient we have :

$$\lambda(\theta) \leq \min_{u \in H} \frac{(\mathbf{A}(\theta)u, u)}{(C(\theta)u, u)}$$

Let any $v \in V$ such that $(C(0)v, v)$ is not zero, upon a restriction on U, there exist constants $c_1 > 0$ and c_2 independent of θ such that $(C(\theta)v, v) \geq c_1$ and $(\mathbf{A}(\theta)v, v) \leq c_2$ for all θ in U. The first eigenvalue $\lambda(\theta)$ is then uniformly bounded by c_2/c_1 and $(C(\theta)u, u)^{1/2} \geq \frac{mc_1}{c_2}$. Upon a restriction on U there exist c_3 such that $(C(\theta)u, u)^{1/2} \geq \frac{mc_1}{c_2} \Rightarrow (C(0)u, u)^{1/2} \geq c_3$ and upon a last restriction on U, there exist α such that $(C(0)u, u)^{1/2} \geq c_3 \Rightarrow (C(\theta)u, u)^{1/2} \geq \alpha$.
$\diamond$ Definition of S : We then define the sequentially compact S such as

$$S = \{u \in H \text{ st } (C(0)u, u)^{1/2} \geq c_3 \text{ and } (u, u)_V \leq \gamma\}$$

$\diamond$ Verification of the properties :
-For every $\theta \in U$ and $u \in H$, If u is a maximizer of $F_u(\theta)$ over H, then u belongs to S, thus $\mathcal{J}_{rob}(\theta)$ is indeed the maximum of $F_u(\theta)$ over S.
The compactness of S comes from the uniform bound on $\|u\|_V$ and the compact injection of V into H
-Because of the bound $(C(\theta)u, u) \geq \alpha$, the differential

$$DF_u(\theta_0).\theta = -(D\mathbf{A}(\theta_0).\theta u, u) + 2(Df(\theta_0).\theta u, u) + \frac{m}{(C(\theta)u, u)^{1/2}}(DC(\theta_0).\theta u, u)$$

exist for all $\theta_0 \in U$ and $u \in S$ and is uniformly bounded by K

B.2 The directional derivative

The directional derivative of F in the point 0 and in the direction $\theta_0 \in X$ exists and is worth $\max_{\zeta \in \partial \mathcal{J}_{rob}(0)} < \zeta, \theta_0 >_{<X^*, X>}$. Let θ_0 be given and let call $\mathcal{J}'_{rob}$ the directional derivative of $\mathcal{J}_{rob} = \max F$ in the direction θ_0, we want to prove that

Proposition B.2.1

$$\mathcal{J}'_{rob} = \max_{u \in \mathcal{M}(0)} -(\mathbf{A}'u, u) + 2(f', u) + \rho^*(C'u, u) \tag{B.2}$$

Where $\mathbf{A}'$ (resp f',C') denotes the differential of $\mathbf{A}(\theta)$ (resp $f(\theta)$,$C(\theta)$) in $\theta = 0$ applied to θ_0

Proof B.2.1.1 *Recall that if $\zeta \in \partial \mathcal{J}_{rob}(0)$ then there exist $\mu \in P[\mathcal{M}(0)]$ such that*

$$< \zeta, \theta_0 >_{<X^*, X>} = \int_S < DF_u(0), \theta_0 >_{<X^*, X>} \mu(du) \tag{B.3}$$

$\diamond$ The first thing that has to be shown is that

$$\max_{u \in \mathcal{M}(0)} < DF_u(0), \theta_0 >_{<X^*, X>} \text{ is attained by a } u^* \in \mathcal{M}(0)$$

It can be done simply by observing that

$$< DF_u(0), \theta_0 >_{<X^*,X>} = -(\mathbf{A}'u, u) + 2(f', u) + \rho^*(C'u, u)$$

and $\mathcal{M}(0)$*, the set of maximizers is finite dimensional and bounded (see Theorem 4.5.4). Take a maximizing sequence that lies inside* $\mathcal{M}(0)$*, by compactness of finite-dimensional bounded subset of vector spaces, it will converge up to a subsequence to a maximum* u^**.*
$\diamond$ *Then whatever measure* $d\mu$*, the convex sum* (B.3) *is always lower than* $< DF_u^*(0), \theta_0 >$ *and the maximum of such convex sum over the measures is therefore attained and equal to* $< DF_u^*(0), \theta_0 >$ *when* $d\mu$ *is taken equal to the Dirac measure which support is* u^**. Then*

$$\begin{aligned} \mathcal{J}'_{rob} &= \max_{\zeta \in \partial \mathcal{J}_{rob}(0)} < \zeta, \theta >_{<X^*,X>} \\ &= < DF_{u^*}(0), \theta >_{<X^*,X>} \\ &= \max_{u \in \mathcal{M}(0)} -(\mathbf{A}'u, u) + 2(f', u) + \rho^*(C'u, u) \end{aligned}$$

Table des figures

1.1 Le problème de la console et une des formes optimales standard . 18

1.2 **Symétries du vecteur déplacement** : On applique d'abord la symétrie pour passer de la première forme à la seconde. On multiplie le terme source par -1 pour passer de la seconde forme à la troisième, par linéarité de l'équation , on multiplie aussi le déplacement par -1. On conclut en remarquant que le terme source ainsi obtenu $-S(f)$ est égal à f. 19

2.1 Shape gradient method (without topological derivative) for the cantilever problem : initializations (left) and optimal designs (right). 34

2.2 Coupled shape and topological gradient method for the cantilever : optimal design (left) and convergence history of the objective function (right). 35

2.3 Optimal cantilever for the coupled shape and topological gradient method : $n_{top} = 10$ (left) and $n_{top} = 1$ (right). 35

2.4 Optimal bridge in 2-d : iterations 6, 11, 16 and 100. 36

2.5 Optimal bridge in 2-d : half domain initialization and optimal shape after 100 iterations. 36

2.6 Convergence history of the objective function (left) and of the weight (right) for the 2-d optimal bridge. 37

2.7 Convergence history of the objective function (left) and of the weight (right) for the 2-d optimal mast of Figure 2.8. 37

2.8 Optimal mast in 2-d : boundary conditions and iterations 6, 11, 16, 21 and 100. 38

2.9 Optimal design (left) for the negative Poisson ratio mechanism, and deformed configuration (right). 39

2.10 Convergence history of the objective function (left) and of the weight (right) for the negative Poisson ratio mechanism. 39

2.11 Boundary conditions and target displacement for the gripping mechanism. 39

2.12 Optimal design (left) for the gripping mechanism, and deformed configuration (right). 40

2.13 Optimal cantilever in 3-d (right). Convergence history of the objective function (left). 40

2.14 Optimal mast in 3-d (right). Convergence history of the objective function (left). 41

3.1 Two merging parts of the boundary leads to a non-regular vector field as seen as a distribution on D. 48
3.2 Boundary conditions for a 2-d cantilever (the black zone is heavier and not subject to optimization). 49
3.3 Initialization and optimal shape for the first eigenvalue of a cantilever. 49
3.4 Mesh-refinement influence on the velocity for the Natural extension (left) and the Hilbertian extension (right). 50
3.5 Initialization and optimal shape of the cantilever. 51
3.6 Mesh-refinement influence on the natural extension (left) and the Hilbertian extension (right). 52
3.7 The definition of the 2-d gripping mechanism and its initialization. 52
3.8 Evolution of the objective function for the first step (left) with a ratio for the weak material equal to 0.01 and the second step with a ratio of 10^{-5} (right). 53
3.9 Optimal shape for the Hilbertian method (left) and the natural method (right) at the end of the first step of optimization. 53
3.10 Optimal shape for the Hilbertian method (left) and the natural method (right) at the end of the second step of optimization. . . 53
3.11 Optimal shape displacement. 54
3.12 The Negative Poisson modulus problem and its deformed solution. 55
3.13 Negative Poisson modulus's evolution of the objective function at the first step (left) with a ratio for the weak material equal to 0.01 and the second step with a ratio of 10^{-5} (right). 55
3.14 Negative Poisson modulus's optimal shape for the Hilbertian method (left) and the natural method (right) at the end of optimization. 55
3.15 The Force inverter problem and its deformed solution. 56
3.16 Force inverter's evolution of the objective function for the first step (left) with a ratio for the weak material equal to 0.01 and the second step with a ratio of 10^{-5} (right). 56
3.17 Force inverter's optimal shape for the Hilbertian method (left) and the natural method (right) at the end of optimization. . . . 56
3.18 The problem of the 3-d gripping mechanism. 57
3.19 Optimal shape for the Hilbertian method (left) and the natural method (right) (isovalue 0 of the level-set is shown). 57
3.20 Objective function (left) and displacement of the Hilbertian shape (right) (density of material ≥ 0.3 is shown). 58
3.21 Initialization for narrow domain (left) and for the big domain (right). 66
3.22 The optimal shape for the first eigenvalue in a big domain (left) and its boundary (right). 67

3.23 Evolution of the three smallest eigenvalue (left) and an interpretation (right) for the big domain. 67
3.24 The optimal shape for the first eigenvalue in a narrow domain (isovalue 0.2 of the density is drawn). 68
3.25 Evolution of the two smallest eigenvalue (left) and the objective function (right) for the narrow domain. 68
3.26 Initialization and optimal shape for the first eigenvalue of a short cantilever. 69
3.27 Evolution of the objective function for the two different methods. 69
3.28 Evolution of the two smallest eigenvalues for the Single eigenvalue optimization (left) and the Multiple eigenvalue optimization (right). 70

4.1 The model example 72
4.2 The model problem. 88
4.3 Compliance as a function of m (log scale). 89
4.4 Compliance as a function of h. 89
4.5 Compliance as a function of the mesh. 90
4.6 Dependency of s_M and s_m with respect to the mesh. 90

5.1 The beam-to-cantilever problem and its initialization. 104
5.2 Increasing values of m in the beam-to-cantilever problem. 105
5.3 The Wheel-bridge problem and its initialization. 105
5.4 Increasing values of m in the wheel-bridge problem. 106
5.5 Mesh and initialization of the 2-d mast problem. 107
5.6 Increasing values of m for the 2d-mast problem (vertical perturbations). 107
5.7 Increasing values of m for the 2d-mast problem (vertical and horizontal perturbations). 108
5.8 Upper and bottom view of the optimal shapes for $m = 10^{-2}, 3 \times 10^{-2}$ and 5×10^{-2} for a volume of 10 percent. 108
5.9 Upper and bottom view of the optimal shapes for $m = 10^{-2}, 3 \times 10^{-2}$ and 5×10^{-2} for a volume of 14 percent. 109
5.10 Optimal shape for $m = 7 \times 10^{-2}$ and a volume of 11 percent (isovalue 0 of the level-set is shown). 110
5.11 Optimal shape of the bridge for $m = 0$ (left) and $m = 1$ (right). . 110
5.12 Loading and optimal shape of the chair for $m = 0$ (left) and $m = .1$ (right). 111

6.1 The beam problem. 122
6.2 Initialization (right) and the solutions for a ratio of the weak material equal to 10^{-2} (center) and then equal to 10^{-5} (left). . . 122
6.3 Evolution of the objective function for the beam problem. 122
6.4 The two-beams problem. 123

6.5 **The two beam reinforcement problem** Top : The standard buckling, Bottom : The extended buckling. From left to right : Initialization, optimal shape, linearized displacement at the buckling point and the two first modes that correspond to the buckling eigenvalue which is always of multiplicity 2. 123
6.6 Top : From left to right : The initialization, The optimal shape and the linearized displacement at the buckling point of the two beam reinforcement in the standard case. Bottom : The first four buckling modes. 124
6.7 From left to right : Initialization, The optimal shape, The linearized displacement at the buckling point and the buckling mode of the two beam reinforcement in the extended case. 124
6.8 The compliant bridge problem (left) and its initialization (right). 125
6.9 Top : The compliant bridge problem optimal shapes. Bottom : The compliant bridge problem buckling modes. 125
6.10 Convergence history of the compliant bridge objective function. . 126
6.11 From left to right : Definition of the gripping mechanism problem, a standard optimal solution and its buckling mode. 127
6.12 From left to right : Optimal shape, the displacement at the buckling point and the buckling mode of the buckling grip. 128
6.13 Convergence history (left) and buckling eigenvalue history (right) for the buckling grip. 128
6.14 Left : A grip calculated by the standard method. Right : A grip computed by using the buckling load with a final buckling eigenvalue equal to 1. 129

7.1 La console courte avec perturbations horizontales. 132
7.2 La console courte avec perturbations mixtes. 132
7.3 En haut, formes optimales pour la première valeur propre de la console courte possiblement multiple (gauche) ou toujours simple (droite). En bas, les trois premiers modes pour la forme optimale de gauche. 134
7.4 Evolution des trois premières valeurs propres de la console courte possiblement multiple (gauche) ou toujours simple (droite). . . . 134
7.5 A gauche, comparaison de l'évolution des fonctions objectifs. A droite, évolution des valeurs propres et du nombre de valeurs propres considérées comme multiples au cours des itérations. . . 135
7.6 La pince du CEA avec une pression p entre les mâchoires de plus en plus fortes. 136
7.7 D'une pince à un amplificateur de déplacement. 137
7.8 Une autre pince pour la méthode hilbertienne (gauche) et sa déformée (droite). 139
7.9 Différentes topologies de pinces optimales avec un ressort entre les mâchoires. 140
7.10 Le problème du mécanisme à coefficient de Poisson négatif (gauche) et son initialisation (droite). 141

7.11 Différentes formes optimales du mécanisme à coefficient de Poisson négatif pour un coefficient k_0 augmentant. 142

8.1 Three different initialisation (left) and three different optimal shapes (right). 144
8.2 Entering a cycle when loosing symmetry if the tolerance parameter is not equal to 1. 145
8.3 History of the objective functions for the three steps of optimization for the Figure 8.1. 147
8.4 The fiber local optimum (left) and the global optimum (right) for the 3-d bridge problem. 148
8.5 Initialization and optimal shape for the first eigenvalue of a short cantilever with islands. 149
8.6 The first three modes of the short cantilever with islands. 149
8.7 The velocity (left) and it's regularization (right) in the local minima induced by islands. 150
8.8 Different successive optimal shapes for the reload operation. . . . 150
8.9 A buckling mode localized on an island. 151
8.10 A locally optimal shape for the CEA grip, its deformed configuration and the value of the velocity on its boundary. 152
8.11 An hinge forbids the algorithm to converge to a grip. 153
8.12 History of convergence rate for the two methods and optimal shape obtained with a Tol parameter greater than one. 153
8.13 The disconnected 'optimal shape' and it's displacement. 154
8.14 A close-up on the displacement of the disconnected "optimal shape". 154
8.15 Up : The optimal grips of the natural extension method. Down : The optimal grips for the Hilbertian extension method. 155

A.1 The functional F for $x = 3$. 158
A.2 The functional F for $x = 3$ (seen from above). 158

Bibliographie

[AB93] L. Ambrosio and G. Buttazzo. An optimal design problem with perimeter penalization. *Calc. Var. Partial Differential Equations*, 1993.

[AB03] M-S. Ashbaugh and D. Bucur. On the isoperimetric inequality for the buckling of a clamped plate. *Z. Angew. Math. Phys*, 2003.

[ABFJ97] G. Allaire, E. Bonnetier, G. Francfort, and F. Jouve. Shape optimization by the homogenization method. *Nümerische Mathematik*, 76 :27–68, 1997.

[AGJT05] G. Allaire, F.de Gournay, F. Jouve, and A-M. Toader. Structural optimization using topological and shape sensitivity via a level set method. *Control and Cyb.*, 2005. to appear.

[AJ05] G. Allaire and F. Jouve. A level-set method for vibrations and multiple loads in structural optimization. *Comp. Meth. Appl. Mech. Engrg.*, 2005.

[AJT02] G. Allaire, F. Jouve, and A-M Toader. A level set method for shape optimization. *C. R. Acad. Sci. Paris*, 334(I) :1125–1130, 2002.

[AJT04] G. Allaire, F. Jouve, and A-M Toader. Structural optimization using sensitivity analysis and a level-set method. *J. comput. Phys.*, 194(1) :363–393, 2004.

[All01] G. Allaire. *Shape optimization by the homogenization method*. Springer Verlag, New York, 2001.

[Auc89] G. Auchmuty. Unconstrained variational principles for eigenvalues of real symmetric matrices. *SIAM J. Math. Anal.*, 20(5) :1186–1207, 1989.

[Ben95] M. Bendsoe. *Methods for optimization of structural topology, shape and material*. Springer Verlag, New York, 1995.

[Ber04] P. Bernardoni. *Outils et méthode de conception de structure mécaniques à déformations et actionnements répartis*. PhD thesis, Université Paris VI, 2004.

[BHR04] M. Burger, B. Hackl, and W. Ring. Incorporating topological derivatives into level set methods. *J. Comput. Phy.*, 194(1) :344–362, 2004.

[BK88] M. Bendsoe and N. Kikuchi. Generating optimal topologies in structural design using a homogeneization method. *Comp. Meth. Appl. Mech. Eng.*, 71 :197–227, 1988.

[Bri98] J-McG Brian. A model-trust region algorithm utilizing a quadratic interpolant. *J. Comput. App. Math.*, 91(2) :249–259, 1998.

[BS03] M. Bendsoe and O. Sigmund. *Topology Optimization. Theory, Methods, and Applications*. Springer Verlag, New York, 2003.

[BT98] D. Bucur and P. Trebeschi. Shape optimisation problems governed by nonlinear state equations. *Proc. Roy. Soc. Edinb.*, 128 (sec A)(5) :945–963, 1998.

[Bur03] M. Burger. A framework for the construction of level set methods for shape optimization and reconstruction. *Interfaces and Free Boundaries*, 5 :301–329, 2003.

[BV02] D. Bucur and N. Varchon. A duality approach for the boundary variation of neumann problems. *SIAM J. Math. Anal.*, 34(2) :460–477, 2002.

[BZ95] D. Bucur and J-P Zolésio. n-dimensional shape optimization under capacitary constraint. *J. Diff. Equa.*, 123(2) :504–522, 1995.

[Céa86] J. Céa. Conception optimale ou identification de formes, calcul rapide de la dérivée directionnelle de la fonction coût,. *Math. Model. Num. Anal.*, 20(3) :371–402, 1986. French.

[CC03] A. Cherkaev and E. Cherkaeva. Principal compliance and robust optimal design. *J. Elasticity*, 72 :71–98, 2003.

[Cha03] A. Chambolle. A density result in two-dimensional linearized elasticity and applications. *Arch. Ration. Mech. Anal.*, 167(3) :211–233, 2003.

[Che75] D. Chesnais. On the existence of a solution in a domain identification problem. *J. Math. Anal. Appl.*, 52 :189–289, 1975.

[Che00] A. Cherkaev. *Variational Methods for Structural Optimization*. Springer Verlag, New York, 2000.

[CL03] A. Chambolle and C-J. Larsen. c^∞-regularity of the free boundary for a two-dimensional optimal compliance problem. *Calc. Var. Partial Diff. Eq*, 18(1) :77–94, 2003.

[Cla90] F. H. Clarke. *Optimization and Nonsmooth Analysis*. SIAM, classic in appl. math. edition, 1990.

[ES94] H. Eschenauer and A. Schumacher. Bubble method for topology and shape optimization of structures. *Structural Optimization*, 8 :42–51, 1994.

[FR98] J. Folgado and H. Rodrigues. Structural optimization with a non-smooth buckling load criterion. *Control and Cybernetics*, 1998.

[GGM01] S. Garreau, P. Guillaume, and M. Masmoudi. The topological asymptotic for pde systems : the elasticity case. *SIAM J. Control Optim.*, 39(6) :1756–1778, 2001.

[Kat76] T. Kato. *Perturbation theory for linear operators*. Springer-Verlag, New York, 1976.

[Lit00] G-W. Litvinov. *Optimization in elliptic problems with applications to mechanics of deformable bodies and fluid mechanics*, volume 119 of *0perator Theory*. Birkhauser, 2000.

[MP01] B. Mohammadi and O. Pironneau. *Applied shape optimization for fluids*. Oxford Clarendon Press, 2001.

[MS76] F. Murat and S. Simon. Etudes de problèmes d'optimal design. In *Lecture Notes in Computer Science*, volume 41, pages 54–62. Springer Verlag, Berlin, 1976.

[Nov53] V. Novozhilov. *Foundation of the Nonlinear Theory of Elasticity*. Graylock Press, New York, 1953.

[NRG95] M. Neves, H. Rodrigues, and J-M. Guedes. Generalized topology design of structures with a buckling load criterion. *Structur. Optim.*, 1995.

[NS04] S.A. Nazarov and Y. Sokolovski. The topological derivative of the dirichlet integral under the formation of a thin bridge. *Siberian. Math. J.*, 45(2) :341–355, 2004.

[NSB02] M. Neves, O. Sigmund, and M. Bendsoe. Topology optimisation of periodic microstructures with a penalization of highly localized buckling modes. *Int. J. Numer. Meth. Engng.*, 2002.

[OS88] S. Osher and J-A. Sethian. Front propagating with curvature dependent speed : algorithms based on hamilton-jacobi formulations. *J. Comput. Phys.*, 78 :12–49, 1988.

[OS01] S. Osher and F. Santosa. level-set methods for optimization problems involving geometry and constraints : frequencies of a two-density inhomogeneous drum. *J. Comput. Phys.*, 171 :272–288, 2001.

[PBH04] B. Protas, T-R Bewley, and G. Hagen. A computationnal framework for the regularization of adjoint analysis in multiscale pde systems. *J. Comput. Phys.*, 195 :49–89, 2004.

[Pir84] O. Pironneau. *Optimal shape design for elliptic systems*. Springer-Verlag, New York, 1984.

[RC90] B. Rousselet and D. Chenais. Continuité et différentiabilité d'élements propres : Application à l'optimisation de structures. *Appl. Math. and Optim.*, 22 :27–59, 1990.

[Set99] J-A. Sethian. *Level-Set Methods and fast marching methods : evolving interfaces in computational geometry, fluid mechanics, computer vision and materials science*. Cambridge University Press, 1999.

[SHSP89] J. Sanchez-Hubert and E. Sanchez-Palencia. *Vibration and coupling of continuous systems. Asymptotic methods*. Springer-Verlag, Berlin, 1989.

[Sim80] J. Simon. Differentiation with respect to the domain in boundary value problems. *Num. Funct. Anal. Optimz.*, 2 :649–687, 1980.

[SJP92] J. Sokolowski and J-P.Zolesio. *Introduction to shape optimization : shape sensitivity analysis, Springer Series in Computational Mathematics*, volume 16. Springer-Verlag, Berlin, 1992.

[Sve93] V. Sverák. On optimal shape design. *J. Math. Pures Appl*, 72(6) :537–551, 1993.

[SW00] J-A. Sethian and A. Wiegmann. Structural boundary design via level-set and immersed interface methods. *J. Comput. Phys.*, 163 :489–528, 2000.

[SZ99] J. Sokolowski and A. Zochowski. On the topological derivative in shape optimization. *SIAM J. Control Optim.*, 37 :1251–1272, 1999.

[SZ01] J. Sokolowski and A. Zochowski. Topological derivatives of shape functionals for elasticity systems. *Mech. Structures Mach.*, 29(3) :331–349, 2001.

[VB96] L. Vandenberghe and S. Boyd. Semidefinite programming. *SIAM review*, 38 :49–95, 1996.

[WWG03] M-Y. Wang, X. Wang, and D. Guo. A level-set method for structural topology optimization. *Comput. Methods Appl. Mech. Engrg.*, 192 :227–246, 2003.

[WX04] Wang M.Y. Wang X., Yulin M. Incorporating topological derivatives into level set methods for structural topology optimization. In Polish Academy of Sciences, editor, *Optimal shape design and modeling*, pages 145–157. T. Lewinski et al, Warsaw, 2004.

Résumé

Dans le contexte de l'optimisation de formes par la méthode des courbes de niveaux, nous nous intéressons à certains nouveaux problèmes : l'optimisation de valeurs propres multiples, l'optimisation de la compliance robuste et l'optimisation du critère de flambement. Nous résolvons aussi deux importants problèmes numériques par le couplage avec le gradient topologique et la méthode de régularisation de la vitesse. Nous proposons aussi dans cette thèse un chapitre destiné à montrer les problèmes numériques propres à la méthode des courbes de niveaux et nous montrons les "trucs" numériques utilisés pour résoudre ces problèmes.

Abstract

In the context of shape optimization by the level-set method, we address some new problems : Multiple eigenvalue optimization, robust compliance optimization and buckling load optimization. We also solve two important numerical issues via the bubble method and the velocity regularisation method. This Ph-D thesis also contains a chapter that unveils some of the most important numerical problems that arise when using the level-set method and the numerical tricks that solve these issues.